UNIVERSITÀ DEGLI STUDI DI SALERNO

UNIVERSITÀ DEGLI STUDI DI SALERNO

Dipartimento di Farmacia

Ph.D. program

in **Drug Discovery and Development**

XXXIII cycle – Academic Year 2020-2021

Ph.D. Thesis in

Design, synthesis and biological evaluation of small molecules able to interact with macromolecular targets involved in tumor pathology

Candidate

Dafne Ruggiero

Supervisor

Prof. Ines Bruno

Ph.D. Program Coordinator: Prof. Gianluca Sbardella

PREFACE

My Ph.D. three years course in Pharmaceutical Sciences at the Department of Pharmacy of Salerno University started in 2017 under the supervision of Prof. Ines Bruno.

My research project was mainly focused on the design, synthesis and biological evaluation of small molecules as new modulators of emerging targets involved in inflammatory and cancer processes. Specifically, my research activity was addressed to the investigation of three major targets:

- the transcription factor, Heat Shock Transcription Factor 1 (HSF1);
- the co-chaperone, Bcl-2-Associated Athanogene 3 (BAG3);
- the membrane enzyme, microsomal Prostaglandin E2 Synthase-1 (mPGES-1).

The entire work was carried out under the direct supervision of Prof. Ines Bruno and Dr. Stefania Terracciano.

Computational guided design of compounds was performed in collaboration with Prof. Giuseppe Bifulco's research group.

Biological screenings were performed in collaboration with Dr. Nuria Vilaboa of Hospital Universitario La Paz (Spain) in the case of HSF1, with Prof. Silvia Franceschelli of University of Salerno in the case of BAG3, and with Prof. Oliver Werz of Friedrich Schiller University (Germany) in the case of mPGES-1. In order to investigate more thoroughly HSF1, in 2019 I joined Dr. Nuria Vilaboa's research group in Madrid where I spent four months. The purpose of the research in Madrid was to screen a small library of molecules potentially able to modulate HSF1 employing a reporter gene assay.

List of publications related to the scientific activity performed during the three years Ph.D. course in Pharmaceutical Sciences.

Papers:

- Di Micco S., Pulvirenti L., Bruno I., Terracciano S., Russo A., Vaccaro M.C., **Ruggiero D.**, Muccilli V., Cardullo N., Tringali C., Riccio R., Bifulco G. "Identification by Inverse Virtual Screening of magnolol-based scaffold as new tankyrase-2 inhibitors". *Bioorg. Med. Chem.* **2018,** *14*, 3953-3957. DOI: 10.1016/j.bmc.2018.06.019.

- De Vita S., Lauro G., **Ruggiero D.**, Terracciano S., Riccio R., Bifulco G. "Protein Preparation Automatic Protocol for High-Throughput Inverse Virtual Screening: Accelerating the Target Identification by Computational Methods". *J. Chem. Inf. Model.* **2019**, *59*, 4678–4690. DOI: 10.1021/acs.jcim.9b00428.

- Lauro G., Terracciano S., Cantone V., **Ruggiero D.**, Fischer K., Pace S., Werz O., Bruno I., Bifulco G. "A Combinatorial Virtual Screening Approach Driving the Synthesis of 2,4-Thiazolidinedione-Based Molecules as New Dual mPGES-1/5-LO Inhibitors". *ChemMedChem*, **2020**, *15*, 481-489. DOI: 10.1002/cmdc.201900694.

- Nemati F., Salehi P., Bararjanian M., Hadian N., Mohebbi M., Lauro G., **Ruggiero D.**, Terracciano S., Bifulco G., Bruno I. "Discovery of noscapine derivatives as potential β-tubulin inhibitors". *Bioorg. Med. Chem. Lett.*, **2020**, *20*, 127489. DOI: 10.1016/j.bmcl.2020.127489

- Di Micco S., Terracciano S., **Ruggiero D.**, Potenza M., Vaccaro M.C., Fischer K., Werz O., Bruno I., Bifulco G. "Identification of 2-(thiophen-2-yl) acetic acid-based lead compound for mPGES-1 Inhibition". *Frontiers in Chemistry*, DOI: 10.3389/fchem.2021.676631.

Conference proceedings:

- **Ruggiero D.**, Terracciano S., Vaccaro M.C., Chini M.G., Russo A., Riccio R., Bifulco G., Bruno I. "Discovery and synthesis of new C-terminal Hsp90 inhibitors as attractive candidates for anticancer drugs". XLIII "A. Corbella" International Summer School on Organic Synthesis, Gargnano (Italy), June 10-14, 2018.

- **Ruggiero D.**, Terracciano S., Di Micco S., Vaccaro M.C., Riccio R., Bifulco G., Bruno I. "Exploration of the aryl bromide scaffold for the development of new potential anti-inflammatory and anti-cancer agents blocking mPGES-1 enzyme". XXXVIII Convegno Nazionale della Divisione di Chimica Organica, Milano (Italy), September 9-13, 2018.

- **Ruggiero D.**, Terracciano S., Russo A., Vaccaro M.C., Lauro G., Bruno I. "Identification of selective Bag domain modulators of Bag 3 protein as a new class of attractive candidates for cancer therapy". XLIV "A. Corbella" International Summer School on Organic Synthesis, Gargnano (Italy), June 9-13, 2019

Table of contents

Abstract

Inflammation and cancer are two complex pathological processes that exploit several molecular actors. The identification of new platforms able to interfere with biological targets placed at the crossroads of these two pathways is strongly needed both, for the development of promising drug candidates, and as chemical probes useful to further investigate less understood biological aspects. Three main targets, involved at different levels in inflammation and cancer, have been thoroughly investigated: the Heat Shock Factor 1 (HSF1), the Bcl-2 associated athanogene 3 protein (BAG3), and the microsomal Prostaglandin E Synthase-1 (mPGES-1). The obtained results can be summarized in the three main sections reported below according to the target of interest:

a) Discovery of new potential modulators of HSF1 by computer-aided approach.

Heat shock factor 1 (HSF1) is the master regulator of the cytoprotective Heat Shock Response (HSR) in eukaryotes. The HSR is an evolutionarily conserved mechanism triggered by proteotoxic stress and involves the rapid and transient expression of Heat Shock Protein (HSP), molecular chaperones that restore cell proteostasis. HSF1 activity is amplified in many tumor contexts in a manner that resembles a chronic state of stress, characterized by high levels of *hsp* gene expression as well as HSF1-mediated non-*hsp* gene regulation. HSF1 and its gene targets are implicated in tumorigenesis as assessed in several experimental tumor models and facilitate metastatic and resistant properties within cancer cells. HSF1 is emerged as a therapeutic target valuable in cancer related disorders although, for several reasons, it can be considered quite “undruggable”. The workflow that guided us in the research of potential HSF1 binders was based on an integrated approach including computational studies, synthesis of the most promising molecules,

biophysical assays, and in-cell assays. Starting from the HSF1-DBD crystallographic structure in complex with an HSE (PDB: 5D5U), two types of virtual screening were performed. The molecules with the best docking score values were purchased or synthesized and their affinity for the full-length protein was evaluated by SPR assay. These studies led us to identify several molecules potentially able to target the protein, in particular, we found that **BD-1** and **LAM17** are able to bind the full-length protein with a dissociation constant in the low micromolar range, and furthermore, basing on in-depth biological studies, they showed to regulate the transcriptional activity of HSF1.

b) Design, synthesis and biological evaluation of BAG3 modulators.

Bcl2-associated athanogene 3 (BAG3) protein is a member of the BAG family of co-chaperones that interacts with the ATPase domain of the Heat Shock Protein 70 (Hsp70) through the conserved BAG domain. BAG3 is the only member of the family to be induced by stressful stimuli, mainly through the activity of HSF1 on *bag3* gene promoter. In addition to the BAG domain, BAG3 also contains a WW domain and a proline-rich (PXXP) repeat that mediate its binding to different partners. These multifaceted interactions underlie the BAG3 ability to modulate key biological processes like apoptosis, development, cytoskeleton organization, and autophagy, thereby mediating the cell adaptive responses to stressful stimuli. In normal cells, BAG3 is constitutively present in a very few cell types, including cardiomyocytes and skeletal muscle cells, in which the protein appears to contribute to cell resistance to mechanical stress. A growing body of evidence indicates that BAG3 is highly expressed in several tumor types where it is proven to sustain cell survival, resistance to therapy, motility, and metastatization. In some tumor types, the down-modulation of BAG3 levels was shown, as a proof-of-principle, to inhibit neoplastic cell growth in animal models. With the aim of exploring the BAG3 protein as cancer target, through a combined approach of *structure-based drug design* and biophysical methods, in 2017 the research group of which I am part

discovered the first selective BAG3 modulator featuring a 2,4-thiazolidinedione scaffold. Basing on these promises, I continued to explore the chemical space around the thiazolidinedione core, and, supported by computational studies, a new compounds collection has been developed. In order to assess the affinity for the target, these molecules were tested, through SPR assay, against both the full-length BAG3 protein and the BAG3-BD. **LK6** proved to be the most promising molecule showing a high affinity for both the full protein (6.3 ± 0.3 μM) and the BAG domain (27.6 ± 1.9 μM). According with its favorable binding properties, **LK6** showed a potent cytotoxicity and the ability to cause a cell accumulation in the G_1 phase, suggesting an apoptosis/necrosis event which was confirmed by the significant dose-dependent reduction of caspase 3 and 9, the main effectors of the programming cell death, in treated cells.

c) Identification of mPGES-1 inhibitors through a multistep approach.

Microsomal prostaglandin E synthase-1 (mPGES-1) is the terminal synthase responsible for the production of prostaglandin E_2 (PGE_2). PGE_2 is a bioactive lipid that can elicit a wide range of biological effects associated with inflammation and cancer. The pleiotropic role of PGE_2 is mainly mediated by the activation of key downstream signaling cascades via transmembrane EP receptors located on the cell surface. Elevated levels of COX-2 and concomitant overproduction of PGE_2 are often found in human cancers leading to the use of non-steroidal anti-inflammatory drugs (NSAIDs) as chemo preventive agents. Their long-term use, however, may be associated with gastrointestinal toxicity and increased risk of adverse effects. Targeting mPGES-1 is considered a valid alternative to the use of NSAIDs because it is an inducible enzyme able to affect only the prostanoids elicited by inflammatory stimuli without affecting those lipid mediators constitutively expressed. In the frame of my Ph.D. project, following a *fragment-based approach* and a *structure-based drug design*, a very promising mPGES-1 inhibitor was

disclosed as well as a dual inhibitor of mPGES-1 and 5-lipoxygenase (5-LO). In the first case, a (4-phenyl-thiophen-2-yl)-acetic acid-based compound, **SZK9**, showed a high selectivity and a potent inhibitory activity against mPGES-1 (IC_{50} = 5.9 ± 1.0 µM). Since this molecule is endowed with a strong cytotoxic effect (IC_{50} = 10.1 ± 1.2 µM) comparable to the known inhibitor **CAY10526** it can represent an attractive candidate for the development of new therapeutics in cancer pathology. In the second case, following a *structure-based approach* a 2,4-thiazolidinedione based molecule, **TZ8**, was identified as a potent inhibitor of both mPGES-1 and 5-LO, two key enzymes involved in inflammatory related disorders. Owing to its dual-target inhibitor profile **TZ3** can be considered an interesting hit for the development of novel therapeutic interventions.

Introduction

CHAPTER 1

Heat Shock Transcription Factor 1 (HSF1)

CHAPTER 1
Heat Shock Transcription Factor 1 (HSF1)

1.1 Introduction

The discovery of the Heat Shock Response (HSR) dates back to the early 1960s when the Italian researcher Ferruccio Ritossa was engaged in the study of puffs in polythene chromosomes of *Drosophila melanogaster* salivary glands. [a,1,2,3] By mistake, the temperature of the incubator containing the *Drosophila* larvae was increased and Ritossa could observe the formation of a unique puff in the polythene chromosomes. It was later discovered that this puff could also form when the larvae were exposed to sodium salicylate or dinitrophenol. Based on this evidence, Tissieres and colleagues, in 1974, discovered a category of proteins, the Heat Shock Proteins (HSPs), which turns out to be up-regulated during chromosomal puffing occurring upon heat stress. [4, 5]

All living organisms have a defense mechanism called Heat Shock Response which allows cells to survive exposure to high temperatures (41-42°C in humans) and other environmental stressors such as hypoxia, pH fluctuations, and heavy metals. HSR is the results of the *hsp* genes expression, controlled by a transcription factors family, the Heat Shock Factors (HSFs). When this cytoprotective mechanism is triggered, high levels of HSPs, such as Hsp27, Hsp40, Hsp70, and Hsp90 are produced. Most of these proteins are molecular chaperones able to preventing protein misfolding and aggregation within cells. Among the HSFs, HSF1 is the master regulator of the transcriptional response to proteotoxic stress and it also plays a pivotal role in controlling genes involved in the maintenance of cell

[a] Polythene chromosomes are giant chromosomes, formed following various replication cycles, able to produce many copies (even hundreds) of sister chromatids that remain united. This kind of chromosomes has the function of increasing cell volume but also entail a metabolic advantage since the puffs are strongly unrolled regions characterized by an intense transcription activity of genetic information in RNA.

structure and metabolism, providing protection against a wide range of cellular stressful mediators, besides heat shock. When HSR is activated by HSF1, the induction of other transcription factors occurs promoting as many stress response pathways, thus amplifying the initial signal. [6] It must be specified that not all the genes are induced at the same time and for the same time. The genes involved in proteostasis restoring are immediately activated (within a few minutes), while other genes involved in DNA damage repair and cellular metabolism are activated later (hours are needed). [6]

1.2 HSF family members

Beyond HSF1, that will be treated in detail in the next section, other three HSFs isoforms are present in vertebrates: HSF2, HSF3, and HSF4. HSF2 is often co-expressed with HSF1 in many tissues and cell lines; HSF3 was originally found only in avian species; and HSF4, the most recently identified member in mammals, is expressed predominantly in lens and brain. [7-9]

The biochemical characterization of HSF2 revealed that, unlike HSF1, which undergoes a transition from monomer to trimer, HSF2, upon activation, is converted from an inactive dimer to an active trimer and is not phosphorylated. The regulation of HSF1 and HSF2 expression is completely different: while HSF1 is stably and constitutively expressed, HSF2 is regulated both transcriptionally and through the stabilization of its mRNA. [10] The rapid accumulation of HSF2 protein, due to the downregulation of the ubiquitin proteolytic pathway, has provided experimental evidence that HSF2 is a labile protein. Upon stress, HSF2 can either form a homotrimer, or it can heterotrimerize with HSF1 in the nucleus driving both the HSF1-mediated expression of HSPs and the transcription of non-coding satellite III DNA repeats in nuclear stress bodies (see below). [11] Furthermore it plays also a key role in neurological and embryonic development, meiosis, and spermiogenesis. [12]

HSF3 is the major heat shock transcription factor in the chicken, where it was initially identified. It exists as a dimer in unstressed cells, however, it can form homotrimers upon heat shock. [13] Its activation levels depend on heat shock severity: it is not activated by mild heat shocks but only by extreme heat shocks (above 44°C). HSF3 is activated by the same stresses that activate HSF1, however, HSF3 activation levels are always lower than HSF1 levels suggesting that it may be much more suitable for extreme stresses than HSF1. [14] It is worth noting that, although HSF3 is considered the avian orthologue of the mammalian HSF1, some evidence suggests its involvement in the regulation of several mediators responses in humans (the interleukins IL-6, IL-1β, and the activating transcription factor 3). [15]

HSF4 is a novel member of the HSF family that lacks the leucine zipper 4 (LZ4) domain (see below). It is localized mainly in the nucleus and preferentially expressed in the human heart, brain, skeletal muscle, and pancreas. [16] Despite having in common with the other HSF proteins many biochemical features, it does not possess the typical properties of the transcriptional activators. Thanks to transient and stable transfection experiments, it has been demonstrated that HSF4 binds DNA as a trimer but without positive stimulating effects on transcription. This unusual feature could be related to the lack of the hydrophobic carboxy-terminal repeat present in all HSF family members. HSF4, specifically, binds DNA at the HSE levels, however, is not still clear if it is present in an activated or repressed state. It remains to be determined whether HSF4 is a new negative regulator of heat shock gene expression capable of exerting its action only in some tissue types. Some evidence suggests that HSF4 is involved in the basal transcription repression of cellular heat shock genes (*hsp90*, *hsp70* and, *hsp72*). [7]

1.3 HSF1

HSF1, the most investigated member of the HSF family, is highly conserved among species, indeed, the analysis of the amino acid sequences of the human, murine, and

bovine forms indicate a sequence identity of approximately 84%. Furthermore, HSF1 shares 32% and 36% of sequence identity with HSF2 and HSF4 in humans, respectively (**Figure 1**).

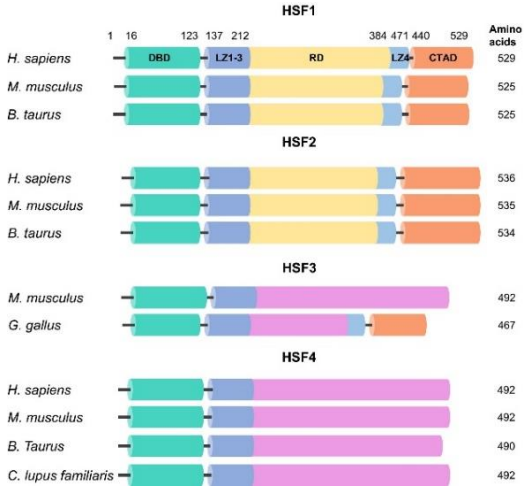

Figure 1: Functional domains of proteins belonging to the HSF family across different species (HSF1-4).

In mammals, HSF1 exists as a monomer and is preferentially localized in the cytoplasm. In the absence of stress, its ability to bind DNA is suppressed both, at the intramolecular and intermolecular levels, and its inhibition is favored by the association with several molecular chaperones, such as Hsp90, Hsp70, and TRiC/CCT. [17-19] Upon stress conditions, HSF1 undergoes a series of activating post-transcriptional modifications (PTM) and forms transcriptionally active trimers that accumulate in the nucleus and bind the Heat Shock Elements (HSEs) on DNA. The HSEs are inverted repeats of the pentameric sequence nGAAn present in the upstream regulatory regions of the *hsp* genes (**Figure 2**). [20] The HSE sequences must have a specific orientation to preferentially guide HSF1 binding to the target loci. [21]

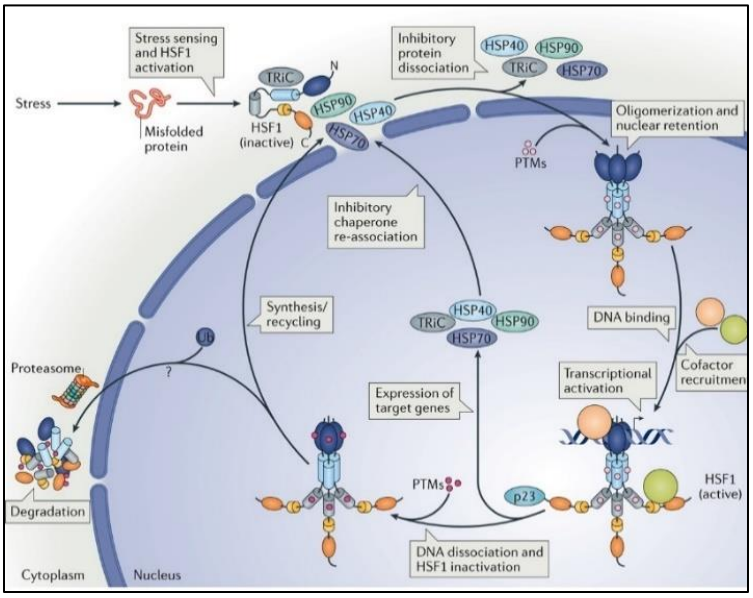

Figure 2: Various types of cellular stressors can activate the HSR by causing the release of HSF1, which in unstressed conditions is basally sequestered by the Hsp90 multichaperone complex. The activated and phosphorylated HSF1 enters the nucleus, homotrimerizes, and binds to the HSE to induce the transcription of its target genes. In the attenuation phase, Hsp70 presents in the nucleus can bind HSF1 to inhibit its function. During this time, HSF1 is also dephosphorylated and shuttles out of the nucleus, resumes its inactivated form, and is once again bound to the Hsp90 multichaperone complex.

When the cell is exposed to stress, distinct and relatively large structures (0.3-3 μm in diameter), called nuclear Stress Bodies (nSBs), corresponding to highly packed forms of ribonucleoprotein complexes, are formed in the nucleus. [22] Simultaneously with the nSBs, the formation of HSF1-HSF2 transcriptionally active heterocomplexes occur along with the Hsp70 nucleolar accumulation. [11] Although the function of the nSBs is still largely unknown, it is noteworthy that the nSBs are formed in the first 5 minutes after the onset of stress and persist for several hours. When HSR declines, Hsp70 levels increase, HSF1 trimers detach from nSBs and dissociate into inactive HSF1 monomers by binding to Hsp70. [23] The HSF1 activity is strictly regulated by protein-protein interactions and PTMs, however, several evidences showed that HSF1-induced HSPs can directly inhibit the transcription factor, providing thus an autoregulatory mechanism able to sense the extent of cellular protein damage and to accordingly calibrate the stress response.

1.3.1 HSF1 structure

HSF1 protein is formed by 529 amino acid residues and it is structurally organized in five functional units: a DNA-Binding-Domain (DBD) responsible for the DNA interaction, two heptad repeat regions (HR-A/B and HR-C), involved in the trimerization step, the trans-activation domain (TAD), which governs the transcriptional activation of the target genes, and a regulatory domain (RD) which keep the TAD in an active condition (**Figure 3**). [24]

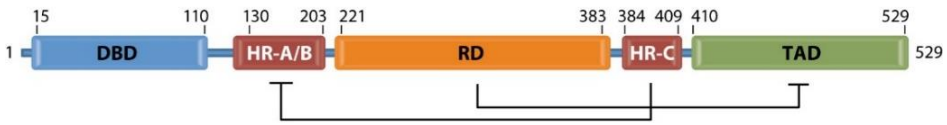

Figure 3: HSF1 protein structure.

In more detail, the human HSF1-DBD corresponds to the amino acid residues from 15 to 110 (**Figure 3**). It is the best-conserved region within the HSF family and it is the only functional domain for which detailed structural data are available. The HSF1-DBD is of a looped helix-turn-helix type, but, unlike many other looped helix-turn-helix transcription factors, the HSF1 loop does not make direct contacts with DNA. The loop has, instead, been proposed to stabilize the binding of HSF1 trimer to DNA by protein-protein interactions. [25]

The HSF1 trimerization is regulated by the oligomerization domain. Although detailed structural information is not available for this domain, spectroscopy studies have shown that is rich in α-helices and is divided into two subdomains, each containing an amphiphilic helix with hydrophobic heptad repeats (HR) (**Figure 3**). The HR-A and HR-B regions, which include the amino acid residues from 130-203, are also commonly called LZ1-3 and LZ4 because they are leucine zippers created by the dimerization, at least, of two specific alpha helix monomers bound to DNA. [26] The spontaneous trimerization of HSF1 can be suppressed by another HR region,

HR-C, located between the regulatory domain and the transactivation domain (amino acid residues 384-409). The HR-C domain can fold back and interact with HR-A/B to keep HSF1 in an inactive state. [16] The trimerization is also modulated by the linker that connects the DBD to the HR-A/B. [27]

The C-terminal region of HSF1 contains 150 amino acids and governs the transcriptional activation of the target genes, as well as the regulation of HSF1 activation intensity (**Figure 3**). It can be divided into two trans-activation domains (TADs), TAD1 and TAD2. [28] In *in vitro* transcription assays, TAD1 and TAD2 are capable of individually stimulating both, the transcriptional initiation and elongation, through the recruitment of BRG1, an ATPase subunit of the SWI/SNF chromatin-remodeling complex. [29, 30]

Under physiological conditions, the HSF1-TAD is maintained in an inactive condition by the regulatory domain (RD), situated between the HR-A/B and HR-C domains (**Figure 3**). The HSF1-RD is inducibly targeted by various forms of PTMs, including phosphorylation, SUMOylation, and acetylation. [28]

1.3.2 HSF1 Post-translational modifications

PTM	Enzyme	Effect	Physiological context	References
Phosphorylation				
Ser121	MK2, AMPK	Hsp90 binding and respression	Cancer (↓), metabolic stress (↑)	[31]
Ser127	-	-		[32]
Thr142	CK2	DNA binding activation	Heat shock (↑)	[33]
Ser195	-	LZ1-3 and LZ4 dissociation and transactivation	Heat shock (↑)	[34]
Ser216	PLK1	Protein degradation, mitotic progression	Mitosis (↑)	[35]
Ser230	CaMKII	Activation	Heat Shock (↑)	[36]
Ser292	-	-		[37]
Ser303	GSK3β, ERK1, MEK1, CK2	Attenuation and degradation	Cancer (↓), HD (↑)	[38]
Ser307	GSK3β, ERK1, MEK1, CK2	Attenuation and degradation	Cancer (↓), HD (↑)	[32]
Ser314	-	-	Cancer (↓)	[31]
Ser319	-	-	-	[39]
Ser320	PKAcα	Activation	Heat Shock (↑)	[40]
Thr323	-	Repression	Heat Shock (↑)	[31]
Ser326	mTOR, ERK1/2, MEK1	Activation	Heat shock (↑), cancer (↓)	[39]
Ser333	PKCθ	Hsp90 dissociation and activation	Cancer (↑)	[41]
Ser344	-	-		[39]
Ser363	PKCα, PKCζJNK	Repression	Heat shock (↓)	[42]
Thr367	-	Repression	Cancer (↓)	[31]
Ser419	PLK1	Nuclear localization and activation	Heat shock (↓)	[39]
Ser444	-	-		[39]
Acetylation				
Lys80	GCN5, p300, SIRT1, HDAC7, HDAC9	Inhibition, DNA binding dissociation	Heat shock (↓)	[43]
Lys116	-	-		[44]
Lys118	p300	Inhibition	Heat shock (↑)	[44]
Lys126, Lys 148	-	-		[44]
Lys157, Lys188	-	-		[44]
Lys208	p300	Protein stabilization	Basal conditions (↑)	[44]
Lys224	-	-		[44]
Lys298	p300	Protein stabilization	Basal conditions (↑)	[44]
Lys524	-	Heat shock response	Heat shock (↑)	[45]
SUMOylation				
Lys62, Lys91, Lys116, Lys118, Lys126, Lys131, Lys 139, Lys148, Lys 157, Lys 162, Lys 184, Lys 208	-	-		[46]
Lys298	UBC9	Repression	Heat shock (↓)	[46]
Lys372	-	-		[46]

Table 1: Summary of post-translational events targeting HSF1. Arrow indicate stress and/or pathological conditions in which alterations in particular modification have been reported. '-' indicates that the function of this post-translation modification is not known or has not been assessed yet.

The HSF1 stress-mediated activation involves a multitude of events which drive the protein trimerization and the active HSF1 transcription complex formation through the recruitment of several regulatory elements and coactivators. Most of these events, inducing conformational changes inside the proteins, are modulated by post-translational modifications (PTM), such as phosphorylation, SUMOylation, and acetylation (**Table 1**).

The HSF1 binding to the DNA is not sufficient for the transcriptional induction of *hsp* genes, suggesting that other mechanisms operate to increase HSF1 *trans*-activating competence. A key feature of HSF1 is its conversion into a transcriptionally active trimer, following the extensive hyperphosphorylation of the serine residues, most of which are within the RD. [47] 20 phosphorylation sites on serine and threonine residues have been so far identified. Some sites, such as S230 and S326, are constitutively phosphorylated and participate in the HSF1 activation, whereas, other sites are subjected to inducible phosphorylation. The phosphorylation can also repress the transcriptional activity of HSF1, as in the case of S303 and S307. [48]

Phosphorylation-Dependent SUMOylation (PDSM) is another PTM occurring on HSF1. The small ubiquitin-like modifier (or SUMO) proteins belong to a family of small proteins, covalently attached to and detached from other proteins in cells at specific lysine residues to modify their function. [49] In HSF1 the SUMOylation and the phosphorylation sites (SP) form together an extensive motif that mediates phosphorylation-dependent SUMOylation (PDSM). [50] The PDSM is induced during stress and it can modulate the *hsp* transcription genes in the late stage of stress. However, the exact proteostatic functions and regulation-driven by this PTM are still poorly understood. [51, 52]

The acetylation also plays a fundamental role in modulating HSF1 activity. [44] It has been observed that HSF1 acetylation on lysine residues increases as a result of the pharmacological inhibition of sirtuins, a class of proteins possessing deacetylase activity, and decreases following the overexpression of sirtuin 1 (SIRT1). HSF1

ability to bind DNA can be prolonged over time or reduced using chemical compounds capable of activating or inhibiting SIRT1, respectively, confirming that SIRT1-mediated deacetylation can hold HSF1 in an active state. [44] Unlike phosphorylation, which occurs mainly at the RD level of the protein, acetylation targets the lysines of domains implicated in the HSF1-DNA recognition, oligomerization, and subcellular localization. [44] Among them, the acetylation of Lys80, located within the HSF1-DBD, in direct contact with the DNA phosphate backbone, induces an attenuation in the HSF1 DNA binding ability, thus leading to a weak HSR. [53]

1.3.3 HSF1 in cancer and neurodegenerative diseases

HSF1 has been well recognized to play a crucial role in several diseases, including cancer, where it has a strong relation with patient outcomes. [54] Cancer cells show a "non-oncogene addiction" to this transcription factor because they experience high levels of proteotoxic stress and a general hostile microenvironment, therefore, they depend on stress response pathways for survival and proliferation. HSF1 is supposed to support malignant transformation by coordinating a network of mechanisms including proliferation, survival, protein synthesis, and glucose metabolism (**Figure 4**).

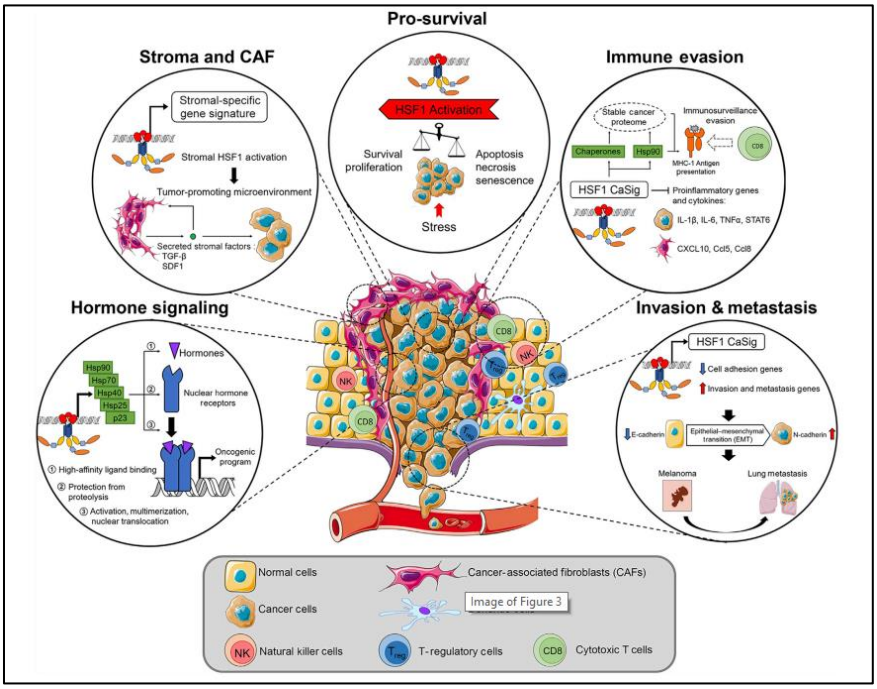

Figure 4: An illustration of a solid tumor disseminating into local circulatory system in order to highlight the functional importance of the HSF1-mediated transcriptional network in key aspects for cancer survival, progression, dissemination, and evasion of immune surveillance.

All the studies, carried out so far, have led to the identification of a single HSF1 transcription program, active in highly malignant cells, known as HSF1 Cancer Signature (HSF1-CaSig). [54] Patients with a high expression of HSF1-CaSig show worse results regardless of cancer tissue origin. Specifically, the phosphorylation of HSF1-Ser326 has been linked to poor prognosis in ovarian cancer, chronic lymphocytic leukemia, and myeloma. Besides, high HSF1 levels correlate with a malignant and very aggressive phenotype in breast cancer. [54, 55]

HSF1 support cancer genesis and progression through different mechanisms, although its cytoprotective role is mainly linked to the induction of HSPs expression. HSF1 target genes codify for molecular chaperones essential for the folding, stability, and activity of many oncoproteins as androgen receptor (AR), BRAF, AKT, TP53, Src, and others. [56] The chaperone network protects the cell from proteomic imbalances resulting from genetic and epigenetic stresses, and post-

translational aberrations, typical phenomena of cancer cells. [57] Furthermore, HSF1 induces high levels of BAG3; this latter is responsible, under stress conditions, for the stabilization of the antiapoptotic factors belonging to the Bcl-2 protein family which determine a decrease of the programmed cell death. [54, 58] HSF1 maintains cellular homeostasis, modulating several processes including the activation of p53 protein that induces cell cycle arrest at G_2/M phase, following the DNA damage, and the increased expression of genes involved in the DNA damage repair. [59] Finally, HSF1 activation has been associated with the negative outcome of radiotherapy treatments and chemotherapeutic drug resistance, both in solid tumors and in hematological malignancies, and an aberrant HSF1 hyperactive state has been observed in several cancer (breast, lung, prostate, colon, myeloma, pancreas, and others) (**Table 2**). [54, 60-63] Hence, considering the crucial role of HSF1 in several processes underlying malignant transformation, it has been well recognized as an attractive target in cancer therapy. Although the identification of HSF ligands is not a simple task for several reason, however, having in the hand selective modulators of this protein can be of great interest for the scientific community in order to develop new potent and attractive drugs for future anticancer strategies.

Cancer types	Clinical relevance	Clinical significance	Reference
Hepatocellular carcinoma	1. HSF1 protein level in HCC tissues is higher than non-cancerous liver tissues. 2. HSF1 protein expression is associated with tumor size, number of tumor nodules, TNM stage, BCLC stage, and histological grade. 3. HSF1 expression is positively correlated with BAG3 expression. 4. Higher HSF1 protein level is associated with shorter overall survival.	HSF1 could be an independent prognostic factor for overall survival in HCC patients	64
Breast cancer	1. Nuclear HSF1 level is increased in situ and invasive tissues. 2. HSF1 expression was associated with high histologic grade, larger tumor size, and nodal involvement at diagnosis. 3. High HSF1 expression is associated with reduced survival in ER-positive patients.	HSF1 could be an independent prognostic indicator in ER-positive patients and a useful therapeutic target for breast cancer.	65
Endometrial carcinoma	High HSF1 protein level is associated with aggressive disease and poor survival	HSF1 may be an independent prognostic marker in ER-positive patients	66
Oral squamous cell carcinoma	1. HSF1 mRNA expression was greater in cancer tissues than in normal tissues. 2. Higher nuclear HSF1 expression was closely related to tumor size and histopathologic types.	HSF1 might be a potential diagnostic biomarker and a therapeutic target for OSCC.	67
Prostate cancer	HSF1 is overexpressed in cancer sections compared to normal sections.		68
Colorectal cancer	HSF1 mRNA levels was increased in cancer tissues compared to normal tissues		69
Stage I non-small cell lung adenocarcinoma	1. Stromal HSF1 activation is correlated with reduced disease-free survival. 2. Stromal HSF1 activation is associated with reduced disease-free survival in patients with KRAS mutant tumors.	Stromal HSF1 could serve as an independent prognostic marker in lung cancer	70

BAG3: Bcl-2-associated athanogene domain 3; BCLC: Barcelona Clinic Liver Cancer; TNM: Tumor Node Metastasis.

Table 2: The clinical relevance and significance of HSF1 in cancer.

In addition to cancer-related processes, HSF1 is also involved in genetic programs underlying the neuronal migration, the formation and maintenance of neuronal synapses, and the resistance to proteotoxic stress. [71, 72] Impairment of HSF1 activity with aging and in neurodegenerative diseases, such as Huntington, Alzheimer's, Parkinson's disease, and amyotrophic lateral sclerosis (ALS) is well documented.

[73] The lower HSF1 activation appears to exacerbate protein misfolding and aggregation by inducing a decreased expression of chaperones, contributing to the reduction of protein quality control, neuronal dysfunction, neuronal cell death, and disease progression. These findings highlight the crucial role played by HSF1 in neurons protection and that could lead to the development of therapeutic approaches for neurodegenerative diseases [74-78] (**Figure 5**).

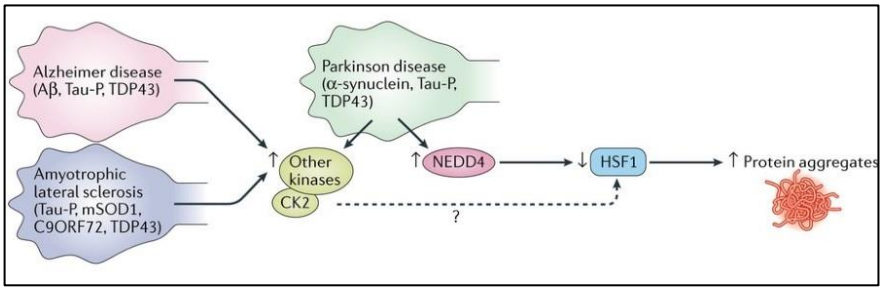

Figure 5: In Parkinson disease, Alzheimer disease and amyotrophic lateral sclerosis (ALS) reduced HSF1 protein levels and/or activity has been reported and are associated with decreased expression of chaperones, exacerbating the aggregation of disease-relevant proteins, including α-synuclein, amyloid-β (Aβ), phosphorylated Tau (Tau-P).

1.4 HSF1 inhibitors

As emerged from the previous discussion, HSF1 is extremely challenging to target with small molecules for several reasons. For example, from a structural point of view, except for the DBD and the leucine zipper domains, HSF1 is a highly unstructured protein, a typical feature of regulatory factors that establish numerous protein-protein interactions. This aspect, and the lack of an effective and specific molecule able to inhibit HSF1 transcriptional activity prevent both, a *structured-based design* and a *ligand-based* approach. Despite the many efforts focused on the identification of a selective inhibitor of HSF1 activity, the molecules disclosed so far remain in the preclinical stage.

1.4.1 Direct inhibitors

A relatively direct interaction and thus an effect on HSF1 action was demonstrated for only two molecules: **KRIBB11** and **I_{HSF115}** (**Figure 6**).

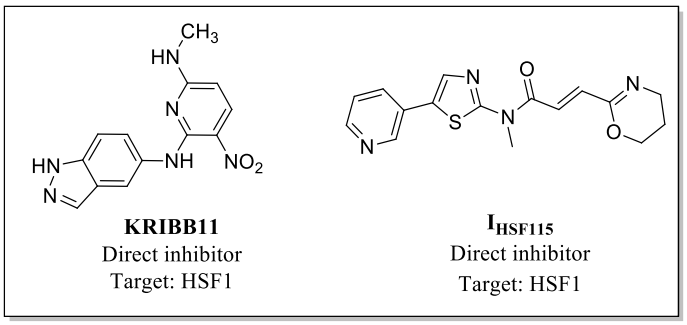

Figure 6: Structures of direct HSF1 inhibitors.

KRIBB11 was the first molecule that showed to interact with HSF1 directly (**Figure 6**). [79] The interaction between HSF1 and **KRIBB11** was shown via western blot using biotinylated-KRIBB11. This molecule inhibits the HSF1-dependent recruitment of the positive transcription elongation factor b (P-TEFb) to the *hsp70* promoter. It induces apoptosis and inhibits the growth of myeloma cells. [79]

I_{HSF115} was the second discovered molecule able to directly bind HSF1. [80] This molecule was identified in the course of an *in silico* screening of a large compounds library, considering, as possible binding pockets, small cavities large enough to accommodate potential binders. More in-depth studies revealed that **I_{HSF115}** regulates HSF1 transcriptional activity inhibiting the binding between HSF1 and ATF1-containing transcription complexes. ATF1 is a pivotal component of the transcription factor complexes that mediate HSF1 target gene transcription in heat-shocked cells. This factor interacts with a region within the DNA-binding domain of HSF1 and this interaction may be weakened by a conformational change of HSF1 induced by **I_{HSF115}**. Alternatively, the inhibitor may interfere directly with ATF1 blocking its interaction with HSF1. **I_{HSF115}** showed cytotoxicity against several

human cancer cell lines, particularly multiple myeloma, and breast cancer. (**Figure 6**). [80]

More recently, an emerged genetic technology led to the discovery of a new way to modulate HSF1. Aptamers are oligonucleotides that have been engineered through repeated rounds of *in vitro* selection to bind a specific target molecule. [81] **APtHSF-RA1** was reported to inhibit HSF1 activity. This aptamer interacts with the DBD and the adjacent linker region of HSF1 and competes with the HSEs to bind HSF1. It prevents HSF1 from binding to HSE, reduces HSP levels, and attenuates the MAPK signaling pathway activation, inducing apoptosis and abolishing the colony-forming capability of cancer cells. [82]

1.4.2 Indirect inhibitors

Several papers describe the identification of both, natural and synthetic molecules able to interact with HSF1, however, functional results were not satisfactory and none of the reported molecules are selective for HSF1 (**Figure 7**, **8**)

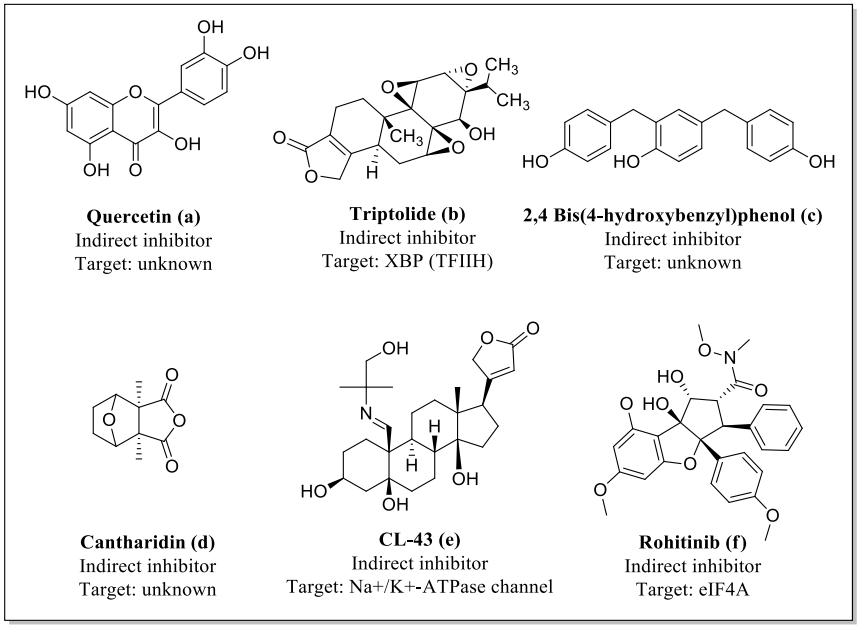

Figure 7: Structures of natural HSF1 inhibitors: **a)** quercetin [83, 84]; **b)** triptolide [85, 86]; **c)** 2,4 Bis(4-hydroxybenzyl)phenol [87]; **d)** cantharidin [88]; **e)** CL-43 [89]; **f)** rohitinib [55].

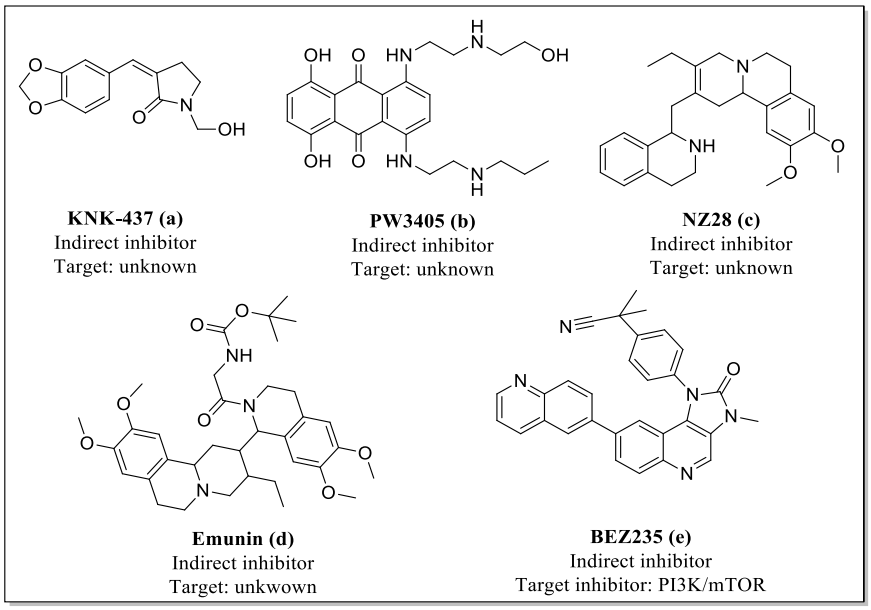

Figure 8: Structures of synthetic HSF1 inhibitors: **a**) KNK-437 [90, 91]; **b**) PW3405 [92]; **c, d**) NZ28 and emunin [93]; **e**) BEZ235 [94].

CHAPTER 2

Bcl-2-associated athanogene 3 (BAG3) antiapoptotic protein

CHAPTER 2

Bcl-2-associated athanogene 3 (BAG3) antiapoptotic protein

2.1 The Human BAG proteins family

The BAG (Bcl-2 associated athanogene) family is an evolutionarily conserved group of proteins, characterized by a common conserved region known as BAG domain, able to regulate key cellular function ranging from apoptosis to tumorigenesis. The BAG domain, made up of 110-121 amino acid residues, is a conserved region at the C-terminus that provides the interactions with both, the constitutive (Hsc70) and the inducible form of Hsp70. Crystallographic studies have shown that the interaction between Hsp70 and the BAG domain induces a conformational change in the ATPase domain of the chaperone which prevents the association with the ATP (the principle has been extended to the whole BAG protein family). [95] Hence, BAG proteins act as Hsp70 chaperone assistants and therefore they are called co-chaperones. [96] The six known members of this family are BAG1 (RAP46/HAP46), BAG2, BAG3 (CAIR stressed-1 or CAIR-1/B), BAG4 (SODD), BAG5, and BAG6 (BAT3/Scythe). They possess other domains in addition to the BAG domain, which allow them to interact with many factors, thereby explaining their multifaced functions (**Figure 9**). [97, 98]

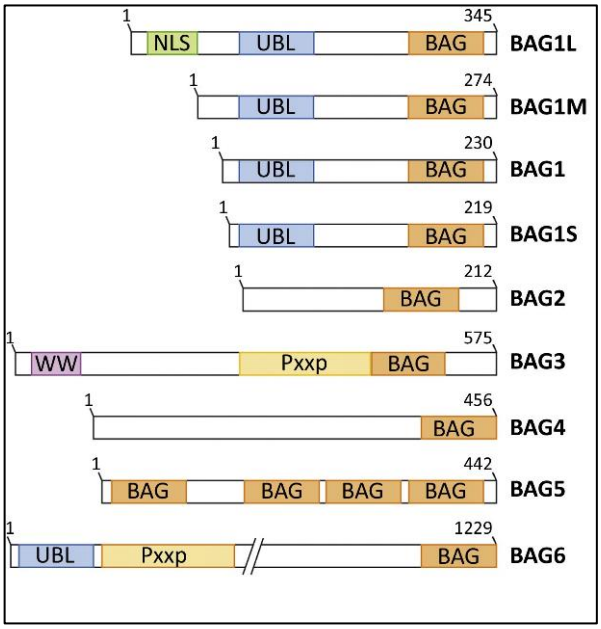

Figure 9: The human BAG family of proteins.

BAG1, occurring as four isoforms structurally differing in their N-terminus, is generally the most abundant protein. Cell studies have shown that BAG1 has several functions: in complex with Hsp70 drives ATP exchange, by stimulating the substrate release, and positively cooperates to direct the client proteins to the proteasomal degradation through its ubiquitin-like domain; however, BAG1 has also a negative regulatory effect on Hsp70. [99] Other functions are independent of its BAG domain. [100]

BAG2, one of the simplest proteins in the BAG family, being characterized only by one BAG domain, is the substrate for MAPK-activated protein kinase 2 (MAPKAP) and a specific inhibitor of CHIP protein (C-terminus of the Hsc70-interacting protein). Via CHIP inhibition, BAG2 can influence the balance of Hsp70-controlled protein folding and degradation of substrate proteins. [101] However, BAG2 has been shown to promote protein degradation via the 20S proteasomal processing pathway, thus, acting independently from ubiquitin. [102] The essential role played by BAG2

in cellular protein quality control allows to understand its involvement in neurodegenerative diseases associated with the accumulation of misfolded proteins. BAG4, like BAG2, has a very simple structure characterized by a single BAG domain. BAG4 acts as a death domain silencer (SODD), by binding the death domains present in members of the TNF receptor family, such as TNF1 and the death receptor 3. [103] BAG5, instead, has four putative BAG domains. The functions of BAG5 are not well known. According to several evidences, it has been possible to connect BAG5 to the pathogenesis of Parkinson's disease (PD), indeed, BAG5 inhibits the activity of *parkin*, a gene that codes for E3 ubiquitin ligase, whose mutations are the main cause of early- PD onset. [104]

Finally, BAG6 is made up of 1229 amino acid residues and is the largest protein belonging to the BAG family. BAG6 is included in BAG family proteins for its homology sequence at the BAG domain level. [105, 106] BAG6, with its UBL domain at the N-terminal end, is involved in the proteasomal pathway by addressing the ubiquitinated Hsp70 substrates to the proteasome. [107]

2.2 BAG3

BAG3, belonging to the Bcl-2 associated athanogene co-chaperones protein family, is highly conserved in mammals and is the only member to be induced by stressful stimuli through the *bag3* gene expression that is under the control of several endogenous physiological factors. The increased BAG3 levels, following stress or treatment with compounds, derives, mostly, from the induction of BAG3 expression by HSF1, which interacts with two HSEs within the *bag3* promoter. [108] The strong BAG3 up-regulation, upon harmful environmental conditions, suggests that it has a fundamental role in key biological processes sustaining cell survival and protection. [109,110]

2.2.1 Structure of BAG3 protein

There are two isoforms of BAG3: the full-length protein (70 kDa) and the shorter version of around 40 kDa (**Figure 10**).

Figure 10: Structure of BAG3 proteins (full-length e shorter isoforms).

The shorter isoform is expressed in synaptosomes and probably derives from alternative splicing or proteolytic process, however, it has not yet been characterized in detail. [111]

BAG3 full-length protein is ubiquitously expressed in human tissues at different levels: high constitutive expression is reported in muscle cells (heart and skeleton) and high levels were also found in different types of cancer (myeloid or lymphoid leukemia, glioblastoma, neuroblastoma and prostate, ovarian, breast, pancreatic carcinomas). [109, 112] Under physiological conditions, it is localized in the cytoplasm, mainly concentrated in the rough endoplasmic reticulum, instead, following acute stress or viral infection, the subcellular distribution of BAG3 varies: it could translocate into the nucleus or be localized in perinuclear aggregates/bodies inclusion. [113] Recently, it has been shown that BAG3 protein interacts with HSF1 through its BAG domain, both under normal and stress conditions, determining the co-translocation of BAG3 into the nucleus. [114]

From a structural point of view, BAG3 is characterized by a multi-modular domain structure that allows a wide range of protein–protein interactions. In detail, the functional regions are a WW domain at the N terminus (21-55 aa), two conserved IPV (isoleucine-proline-valine) motifs (87-101 and 200-213 aa), a PxxP motif (302-412 aa), and highly conserved BAG domain (420-499 aa) (**Figure 11**). [115]

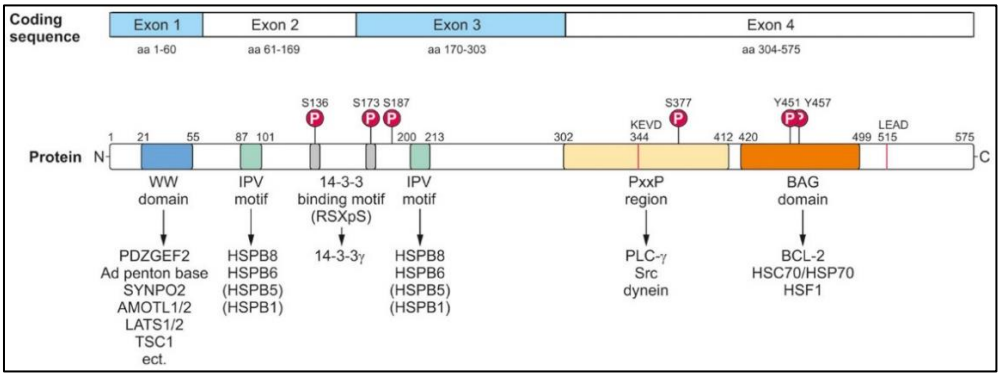

Figure 11: BAG3 modular protein structure.

The BAG domain, in the C-terminal region, can bind the ATPase domain of the Hsc/Hsp70 chaperone, but also, as recently found, HSF1. The WW domain binds to proline-rich ligands, such as guanine nucleotide exchange factor 2 containing a PDZ domain (PDZGEF2); the PDZ domain is a common structural domain of 80–90 amino acids found in different signaling proteins. The WW domain plays a key role in chaperone-assisted selective autophagy. [116-118] Two conserved IPV motifs were identified at N-terminus and in the middle of BAG3 and mediate its binding to the small heat shock proteins HspB8 (Hsp22), HspB6 (Hsp20) and, to some extent, also to HspB5 (α-crystallin B) and HspB1 (Hsp7). The proline-rich PxxP region mediates the binding to phospholipase Cγ. [118] Finally, there are also a cleavage caspase sites both, within the PxxP region, (^{344}KED) and the C-terminus. [119] Besides these highly structured domains and motifs, BAG3 protein exhibits several disordered regions that are not only "linker" segments between structured protein domains, but are also functional sites able to mediate protein–protein interactions and subjected to post-translational modifications. [120] Phosphorylation is one of the most important post-translational modifications of BAG3 that regulates its functional activity. [121] Moreover, BAG3 is subjected also to ubiquitination by the ubiquitin ligase STUB1; BAG3 may be degraded by the proteasome during the formation of the autophagosome in myocytes. [122]

The analysis of BAG3 interactome allowed to identify 382 proteins interacting with BAG3, including proteases, transferases, transcription factors, and signaling molecules, hence, given the dense network of partners interaction, BAG3 occupies a central role in several important biological processes such as apoptosis, cell proliferation, development, cytoskeletal rearrangement, cell adhesion, cell motility, viral replication, and selective macro-autophagy. It is not surprising that BAG3 dysfunction or dysregulation can have devastating effects on cells and tissues. To better understand the importance of BAG3 in physiological and pathological conditions is useful to discuss some functional aspects in more detail.

2.2.2 BAG3 pathways

BAG3 appears to influence cell survival activating multiple pathways. [115, 123-125] In particular, the formation of BAG3-Hsp70 complex regulates the turnover of several proteins through the two main protein degradation pathways: proteasomal degradation and macroautophagy. The BAG3 ability in controlling apoptosis and autophagy suggests a key role of the protein in the crosstalk between these two pathways, although the exact mechanism remains still unclear (**Figure 12**). However, its involvement in controlling the cellular levels of key proteins can explain its ability to modulate a wide range of physiological processes including, besides apoptosis, cellular stress response, development, and cytoskeletal organization.

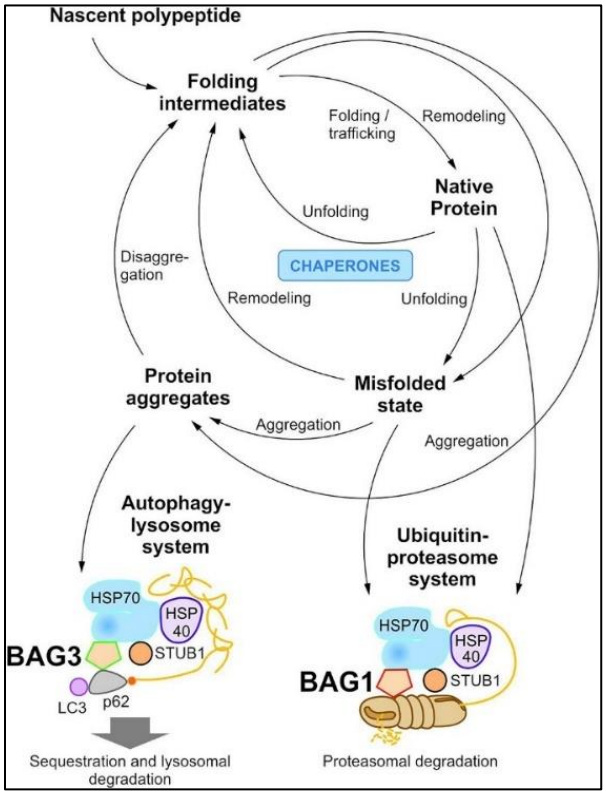

Figure 12: The cellular proteostasis network and its degradation systems. In cellular protein quality control, molecular chaperone systems function in concert with protein transport and degradation systems to ensure cellular proteostasis. In addition to the ubiquitin-proteasome system, the autophagy-lysosome system mediates the disposal of degradation-prone substrates.

BAG3 can interfere at several levels in the apoptotic cascade, representing a key factor in contrasting death signals. A possible mechanism for BAG3 anti-apoptotic activity involves its role, as co-chaperone, in proteins delivery to the proteasome by competing with BAG1. [100, 126, 127] Several evidences showed that BAG3 has a stabilizing effect on the pro-survival members of Bcl-2 family (Bcl-2, Bcl-xL, and Mcl-1) because it interferes with their Hsp70-mediated delivery to the proteasomal pathway, thereby counteracting the activity of the proapoptotic Bcl-2 family members (BH3-only and BAX like proteins), whose effects finally culminate in the caspases activation, the main effectors of the apoptotic process. In osteosarcoma

and melanoma cells, BAG3 prevents the IKK-γ proteasome delivery and this results in the activation of the antiapoptotic NF-κB pathway (**Figure 12**). [125,128]

BAG3 protein also mediates a selective macroautophagy pathway, indeed, through its PxxP domain, associates with dynein, exploiting the microtubule-based retrograde transport to the aggresome, an accumulation of misfolded proteins. This mechanism is recognized as a cytoprotective response providing to the sequester of potentially toxic misfolded proteins and to facilitate their clearance by autophagy; the fusion of the aggresome with the lysosomes leads to the degradation of the enclosed material (**Figure 13**). [129]

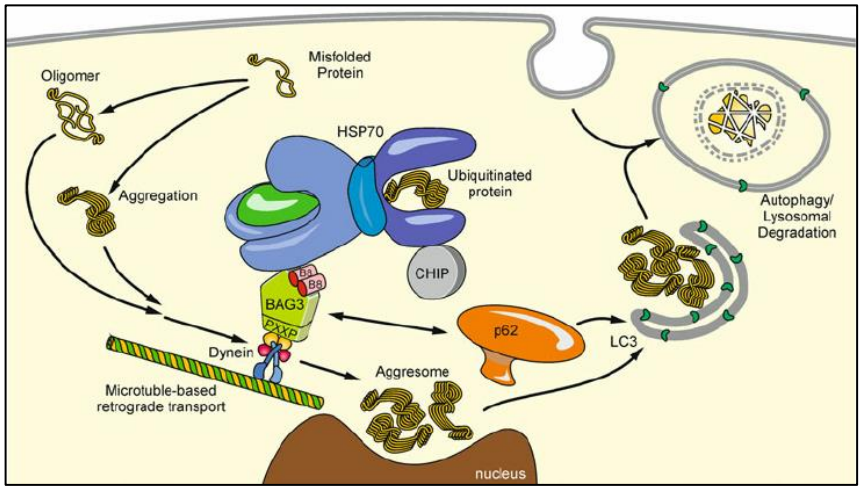

Figure 13: Aggresome formation and induction of BAG3-mediated selective macroautophagy.

During cellular aging, as well as under acute oxidative or proteasomal stress conditions, BAG1 and BAG3 expression levels are reciprocally regulated, indicating an adaptive response of the chaperone system to a changing cellular environment. [113] Under physiological conditions the protein turnover is mainly regulated by BAG1-dependent and Hsp70-mediated proteasomal degradation of polyUb proteins, while, in pathophysiological conditions, there is an increasing demand for protein degradation and BAG3-mediated selective macroautophagy is turned on. [130] This means that the BAG1-BAG3 expression is followed by a

functional switch from BAG1-mediated proteasomal to BAG3-mediated autophagic activity (**Figure 14**). [113]

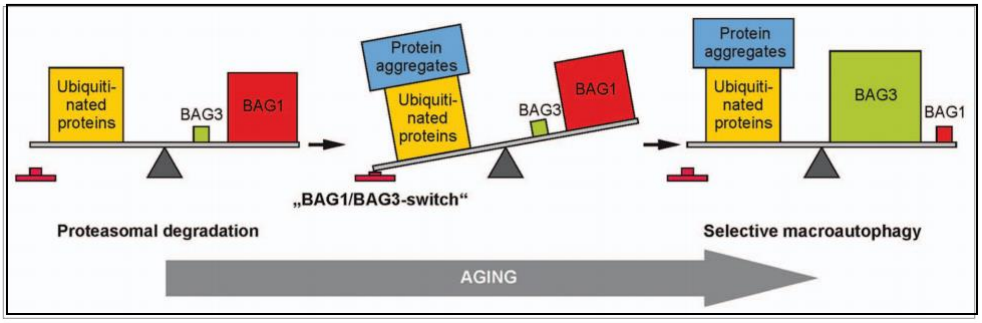

Figure 14: The shift from BAG1 to BAG3 to maintain intracellular proteostasis under enhanced protein stress.

Basing on all these considerations that highlight the key role of BAG3 in ensuring cellular proteostasis and protection, it can be well understood why an impaired BAG3 expression/activity can have a great effect in cancer genesis and progression. Furthermore, interestingly, its role in contrasting misfolded protein aggregations makes it a valuable target also in neurodegenerative disease and in aging related disorders. [131]

2.2.3 BAG3 in cancer

As previously discussed, owing to its multiple interactions with key cellular proteins, BAG3 is emerged as an important survival factor for cancer cells. Accordingly, BAG3 is often found overexpressed in several cancers where it is correlated with a poor prognosis (**Table 3**). Recent evidences highlight that the co-chaperone drives several hallmarks of cancer like cell adhesion, metastasis, angiogenesis, and apoptosis inhibition, through different mechanisms. Furthermore, BAG3 has been found to regulate the nucleocytoplasmic shuttling of HSF1, interfering in the cellular response to different types of stress and in proteomic homeostatic changes in cancer and other pathologies. [132] BAG3 also

promotes cancer invasiveness through direct or indirect effects on proteins involved in adhesion or actin-cytoskeleton dynamics (FAK, Rac1, PDZGEF2, E/N-cadherin, vimentin), or in the regulation of the cellular capacity to degrade components of the extracellular matrix, through the increased expression of metalloproteinases. [117, 133-135]

Altogether these results consolidate the eminent role played by BAG3 in tumorigenesis and provide a new attractive target for cancer therapy (**Table 3**).

Tumor	%positivity	Poor prognosis	Resistance to treatment	References
Thyroid carcinomas	0.96%	ND	ND	[136]
Prostate carcinomas	ND	ND	ND	[137]
Astrocytomas	20-50%	ND	ND	[128]
Melanomas	67-70%	YES	ND	[138]
Colorectal carcinomas	ND	YES	ND	[139]
Ovarian carcinomas	ND	YES	ND	[140]
Lung cancer	62-100%	ND	ND	[141]
Liver cancer	1	YES	YES	[135]
Breast cancer	ND	ND	ND	[142]
Endometrial cancer	1	ND	ND	[143]
Pancreatic ductal carcinoma	1	YES	ND	[144]

Table 3: Intracellular BAG3 in human tumors.

2.3 BAG3 inhibitors

As stated before, one of the main mechanisms related to the anti-apoptotic activity of BAG3 is the interaction, via its BAG domain, with the Hsp70 chaperone. Hsp70 collaborates with several co-chaperones, however, its interaction with BAG3 is fundamental in cancer progression. Many studies have shown the cytoprotective effect of the Hsp70-BAG3 complex, consequently, the block of this interaction, through mutations or *bag3* gene knockdown, produces an anti-proliferative effect in tumor cells, paving the way for a non-canonical way of interrupting the pathways mediated by this complex. These considerations have prompted the scientific community to search for an allosteric inhibitor able to weak the Hsp70-BAG3 interaction. It is well known that the Hsp70-BAG3 interaction is significantly weakened (13fold) by the presence of ADP, suggesting that the ADP-bound state stabilization of Hsp70 may represent a way of blocking this tight contact. Using this approach, Li et al. identified **JG-98** and **YM-01**, two potential allosteric inhibitors of Hsp70 (**Figure 15**). [145]

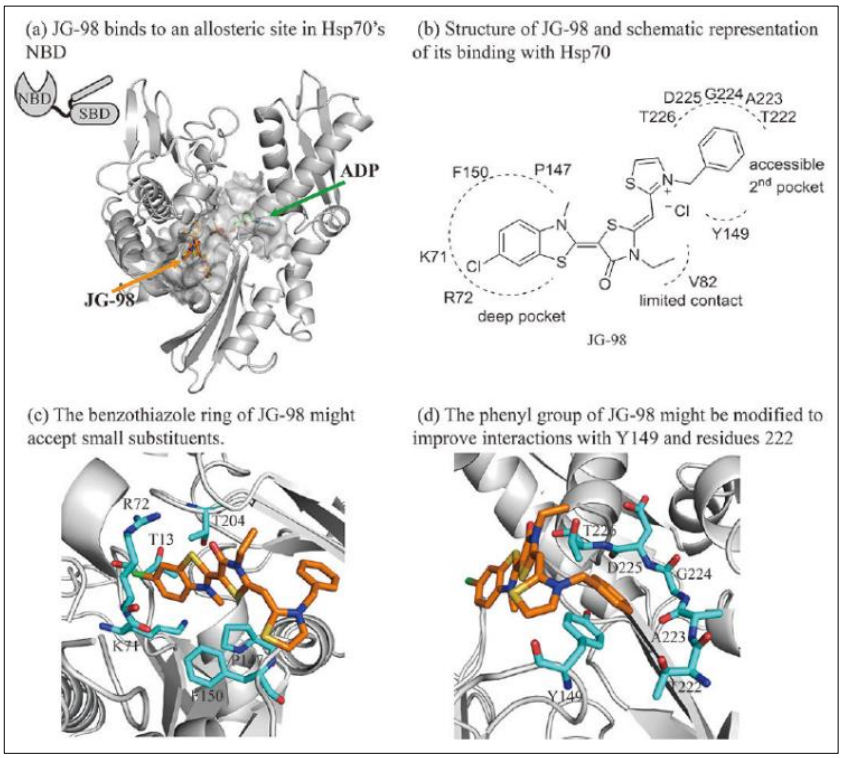

Figure 15: **a) JG-98** is predicted to enhance turnover of cancer signaling proteins by blocking BAG3 binding to HSP70; **b-d)** it binds an allosteric pocket in the NBD of Hsp70 that doesn't overlap with the nucleotide-binding cleft, the BAG3-interaction motif, or other PPI regions.

YM-01 and **JG-98** bind Hsp70 and stabilize the ADP-bound form, therefore it has been hypothesized that these molecules could destabilize the Hsp70-BAG3 interaction. ELISA experiments have shown that **JG-98** bound Hsp70 60-times tighter than **YM-01**, and the biological assays on it showed that the molecule possesses a relevant antitumor activity. This result suggested that the Hsp70-BAG3 interaction could be a promising target for further exploration and that **JG-98** could represent a starting point in this strategy. [145]

Despite all the efforts made in this research area, the development of strategies capable of selectively inhibiting the Hsp70 pathological role, without interfering with its physiological role proved to be quite challenging. One alternative way to block the Hsp70 activity can be represented by directly targeting BAG3 protein which, as previously discussed, represents itself an attractive strategy for cancer

therapy. Basing on these considerations, in 2017, our research group, succeeded to identify, using a multidisciplinary approach, a 2,4-thiazolidinedione based molecule, **LK1**, as a promising chemical platform able to selectively bind and inhibit Hsp70-BAG3 protein-protein interaction. These outcomes were extremely relevant because they provided to disclose the first reported BAG3 modulator useful for the development of a novel class of therapeutic agents (**Figure 16 a**,**b**). [146]

A

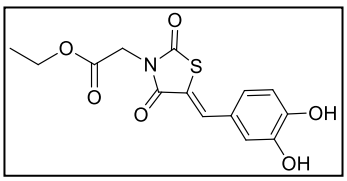

B

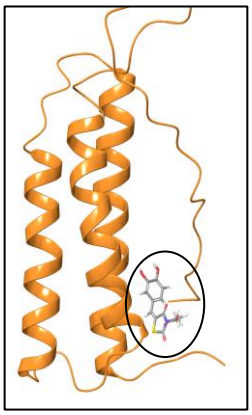

Figure 16: a) (Z)-ethyl 2-(5-(3,4-dihydroxybenzylidene)-2,4-dioxothiazolidin-3-yl)acetate (**LK1)**; **b)** Putative BAG3-BD binding site of **LK1** and its interactions.

CHAPTER 3

Microsomal Prostaglandin E Synthase-1 (mPGES-1)

CHAPTER 3

Microsomal Prostaglandin E Synthase-1 (mPGES-1)

3.1 Introduction

Prostaglandins (PGs) represent an important class of potent biological lipid mediators that are ubiquitously found in animal tissues and are associated with physiological and pathological processes. [147, 148] The most abundant PG in humans is prostaglandin E2 (PGE_2), a key mediator of inflammation, pain, and fever, also involved in the protection of the gastrointestinal mucosa, blood pressure regulation, and ovulation. [149, 150] PGE_2 is secreted from cells and carries out its actions through one or more specific G-protein coupled receptors, EP1-EP4. [151]

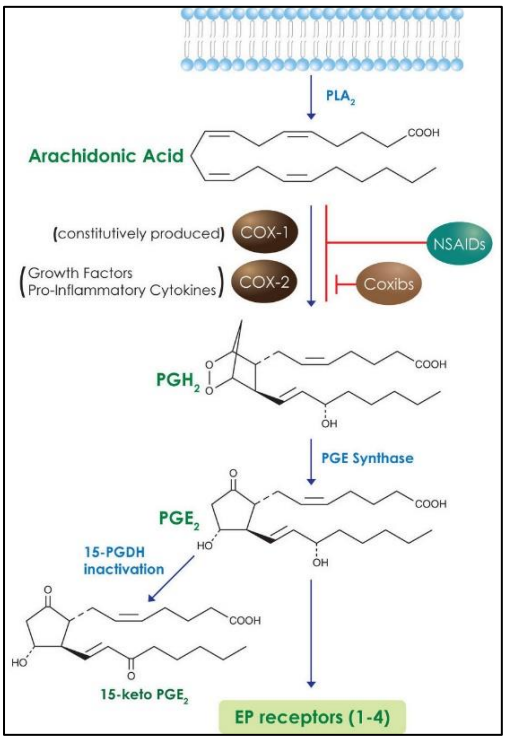

Figure 17: Phospholipases A_2 (PLA_2) release polyunsaturated fatty acids, including arachidonic acid (AA), from membrane lipid. Oxygenation of these fatty acids by cyclooxygenases (COX) and PGE synthase (mPGES-1) leads to one of the final products, PGE_2, that carries out its action through EP receptors.

The PGE_2 biosynthesis starts with the release of arachidonic acid (AA) from the phospholipid membrane through the action of phospholipases A_2 (PLA_2) and phospholipase C (PLC). [152] PLA_2 hydrolyzes phosphatidylcholine and phosphatidylethanolamine, the main source of AA, while PLC hydrolyzes phosphatidylinositol and phosphatidylinositol phosphate to form diacylglycerol (DAG), which, in turn, is converted by DAG lipase into 2-arachidonoyl glycerol (2-AG), an important precursor of AA. [153] The oxygenation of AA is performed by cyclooxygenases 1 and 2 (COX-1/COX-2): COX-1 is constitutively expressed in most tissues and contributes to the homeostatic PGE_2 production, while COX-2 is induced following pro-inflammatory stimuli and is essential for PGE_2 production in inflammatory processes. The COXs action produces the prostaglandin G_2 (PGG_2), which is subsequently reduced to prostaglandin H_2 (PGH_2). PGH_2 is then converted by different synthases into a variety of prostanoids ($PGF_{2\alpha}$, PGD_2, PGI_2), including PGE_2 and thromboxane A_2 (TxA_2) (**Figure 17**). In particular, the conversion of PGH_2 into PGE_2 is due to the action of PGE_2 synthases (PGES). [154]

Currently, three PGES isoenzymes have been identified: the cytosolic PGES (cPGES) and two microsomal PGESs, mPGES-1 and mPGES-2. cPGES is constitutively expressed in most tissues and functionally coupled to COX-1. It is considered the main responsible for homeostatic PGE_2 production and requires GSH as an essential cofactor. cPGES can be induced under special conditions (LPS-treatment enhanced its expression in the rat brains) and the phosphorylation at Ser113 and Ser118 by casein kinase 2 (CK2) protein increases its activity. [155, 156] mPGES-1, which will be discussed in detail later, is similarly constitutively expressed, but at low levels, in some organs; it is up-regulated in inflammatory tissues and overexpressed in tumors. [157] Finally, mPGES-2 can convert PGH_2 derived from both COX-1 and COX-2 in PGE_2. [158] Unlike mPGES-1 and cPGES, mPGES-2 does not require GSH as a cofactor. [159] It is integrated into the Golgi apparatus, through its N-terminal hydrophobic domain, and the proteolytic cleavage of this domain releases the active enzyme into the cytosol. [156] mPGES-2 is highly

expressed in the brain, heart, skeletal muscle, kidney, liver, and less in other tissues. [159]

These three terminal enzymes participate in the production of prostaglandin PGE_2, whose pleiotropic functions are mediated by EP1-EP4 receptors, each of them owns different homeostatic and pathophysiological properties. During the initial phase of the inflammatory response, PGE_2 and related prostanoids, such as PGI_2, act as vasodilators to facilitate the tissue influx of neutrophils, macrophages, and mast cells from the bloodstream, leading to swelling and edema of the infection or the injury site. [160] PGE_2 possesses the ability to stimulate the eicosanoid class switch, indeed, it blocks the biosynthesis and the release of pro-inflammatory mediators, such as TNFα, IL-1β, IL-8 during the terminal phase of inflammation, and stimulates the formation of IL-10, lipoxins, resolvins, and protectins which actively antagonize inflammation. [161, 162] PGE_2, furthermore, stimulates the sensory nerves to increase the pain response, acts on neurons to promote pyrogenic effects, and activates a subset of T helper cells, which are characterized by the production of interleukin 17 (IL-17), important in the recruitment of monocytes and neutrophils to the site of inflammation.

3.2 mPGES-1

As already stated, along the arachidonic acid cascade, mPGES-1 is the terminal enzyme responsible for the conversion of PGH_2 into PGE_2. It is a member of the MAPEG family (Membrane-Associated Proteins in Eicosanoid and Glutathione metabolism), and it is well established to play a key role in inflammation and multiple diseases with an inflammatory component, such as rheumatoid arthritis, atherosclerosis, stroke, multiple sclerosis, Alzheimer's, and cancer. [163,164] In this respect, most studies claim that mPGES-1 supports tumorigenesis by promoting cancer cell proliferation, angiogenesis, and metastasis. [165]

From a structural point of view mPGES-1 is a transmembrane homotrimer (16kDa) whose monomers are made up of 152 amino acid residues. The single monomer is characterized by four transmembrane helices. [166]

MPGES-1 shows significant homology with other MAPEG superfamily proteins, including microsomal glutathione-S-transferase-1-like-1 (MGST1-L1), MGST-1, MGST-2, MGST-3, 5-lipoxygenase-activating protein (FLAP), and leukotriene C4 synthase (LTC4S). [166] A unique feature among the MAPEG family members is a small cytosolic domain inserted between the transmembrane helices (TH) TH1 and TH2. MPGES-1 is the first PGES isoform identified and cloned by Jakobsson et al. in 1999 as an inducible and glutathione (GSH) dependent enzyme. [167] A clearer enzyme topology has been defined thanks to the growing amount of structural information obtained by the increasingly resolved enzyme crystal structures published over the last ten years. The first low-resolution structure was reported by Jegerschöld in 2008 and it refers to the inactive closed conformation of the enzyme. [166] Later on, in 2013, Sjögren reported the first high-resolution X-ray structure of human mPGES-1 in the active conformation. [168] Finally, between 2014 and 2015, the high-resolution X-ray structures of human mPGES-1 in complex with new and potent enzyme inhibitors were published (e.g. PDB code: 4BPM, 4YL1, 5BQH, and 5BQI). [169, 170]

The crystallographic analysis revealed that the secondary structure of this protein is predominantly composed of alpha-helix regions (74%). The trimer inner core consists of three TH2 domains that shrink towards the luminal side, via the side chains of four aromatic amino acids (Tyr80, Phe84, Phe87, and Phe91) (**Figure 18 a**,**b**). The cytoplasmic side of the core, instead, is completely open, giving the core a funnel shape. The essential mPGES-1 cofactor, GSH, binds with a U-shaped geometry to a site consisting of three distinct regions of two monomers (**Figure 18c**). [166]

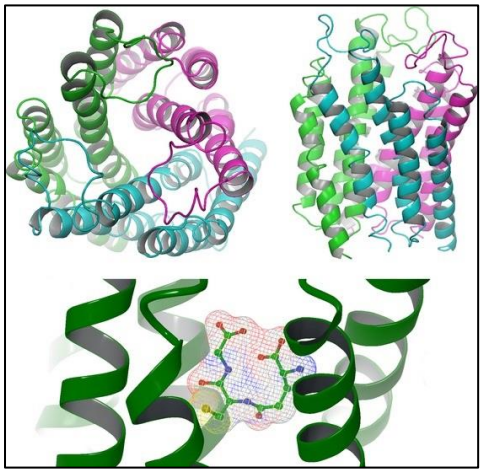

Figure 18: Structures of mPGES-1 trimer: **a)** top view; **b)** side view; **c)** U-shaped geometry of glutathione molecule. Chains of trimer are colored differently.

The three active sites are located in the membrane-spanning region at the interface between the monomers. The analysis proposed five key amino acid residues essential for substrate binding and catalytic functioning: Gln36, Arg110, Thr114, Tyr130, and Gln134. Tyr130 is important for PGH_2 binding and catalytic function, Arg110 and Thr114 are responsible for the interaction with the PGH_2 carboxyl tail, while Gln36 and Gln134 are important for PGH_2 binding affinity. [171] Other five aminoacidic residues (Thr131, Leu135, Ala138 and potentially Arg52 and His53) act as gate keepers and limit the access of inhibitors to the active site. The active sites cavities are separated from the internal core by the side chain of Arg73. A conformational change can create a large continuous pocket with an unknown function. [172]

3.2.1.1 mPGES-1 mechanism

mPGES-1 mechanism of action has been hypothesized based on the 3D structure of its closed form. Most likely, the closed state of the trimer is in rapid equilibrium with its open state, and the equilibrium is shifted in favor of product formation, when the substrate comes close to mPGES-1. [166]

The GSH is enveloped by the rest of the enzyme and protected from unwanted reactions, such as oxidation. Modeling studies suggest that PGH_2 enters the active site, via its peroxofuran core and with the two flexible aliphatic tails that point inside the lipid membrane.

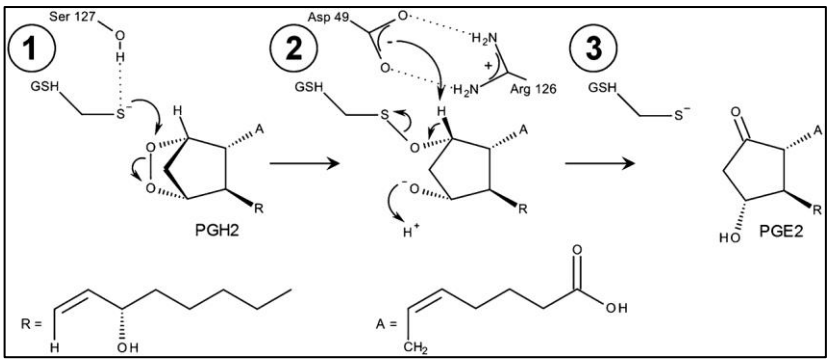

Figure 19: Chemical mechanism for the catalysis of PGH_2 to PGE_2.

Sjögren et al. also proposed a mechanism for the PGH_2 isomerization to PGE_2 mediated by the GSH cofactor. According to this suggested mechanism, Ser127 activates the thiol function of GSH to form a thiolate anion that exerts a nucleophilic attack on the endoperoxide oxygen atom of PGH_2, producing an unstable intermediate. Subsequently, Asp49 mediates the abstraction of the proton at C-9 followed by the cleavage of the S-O bond, which results in the regeneration of GSH and the formation of PGE_2 (**Figure 19**). [168]

Kinetic experiments suggest that potent mPGES-1 inhibitors bind the enzyme active site. Currently, no allosteric inhibitor has been reported, probably owing to the rigid structure of mPGES-1 determined by interhelix hydrogen bonds which prevent the possible conformational changes. [168, 173] All the high-affinity inhibitors are supposed to act or displacing the substrate from the enzyme active-site, or blocking GSH interaction. [174]

3.2.1.2 mPGES-1 pharmacological target

As already reported, COX-1 is constitutively expressed under normal conditions in most cells, especially in the gastric mucosa and kidneys, while COX-2 is inducible under inflammatory conditions. The classical NSAIDs, which inhibit both COX-1 and COX-2, lead to severe side effects, such as gastric irritation, kidney problems, hypertension owing to the massive suppression of PGE_2 which exerts pleiotropic functions included gastric protection. On the other hand, selective inhibition of COX-2 leads to cardiovascular diseases. [175] For this reason, the specific inhibition of mPGES-1, the terminal synthase in PGE_2 biosynthesis, should suppress the synthesis of prostanoids induced by inflammatory stimuli, without affecting PGE_2 constitutively expressed, indicating for mPGES-1 inhibitors fewer side effects and, thus, a better pharmacological profile. Hence, in the last years, mPGES-1 has been the focus of extensive investigations aiming at clarifying its involvement in a range of pathological conditions like inflammatory related disorders. Furthermore, only recently mPGES-1 has been established to be significantly implicated in cancer genesis and progression; accordingly, high levels of the enzyme and its biosynthesized product, PGE_2, have been found in several human cancers, including colon, lung, pancreas, and brain tumors. mPGES-1 overexpression appeared to be strictly correlated to a worse prognosis.[176-178] Often, high levels of mPGES-1 are associated with a concomitant COX-2 overexpression, however, recent studies outlined that the terminal synthase can be induced also apart from COX-2, providing evidence that these enzymes can be independently regulated. These data strongly support the possibility to target mPGES-1 activity in order to obtain the concomitant PGE_2 suppression, avoiding the toxicity associated with COX-2 inhibition.

3.2.1.3 The crosstalk between cancer and inflammation

The close relationship between cancer and inflammation deserves some consideration. Although the correlations between them are not yet fully understood, the crosstalk between cancer progression and inflammatory processes has been known for a long time. [179] The first example of a correlation was reported in the 19th century by the German physicist Rudolf Virchow, who described leukocyte infiltrates in tumors. [180] The presence of leukocytes was initially attributed to immunosurveillance and anti-tumor response, but now it is well known that they can act both as tumor-suppressors and tumor-promoters. [181] Relevant aspects of cancer-associated inflammation include the infiltration of white blood cells (mainly tumor-associated macrophages), the presence of inflammatory mediators (cytokines and chemokines), tissue remodeling and angiogenesis. [182] Both intrinsic and extrinsic inflammatory pathways have been linked to cancer. [183] The intrinsic pathway is activated by genetic events, in particular by the activation of oncogenes, resulting in cell transformation which contributes to the creation of an inflammatory environment. [184] In the extrinsic pathway, the conditions of chronic inflammation or infections increase the risk of developing cancer (e.g. prostatitis for prostate cancer, papillomavirus for cervical cancer). [185] The two pathways converge in the activation of transcription factors, such as NF-κB and STAT3, which are the key mediators of cancer development and progression (**Figure 20**). [186, 187]

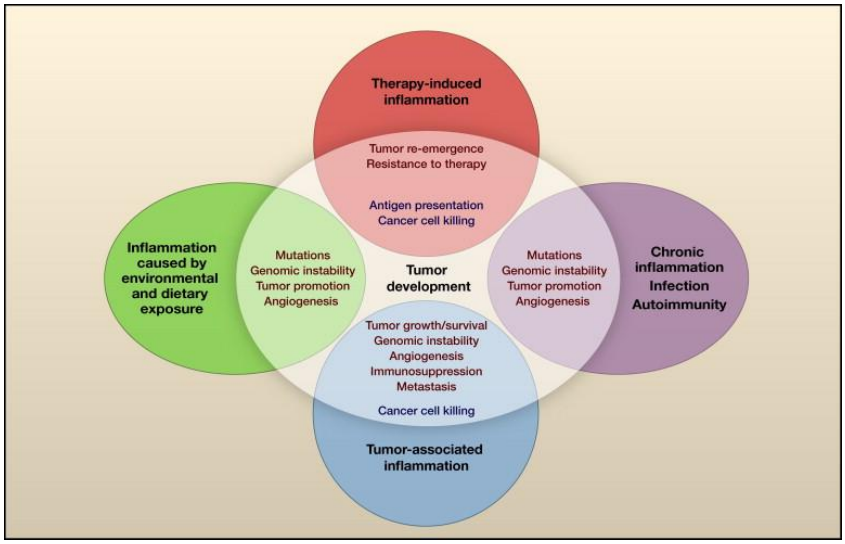

Figure 20: Chronic inflammation associated with infections or autoimmune disease precedes tumor development and can contribute to it through induction of oncogenic mutations, genomic instability, early tumor promotion, and enhanced angiogenesis.

Both malignant and premalignant tissues were found in an inflammatory state driven by cells of the immune system which showed a tumor-promoting effect in the inflammatory response. Furthermore, inflammatory mediators contribute to genomic instability and mutations associated with tumors, since many of them act as direct mutagens or deregulators of the DNA repair mechanism and cell cycle checkpoints, providing cancer cells to acquire the ability to proliferate, invade and escape from host defense. [188]

Many of the evidence gathered suggest that improved therapeutic efficacy can be achieved by blocking the two signaling networks. [189] Consequently, targeting inflammatory and neoplastic pathways can be performed at different levels through the modulation of specific proteins involved in the key steps of these processes. In this regard, mPGES-1 is supposed to act at the crossroad of the inflammation and tumorigenesis pathways, deserving thus an eminent consideration as an attractive drug target.

3.2.2 mPGES-1 inhibitors

A significant problem in mPGES-1 targeting is the sequence dissimilarity of the enzyme isoforms in the different species. For example, potent inhibitors against the human enzyme may partially or completely lose potency against the rat isoform, mainly due to the variation of three amino acids located in the transmembrane helix IV, which play a crucial role as gatekeepers for the active site of mPGES-1, regulating the access of a possible inhibitor. In the human enzyme, these residues are rather small (Thr131, Leu135 and Ala138) but in the rat isoform they are bulkier or aromatic (Val131, Phe135 and Phe138), and thereby prevent the access to inhibitors for steric hindrance reasons. Although a large number of potential natural and synthetic mPGES-1 inhibitors are reported in literature (**Figure 21**, **22**), none of them have passed yet all the clinical trials and consequently no drug useful for the treatment of inflammatory and pathological states resulting from the PGE_2-synthase deregulation has been developed.

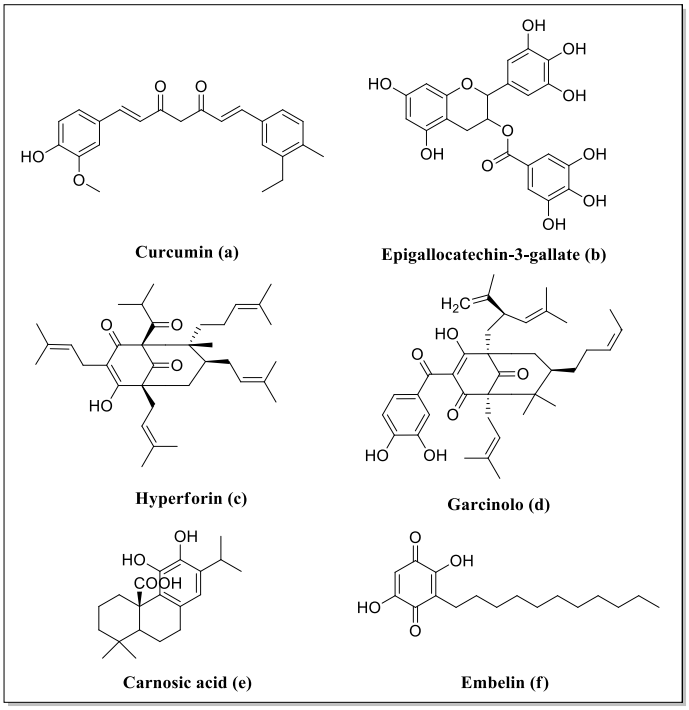

Figure 21: Structures of natural mPGES-1 inhibitors: **a)** curcumin [190]; **b)** epigallocatechin-3-gallate [191]; **c)** hyperforin [192]; **d)** garcinol [193]; **e)** carnosic acid [194]; **f)** embelin [195].

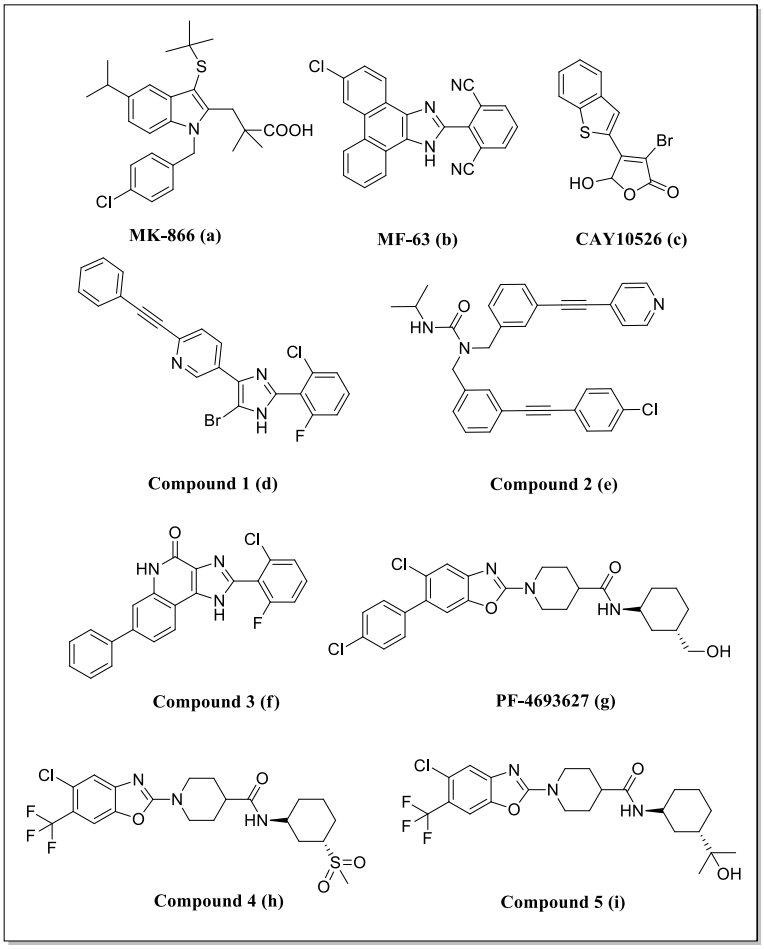

Figure 22: Structure of synthetic mPGES-1 inhibitors: **a)** MK-866 [196]; **b)** MF63 [197, 198]; **c)** CAY10526 [199] ; **d)** compound 1 [200]; **e)** compound 2 [201]; **f)** compound 3 [202]; **g)** PF-4693627 [203]; **h, i**) Compound 4 and 5 [204].

Despite the challenging problems connected with the exploration of this biological target, selective inhibition of mPGES-1 might represent a promising approach for the design of effective anti-inflammatory drugs lacking the severe side effects related to the use of the classic NSAIDs. Hence, the identification of potent and selective mPGES-1 inhibitors with good ADME properties is a goal that must be still achieved.

To date, two compounds entered the clinical trials: **GRC27864** and **LYS3023703** (**Figure 23**).

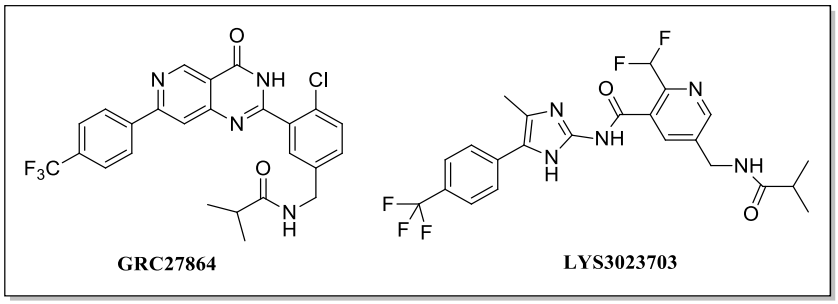

Figure 23: **GRC27864** and **LYS3023703** structures.

GRC27864 presents a pyrimidine scaffold. It inhibits the enzyme with an IC_{50} of 5 nM in the cell-free assay and 376 nM in human whole blood assay; moreover, it was able to interfere with the production of PGE_2 in synovial fibroblasts and chondrocytes deriving from tissues affected by rheumatoid arthritis and osteoarthritis. Other biological assay demonstrated that it is also a potent inhibitor of recombinant guinea pig mPGES-1 enzyme (IC_{50} = 12 nM) and 1000-fold selective over COX-1, COX-2, mPGES-2, cPGES, and the other enzymes of arachidonic acid cascade. It is currently in phase 2 of clinical trials (**Figure 23**). [205] **LY3023703**, the second compound that entered the clinical trials, showed a higher potency in enzyme inhibition than celecoxib. The identified side effects were diarrhea, abdominal pain, and one of the patients reported an increase of the level of aminotransferase, which is index of liver toxicity (**Figure 23**). [206]

Results and discussion

CHAPTER 4

Identification of small molecules as potential modulators of HSF1

CHAPTER 4

Identification of small molecules as potential modulators of HSF1

4.1 Aim of the work

In recent years, the growing amount of information about the structure, regulation, and functions of HSFs has allowed to understand their roles in protein misfolding, metabolism, neurological diseases, and cancer. Despite the steps forward, a systematic view of the entire network of HSF isoforms encoded by the human genome, their complete structures, and how they interact within the family and with other proteins in unique combinations to regulate gene expression, remained to be gained. Furthermore, the HSFs proteins are subjected to a multitude of PTMs but the knowledge of their specific and context-dependent roles in normal or pathological conditions is still limited.

A part of my Ph.D. project was devoted to the identification of potential HSF1 modulators. HSF1 is a promising target for anti-cancer therapy although, for several reasons, it can be considered quite "undruggable". HSF1 functions have not yet been completely clarified and none of the known inhibitors are sufficiently selective. Moreover, the mechanism underlying its regulation in the broad context of unbalanced metabolism, protein misfolding, and cancerous signaling pathways remains to be fully elucidated. All these aspects, together with the still uncertain possible binding pockets for small molecules, make the identification of HSF1 modulators quite difficult. [207]

The workflow followed in the research of potential HSF1 binders was based on an integrated approach including computational studies, identification of the most promising molecules, biophysical assays, and in-cell assays. Starting from the HSF1-DBD crystallographic structure in complex with an HSE (PDB: 5D5U[24]), two types of virtual screening were performed. In the first case, the amino acid residues involved in the interaction between HSF1 and its known inhibitor, **I_{HSF115}**,

both on monomeric and dimeric forms of the protein were considered. In the second case, a small deep pocket, related to DBD-DBD interactions, was considered as possible binding site, using another known HSF1 inhibitor, **KRIBB11**, as reference. These studies led us to identify several molecules potentially able to target the protein.

4.2 Virtual screening – I type

To identify new potential HSF1 inhibitors, we focused our attention on the DNA Binding Domain (DBD) of the protein: a modulator able to bind the DBD would prevent HSF1 activity. Using the crystallographic structure of the complex between the human HSF1-DBD and an HSE (PDB: 5D5U[24]) and performing a molecular docking of the known inhibitor **I_{HSF115}** (see paragraph 1.4.1[80]), two key amino acids potentially important for HSF1 interaction, Lys80 and Asn74, have been identified (**Figure 24**).

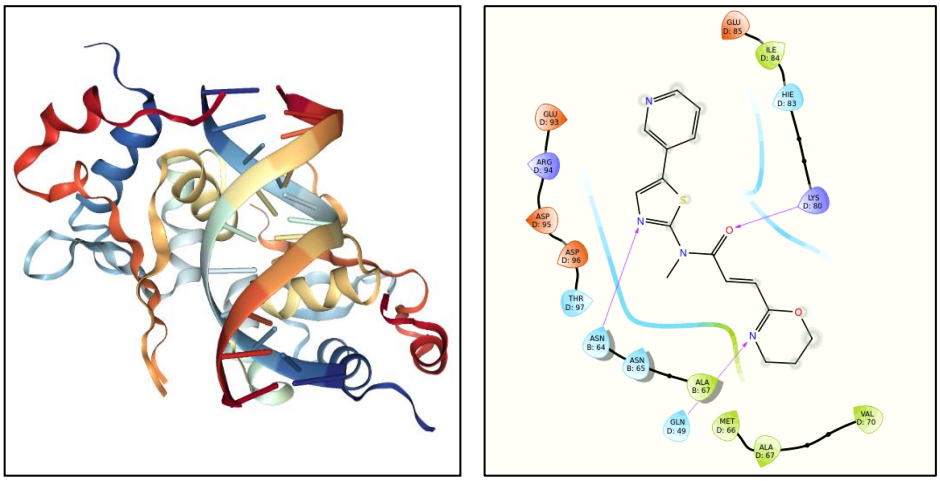

Figure 24: Crystal structure of human HSF1 with HSE DNA (PDB: 5D5U[24]) and molecular docking studies for **I_{HSF115}**. H bond interactions are reported as pink arrows. Hydrophobic residues are depicted in green, positive and negative charge residues in blue and orange respectively, and polar residues in light blue.

The gathered interactions were used as a filter in the virtual screening performed on a large collection of molecules including two commercially available compounds libraries (Otava Chemicals + Sigma Aldrich Market) (Group 1 and 2 respectively; **Figure 25**, **26**), and a wide selection of molecules available in our Organic Chemistry laboratory (Group 3; **Figure 27**). Furthermore, the CombiGlide procedure has been utilized for the *de* novo design of other two compound collections (MO and BR collection) which were similarly subjected to virtual screening. The molecules resulting from this first screening traced the elongated shape of the known inhibitor used as reference, and those with the best docking score values, were selected for the next processing phase in order to verify their ability to bind the target protein.

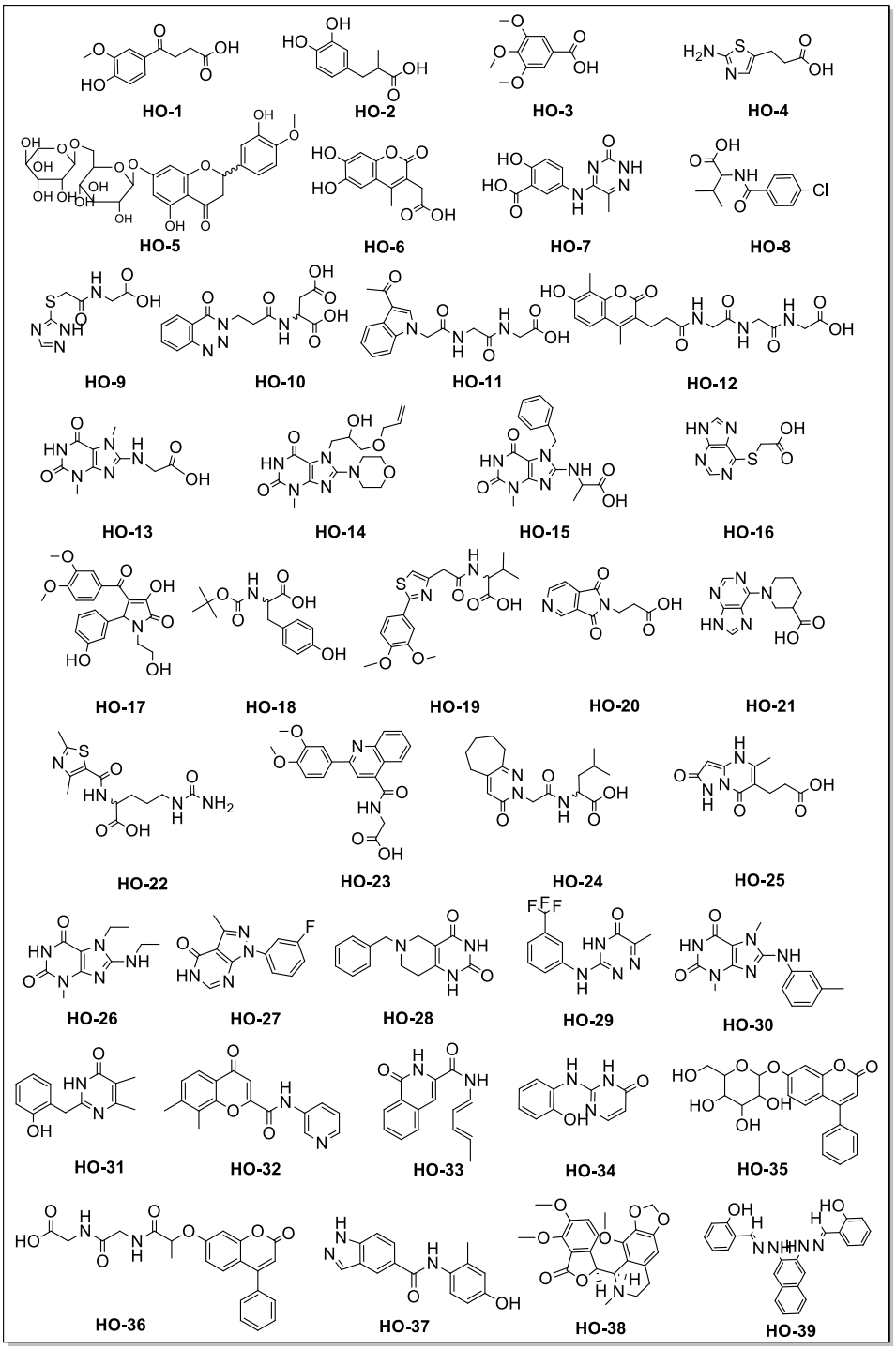

Figure 25: Structures of the Otava commercially available compounds selected by virtual screening (**Group1**).

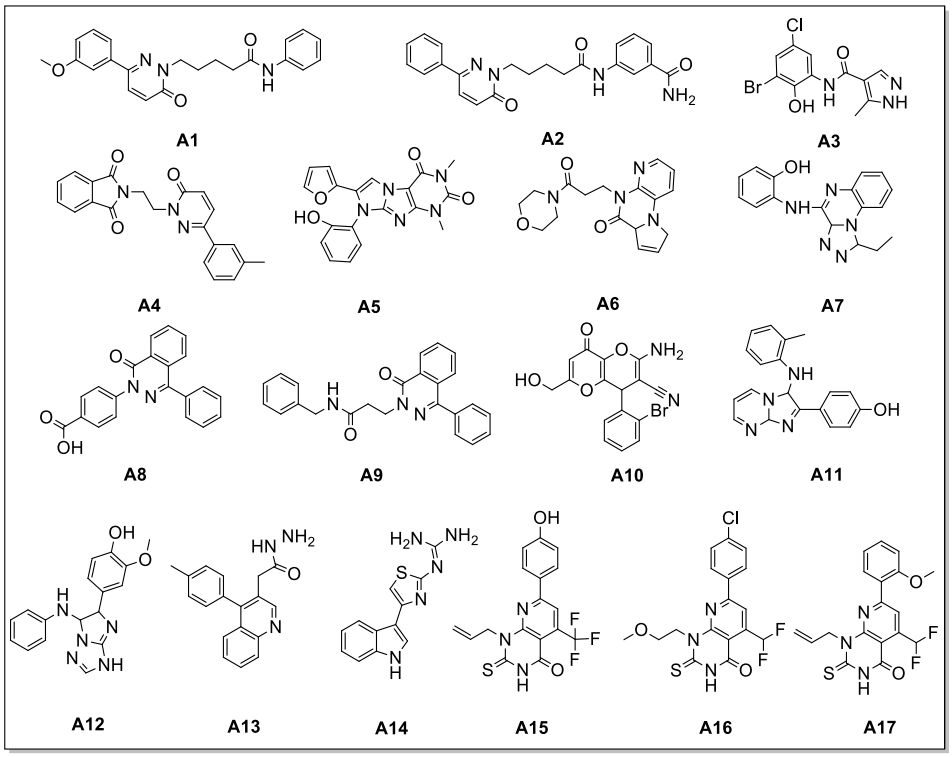

Figure 26: Structures of the Sigma commercially available compounds selected by virtual screening (**Group2**).

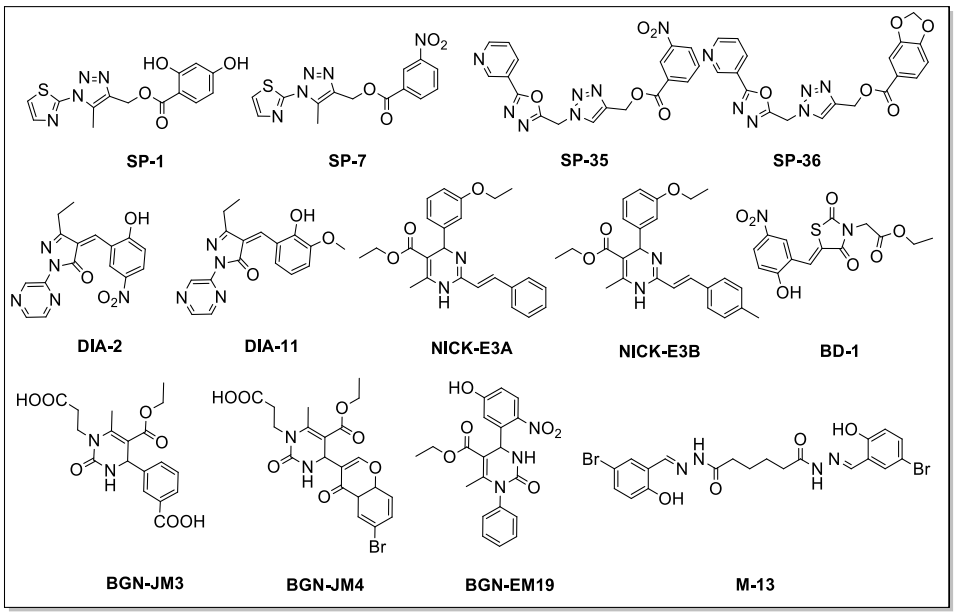

Figure 27: Structures of the molecules available in our laboratory selected by virtual screening (**Group3**).

4.2.1 Synthesis of MO compounds

The first CombliGlide procedure generated the **MO** library (8772 compounds) containing a quinazolinedione scaffold which represents a privileged structure useful for the rapid discovery of leads with enhanced drug-like properties. For the construction of the combinational libraries *in silico*, the CombiGlide software, available in the Schrödinger suite, was used. The combinatorial approach was applied on three quinazolinedione items, **3a-3c**, for the generation of three different libraries endowed with a 5, 6, or 7 carbon chain respectively, in order to trace the elongated shape of the reference molecule. Furthermore, commercially available aromatic amines (2924) were combined with each selected scaffold. Then, LigPrep was applied for the generation of all possible tautomers, stereoisomers, and protonation states at physiological pH, while, QikProp determined pharmacokinetic parameters for each item of the libraries. The molecules showing the highest docking score have been synthesized (**Figure 28**, **29**).

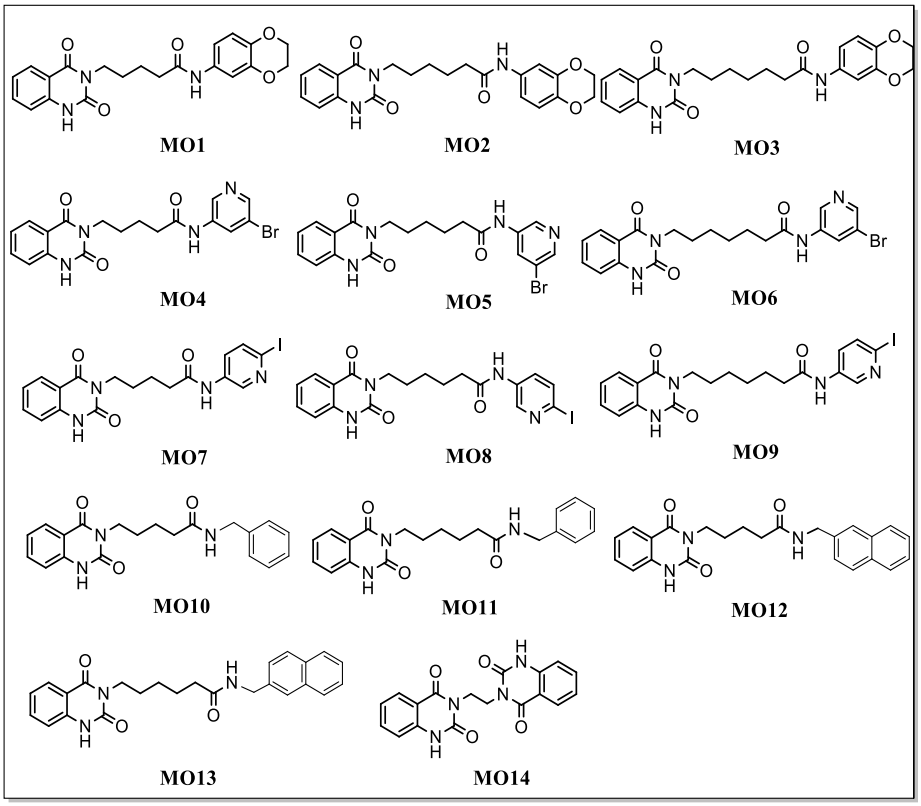

Figure 28: Chemical structures of the compounds selected by virtual screening (**MO** collection).

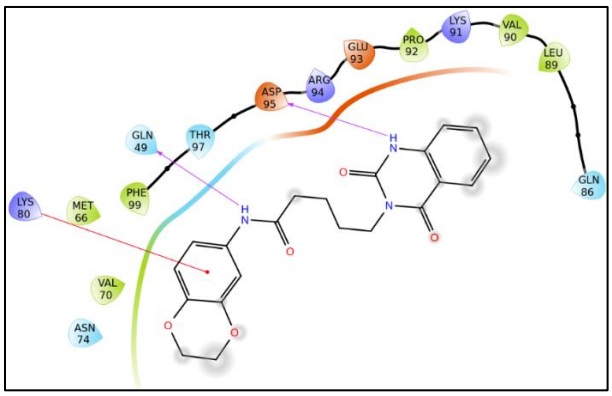

Figure 29: 2D representation of **MO1** in the binding site of the crystal structure of human HSF1-DBD in complex with a HSE (PDB: 5D5U[24]). H bond interactions are reported as pink arrows while π-cation interaction as red line. Hydrophobic residues are depicted in green, positive and negative charge residues in blue and orange respectively, and polar residues in light blue.

The synthesis of the selected compounds, showing as central core a dihydroquinazoline scaffold, started from the isatoic anhydride (1*H*-3,1-benzoxazine-2,4-dione), a suitable synthetic building block. When the isatoic anhydride reacts with primary amines, aliphatic or aromatic, two products can be formed: anthranilamide and *o*-ureidobenzoic acid, depending on the experimental conditions. Following the amine nucleophilic attack at the C-4 of the anhydride, the corresponding carbamic acid is formed and, this latter, rapidly decarboxylates to give the anthranilamide (**Figure 30a**). *O*-ureidobenzoic acid, instead, is the product of an amine attack at C-2 of the anhydride. [208] The formation of this acid is favored in presence of bulkier amines or when the amine is used in large excess; with less bulky amines, the formation of anthranilamide prevails. [209] When the isatoic anhydride reacts with less sterically hindered primary amine, in the presence of a base, *o*-ureidobenzoic acid is mainly formed, while anthranilamide is present only in little amounts. This different outcome depends on the conversion of isatoic anhydride (pKa = 8.6) into its anion which, in turn, rapidly and reversibly converts into the corresponding isocyanate. This latter, reacting with the amine, leads to the formation of *o*-ureidobenzoic acid (**Figure 30b**). [208]

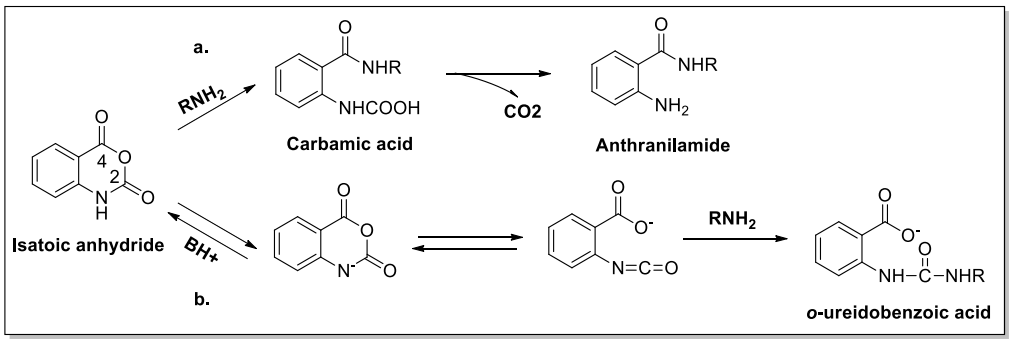

Figure 30: **a)** Anthranilamide formation; **b)** *O*-ureidobenzoic acid formation.

The further cyclization of *o*-ureidobenzoic acid to form the desired dihydroquinazoline scaffold occurs when an excess of amine is used and it is promoted by acid conditions which, activating the carboxylic function, favor the

nucleophilic attack of the amide nitrogen (**Figure 31**). [209] In this way, following the loss of a water molecule, the quinazolinedione is formed.

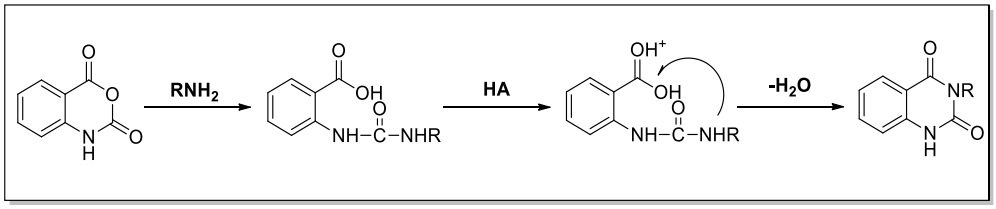

Figure 31: Acid catalyzed cyclization of *o*-ureidobenzoic acid.

In our case, by reacting isatoic anhydride (**1**) with aminopentanoic/esanoic/eptanoic acid (**a-c**) or ethylenediamine (**2**) in presence first of triethylamine and then of formic acid we obtained, respectively, the intermediates **3a-3c** and **4** (**Scheme 1**). Furthermore, by reacting compound **4** with isatoic anhydride, under the same experimental conditions just described, we obtained the final compound **MO14**.

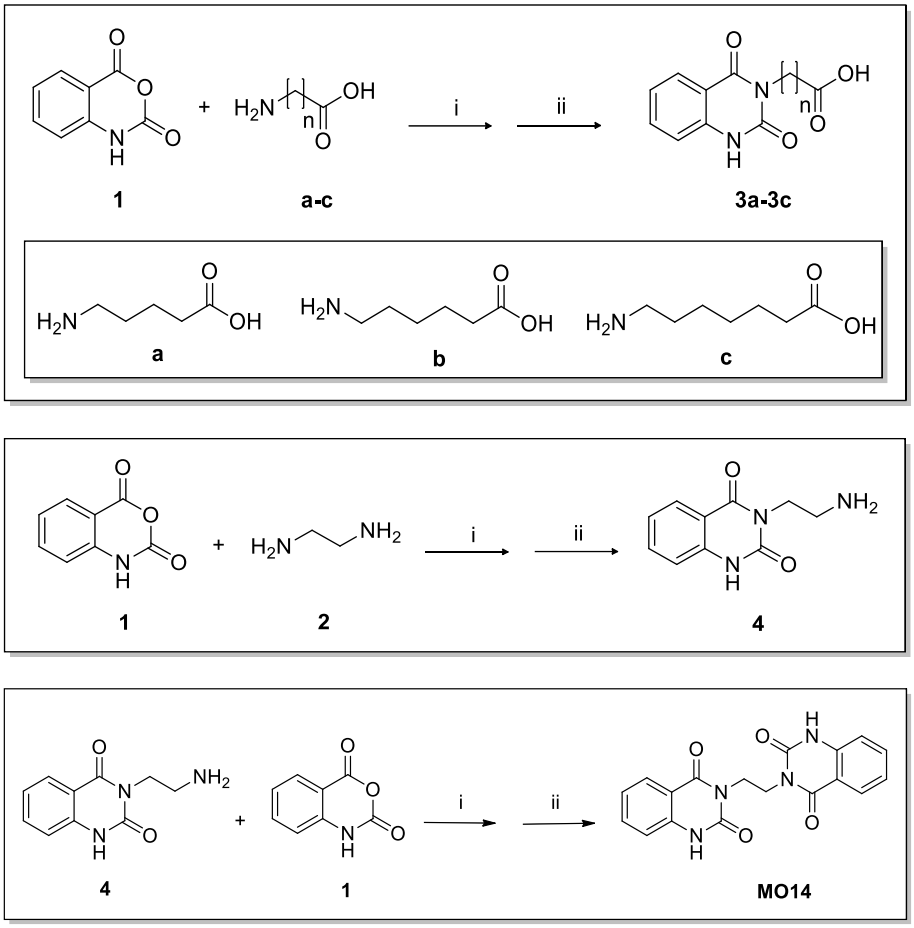

Scheme 1: Synthetic procedure for **3a-3c**, **4** and **MO14** compounds.
Reagents and conditions: i) Et_3N, H_2O, 2h, rt; ii) HCOOH, 7h, reflux.

The second step for the synthesis of MO collection involved the amide bond formation. Among the wide selection of activation methods developed over the years, the diisopropylcarbodiimide (DIC) as condensing agent and 1-hydroxybenzotriazole (HOBt) as additive were chosen. [210, 211] The reaction was carried out in DMF, an aprotic polar solvent, in order to increase the product yield. [212] The detailed synthetic procedure used for obtaining **MO1-MO13** compounds is depicted in **Scheme 2** and the experimental details are reported in the last section.

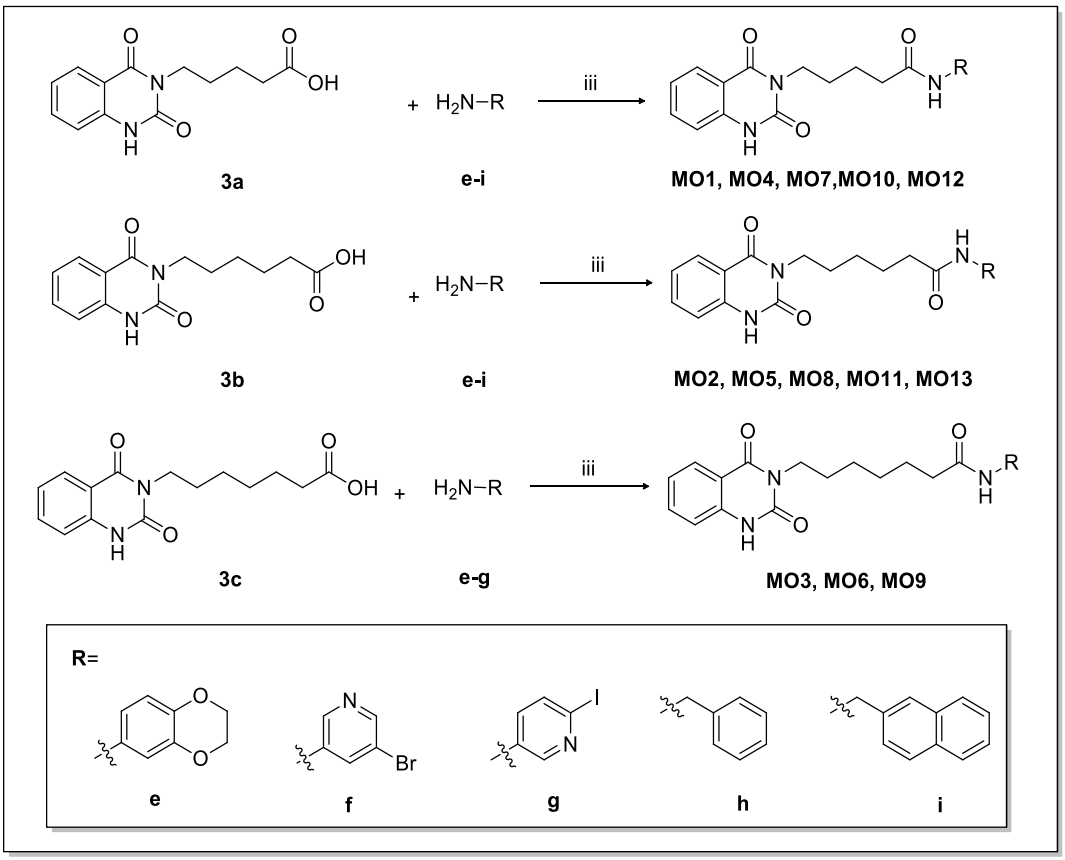

Scheme 2: Synthetic procedure for **MO1-MO13** compounds.

Reagents and conditions: iii) HOBt, DIC, DMF, 16h, rt.

4.2.2 Synthesis of BR compounds

The second library generated by using the CombiGlide procedure was called **BR** (1767 compounds). It was built *in silico* featuring the 5-aminopyrimidine-2,4(1H,3H)-dione (**5**), the 5-methylpyrimidine-2,4(1H,3H)-dione (**6**), and the pyrimidine-2,4(1H,3H)-dione (**7**) chemical cores substituted at N-1 in position (**Scheme 3**). In this way, for each accounted chemical core, 589 compounds (basing on the commercially available boronates and according to the related synthetic routes) were built and submitted to the subsequent molecular modeling

experiments. The most promising compounds were successfully synthesized (**Figure 32, 33)**.

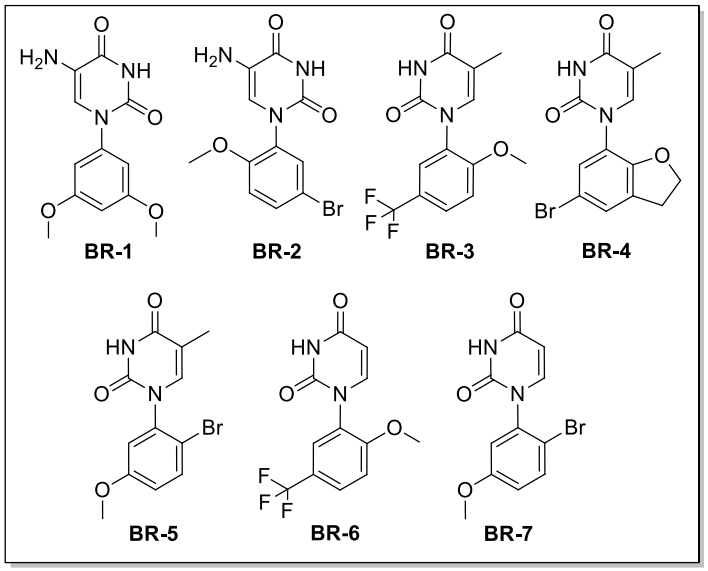

Figure 32: Chemical structures of the **BR** compounds collection selected by virtual screening.

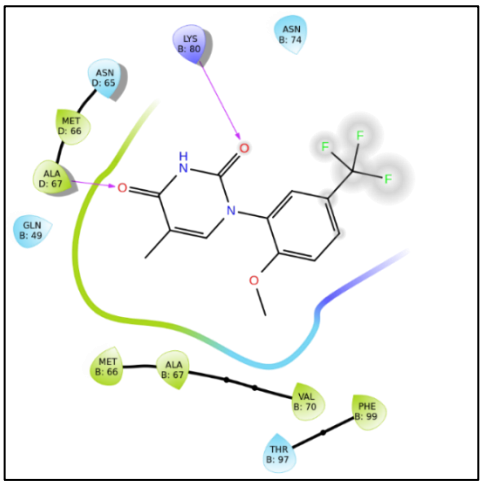

Figure 33: 2D representation of **BR3** in the binding site of the crystal structure of human HSF1-DBD in complex with a HSE (PDB: 5D5U[24]). H bond interactions are reported as pink arrows while π-cation interaction as red line. Hydrophobic residues are depicted in green, positive charge residues in blue, and polar residues in light blue.

The central core of BR molecules is represented by a dihydropyrimidine scaffold, which is, also in this case, considered a "privileged scaffold". As previously reported by Evans, a privileged scaffold is a structure "that is able of providing high-affinity ligands for more than one type of receptor". This statement has led, during the years, to a controversial debate between those researchers, who consider these structures as "promiscuous hitters" able to interfere with a plethora of targets, and therefore poorly suitable in drug discovery, and others, who consider them a promising tool for a quick identification of a hit, whose selectivity can be appropriately tailored in subsequent structural optimization steps. This more positive perspective guided us to select the dihydropyrimidine scaffold to generate a new compounds collection using a direct N-arylation with phenylboronic acids for the C-N selective bond formation. [213]

The possible reaction mechanism is shown in the **Figure 34**. Upon the addition of the pyrimidine scaffold, the cupric acetate dissolves instantly to give a dark blue complex (**1**) as the first step of the reaction. The transmetallation of an arylboronic species with this heterocycle-copper (II) complex (**1**) allows to obtain compound (**2**) which undergoes to reductive elimination to give the N-arylated compounds (**4**). Air oxidation or possible dismutation of copper (II) to copper (III) leads to compound (**3**) which, in the same way incurs a reductive elimination to give the cross-coupled compound (**4**). [214]

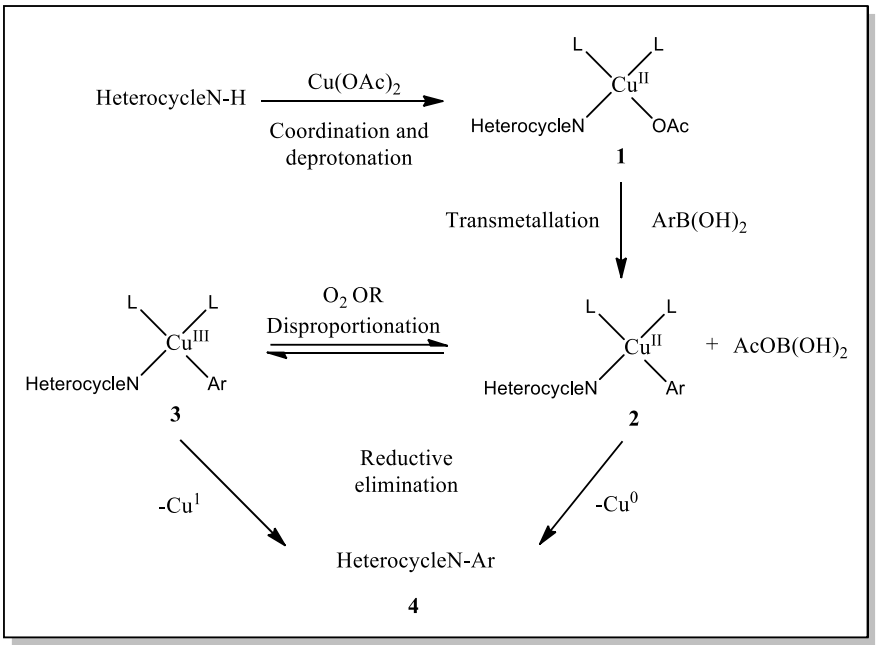

Figure 34: N-arylation mechanism.

In our case, compounds **5-7** were allowed to react with the appropriate boronic acids **(a-e)** in the presence of cupric acetate and TMEDA in a mixture of methanol/water (4:1 ratio) at room temperature overnight, to afford the desired molecules **BR1-BR7** (**Scheme 3**). [215]

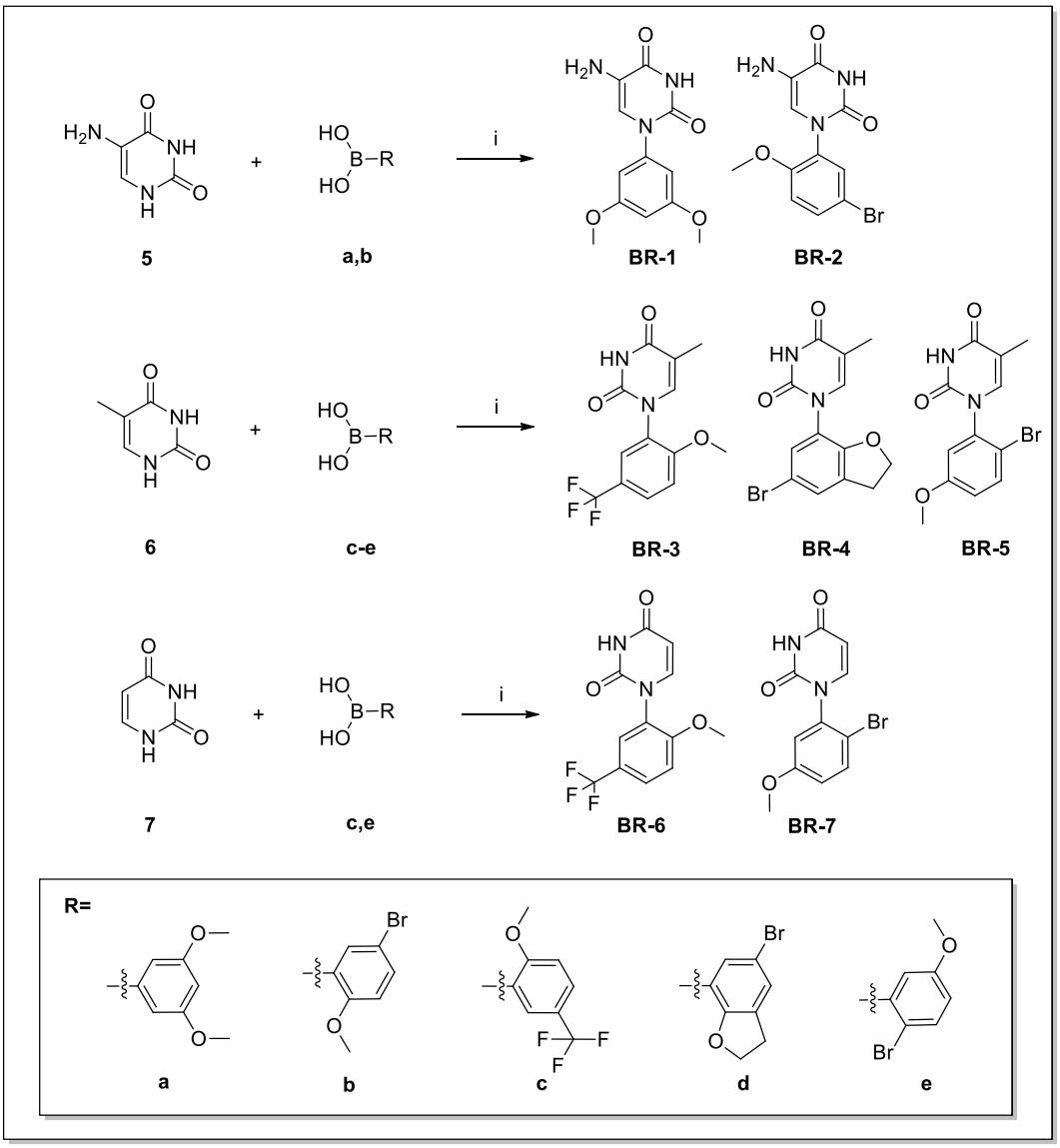

Scheme 3: Synthetic procedure for **BR1**-**BR7** compounds.

Reagents and conditions**:** i) $Cu(OAc)_2 \cdot H_2O$, dry TMEDA, $MeOH/H_2O$, rt overnight.

4.3 Virtual screening – II type

Since there is no co-crystallized ligand-inhibitor structure, to not discard any option, we also considered as a starting point another site for computational studies. According to the structural information recently reported in the literature, the little site at the interface between the DBDs of two HSF1 monomers (Asp48, Gln49, Gly50, Gln51, Lys54, Asp95) was selected for docking studies. [24] Considering that only very few molecules have shown to interact with this biological target, the known direct HSF1 inhibitor, **KRIBB11**[79], was used as a reference compound in this new docking studies. Although the precise mechanism of protein-inhibitor interaction remains still elusive, the possible interactions with the HSF1-DBD were analyzed. **KRIBB11** has been shown to position itself in a good way at the interface between the DBDs (interactions with the Asp48, Gln49, Gly51 on one monomer, and Gly50 and Lys54 on the other monomer) (**Figure 35**).

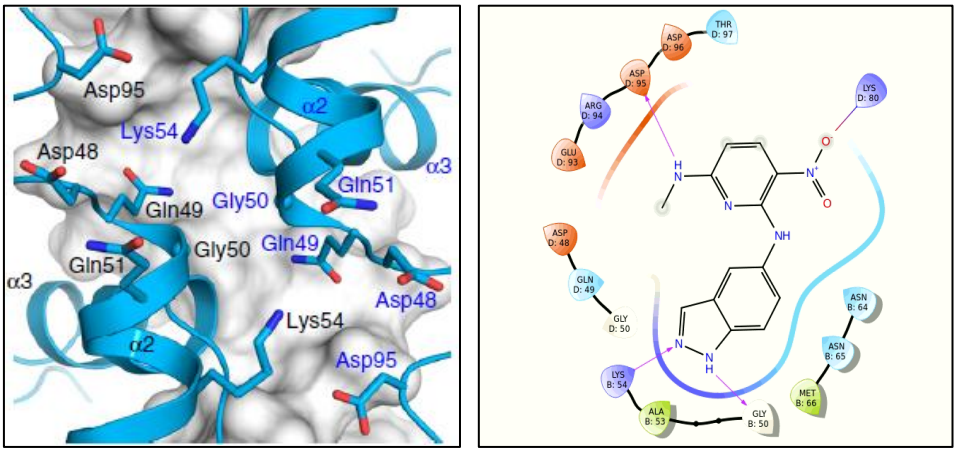

Figure 35: Crystal structure of human HSF1 with HSE DNA (PDB: 5D5U[24]) and molecular docking studies for **KRIBB11**. H bond interactions are reported as pink arrows. Hydrophobic residues are depicted in green, positive and negative charge residues in blue and orange respectively, and polar residues in light blue.

The above-mentioned interactions were used as filter in the third CombiGlide (LAM collection). Unlike the molecules belonging to the previous collections,

LAMs have a more compact and less elongated shape similar to **KRIBB11**, in order to respect the interactions that this latter establishes with the protein counterpart (**paragraph 1.4.1**).

4.3.1 Synthesis of LAM compounds

The third CombiGlide led to the **LAM** collection. For the realization of the library, 4 starting scaffolds were designed, the 7-chloro-2-methyl-4H-pyrimido[1,2-b]pyridazin-4-one (**LAM3**), the 2-(4-bromophenyl)-7-methyl-5H-[1,3,4]thiadiazolo[3,2-a]pyrimidin-5-one (**LAM4**), the 2-bromo-7-(p-tolyl)-5H-[1,3,4]thiadiazolo[3,2-a]pyrimidin-5-one (**14**), and the 2-bromo-7-methyl-5H-[1,3,4]thiadiazolo[3,2-a]pyrimidin-5-one (**16**) (**Scheme 4**). Subsequently, 589 commercially available boronic derivatives were inserted in the reactive positions of the designed cores containing bromine. At the end of all the operations necessary for the generation of the library, 2356 molecules were obtained and then subjected to pharmacokinetic filters: 1798 compounds met the filter criteria and passed to the next phase of molecular docking calculations. The most promising compounds, based on the docking score values and on the interactions with fundamental amino acids, were selected for the next synthetic step (**Figure 36**, **37**).

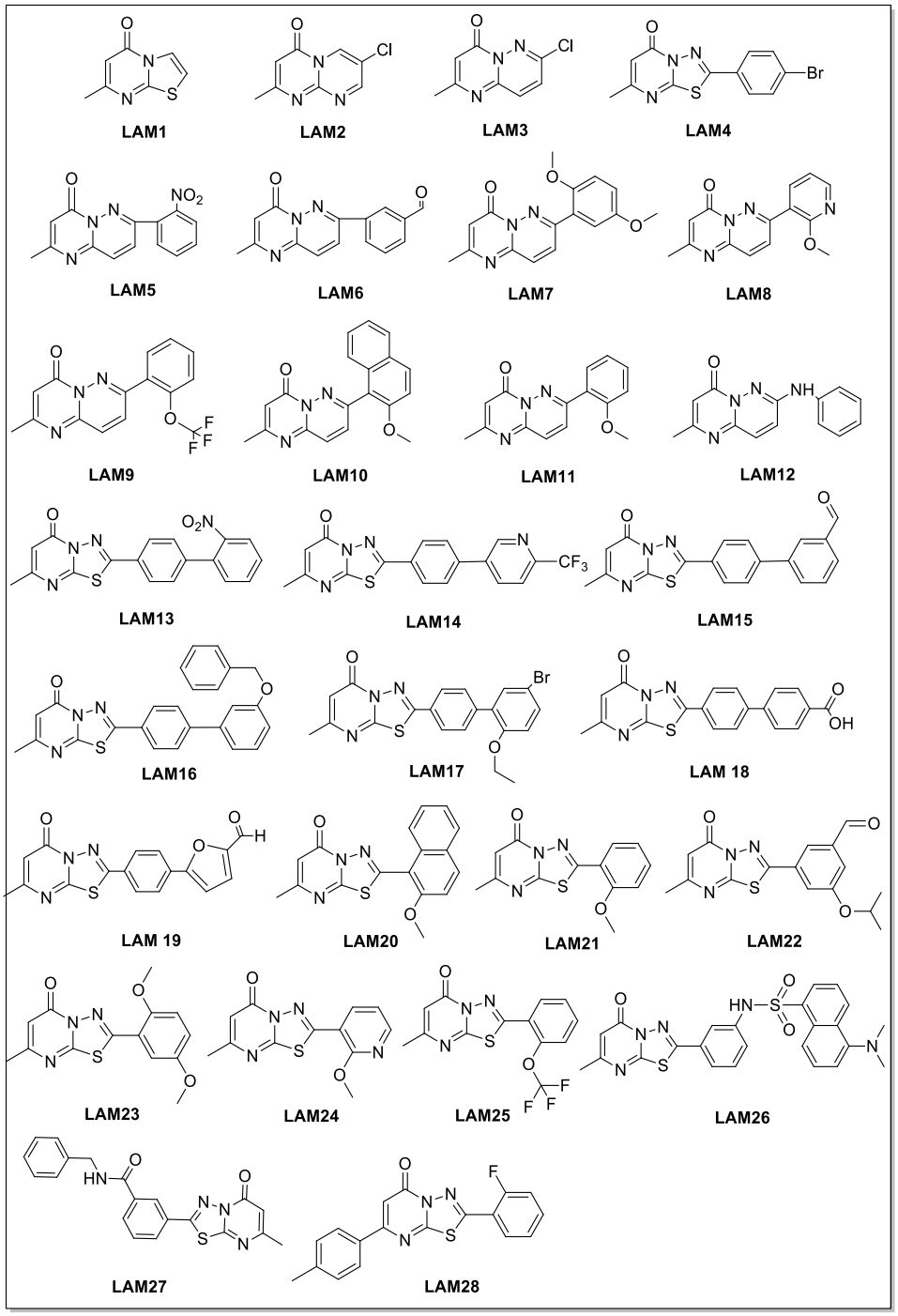

Figure 36: Chemical structures of compounds selected by virtual screening (**LAM** collection).

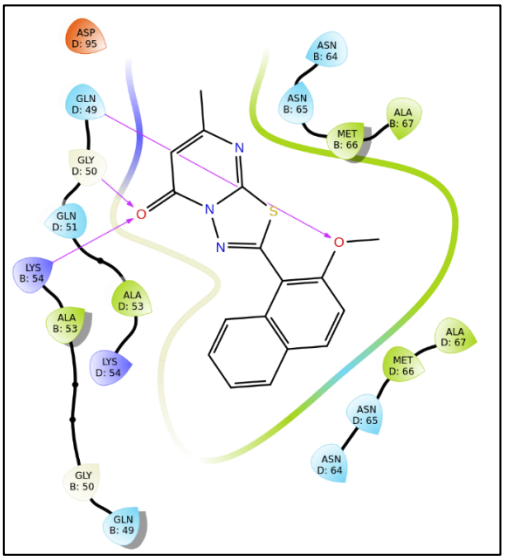

Figure 37: 2D representation of **LAM20** in the binding site of the crystal structure of human HSF1-DBD in complex with a HSE (PDB: 5D5U[24]). H bond interactions are reported as pink arrows. Hydrophobic residues are depicted in green, positive and negative charge residues in blue and orange respectively, polar residues in light blue, and glycine in light grey.

According to the procedure reported by Takayuki, the pyrimidones containing bis-heterocycles were synthesized exploiting a condensing ring-closure reaction. Upon heating with polyphosphoric acid (PPA), the beta-keto-esters and the appropriate heterocyclic amines were allowed to condense to give the pyrimido-heterocycles derivatives, likely through the initial imine formation which undergoes cyclization (**Figure 38**). [216]

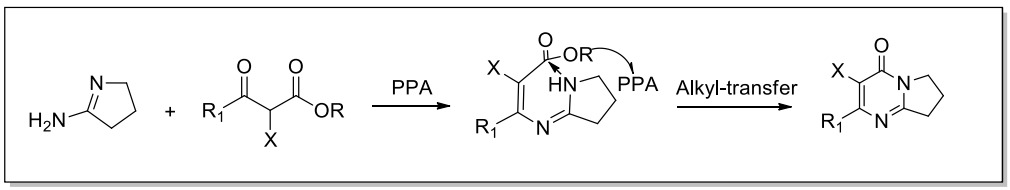

Figure 38: Suggested reaction mechanism for the synthesis of pyrimidone derivatives.

In more details, the beta-keto-esters **8** and the heterocyclic amines **9-13** were put to react with PPA at 140-160°C for 1.5 h, obtaining the molecules **LAM1-LAM4** and

the core **14**, while the core **16** was obtained by reaction between **12** and a different beta-keto-ester **15** (**Scheme 4**). [217]

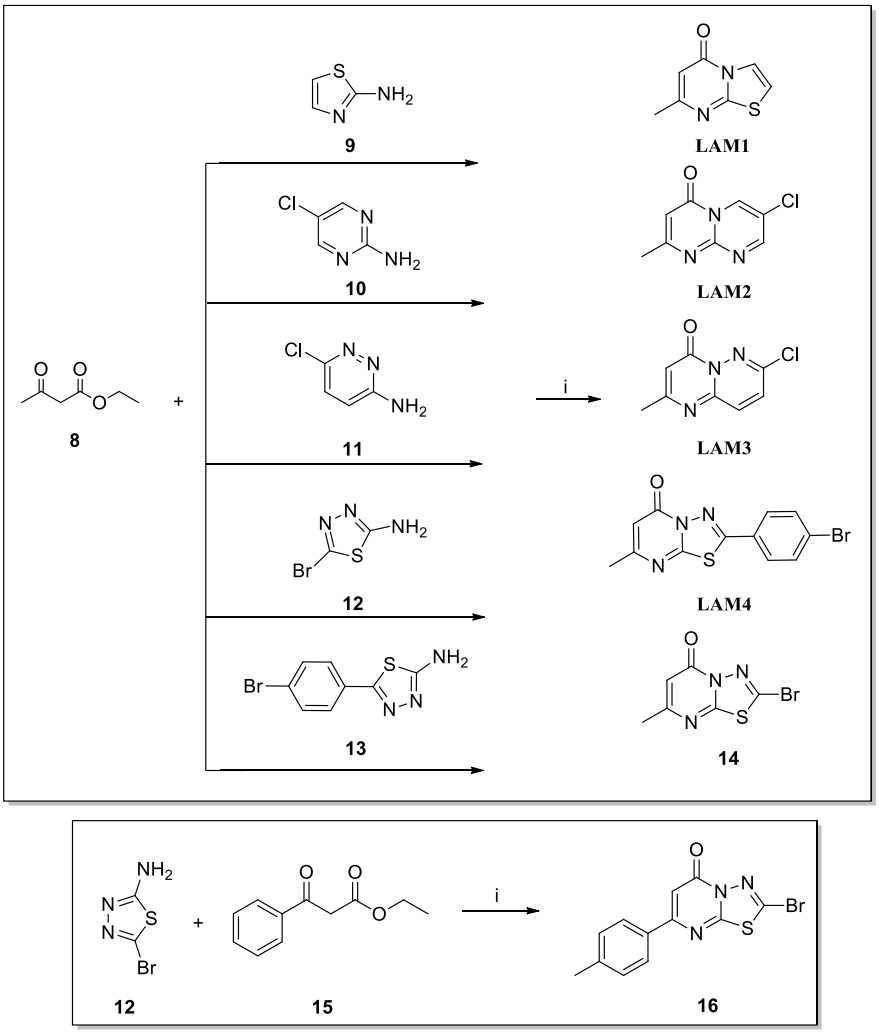

Scheme 4: Synthetic procedure for **LAM1-LAM4, 14** and **16.**
Reagents and conditions: i) PPA, 140-160°C, 1.5h.

The second synthetic step involved the Suzuki reaction, since the bromide atom on the heterocycle moiety give access to a further functionalization reaction. The Suzuki reaction is a versatile cross-coupling reaction between a boronic acid and an organohalide catalyzed by a palladium(0) complex, in the presence of a base. [218]

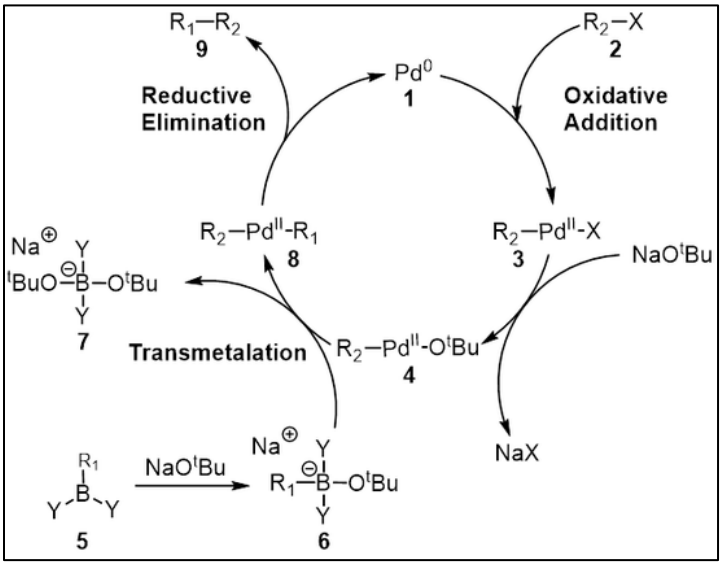

Figure 39: Suzuki reaction mechanism.

The mechanism begins with an oxidative addition of the organohalide (**2**) to the Pd (0) to form a Pd (II) complex (**3**), then, a molecule of the base replaces the halide on the palladium complex, while another adds to the organoborane to form a borate reagent (**6**) which is more prone to give the transmetallation process. Finally, the reductive elimination of the complex (**7**) gives the coupled product, regenerating the palladium catalyst (**1**) (**Figure 39**).

To obtain **LAM5-LAM11**, **LAM3** was placed to react with boronic acids **a-g**, while, to obtain **LAM13-LAM19**, we started from **LAM4** that was placed to react with the boronic acids **a**,**c**,**h-l** (**Scheme 5**). [219]

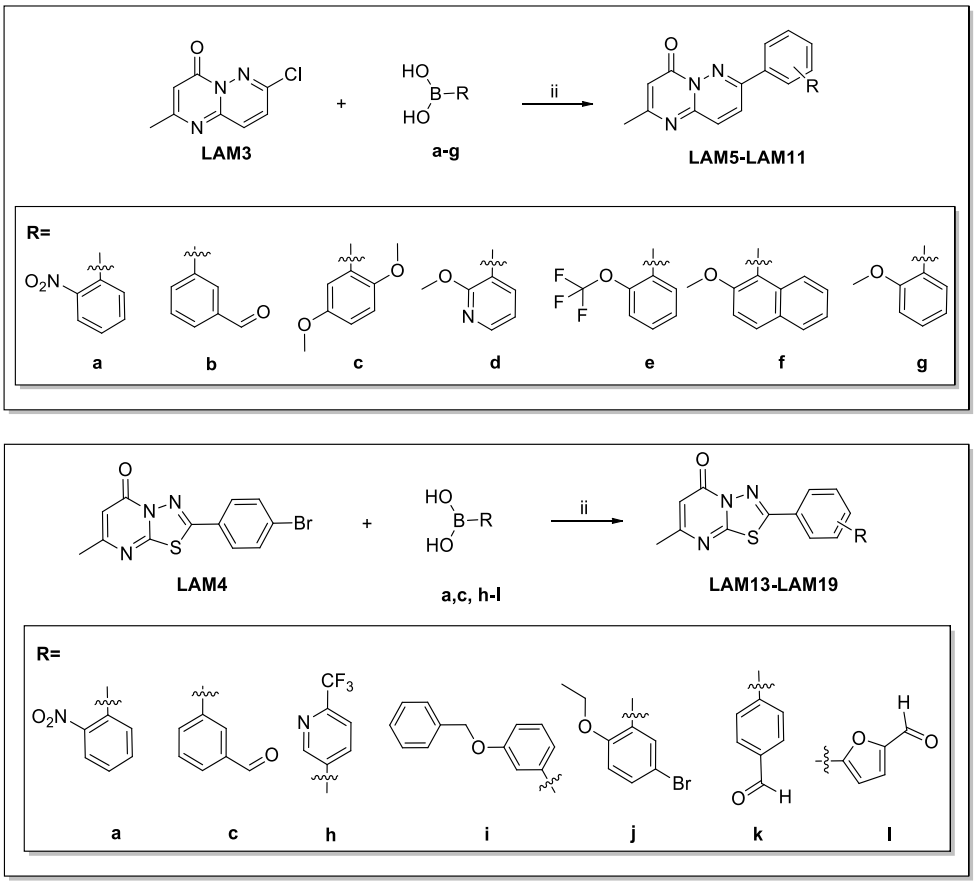

Scheme 5: Synthetic procedure for **LAM5-LAM11** and **LAM13-LAM19.**

Reagents and conditions: ii) $Pd(PPh_3)_4$, K_2CO_3, dioxane/H_2O (2:1), reflux, overnight.

Finally, to obtain **LAM20-LAM27**, we used a modified synthetic protocol. Compound **14** was placed to react at 100°C for 16h with the corresponding arylboronic acids (**c-g, m-o**) in presence of palladium(II)acetate, xantphos, a bidentate diphosphine ligand, and potassium carbonate using as solvent reaction dry 1,4-dioxane. Compound **16** was placed to react with the (2-fluorophenyl)boronic acid (**p**) in the same experimental conditions to give **LAM28** (**Scheme 6**). [220]

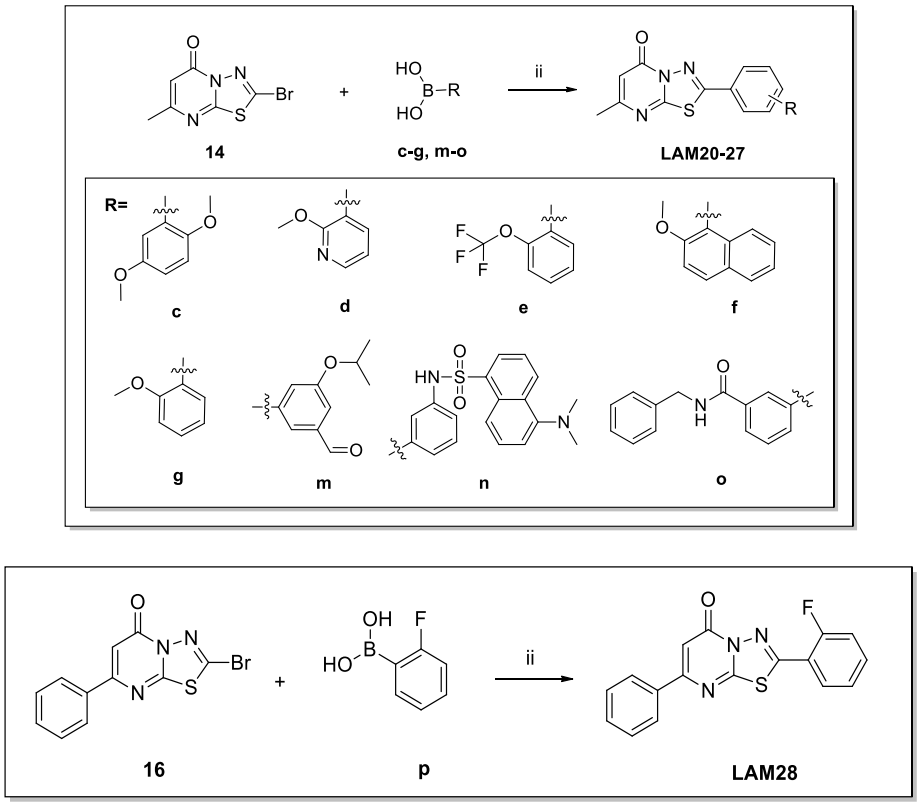

Scheme 6: Synthetic procedure for **LAM20**-**28**.

Reagents and conditions: ii) $Pd(AcO)_2$, K_2CO_3, xantphos, dry 1,4-dioxane, 100°C, 16h.

Only for **LAM12,** the second step was an aromatic nucleophilic substitution. **LAM3** and aniline **17** were resuspended in ethanol and refluxed for 24h (**Scheme 7**).

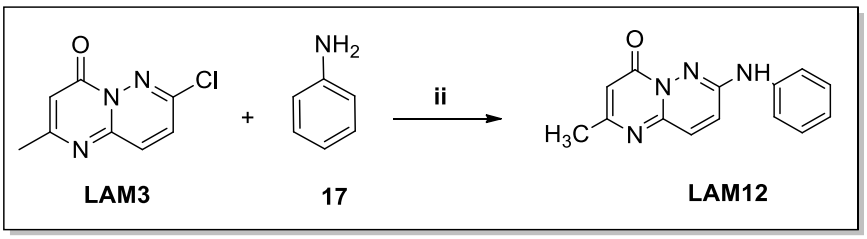

Scheme 7: Synthetic procedure for **LAM12**.

Reagents and conditions: ii) EtOH, reflux, overnight.

4.4 Biochemical evaluation of the selected molecules

On the molecules selected by virtual screening, a Surface Plasmon Reference (SPR) assay was performed in order to establish their binding affinity for the selected target.

SPR is one of the commonly used technologies for detailed and quantitative studies of protein-protein interactions and determination of their equilibrium and kinetic parameters; furthermore, this method provides excellent instrumentation for a label-free, real-time investigation of protein-protein interactions. The SPR-based binding method involves the immobilization of a ligand on the surface of a sensor chip which has a monolayer of carboxymethylated dextran covalently attached to a gold surface. The ligand of interest is immobilized on the surface of the sensor chip, using a well-defined chemistry and allowing solutions, with different concentrations of an analyte, to flow over it and to perform interactions with the immobilized ligand (**Figure 40**). The SPR signal originates from changes in the refractive index at the surface of the gold sensor chip. The increase in mass, associated with a binding event, causes a proportional increase in the refractive index, which is observed as a change in response. These changes are measured as changes in the resonance angle (θ) of refracted light when the analyte, flowing in a microfluidic channel, binds to the immobilized ligand and increases the density at the sensor chip. The response signal is quantified in resonance units (RU) and represents a shift in the resonance angle. When a steady-state is achieved (all binding sites occupied), the maximum RU is determined.

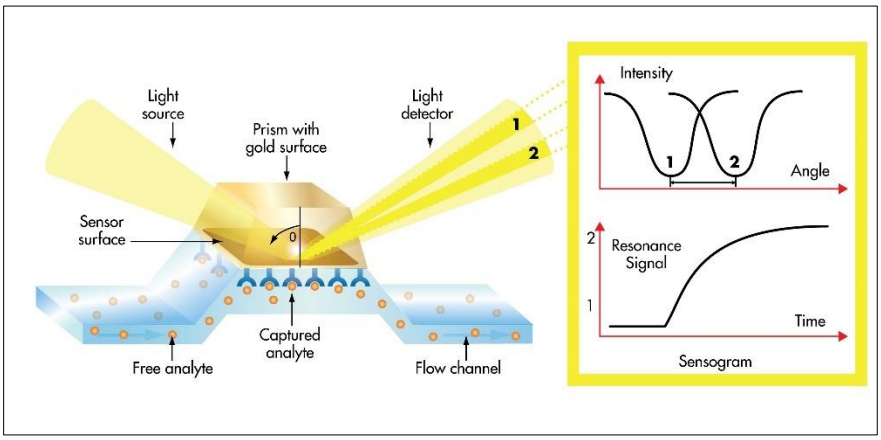

Figure 40: Experimental setup of a SPR assay.

SPR analyses were performed using a Biacore 3000 optical biosensor equipped with research-grade CM5 sensor chips. Using this platform, a recombinant HSF1 surface and one unmodified reference surface were prepared for simultaneous analyses. The recombinant HSF1 full-length protein was immobilized to obtain densities of 8–12 kRU. The compounds were tested at six different concentrations, 0-6-12-25-50-100µM and a known and commercially available inhibitor of HSF1, **KRIBB11**, was used as a positive control.

The table below shows the K_Ds of the molecules for which the affinity for the target protein was assessed (**Table 4**). 79 molecules were tested and 28 were able to bind the full-length protein with K_Ds in the low micromolar range (**Experimental section 7.5**). The known inhibitor used as a reference, **KRIBB11**, also bound the protein with a K_D in a similar order of magnitude.

The 28 HSF1 binders, together with other molecules selected through previous screening were subjected to further in-cell tests during the time I spent at the IdiPAZ Institute in Madrid.

Compound	K_D (μM) ± SD	Compound	K_D (μM) ± SD
HO-1	0.49 ± 0.10	**SP-7**	8.25 ± 1.10
HO-2	4.05 ± 1.10	**SP-35**	No binding
HO-3	No binding	**SP-36**	No binding
HO-4	No binding	**DIA-2**	No binding
HO-5	No binding	**DIA-11**	No binding
HO-6	No binding	**NICK-E3A**	No binding
HO-7	No binding	**NICK-E3B**	No binding
HO-8	No binding	**BD-1**	1.13 ± 0.65
HO-9	No binding	**BGN-JM3**	No binding
HO-10	No binding	**BGN-JM4**	3.57 ± 0.80
HO-11	9.80 ± 3.1	**BGN-EM19**	No binding
HO-12	No binding	**M-13**	No binding
HO-13	No binding	**MO1**	4.15 ± 0.43
HO-14	No binding	**MO2**	3.66 ± 0.24
HO-15	0.75 ± 0.80	**MO3**	0.56 ± 0.05
HO-16	5.05 ± 4.46	**MO4**	2.50 ± 0.52
HO-17	No binding	**MO5**	4.99 ± 0.39
HO-18	No binding	**MO6**	0.81 ± 0.02
HO-19	0.38 ± 0.15	**MO7**	1.81 ± 0.89
HO-20	No binding	**MO8**	0.23 ± 0.01
HO-21	No binding	**MO9**	0.59 ± 0.04
HO-22	No binding	**MO10**	No binding
HO-23	21.90 ± 1.98	**MO11**	No binding
HO-24	No binding	**MO12**	No binding
HO-25	No binding	**MO13**	0.38 ± 0.03
HO-26	No binding	**MO14**	0.07 ± 0.002
HO-27	0.08 ± 0.004	**LAM1**	0.67 ± 0.08
HO-28	0.09 ± 0.002	**LAM2**	No binding
HO-29	No binding	**LAM3**	No binding
HO-30	No binding	**LAM4**	No binding
HO-31	No binding	**LAM5**	No binding
HO-32	No binding	**LAM6**	No binding
HO-33	No binding	**LAM12**	0.19 ± 0.04
HO-34	No binding	**LAM13**	No binding
HO-35	No binding	**LAM14**	No binding
HO-36	No binding	**LAM15**	No binding
HO-37	No binding	**LAM16**	No binding
HO-38	0.21 ± 0.57	**LAM17**	0.44 ± 0.03
HO-39	3.44 ± 0.91		
SP-1	No binding	**KRIBB11**	5.12 ± 1.15

Table 4: Thermodynamic constants measured by SPR for the interaction between the selected molecules and the immobilized HSF1. Data are given as mean ± S.E.M., n = 3.

4.5 Evaluation of biological effects

During my period abroad, at the IdiPAZ Institute in Madrid, under the supervision of Dr. Nuria Vilaboa I took care of evaluating the biological effects of the molecules selected by the previous reported screening assays. To find any molecule able to modulate HSF1 through its DNA binding domain (DBD), the small library was screened employing a gene reporter assay, a very sensitive method to assess the expression and the regulation of a target gene (**Figure 41**).

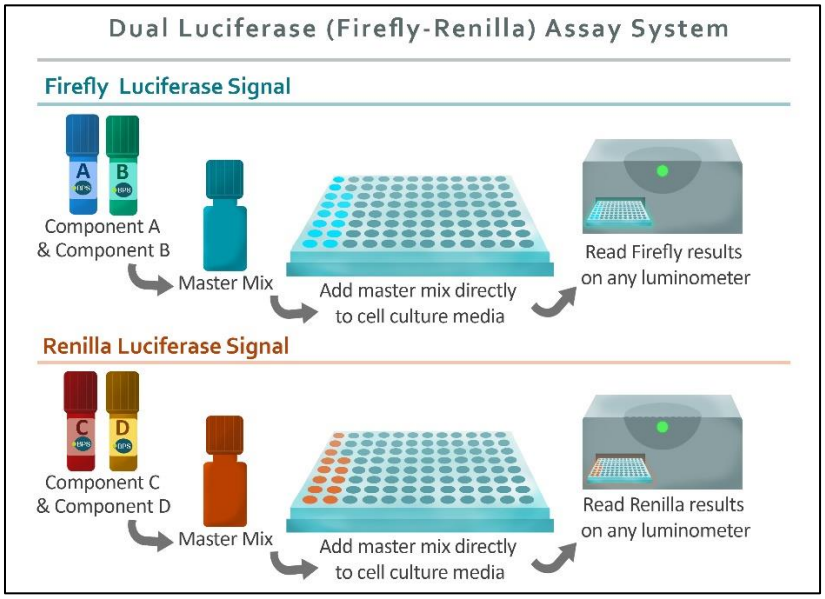

Figure 41: Dual-Luciferase reporter assay system.

Genetic reporters are widely used in drug development, biomedical research, and biochemistry. In a nutshell, the reporter gene is fused with the gene of interest and cloned into an expression vector. The expression vector with the chimeric sequence is transferred into suitable cells. The expression of the gene in the cell is measured by the activity of the reporter protein. The most common reporters are bioluminescent reporters whose detection is based on the enzymatic reaction with an enzyme. We used a dual luciferase assay system, indeed, the activities of Firefly

(*Photinus pyralis*) and Renilla (*Renilla reniformis*) luciferases were measured sequentially from a single sample. Renilla luciferase is often used as an internal control fused with housekeeping or constitutively expressing promoters. Hence, the firefly luciferase reporter is measured first by adding Luciferase Assay Reagent II (LAR II) to generate a luminescent signal lasting at least one minute. After quantifying the firefly luminescence, this reaction is quenched, and the Renilla luciferase reaction is initiated simultaneously by adding Stop & Glo Reagent to the same sample.

The research group of Dr. Nuria Vilaboa developed a stable cell line, Z74, transfected with gene constructs that allow to analyze the effects of a compound on the activities of both the wild type HSF1 and a chimeric one. To exclude indirectly acting compounds, given the HSF1 modular nature, its DNA-binding domain was replaced with an unrelated DNA-binding unit in order to create a chimeric transcription factor that is recruited to a different target promoter, but whose activity is regulated like that of the endogenous HSF1. Z74 cells, indeed, contain the expression construct LEXA-hHSF1 controlled by the promoter *CMV* and whose transcript trigger the downstream *FLUC* gene, and a *RLUC* gene functionally linked to an *HSP70B* (*HSPA7*) heat shock gene promoter and, therefore, controlled by endogenous HSF1. Both reporter genes are activated by heat shock in a similar dose-dependent way (**Figure 42**). [80]

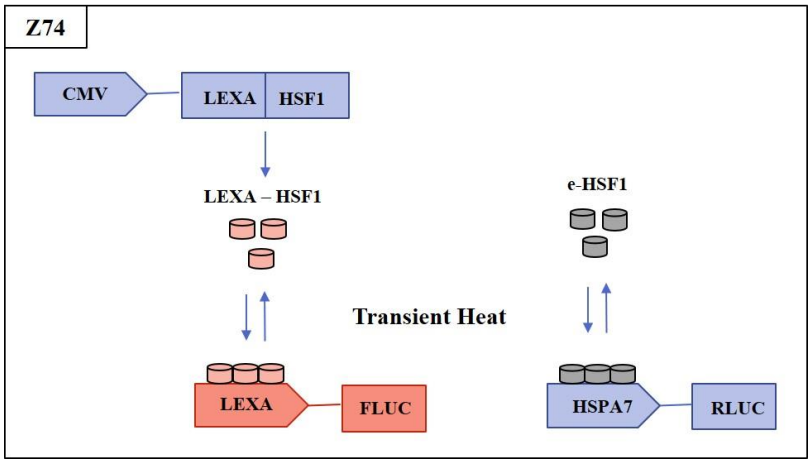

Figure 42: Z74 cells harbor an *RLUC* gene that is linked to an *HSPA7* gene promoter. The latter promoter is responsive to endogenous human transcription factor HSF1 (eHSF1). Z74 cells also contain a CMV promoter-driven gene for chimeric transcription factor LEXA-HSF1 as well as a *FLUC* gene controlled by a promoter responsive to LEXA-HSF1

To be considered a true hit, a compound should inhibit the heat-induced activity of wild type HSF1 (i.e. RLUC activity) but not that of chimeric HSF1 (i.e. FLUC activity) in the Z74 cells (**Figure 42**). [80] In this assay, the known commercially available HSF1 inhibitor, **KRIBB11**, was used as a positive control, and a **HO-18**, a molecule not able to bind the full-length protein, as a negative control. The obtained results on the Z74 cell line are reported in the table below (**Table 5**).

Compound	FLUC – Z74 (25µM)	FLUC – Z74 (12.5 µM)	RLUC – Z74 (25µM)	RLUC – Z74 (12.5µM)
HO-1	113.08%	128.38%	82.26%	76.60%
HO-2	120.51%	140.09%	89.40%	72.11%
HO-11	115.05%	107.12%	78.12	82.60%
HO-15	91.79%	92.32%	108.40%	126.78%
HO-16	134.37%	125.91%	90.33%	108.82%
HO-18	137.09%	127.83%	94.47%	103.52%
HO-19	138.62%	124.01%	84.56%	99.46%
HO-23	138.74%	122.62%	93.40%	97.65%
HO-27	110.97%	102.29%	83.24%	87.06%
HO-28	97.74%	114.79%	102.93%	144.15%
HO-38	56.09%	100.59%	87.48%	107.12%
HO-39	95.30%	108.27%	94.25%	97.43%
SP7	87.16%	68.98%	99.43%	121.74%
BD-1	100.86%	96.92%	64.83%	84.85%
BGN-JM4	94.87%	72.91%	102.27%	109.04%
MO1	77.54%	87.50%	108.27%	98.38%
MO2	74.91%	87.50%	117.42%	98.38%
MO3	59.33%	82.24%	86.57%	87.51%
MO4	92.00%	95.79%	115.08%	107.13%
MO5	69.59%	82.81%	95.28%	95.37%
MO6	59.33%	73.57%	96.17%	87.65%
MO7	93.13%	86.67%	110.34%	105.09%
MO8	88.21%	86.67%	97.47%	105.09%
MO9	29.42%	54.75%	27.98%	45.75%
MO13	86.47%	91.27%	87.86%	90.39%
MO14	103.26%	93.57%	97.99%	102.42%
LAM1	93.35%	80.08%	102.83%	109.04%
LAM12	112.54%	145.93%	95.46%	85.81%
LAM17	104.96%	104.23%	63.65%	73.12%
A1	60.19%	82.01%	81.36%	100.88%
A2	111.83%	120.07%	89.21%	102.35%
A3	94.11%	107.31%	76.79%	93.80%
A4	89.47%	106.14%	77.63%	91.84%
A5	114.46%	123.61%	87.45%	95.76%
A6	96.91%	107.95%	85.22%	90.19%
A7	112.29%	96.14%	108.93%	110.95%
A8	101.02%	101.12%	104.34%	116.02%
A9	93.86%	96.11%	91.44%	98.98%
A10	90.73%	94.58%	77.40%	92.97%
A11	67.56%	70.83%	93.28%	99.83%
A12	130.80%	116.52%	76.65%	94.26%
A13	110.10%	114.35%	101.68%	106.13%
A14	96.44%	114.19%	44.94%	101.64%
A15	8.86%	10.37%	12.15%	29.00%
A16	108.92%	122.57%	103.49%	98.09&
A17	78.00%	89.22%	78.72%	74.58%
BR-1	112.71%	123.56%	100.28%	95.10%
BR-2	84.18%	79.54%	109.29%	124.63%
BR-3	84.39%	79.80%	92.20%	118.96%
BR-4	82.70%	76.95%	87.75%	112.75%
BR-5	89.43%	86.55%	85.12%	109.52%
BR-6	87.02%	87.13%	81.63%	102.90%
BR-7	101.28	93.69%	84.55%	101.89%
KRIBB	3.24%	10.15%	31.34%	55.91%

Table 5: Average percentage of RLUC and FLUC activity in Z74 cells following treatment with selected molecules. Z74 cells, exposed to the molecules at the indicated concentrations for 2h, or exposed to DMSO, were heat-treated (HS) at 43°C for 30 min and post-incubated at 37°C for 6h. The data were normalized to the values of reporter genes of heat-exposed/ untreated cells, which were given the arbitrary value of 100. Data are given as mean ± S.E.M., n=3.

The analysis of the results allowed to gather the following information:

- **BD-1** and **LAM17** reduce heat-induced RLUC activity and do not interfere with FLUC activity;
- **MO9** and **A15** reduce both heat-induced RLUC and FLUC activities;
- **KRIBB11** behaves as an HSF1 inhibitor, although the effect on FLUC expression suggests that it does not exert its action through the DBD domain of HSF1. **HO-18**, used as a negative control, do not have any effect on the expression of the both reporter genes;
- All the other tested compounds do not affect the heat-induced activity of the reporter genes.

Basing on these results we selected **BD-1**, **LAM17**, **MO9**, and **A15** for further investigations, and in particular their cytotoxicity has been assessed. The viability of HeLa cells (Human cervix epitheloid carcinoma), the parental cell line of Z74, treated with different concentrations of the selected compounds, was investigated using an Alamar blue assay. The live cells were then stained with crystal violet and observed under a microscope with a magnification of 4X (**Figure 43, 44**).

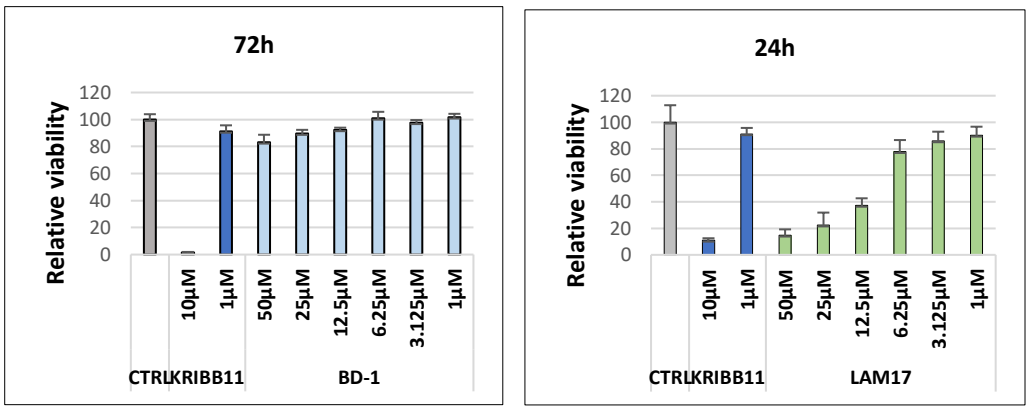

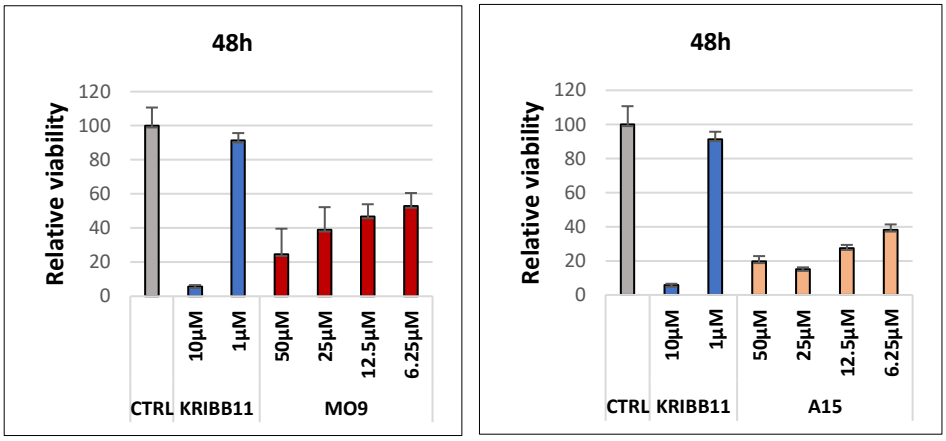

Figure 43: The viability of HeLa cells exposed for 24 or 48 or 72h to the indicated concentrations of **BD-1**, **LAM17**, **MO9**, **A15** was investigated through an Alamar blue assay. DMSO was used as negative control and **KRIBB11** as positive control. Data are given as mean ± S.E.M., n=3.

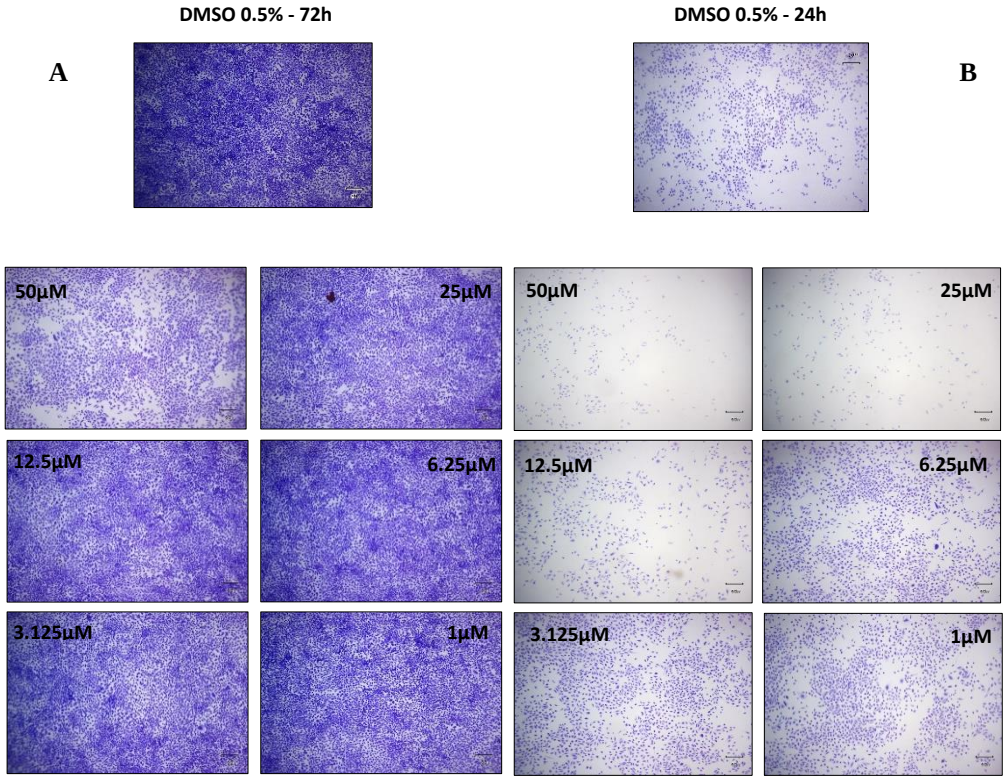

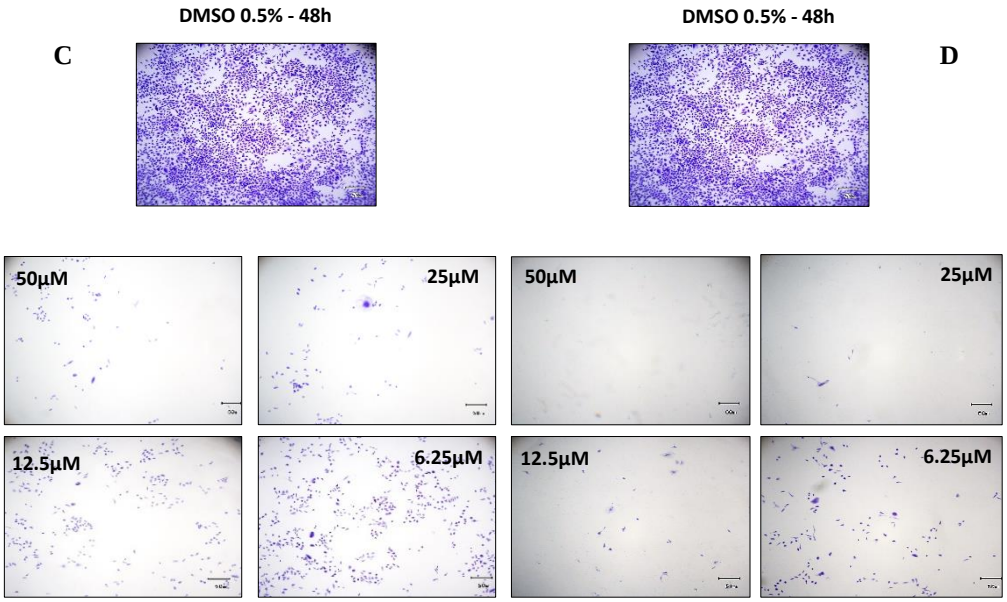

Figure 44: HeLa cells exposed to **a) BD-1** for 72h, **b) LAM17** for 24h, **c) MO9** for 48h, and to **d) A15** for 48h were stained with crystal violet. DMSO was used as reference.

The tests showed that **LAM17**, **MO9**, and **A15** are very cytotoxic: at 50µM they induce about 80% mortality in HeLa cells already at 24-48h. **BD-1**, on the other hand, showed a 20% mortality after 72h. In order to confirm if the activity of the potential modulators caused an inhibition at transcriptional level, the mRNAs levels governed by HSF1 in Z74 cells, *RLUC*, *FLUC*, and *HSPA7* were monitored after the exposure to the selected molecules. It was necessary to choose the most suitable time, following heat shock, to set the experiment. To this purpose, the mRNA levels were measured at different recovery times (1h, 3h, and 6h) at 37ºC after heat shock, using the qRT-PCR technique.

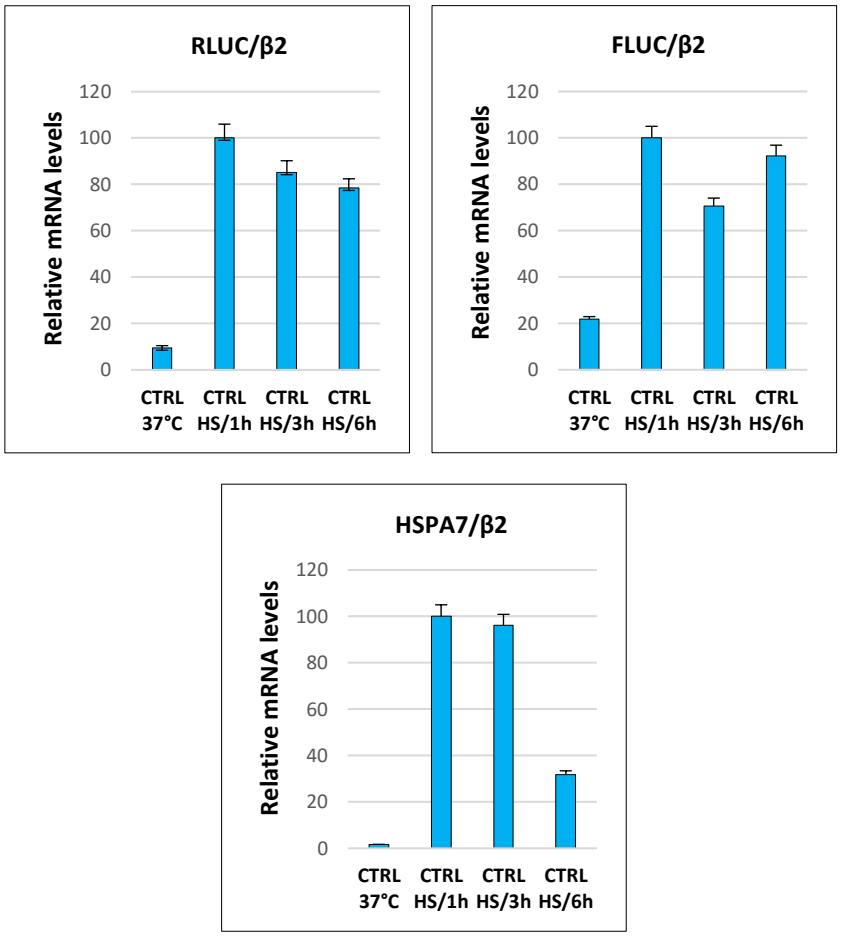

Figure 45: mRNA levels of *RLUC*, *FLUC* and *HSPA7* after 1h, 3h or 6h from the heat shock.

The results showed a progressive reduction in mRNA levels after heat shock, although they remain substantially high even after 6h, especially in the case of *RLUC* and *FLUC* (**Figure 45**).

Finally, the mRNA levels in Z74 cells treated with **BD-1** and **LAM17** heated and let recover for 1h after heat shock were evaluated.

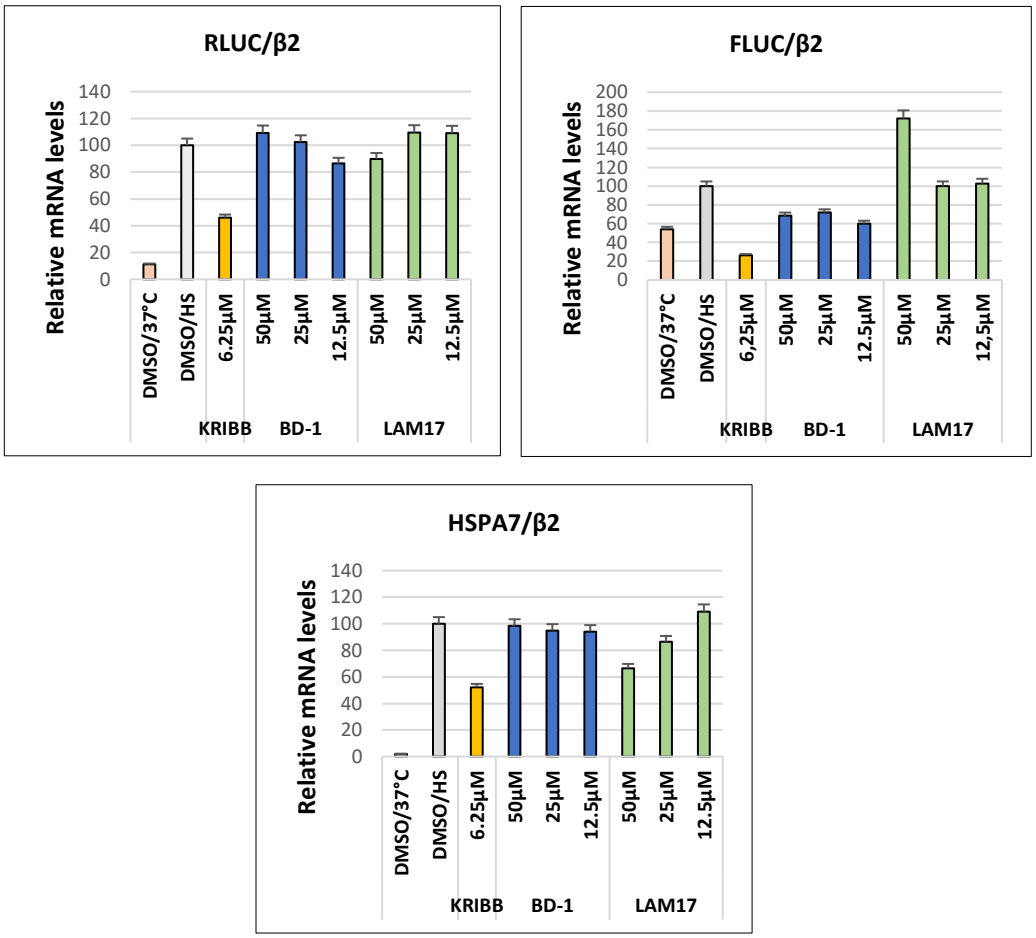

Figure 46: mRNA levels of *RLUC*, *FLUC* and *HSPA7* following treatment with **BD-1**, **LAM17**, and **KRIBB11**. Z74 cells, exposed to the compounds at the indicated concentrations for 2h, or exposed to DMSO, were heat-treated (HS) at 43°C for 30 min and post-incubated at 37°C for 1h. Data are given as mean ± S.E.M., n=3.

The results showed a slight reduction of *RLUC* (about 10%) and *HSPA7* (about 40%) mRNA levels in the case of Z74 cells treated with 50 µM of **LAM17**, while no relevant effect was detected with the doses 25 and 12.5 µM used in the previous screening assays. No effect was observed in cells treated with **BD-1** (**Figure 46**). To confirm this result, a new qRT-PCR experiment with **BD-1** was performed after 6h from the heat shock.

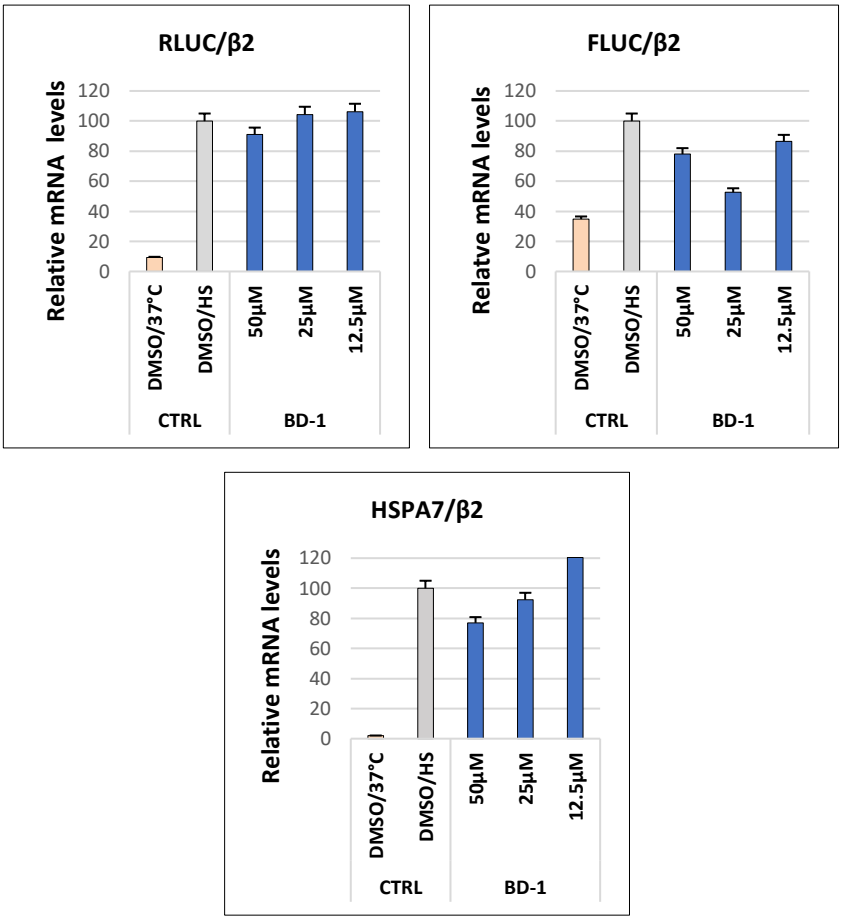

Figure 47: mRNA levels of *RLUC*, *FLUC* and *HSPA7* following treatment with **BD-1**. Z74 cells, exposed to **BD-1** at the indicated concentrations for 2 h, or exposed to DMSO, were heat-treated (HS) at 43°C for 30 min and post-incubated at 37°C for 6h. Data are given as mean ± S.E.M., n=3.

In this case a slight reduction of *HSPA7* (about 25%) and *RLUC* (15%) mRNA levels at the maximum dose was observed. (**Figure 47**)

The same procedure was used to test also **MO9** and **A15**, however no substantial effect was monitored, as showed in **Figure 48** reporting the *HSPA7* mRNA levels following treatment with the two compounds.

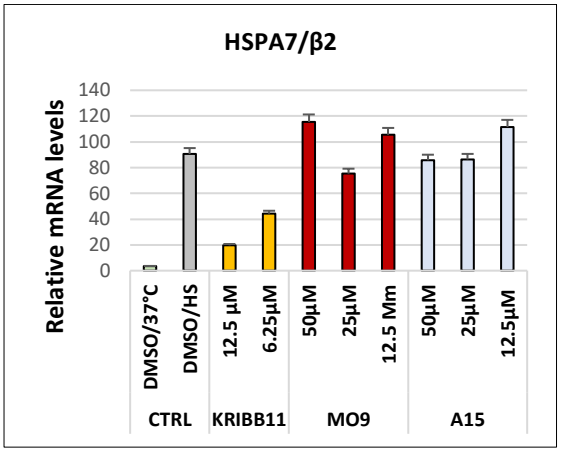

Figure 48: *HSPA7* mRNA levels following treatment with **MO9**, **A15** and **KRIBB11**. Z74 cells, exposed to the compounds at the indicated concentrations for 2h, or exposed to DMSO, were heat-treated (HS) at 43°C for 30 min and post-incubated at 37°C for 1h. Data are given as mean ± S.E.M., n=3.

Taking the data reported all together we can conclude that **BD-1** and **LAM17**, although are not potent and selective modulators of HSF1, may represent interesting starting point for further medicinal chemistry studies aimed at identifying tighter HSF1 binders useful both, as chemical probe to interrogate the target, and as attractive drug candidates.

By analyzing the results obtained so far, we decided to follow a different way for **LAM7**-**LAM11** and **LAM18**-**LAM28**, the last synthesized molecules. The SPR assays conducted on the full-length protein produced many false positives, possibly due to the highly unstructured nature of HSF1, hence we decided to evaluate first the cytotoxic profile of these molecules through a MTT assay. In order to standardize the data, all the molecules were all tested on HeLa cell line at 72 h at two concentrations, 50 and 10 μM, and **KRIBB11**, used as a positive control, was tested at 10 and 1 μM respectively (**Figure 49**).

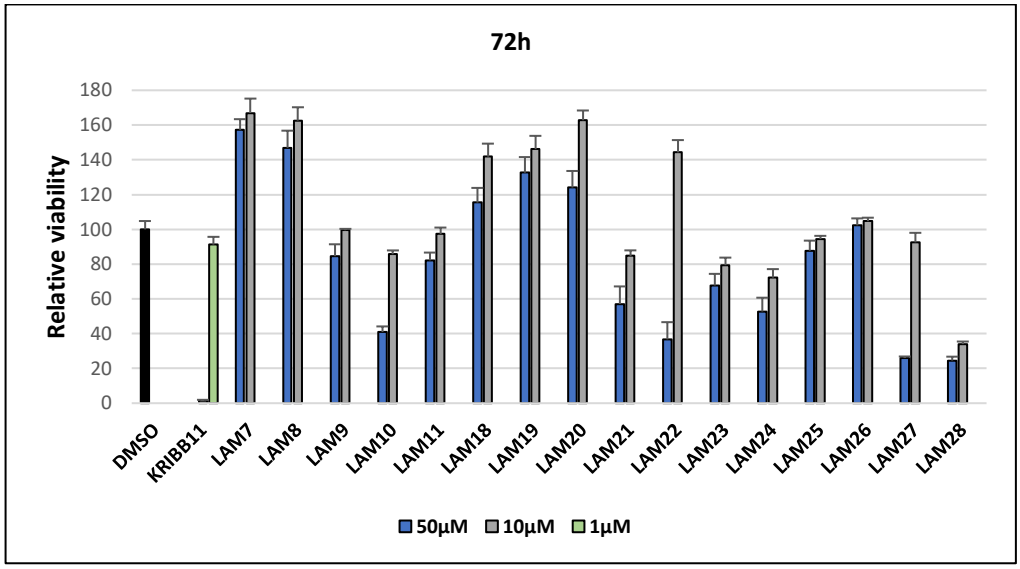

Figure 49: MTT assay performed on HeLa cells at 72 h for **LAM7-LAM11** and **LAM20-LAM28**. DMSO was used as negative control and **KRIBB11** as positive control. Data are given as mean ± S.E.M., n=3.

From this assay, it emerged that the most promising compounds are **LAM10**, **LAM22**, **LAM27** and **LAM28**. In particular, **LAM28** induce ~80% of mortality at 10 µM, showing a comparable profile to **KRIBB11**. For these molecules we will perform a SPR assay, not anymore on full-length protein but on the isolated DBD, in order to avoid false positives, by working on a structured region of the protein. In depth evaluation of the biological profile of these cytotoxic molecules are currently under investigation.

CHAPTER 5

Design, synthesis and biological evaluation of 2,4-thiazolidinedione derivatives as new BAG3 modulators

CHAPTER 5

Design, synthesis and biological evaluation of 2,4-thiazolidinedione derivatives as new BAG3 modulators

5.1 Introduction

The BAG protein family regulates various biochemical events through the modulation of protein kinases, receptor signaling, and transcription factors. [221, 222] BAG3 protein has recently gained the attention of the scientific community as it is involved in many crucial cellular pathways. [129, 131, 223] Although the physiological role of BAG3 has not yet been fully elucidated, most of its cytoprotective effects are due to the interaction with Hsp70. The Hsp70-BAG3 complex detects the formation of aberrant protein complexes upon proteasome decline, transmits this information to the downstream pathways, allowing cells to activate protective responses against stressful environmental conditions. [97, 125, 224] The cytoprotective role of the Hsp70-BAG3 complex, along with the high expression levels of BAG3 and Hsp70 found in several cancer types, highlighted BAG3 as a new therapeutic option against tumor genesis. The discovery of protein modulators has been limited by the absence of the three-dimensional crystallographic structure of the human form. Several studies on mouse protein structures have shown that BAG3 possesses a conserved BAG domain (BD), present in other members of the BAG protein family, through which it interacts with the ATPase domain of the chaperone Hsp70. [97, 145, 221, 224, 225] By leveraging this information, the Organic Chemistry Research Group of Salerno University recently reported the first synthetic BAG3 modulator considered both, as an attractive drug candidate and as a chemical probe to deeply interrogate the biological role of this protein. Indeed, by using a combined approach of virtual screening, biophysical techniques, and biological assays, the 2,4-thiazolidinedione based molecule, **LK1**, was successfully identified as an interesting modulator of Hsp70-BAG3 protein-protein interaction. [146] Taking into

account the fundamental interactions between **LK1** and the BD domain of BAG3, the 2,4-thiazolidinediones library, previously built around the privileged scaffold, was re-evaluated using the shape similarity parameters, performing, thus, a *ligand-based approach*. Then, the most promising compounds were synthesized and their affinity for both, the full-length BAG3 protein and the BD domain, was evaluated by SPR analysis. These studies allowed us to identify **LK6** as a new modulator of BAG-BD endowed with an anti-proliferative profile better than the lead compound.

5.2 Computational studies

To identify novel 2,4-thiazolidinedione-based BAG3-BD modulators, a fast *ligand-based* Virtual Screening campaign was performed (**Figure 50**).

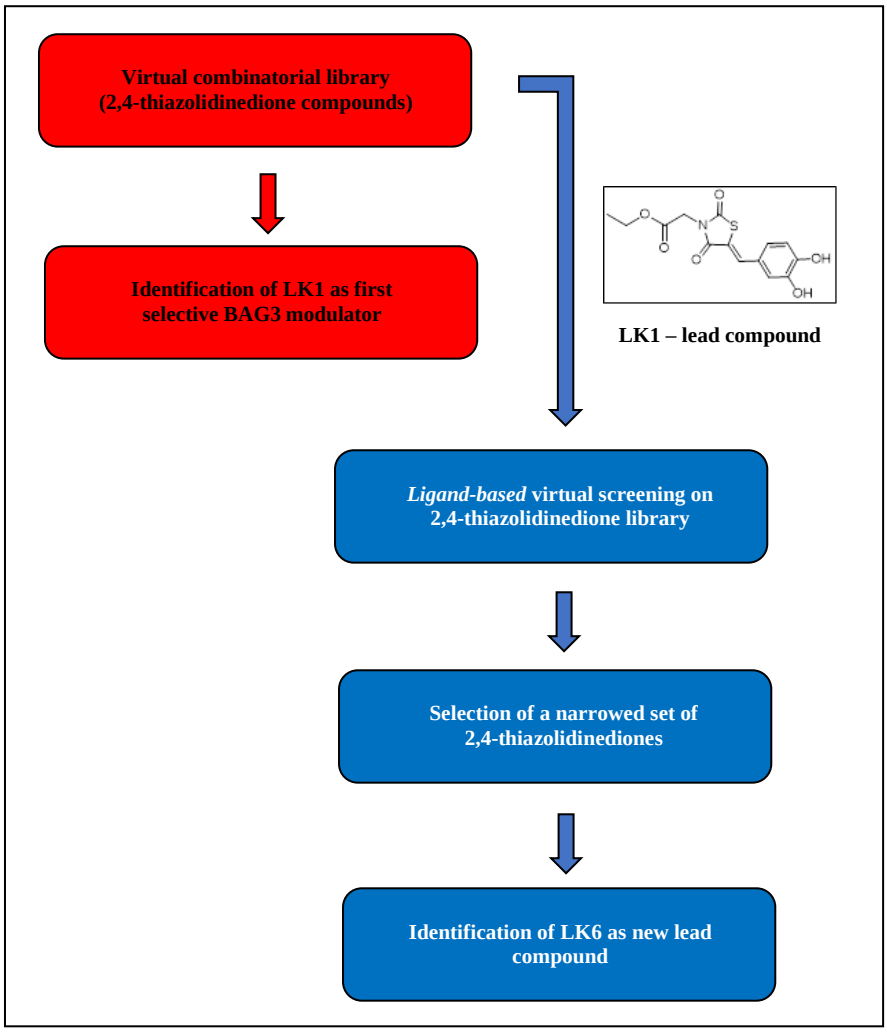

Figure 50: The Virtual Screening workflow for the identification of BAG3 ligands.

The library of ~2.3 × 10^4 2,4-thiazolidinedione-based compounds, built in our previous study, was screened against the lead compound **LK1** computing the related shape similarity values (Phase; Schrödinger; LLC, *New York*, *NY* **2017**). [146]

A restricted set of compounds was selected from the original library with a shape comparable to the lead compound, following the principle that similarly shaped molecules could likely show similar binding modes on the protein counterpart. [226, 227] This protocol envisages a first conformational search round on each item of the accounted library of 2,4-thiazolidinedione-based compounds, and afterward the obtained conformers are aligned and compared to the reference compound. In this way, the "shape similarity" parameter is computed for each screened molecule. Specifically, the related numerical value can range from 0 (no one atom matching between screened and reference compounds) to 1 (all atoms matching). Using this filter, the starting library was reduced to a small set of 8 promising molecules (**Figure 51**).

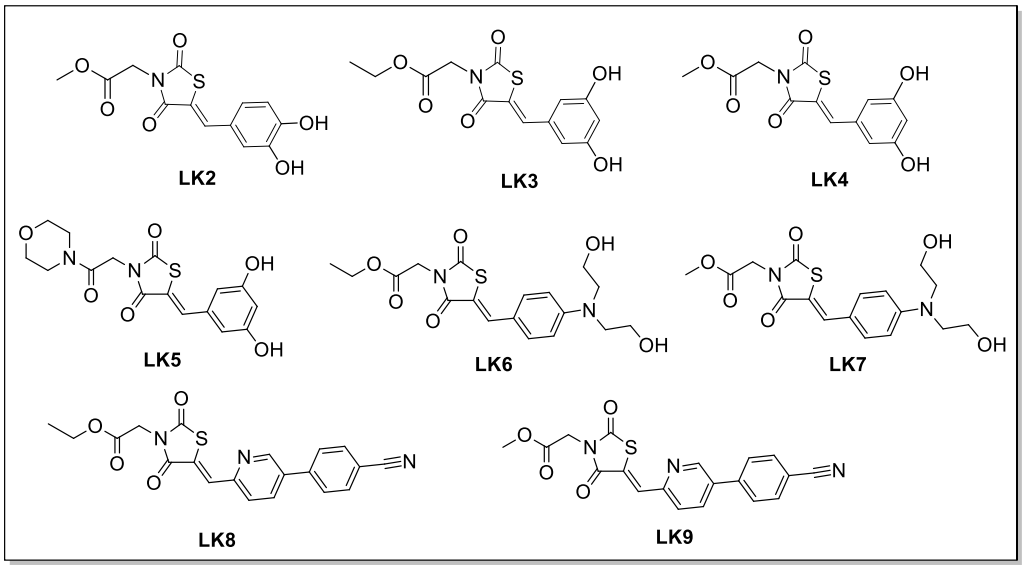

Figure 51: Chemical structures of compounds **LK2**-**LK9**.

5.3 Synthesis of 2,4 thiazolidinedione derivatives

The synthesis of **LK2-LK4** and **LK6-LK9** required two steps, while the synthesis of **LK5** three steps. The first step involved the formation of the (Z)-5-arylidene-2,4-thiazolidinediones through the Knoevenagel condensation, widely used in organic chemistry for C=C bond formation, of the 2,4-thiazolidinedione with aromatic aldehydes. [228] The second step consisted of a nucleophilic substitution between ethyl or methyl bromine acetate and the (Z)-5-aryliden-2,4-thiazolidinediones. [229] Finally, for **LK5** an amine coupling was further performed.
In the Knoevenagel condensation, piperidine plays a role of an organocatalyst. Organocatalysis uses small organic molecules predominantly composed of C, H, O, N, S, and P to accelerate chemical reactions. The advantages of organocatalysts include their lack of sensitivity to moisture and oxygen, their ready availability, low cost, and low toxicity, which gives a huge direct advantage in the production of pharmaceutical intermediates over metal (transition) catalysts. Specifically, the Knoevenagel condensation involves the nucleophilic addition of an activated methylene compound to an aldehyde or ketone using an amine base (e.g., pyridine or piperidine) as a catalyst, followed by a dehydration reaction in which a molecule of water is eliminated (condensation). The product is an α,β-unsaturated carbonyl compound (enone). As depicted in **Figure 52**, the reaction initiates by the formation of the iminium ion and enolate; the next step is the nucleophilic attack of the enolate to iminium ion leading to the elimination of the piperidine catalyst, which is regenerated. [230]

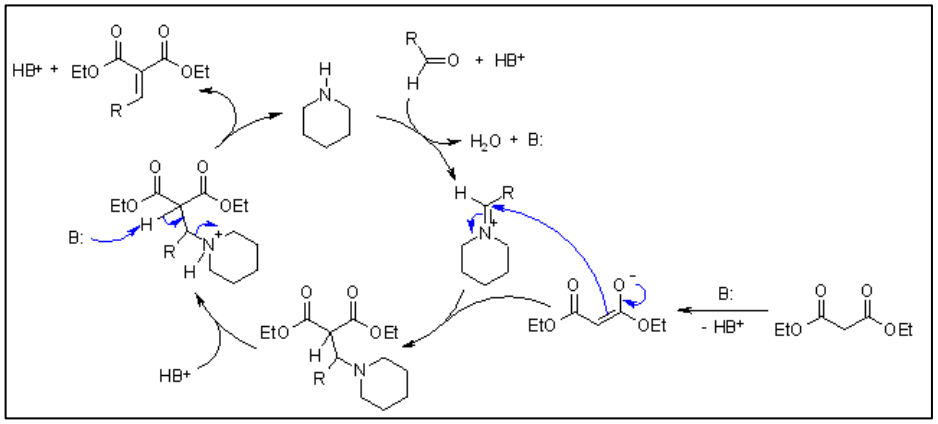

Figure 52: Knoevenagel condensation mechanism.

Hence, the synthesis of **LK2-LK9** was performed through a Knoevenagel condensation, in basic conditions for piperidine, between the commercially available 2,4-thiazolidinedione **18** and the selected aromatic aldehydes (**a-d**), affording the (Z)-5-arylidene-2,4 thiazolidinediones **19a-19d** in high yields (**Scheme 8**). The Z configuration of compounds was assigned based on the comparison of ^{1}H and ^{13}C NMR data of the obtained molecules with the spectral data of (Z)-5-arylidene-2,4 thiazolidinediones reported in the literature. [228]

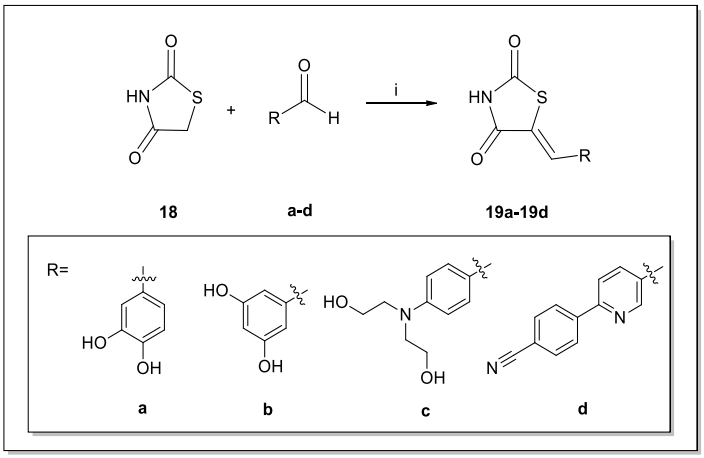

Scheme 8: Synthesis of **19a-19d**.

Reagents and conditions: i) piperidine, EtOH, reflux 16-24h.

The second step involved a nucleophilic substitution reaction at N-3 position of the (Z)-5-arliden-2,4-thiazolidinedione with the formation of N-alkylated products. [229] In detail, the treatment of **19a-19d** with bromo acetic acid esters (**e-g**), in presence of NaH and DMF dry as a solvent, provided the desired compounds **LK2-LK4** and **LK6-LK9** along with the intermediate **20bg** (**Scheme 9**). [228]

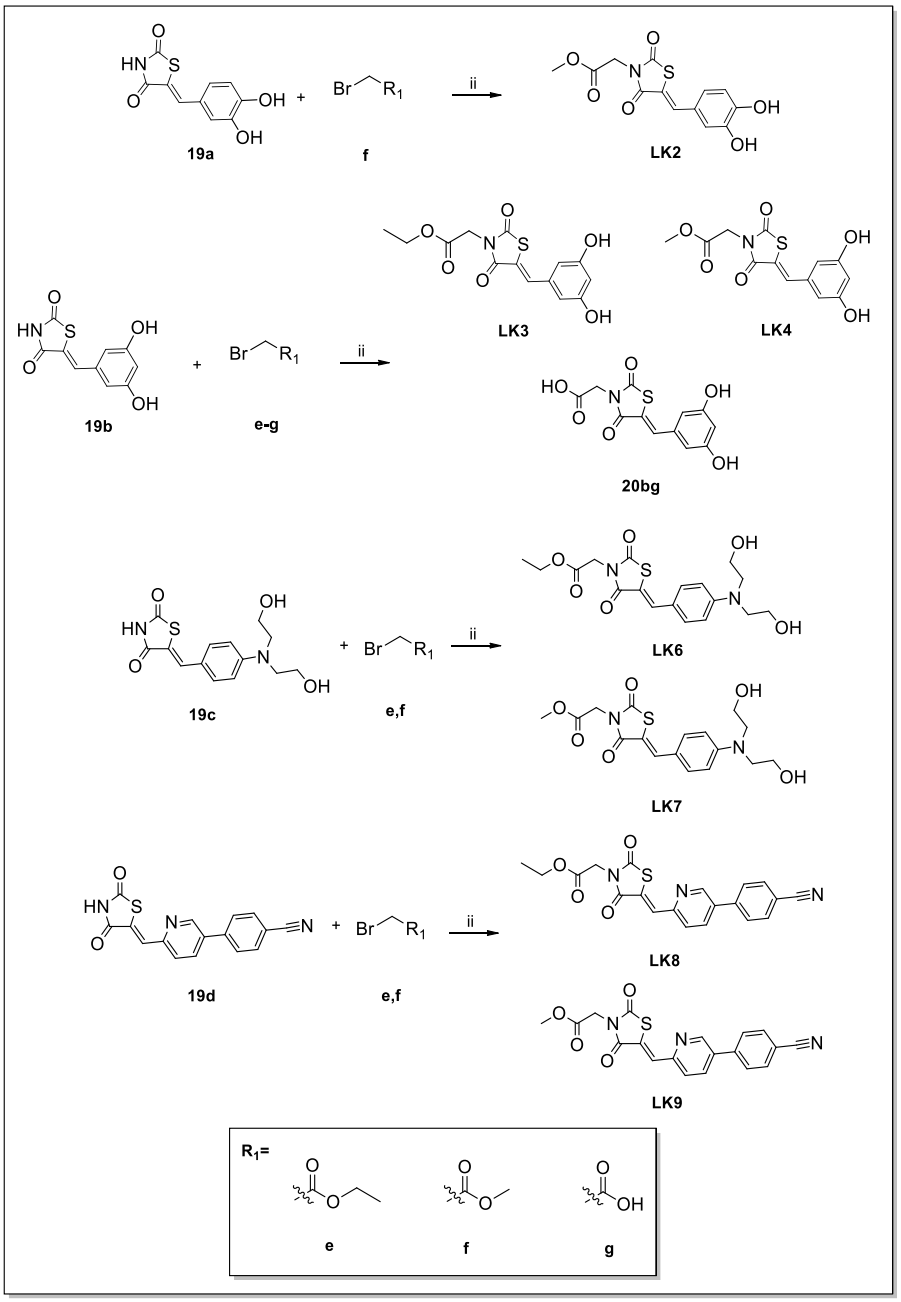

Scheme 9: Synthesis of **20bg**, **LK2-LK4**, and **LK6-LK9**.
Reagents and conditions: ii) NaH, DMF dry, 80°C 16-20h.

Finally, to obtain compound **LK5**, the intermediate **20bg** was further coupled with morpholine (**21**). The reaction was performed in presence of 1-

hydroxybenzotriazole (HOBt) and *N*,*N*-diisopropylcarbodiimide (DIC) as coupling agents (**Scheme 10**). [210-212]

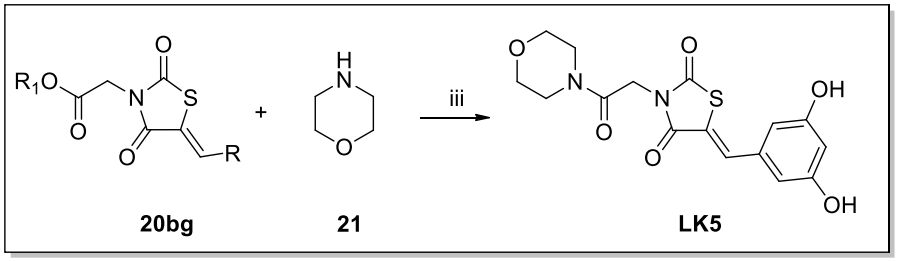

Scheme 10: Synthesis of **LK5**.

Reagents and conditions: iii) HOBt, DIC, DMF, rt, overnight.

5.4 Biophysical assays

The synthesized molecules have been subjected to the post-processing phase to verify their ability to physically bind the target protein. A Surface Plasmon Resonance (SPR) assay, using a recombinant BAG3 protein, was performed and, in order to explore the potential selectivity of our molecules, the affinity for BAG4, the most closely BAG3 related protein, among human BAG protein, was also evaluated. Moreover, since BAG3 contains several functional domains, to gather more information about the binding site, we decided to test their ability to bind the isolated BAG3-BD. The SPR analyses were performed using a Biacore 3000 optical biosensor equipped with research-grade CM5 sensor chips. Using this platform, three separates recombinant rBAG protein surfaces (BAG3, BAG4, and BAG3-BD) and one unmodified reference surface were prepared for simultaneous analyses. Proteins were immobilized on individual sensor chip surfaces at a flow rate of 10 μL min^{-1}, using standard amine-coupling protocols to obtain densities of 8–12 kRU. The assays were performed using the previously identified BAG3-BD inhibitor, **LK1**, as a positive control.

Compound	rBAG3 (full-length) K_D (nM) ± SD	rBAG3BD (domain) K_D (nM) ± SD	rBAG4 (full length) K_D (nM) ± SD
LK1 (lead)	11.1 ± 3.9	6.4 ± 2.2	No binding
LK2	115.2 ± 1.4	No binding	No binding
LK3	No binding	Not evaluated	Not evaluated
LK4	No binding	Not evaluated	Not evaluated
LK5	12.4 ± 1.2	No binding	No binding
LK6	6.3 ± 0.3	27.6 ± 1.9	No binding
LK7	53.1 ± 9.1	45.7 ± 1.7	No binding
LK8	143.5 ± 1.5	No binding	No binding
LK9	24.7 ± 1.8	22.4 ± 0.7	No binding

Table 6: SPR assays of compounds **LK1-LK9** on rBAG3 protein full length, BAG3-BD, and BAG4. Data are given as mean ± S.E.M., n=3.

All the tested molecules, except **LK3** and **LK4**, bound the BAG3 full-length protein with dissociation constants in the low-medium micromolar range. The most promising compounds were: **LK5** (K_D = 12.4 ± 1.2 μM), **LK6** (K_D = 6.3 ± 0.3 μM), and **LK9** (K_D = 24.7 ± 1.8 μM). In particular, **LK6** showed the lowest dissociation constant also compared to the reference compound **LK1** (K_D = 11.1 ± 3.9 μM) (**Experimental section 8.3**). Instead, analyzing the data obtained on isolated BD domain, three molecules bound this protein portion: **LK6** (K_D = 27.6 ± 1.9 μM), **LK7** (K_D = 45.7 ± 1.7 μM), and **LK9** (K_D = 22.4 ± 0.7 μM) (**Experimental section 8.3**). Finally, none of the synthesized molecules were shown to bind the BAG4 protein.

5.5 Biological assays

As the next step, the antiproliferative potency of the molecules was assessed. In more detail, all the compounds have been tested on A375 and HeLa cells, which are known to overexpress BAG3 protein, by a MTT cell viability assay, using

different concentrations (5-50 μM). The IC_{50} values have been calculated after 48 hours of treatment (**Table 7**). [231]

Compound	A375 cell line $IC_{50} \pm SD$ (μM)	HeLa cell line $IC_{50} \pm SD$ (μM)
LK1 (lead)	15.08 ± 0.9	>50
LK2	>50	27.30 ± 1.2
LK3	27.32 ± 1.1	29.54 ± 1.4
LK4	15.47 ± 0.7	42.89 ± 1.2
LK5	25.46 ± 1.1	30.02 ± 1.3
LK6	19.36 ± 1.2	18.67 ± 0.9
LK7	>50	49.37 ± 1.4
LK8	23.15 ± 1.0	25.90 ± 0.8
LK9	28.40 ± 0.9	31.28 ± 1.0

Table 7: The cytotoxic activity of **LK1-LK9** was evaluated as IC_{50} (μM): the concentration of compound that affords cell growth by 50% as compared to control on the following cell lines: A375 and HeLa. Data are given as mean ± S.E.M., n=3.

Several molecules showed IC_{50} values in the micromolar range in both cell lines and, among these, **LK6** displayed the best profile. Therefore, we have evaluated if this compound was capable of inducing a mortality rate in the A375 cell line comparable to the reference **LK1** (**LK1**: IC_{50} = 15.08 ± 0.9 μM; **LK6**: IC_{50} = 19.36 ± 1.2 μM). In addition, for **LK6** an antiproliferative activity against HeLa cell line was also observed (**LK1**: IC_{50} = major than 50 μM; **LK6**: IC_{50} = 18.67 ± 0.9 μM). Having identified **LK6** as the most promising molecule, we decided to further investigate its biological properties in the attempt to clarify how BAG3 activity was functionally modulated. One parameter exploited to evaluate the number of apoptotic cells is the internucleosomal cleavage of DNA, analyzed through the cell cycle analysis method. The propidium iodide (PI) stoichiometrically binds the double helix of the DNA (or double-stranded RNA) providing information on the amount of DNA contained in the cells in relation to the fluorescence intensity (the higher the content of DNA the greater the fluorescence). It is known that the DNA

content varies according to the phase of the cycle reached by a cell. In particular, the G_2 phase and the mitosis (M) have twice the amount of DNA than the phase G_1, while, during the DNA synthesis phase (phase S), the cell has an intermediate amount of DNA between the content in G_1 and G_2. Since the apoptotic cells, when resuspended in an appropriate buffer, lose small fragments of DNA, a reduction of PI fluorescence (related to the decrease in DNA content) can be observed. In this way it is possible to evaluate the percentage of apoptotic cells that are positioned in the so-called hypodiploid peak (subG_0/G_1 phase) and, in addition to this, it is possible to evaluate the percentage of cells in the various phases of the cell cycle: G_0/G_1, S, and G_2/M (**Figure 53**). [232]

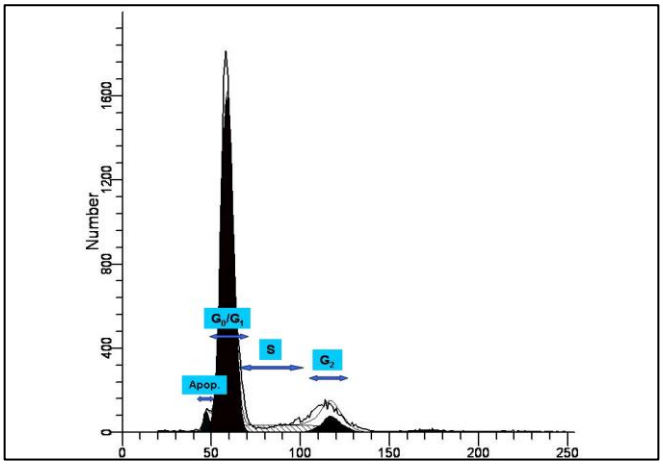

Figure 53: Cell cycle distribution graph observed by propidium iodide staining.

Since BAG3 possesses an antiapoptotic activity, the effect of **LK6** on A375 and HeLa cell cycle distribution by flow cytometry analysis was analyzed. The cells were incubated for 48 h with **LK1** and **LK6** at concentrations 5-10-25μM. Upon treatment with **LK6,** a dose-dependent accumulation in the G_2 phase was observed both in HeLa and A375 cells (**Figure 54a, 55a**). Concerning **LK1**, an accumulation in the G_2 phase was observed in A375 cells, while no evident effect was found in HeLa cells (**Figure 54a**). In agreement with these results, **LK6** treatment in both

cell lines induced a significant increase of the apoptotic response in a dose dependent manner, as depicted in **Figure 54b** and **55b** displaying the hypodiploid nuclei. A dose-dependent increase in hypodiploid nuclei was also observed for **LK1** only in A375 cells (**Figure 54b**).

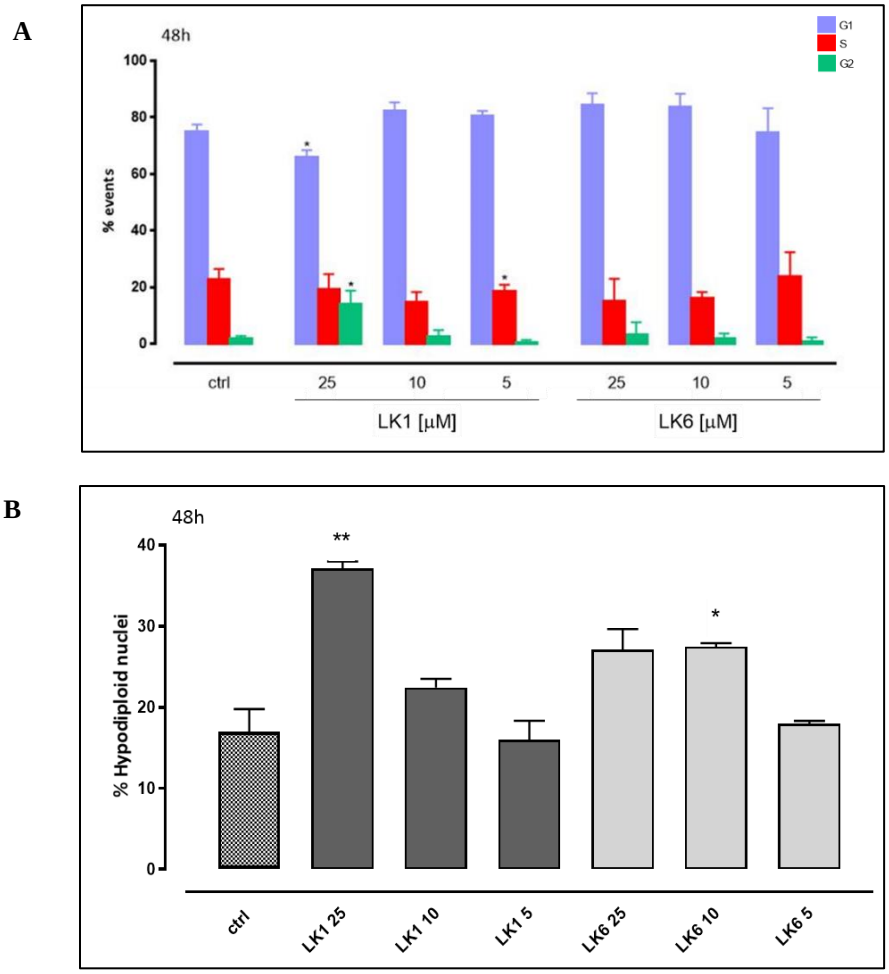

Figure 54: Cell cycle analysis of **a)** DNA content and **b)** hypodiploid nuclei, with propidium iodide staining, were evaluated by flow cytometric assay. A375 cells treated respectively with **LK1** or **LK6** (both 5-10-25 µM) for 48 h. Results are expressed as mean ± S.E.M. of three independent experiments each performed in duplicate. Data were analyzed by Student's t-test. *P<0.05 and **P<0.005 vs non-treated.

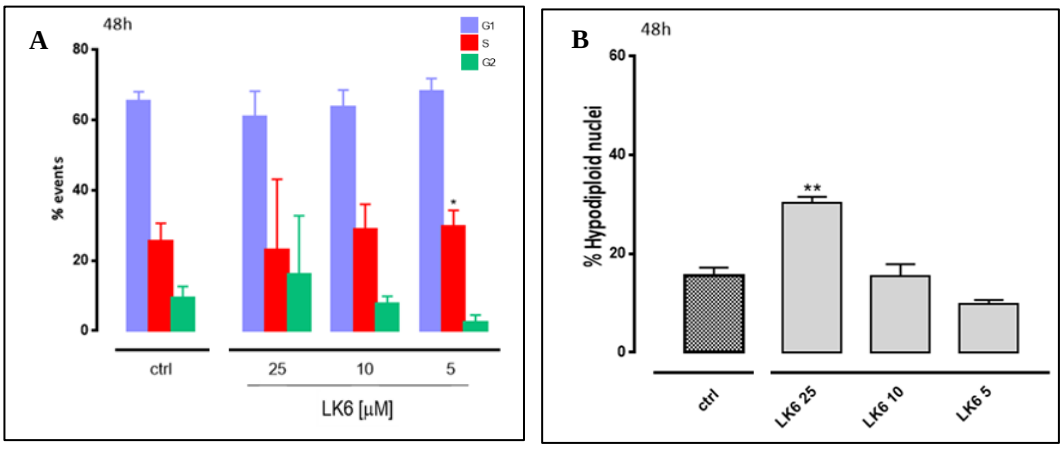

Figure 55: Cell cycle analysis of **a)** DNA content and **b)** hypodiploid nuclei, with propidium iodide staining, were evaluated by flow cytometric assay. HeLa cells treated with **LK6** (5-10-25 µM) for 48 h. Results are expressed as mean ± S.E.M. of three independent experiments each performed in duplicate. Data were analyzed by Student's t-test. *P<0.05 and **P<0.005 vs non-treated.

Since, unlike **LK1**, **LK6** showed to be effective towards HeLa cells, this last was selected to evaluate the expression of caspases. The caspases are a conserved family of cell death proteases that cleave intracellular substrates at Asp residues to modify their function and promote apoptosis. [233] The flow cytometry analysis showed significant and dose-dependent activation of both caspase 3 and caspase 9 levels in cells treated with **LK6** (**Figure 56**).

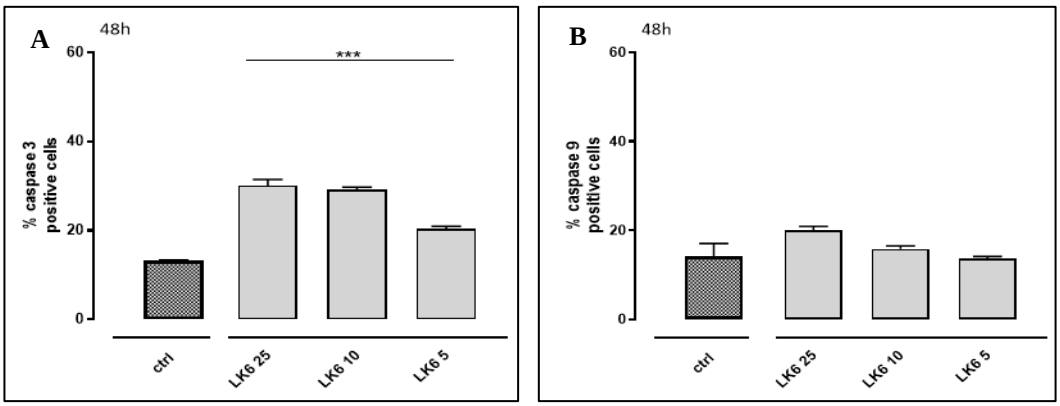

Figure 56: **a)** Caspase 3 and **b)** caspase 9 expressions were detected by flow cytometric analysis. HeLa cells were treated with **LK6** (5-10-25 µM) for 48 h. Results are expressed as mean ± S.E.M. from at least three independent experiments each performed in duplicate. Data were analyzed by Student's t-test. *P<0.05, **P<0.005 and P<0.0001 vs non-treated.

Furthermore, an expression decrease of BAG3 was observed upon **LK6** treatment on HeLa cells. This result confirms the direct interference of **LK6** on BAG3 which is known to self-regulate its levels through a positive feedback mechanism (**Figure 57**). [234]

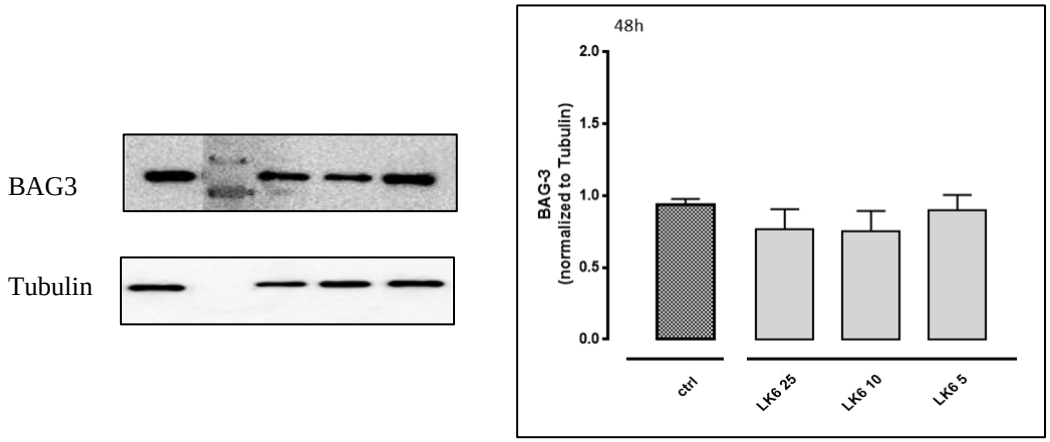

Figure 57: HeLa cells were treated with **LK6** (5-10-25 μM) for 48 h. BAG3 expression was detected by Western blotting. Tubulin protein expression was used as loading control. Results are expressed as mean ± S.E.M. from at least three independent experiments each performed in duplicate. Data were analysed by Student's t test vs non treated.

Taking together, all these data point out the important role of **LK6** in disrupting Hsp70-BAG3 protein-protein interaction, emerging thus both, as an attractive candidate for drug development and a useful tool for further biological investigations of the multifaceted role of this interesting molecular co-chaperone. Hence, by using a *ligand-based approach*, biophysical techniques, and biological assays, the 2,4-thiazolidinedione scaffold was successfully confirmed as a promising chemical platform able to selectively bind and inhibit BAG3-Hsp70 protein-protein interaction.

CHAPTER 6

Identification of mPGES-1 inhibitors

CHAPTER 6
Identification of mPGES-1 inhibitors

6.1 Introduction

In recent years, mPGES-1 is attracting more and more attention as a strategic therapeutic target both, inflammatory and cancer diseases, since its inhibition affects only PGE_2 levels upregulated in pathological conditions, leaving unchanged the levels of the other prostanoids, responsible for key physiological cellular functions. [235] Hence, targeting this synthase it is possible to avoid the gastrointestinal and cardiovascular side effects typical of COX-1/2 or selective COX-2 inhibitors. [236] Despite all the efforts made in developing potential mPGES-1 modulators so far, no inhibitor has reached the market, also because none of the reported potent inhibitors of human mPGES-1 showed to be effective on mouse mPGES-1, preventing, thus, the use of well-established mouse models of inflammatory diseases for preclinical studies. For this reason, the discovery of new promising chemotypes for clinical practice are highly requested. [237]

In the frame of my Ph.D., I have been involved in a project aimed at discovering new mPGES-1 inhibitors as attractive candidates for drug development. Following a *fragment-based* approach and a *structure-based* drug design, a very promising enzyme inhibitor has been disclosed, as well as a dual inhibitor of mPGES-1 and 5-lipoxygenase (5-LO). The phenyl propionic acid, the thiophenyl acetic acid, and the 2,4-thiazolidinedione chemical cores were selected as starting templates for the development of small molecules whose biological properties have been investigated.

6.2 Identification of mPGES-1 modulators

6.2.1 Molecular modelling

In order to develop a small collection of molecules as potential mPGES-1 modulators we decided to rely on commercially available aryl bromides fragments as starting seeds for the construction of more expanded molecular structures, exploiting the Suzuki-Miyaura reaction. [238] We focused on aromatic fragments as starting scaffold, basing on the observation that in the 3D protein structure, several aromatic residues, such as Phe44, His53, and Tyr 130 flank the mPGES-1 binding site. [239]

For this aim a *virtual fragment screening approach* was followed starting from commercially available aromatic bromides (Sigma Aldrich + Otava Chemicals) (**Figure 58**). [240]

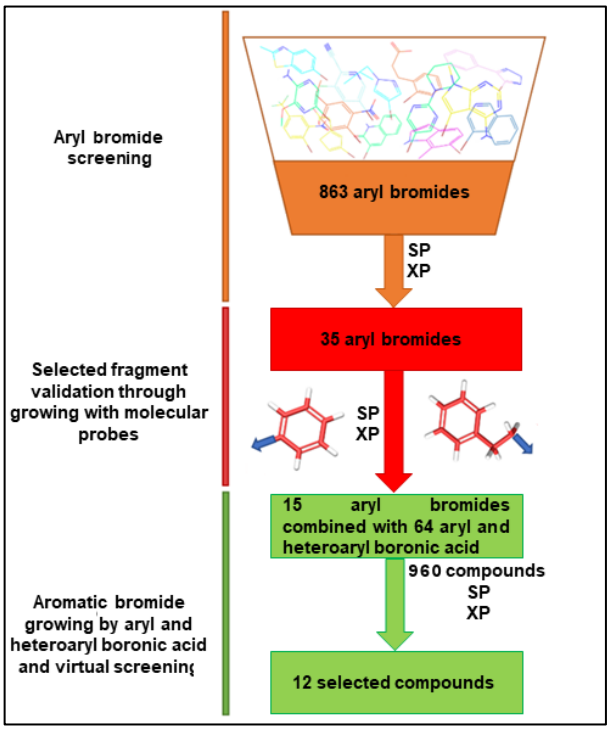

Figure 58: Fragment-based approach workflow.

The library of 863 fragments was virtually screened into the catalytic site of mPGES-1 through the Glide software. [241] As protein model, the high-resolution crystallographic structure of the enzyme linked to GSH (PDB: 4AL0[168]) was employed, as no significant structural changes upon inhibitor binding are observed by comparing the different reported experimental structures. Particular attention was paid to the orientation of the bromine atom representing the functionalization point. The docking results suggested 35 potential scaffolds to be used for chemical modifications. These fragment candidates were expanded by substituting the bromine both, with an aryl, and a phenylethyl moiety as molecular probes, mimicking the boronic acid partners into Suzuki reactions, to evaluate their influence on the binding mode of the parent molecular core. The so built 70 small molecules were subjected to virtual screening which provides to select 15 potential aromatic bromides as electrophile partners in the Suzuki-Miyaura reaction. The docked poses of the selected fragments showed that the bromine atom points towards a 9Å cavity delimited by the transmembrane helices. [238] Consequently, the selected fragments were combined with 64 boronic acids endowed with two aromatic rings, in order to occupy the 9Å pocket, and able to establish π-π interactions, van der Waals contacts, and hydrogen bonds with the macromolecular counterparts. The 960 compounds generated were screened by molecular docking and the results obtained restricted the library to at least two small collections of compounds **SZK1-SZK6** and **SZK7-SZK12** helpful for grasping a basic structure-activity profile (**Figure 59**).

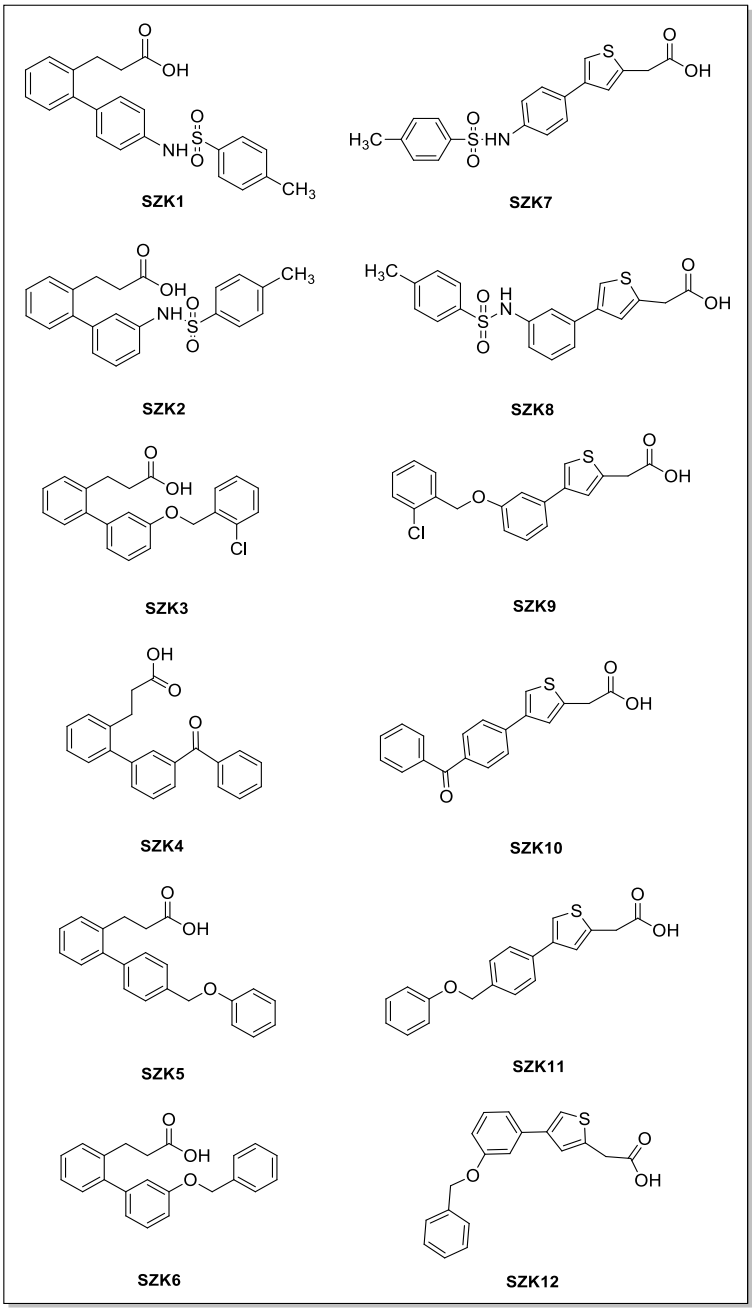

Figure 59: Molecular structure of compound **SZK1-12**.

The two sets of molecules contain as basic units, respectively, a 3-biphenyl-2-yl propionic acid and a 4-phenyl-(thiophen-2-yl) acetic acid, derived from the aromatic bromide fragments coupled with six different boronic acids. The analysis

of the docking poses showed that all the compounds fill equivalent spaces in the catalytic pocket, resulting in a pattern of similar interactions with protein counterparts. They establish H-bonds with Arg52, His53 and Tyr130, like the reported co-crystallized binders of mPGES-1, whereas the 3-phenylpropanoic acid **(SZK1-6**) and the 2-(thiophen-2-yl) acetic acid (**SZK7-12**) portions establish van der Waals contacts with Gly35, Leu39, Phe44, Arg52, His53, Ala123 and Pro124. [169, 170, 174] An example is shown in **Figure 60**.

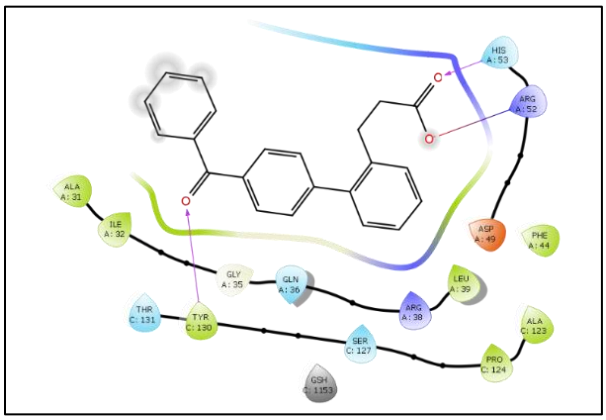

Figure 60: 2D representation of **SZK4** in the binding site of the crystal structure of human mPGES-1 (PDB: 4AL0[168]). H bond interactions are reported as pink arrows. Hydrophobic residues are depicted in green, positive and negative charge residues in blue and orange respectively, polar residues in light blue, and glycine in light grey.

6.2.2 Chemical synthesis

The synthesis of compounds **SZK1-6** and **SZK7-12** was accomplished by a Suzuki–Miyaura cross-coupling reaction of 3-(2-bromo-phenyl)-propionic acid (**22**) or (4-bromo-thiophen-2-yl)-acetic acid (**23**) with selected arylboronic acids/esters (**a-f**), bearing various substitution patterns, as reported in **Scheme 11**. By means of the conventional Suzuki-reaction protocol the designed compounds were easily prepared in goods yields and under mild conditions. [238, 242]

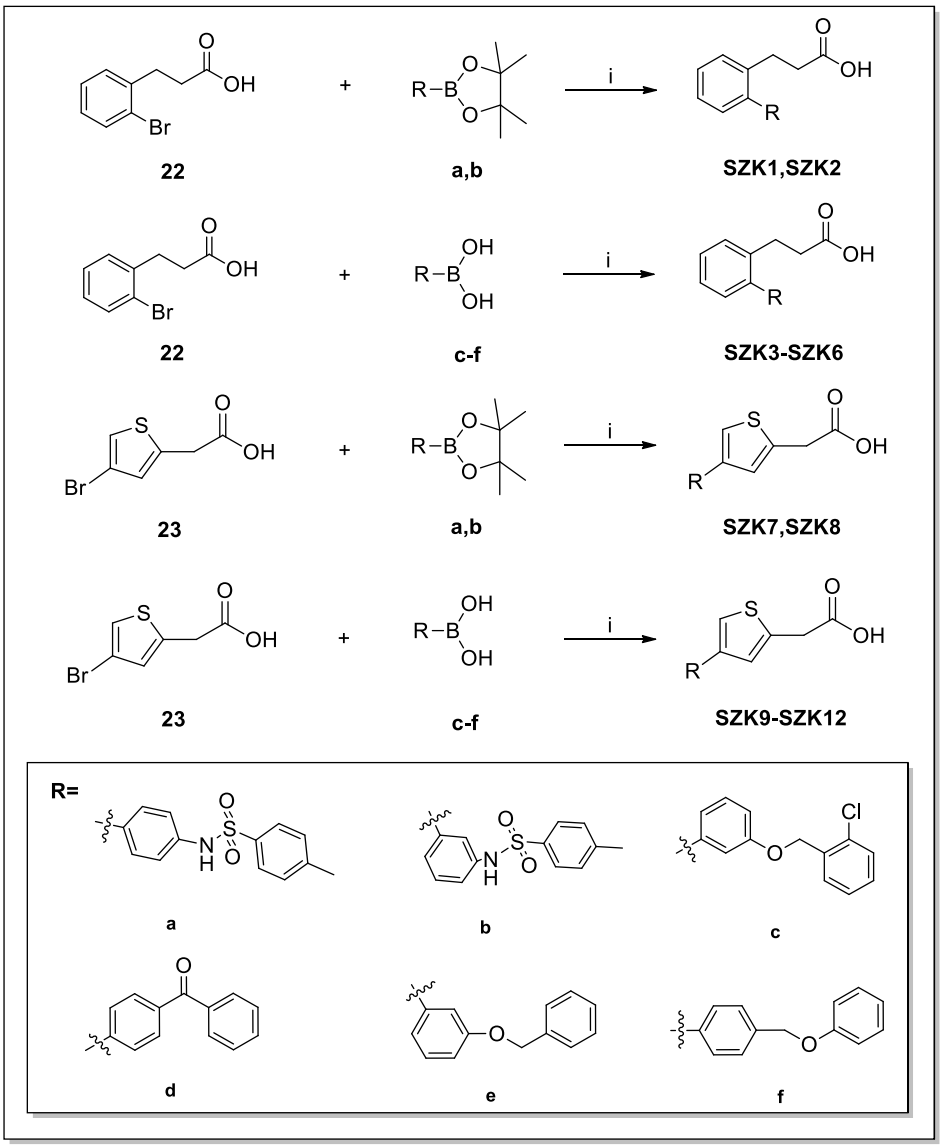

Scheme 11: Synthetic procedure for the **SZK1-SZK12** compounds.

Reagents and conditions: i) $Pd(PPh_3)_4$, K_2CO_3, dioxane/H_2O (2:1), reflux, overnight.

6.2.3 Biological investigation

In order to evaluate the inhibitory activity of compounds **SZK1-SZK12** on the target enzyme, the human mPGES-1, derived from the microsome interleukin-1β-stimulated of A549 cell line, was used in a cell free assay. All the compounds were tested at 10μM and the residual mPGES-1 activity was detected. The experiments showed that **SZK3** and **SZK9** exhibit the highest inhibitory activity (>60%). **SZK2** displayed a less potent activity (enzyme inhibition of 42%), while the remaining compounds were able to produce an inhibition of only 20-25% (**Figure 61**).

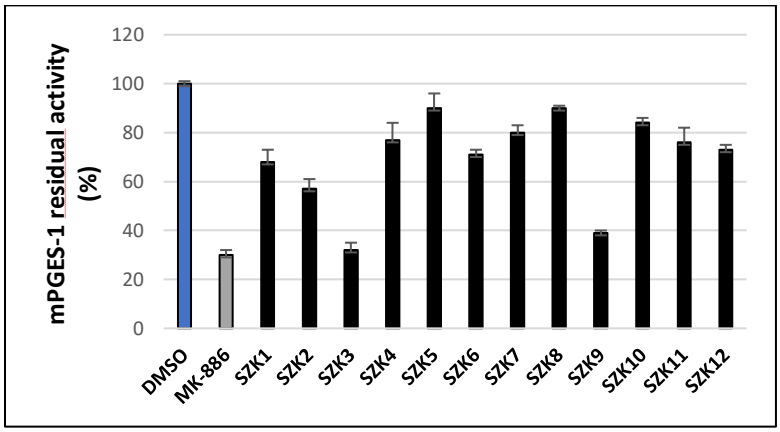

Figure 61: Inhibition of mPGES-1 by compounds **SZK1-12** and **MK-886** (10 μM) in a cell-free enzyme activity assay. The percentage of residual mPGES-1 activity is calculated respect to the control. Data are given as means ± S.E.M., n = 3. ***, p <0.001.

The inhibitory activity of **SZK3** and **SZK9** was then further investigated in order to evaluate their IC_{50} values against mPGES-1, using the same assay. Comparable IC_{50} values in the low micromolar range were observed: **SZK3** (IC_{50} = 3.4 ± 0.5 μM) and **SZK9** (IC_{50} = 5.9 ± 1.0 μM). To verify the downstream effects of these molecules, an ELISA experiment was set in order to assess the PGE_2 production in cell. Both molecules significantly reduce cytokine-induced PGE_2 production (>80%) as shown in **Figure 62**.

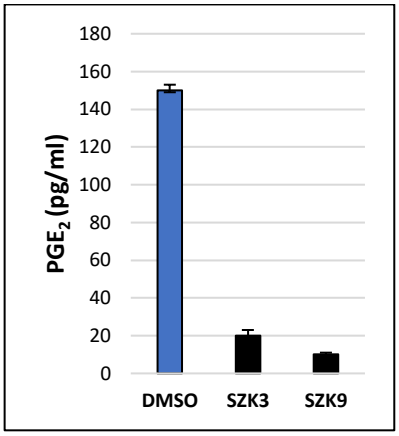

Figure 62: The A549 cells was incubated for 24 h with 10 µM of compounds in conditioned medium (1% FBS and 10 ng/ml IL-1β). The PGE_2 released into medium was quantified using a specific ELISA kit assy. The results were compared with control cells IL-1β stimulated and treated with chemical vehicle (DMSO) and expressed as mean ± S.E.M. (pg/ml) of two different experiments.

To exclude the possible effects on the formation of other prostanoids, the impact of **SZK3** and **SZK9** on both COX-1 and COX-2 was investigated by cell free assay. These two enzymes were incubated with **SZK3** and **SZK9** at 10µM or with the vehicle (0.1% DMSO) and the formation of 12-hydroxyheptadecatrienoic acid (12-HHT) was quantified. The compounds do not compromise the activity of the COXs, confirming their selectivity against mPGES-1, which is functionally linked to the inducible isoform COX-2 (**Figure 63a,b**).

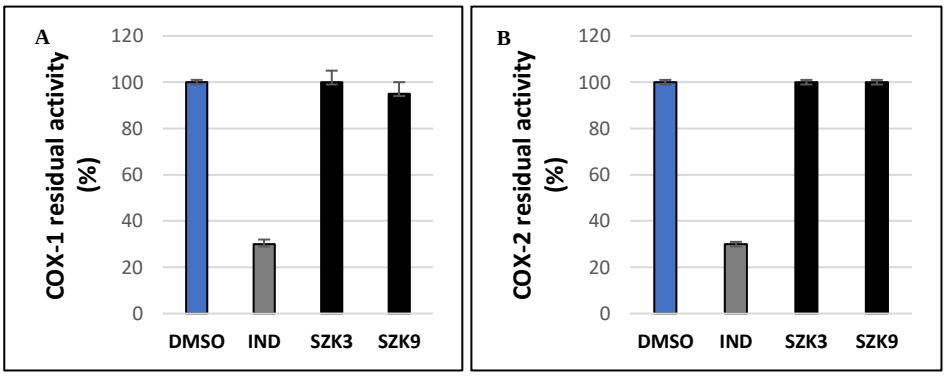

Figure 63: Residual activity of **a)** COX-1 and **b)** COX-2 after incubation with compounds **SZK3**, **SZK9** and indomethacin (10 µM) or vehicle (0.1% DMSO). Data are expressed as percentage of control (100%), n = 3.

As discussed in the previous section, mPGES-1 is highly expressed and strongly associated with signaling pathways in several types of malignant cells, hence, the decrease in mPGES-1 activity could inhibit cell proliferation, induce apoptosis and cell cycle arrest. Basing on these premises, the anti-proliferative activity or cytotoxic effect of **SZK3** and **SZK9** (5-100μM) were assessed after an exposure for 24, 48, and 72 h in A549 cells, determining cell viability by MTT assay. A known inhibitor of mPGES-1, **CAY10526**, was used as a positive control. [199] As showed in **Table 7**, compounds **SZK3** and **SZK9** inhibit cancer cell viability, showing a good cytotoxic activity comparable to the known inhibitor.

Compound	**IC_{50} ± SD (μM)**		
	24h	**48h**	**72h**
SZK3	90.3 ± 1.5	48.2 ± 1.1	36.4 ± 1.5
SZK9	65.5 ± 1.2	18.1 ± 0.9	10.1 ± 1.2
CAY10526	62.5 ± 0.5	12.5 ± 1.1	9.1 ± 1.3

Table 7: Cell viability assay of mPGES1 inhibitors in A549 cancer cell line. IC_{50} (μM) values are given as mean ± S.E.M. of single determinations obtained in three independent experiments at different exposures (24, 48,72 h).

Since **SZK9** showed the best IC_{50} value after 48 and 72h of exposure, it was chosen for further analysis, and in particular its effect on cell-cycle was determined. The cell cycle progression of A549 cells by flow cytometry was evaluated using concentrations close to its IC_{50} value (**Figure 64**).

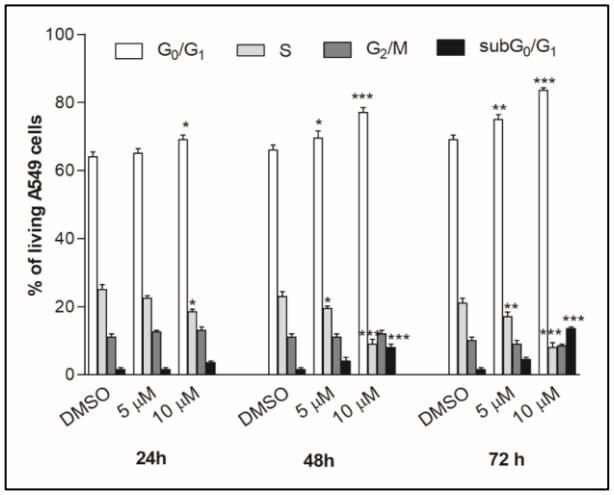

Figure 64: Cell cycle progression. A549 cancer cells were treated for 24, 48 or 72 h with compound **SZK9** used in different concentrations. Percentage of cell cycle stages was analyzed by flow cytometry with DNA propidium iodide staining. Results are expressed as means ± S.E.M. of two independent experiments performed in triplicate (*P < 0.05, **P < 0.005, ***P < 0.001).

SZK9 showed a modest cytostatic activity after 24h and this effect increased after 48 and 72h. Furthermore, the cell exposure to **SZK9** at 10µM for 48 and 72h caused an increase of $subG_0/G_1$ fraction (about 8.0 ± 0.9% and 13.5 ± 0.5%, respectively), suggesting an apoptosis/necrosis event.

This compound, therefore, can be considered an interesting hit particularly worthy of attention for the development of tighter mPGES-1 binders with anti-cancer properties.

6.3 Identification of mPGES-1/5-LO inhibitors

6.3.1 Computational studies

In the frame of the project focused on mPGES-1, a part of the research was devoted to identify new interesting hits able to inhibit the enzyme starting from the 2,4-thiazolidinedione core, representing a "privileged scaffold" and, thus, was useful for the rapid discovery of leads with drug-like properties. [243-245] Hence, as first step a molecular modeling was performed in order to dock the 2,4-thiazolidinedione

core (with minimal substitutions in positions 3 and 5) on the crystallographic structure of mPGES-1 and to evaluate the binding mode and the appropriate decorations required for assuring an optimal interaction with the receptor counterpart. The analysis of the docking poses highlighted that the 2,4-thiazolidinedione core is positioned in the central part of the mPGES-1 binding site near the glutathione cofactor (GSH), suggesting that the modifications in position 3- and 5- of the scaffold could be favorable for increasing the binding affinity (**Figure 65**).

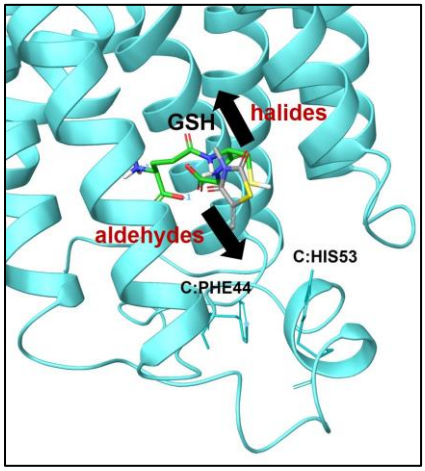

Figure 65: Molecular docking pose of the 2,4-thiazolidinedione core (with minimal substitutions at positions 3 and 5) highlighting the directions for the subsequent substitutions with aldehydes and halides.

Preliminary substitutions of the C-5 position with aldehydes oriented the newly introduced groups towards the cytoplasmic part of the protein, thus close to C:His53 and C:Phe44 residues. Therefore, aromatic aldehydes were preferred in order to establish edge-to-face π-π interactions with these residues which turned out to be essential for the enzyme inhibition.

The other available position (N-3) was exposed toward the endoplasmic reticulum membrane, so that, a substituent placed there could establish further edge-to-face π-π interactions (with A:Phe130 and or C:Tyr28) and polar interactions (with

A:Gln134 and peptide bond of the close residues). For this reason, a small set of halides with aromatic and polar groups was selected. The choice of the reactants was limited both, by the need to respect the molecular weight filter on the final molecules imposed to obtain compounds with good drug-like properties, and to ensure satisfying structured viability inside the library.

Basing on these premises, a large library of compounds with a 2,4-thiazolidinedione core substituted in the 3- and 5- positions was built *in silico*. The commercially available synthons were 33229, then narrowed to 20542 by filtering the "non-drug like" compounds (**Figure 66**).

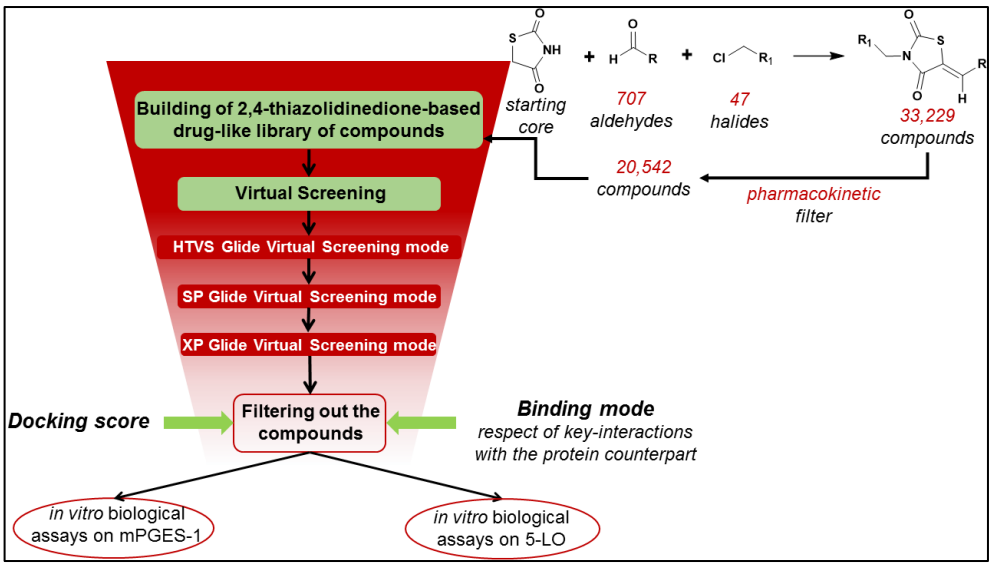

Figure 66: The workflow for the identification of the 2,4-thiazolidinedione-based mPGES-1/5-LO inhibitors.

The obtained library was then screened by molecular docking calculations on mPGES-1. Specifically, the semi-flexible docking procedure, considering the protein as rigid and the ligand as flexible, was used. The 3D protein structure used for molecular modeling experiments was related to the crystallographic structure of the enzyme co-complexed with the powerful 4UL inhibitor (PDB code: 5BQI). [169]

The highest scoring molecules, reported in **Figure 67**, were selected for chemical synthesis.

6.3.2 Chemical synthesis

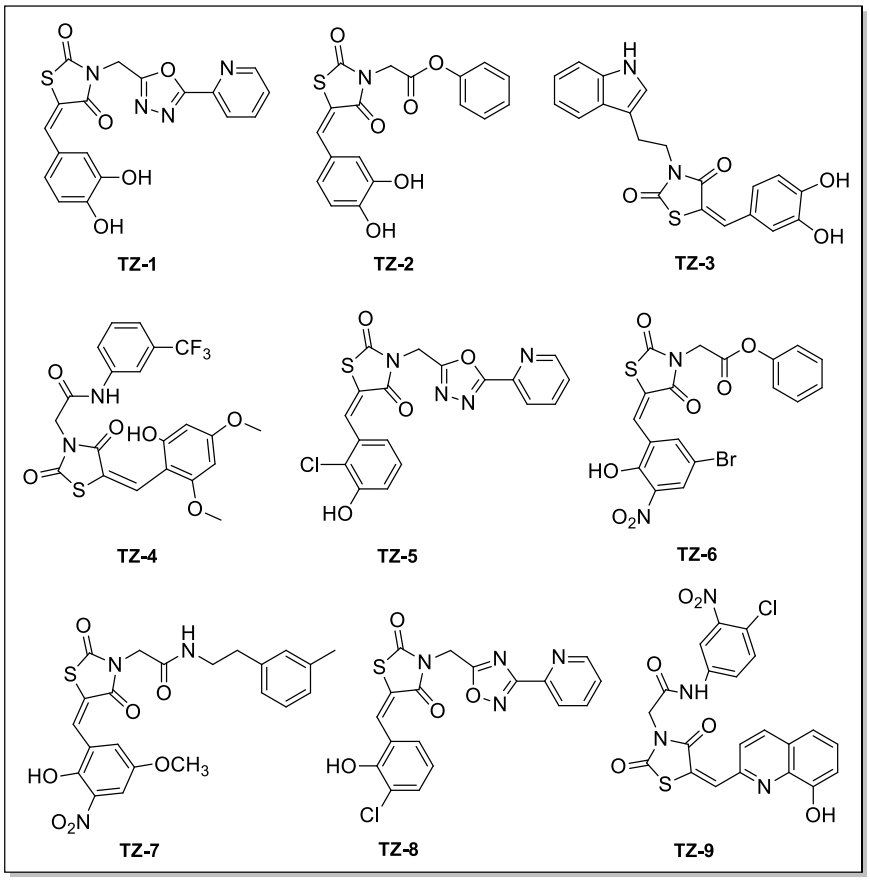

Figure 67: Chemical structures of **TZ1**-**TZ9**.

For the synthesis of **TZ1-TZ9** we started with the N-alkylation of the commercially available 2,4-thiazolidinedione (**24**) to obtain the N-substituted derivatives (**25a-25d**) (**Scheme 11**). [228]

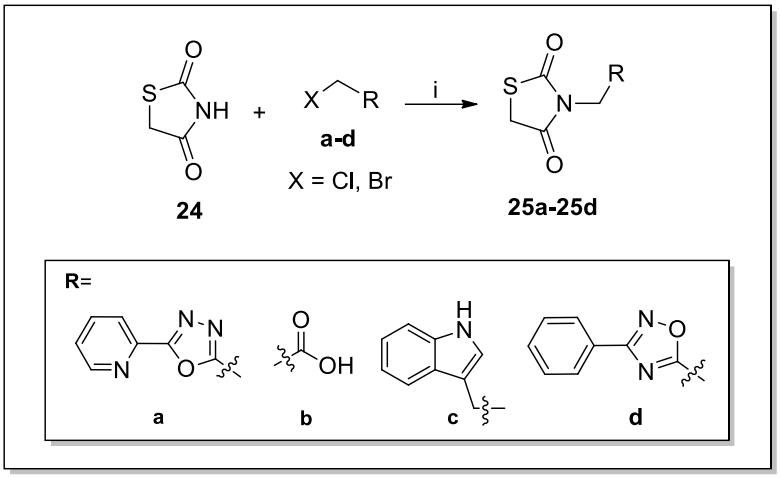

Scheme 11: Synthetic procedure for compounds **25a-25d.**
Reagents and conditions: i) NaH, THF dry, reflux, 24h.

25a-25d were subjected to Knoevenagel condensation using differently substituted aromatic aldehydes (**e-k**) (**Scheme 11**). [228] According to this procedure, we synthesized compounds **TZ1**, **TZ3**, **TZ5**, and **TZ8** and the intermediates **26be, 26bf, 26bh, 26bj,** and **26bk**.

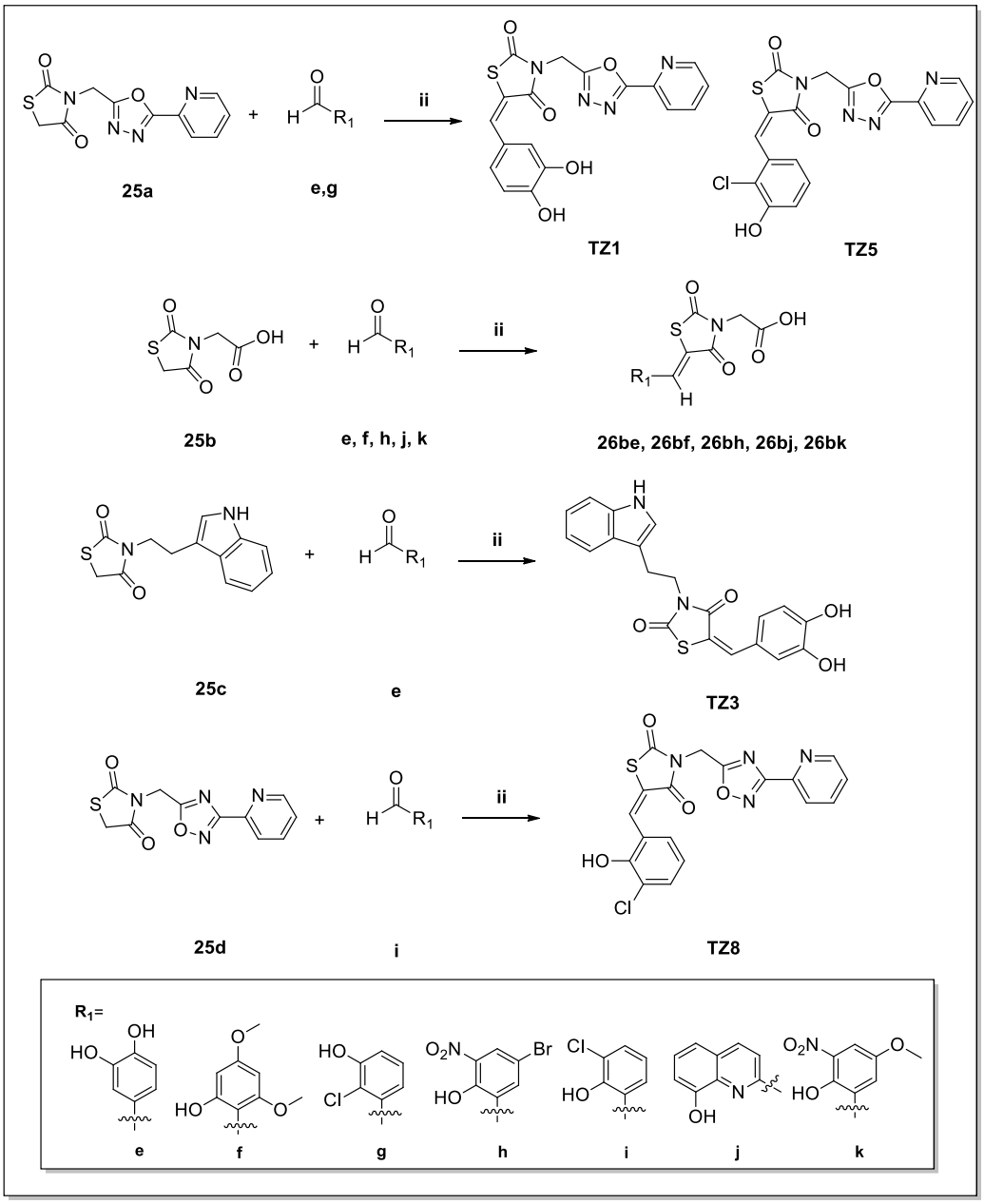

Scheme 12: Synthetic procedure for **TZ1**, **TZ3**, **TZ5**, **TZ8**, **26be**, **26bf**, **26bh**, **26bj**, and **26bk**
Reagents and conditions: ii) piperidine, EtOH, reflux, overnight.

The synthesis of **TZ2** and **TZ6** was performed by esterification of **26be** and **26bh** with phenol; while compounds **TZ4**, **TZ7** and **TZ9** were obtained by amide

coupling of **26bf**, **26bk** and **26bj**, respectively, with different decorated anilines (**m-o**) (**Scheme 13, 14**).

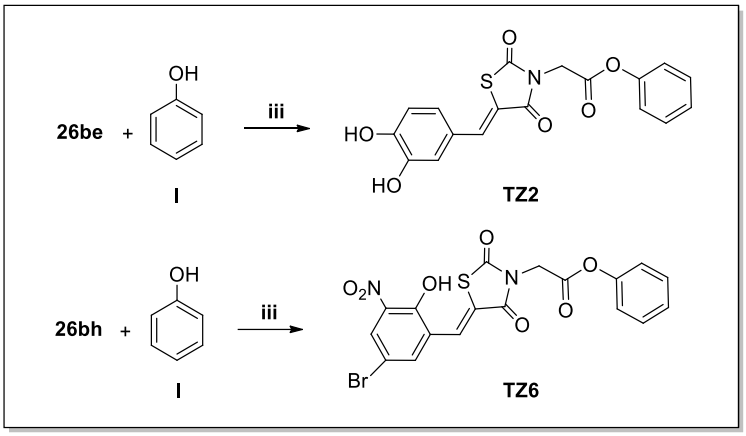

Scheme 13: Synthetic procedure for compounds **TZ2** and **TZ8**.
Reagents and conditions: iii) DMAP, DIC, DCM, rt, overnight.

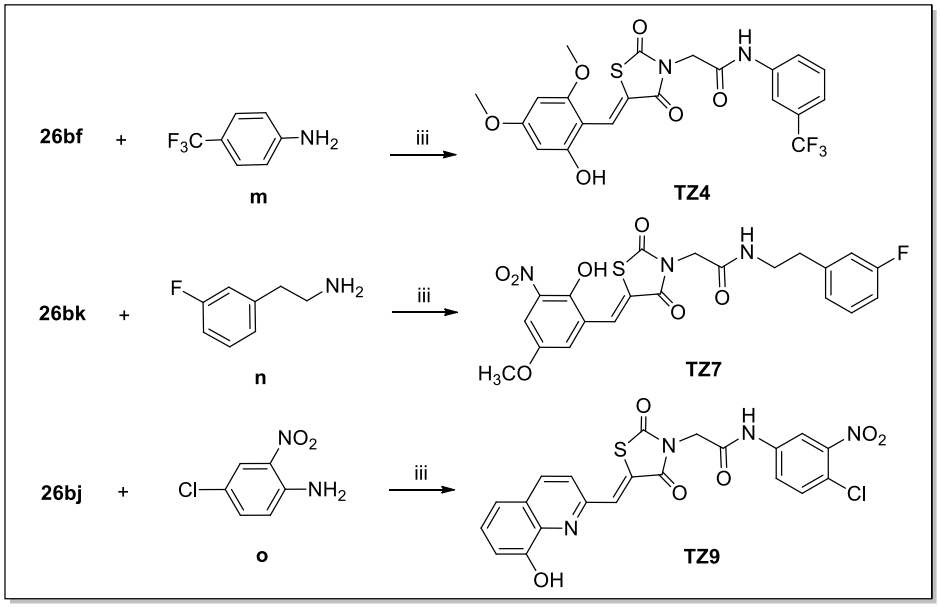

Scheme 14: Synthetic procedure for compounds **TZ4**, **TZ7**, and **TZ9**.
Reagents and conditions: iii) HOBt, DIC, DMF, rt, overnight.

6.3.3 Biological assays

In order to investigate the biological profile of the synthesized molecules, their ability to inhibit mPGES-1 activity was determined by means of a cell-free based, using the microsomal fractions of A549 cells stimulated by IL-1β as a source of human mPGES-1. The synthesized molecules, solubilized in DMSO, were tested at a final concentration of 10μM.

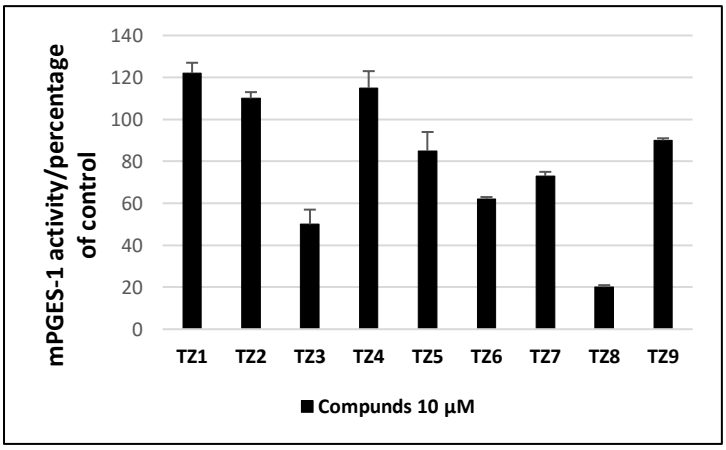

Figure 68: mPGES-1 remaining activity in the presence of compounds **TZ1-TZ9** at 10μM final concentration. Data are given as mean ± S.E.M., number of replicates (n) = 3.

TZ8 showed the most promising inhibitory activity (~85% inhibition), **TZ3** and **TZ6** partially inhibited the enzyme (~50% inhibition), while **TZ7** showed a modest inhibition (~25% inhibition) (**Figure 68**). In order to assess their potency, their IC_{50} was determined. Compound **TZ8** (IC_{50} = 3.5 ± 0.4μM) proved to be the most potent inhibitor of mPGES-1 (**Table 8**).

Compound	Cell-free mPGES-1 remaining activity at 10μM compound	Cell free mPGES-1 IC_{50} (μM)
TZ1	100%	ND
TZ2	100%	ND
TZ3	50%	10.2 ± 3.6
TZ4	100%	ND
TZ5	80%	ND
TZ6	60%	14.0 ± 1.7
TZ7	70%	22.5 ± 4.9
TZ8	15%	3.5 ± 0.4
TZ9	90%	ND

Table 8: Cell-free mPGES-1 remaining activity at [ligand]=10μM, cell-free mPGES-1 IC_{50} values for tested compounds **TZ1-TZ9**. Data are given as mean ± S.E.M., n=3.

To rationalize its interesting biological outcome, the putative binding mode of **TZ8** was analyzed in details. The docking studies showed a favorable accommodation of **TZ8** in the mPGES-1 binding site where it established a large set of interactions with key residues. Specifically, edge-to-face π-π interactions between the terminal 3-chloro-2-hydroxyphenyl group of **TZ8** with C:Phe44 and C:His53 were detected; also, a series of polar interactions were established with A:Arg126, A:Thr131, C:Gln36, and C:Asp49 as well as edge-to-face π-π interaction and hydrogen bond with A:Tyr130 in a region close to the GSH cofactor (Figure X). Similar interactions were found for compounds **TZ3**, **TZ6,** and **TZ7** (**Figure 69**).

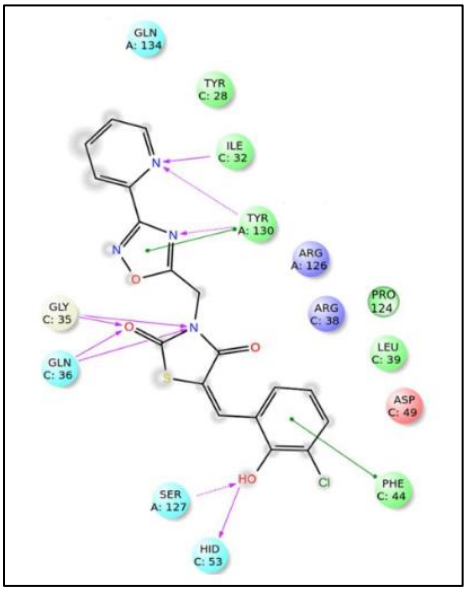

Figure 69: Selected 2D pose of **TZ8** in docking with human mPGES-1 representing interactions (violet arrows representing H-bonds, and green lines representing π-π stacking interactions).

Since several lipophilic mPGES-1 inhibitors have been reported to suppress the activity of 5-LO, the enzyme responsible for leukotriene biosynthesis, to fully understand the biological profile of the most active molecules, their effects against 5-LO were also evaluated. Cell-free assays were performed using partially purified human recombinant 5-LO. The results obtained showed a potent inhibitory activity for **TZ3**, **TZ6-TZ8** with IC_{50} values in the low micromolar, in particular, **TZ3** turned out to possess the highest potency ($IC_{50} = 0.2 \pm 0.1$ μM) (**Table 9**).

Compound	Cell-free 5-LO IC_{50} (µM)[a]
TZ1	ND
TZ2	ND
TZ3	0.2 ± 0.1
TZ4	ND
TZ5	ND
TZ6	3.9 ± 0.8
TZ7	11.8 ± 2.4
TZ8	9.4 ± 4.0
TZ9	ND

Table 9: Cell-free 5-LO IC_{50} values for tested compounds **TZ1-TZ9**. Data are given as mean ± S.E.M., n=3.

The dual inhibition of both mPGES-1 and 5-LO, two crucial enzymes in the production of the pro-inflammatory mediators PGE_2 and leukotrienes, respectively, can provide a better resolution of inflammatory disorders, including inflammation-triggered cancer, considering that one hallmark of unresolved inflammation is the elevated levels of both these lipid mediators. Hence, the disclosed compound **TZ3**, based on its favorable dual-target inhibitor profile, can be of interest for the development of novel therapeutic interventions.

Conclusions

Conclusions

The research work carried out in the frame of my Ph.D. project has been devoted to the study of new and attractive biological targets involved in inflammation and cancer progression. The crosstalk between cancer cells and inflammatory mediators has been known for a long time, even though the complex pathways and correlations have not been fully clarified yet; however, the discovery of small molecules able to act at the crossroad of these two signaling pathways is highly requested. In this research field, considerable efforts have been carried out leading to the identification of new modulators of emerging macromolecular targets involved, at different levels, in cancer and inflammatory-related diseases. Among these, the Heat Shock Factor (HSF1), the Bcl2-associated athanogene 3 (BAG3), and the microsomal Prostaglandin E Synthase-1 (mPGES-1) are of great interest in virtue of their biological importance and their potential for therapeutic applications. The workflow that guided the research of potential modulators of these three targets was based on an integrated approach including computational studies, chemical synthesis, biophysical assays, and in-cell assays.

Concerning HSF1, starting from the HSF1-DBD crystallographic structure in complex with an HSE, two types of virtual screening, considering two different possible binding pockets for small molecules were performed both, on a large library of commercially available compounds, and molecules generated through CombiGlide procedure. The selected molecules were purchased or synthesized and, to evaluate the affinity for the considered target, SPR assays were carried out. The more promising molecules, during my period abroad, were screened employing a gene reporter assay to assess their ability to interact with HSF1 through its DBD. After an extensive biological evaluation, two interesting compounds as HSF1 modulators were identified: **BD-1**, possessing a 2,4-thiazolidinedione scaffold, and **LAM17**, showing a pyrimidone containing bis-heterocycles structure. Although they are not very powerful, they may represent an interesting starting point for

further medicinal chemistry studies. In particular, **BD-1** and **LAM17** will be subjected to further in-depth computational studies in order to understand their binding mode with the receptor counterpart; afterwards, they will be used as lead compounds for the generation of new molecules collections useful for the identification of more potent and selective inhibitors.

Starting from the first disclosed BAG3 inhibitor, **LK1**, discovered by our research group, using a *structure-based drug design*, a new collection of differently decorated compounds featuring a 2,4-thiazolidinedione core, potentially able to modulate BAG3, was designed and synthesized. The affinity towards the target of interest was evaluated by performing SPR assays using both, the full-length BAG3 protein, and the isolated BAG domain. Performing a more extensive biological evaluation of the selected molecules, an interesting compound, **LK6**, was disclosed as a new antiproliferative agent which interferes with BAG3-Hsp70 complex formation. These promising results may stimulate further research toward the identification of more potent and selective inhibitors of this protein-protein interaction. **LK1** and **LK6**, the two molecules currently known as selective modulators of the BAG3-BD, both possess a 2,4-thiazolidinedione core, consequently, as next step a scaffold hopping procedure can be applied in the aim of discovering structurally novel compounds as potential BAG3 modulators.

The use of a proper qualitative *structure-based* filter, together with the docking binding predicted affinities, represented an excellent approach for the discovery of new mPGES-1 inhibitors. This strategy allowed to exploit the phenyl propionic acid, the thiophenyl acetic acid, and the 2,4-thiazolidinedione as starting templates for the development of small molecules whose biological properties have been investigated. Thanks to this method, a very promising compound **SZK9**, possessing a substituted thiophenyl acetic acid core, with a potent and selective inhibitory activity towards mPGES-1 was successfully identified. Furthermore, following a "privileged structure" repurposing strategy, another interesting compound, **TZ3**, showing a decorated thiazolidinedione scaffold was discovered. This compound

displayed a dual inhibitory profile, being able to affect both, mPGES-1 and 5-LO, two key enzymes in the production of proinflammatory mediators and therefore potentially useful for the development of new effective anti-inflammatory drug candidates. Currently, in order to better define the pharmacological profile of these two disclosed molecules *in vivo* tests on mice are underway.

Experimental section

CHAPTER 7

Synthesis of a small collections of potential HSF1 modulators

CHAPTER 7

Synthesis of a small collections of potential HSF1 modulators

7.1 General synthetic methods

All commercially available starting materials were purchased from Merck or Fluorophen Ltd© and used without further purification. The solvents for the synthesis were of HPLC grade (Merck). NMR spectra (^{1}H, ^{13}C) were recorded on Bruker Advance 400 MHz or 500 MHz instruments, T = 298 K. Compounds were dissolved in 0.5 mL of CD_3OD, $CDCl_3$ or $(CD_3)_2SO$ (Merck, 99.8 Atom %D). Coupling constants (*J*) are reported in Hertz, and chemical shifts are expressed in parts per million (ppm) on the delta (δ) scale relative to the solvent peak as the internal reference. Multiplicities are reported as follows: s, singlet; d, doublet; dd, doublet of doublets; ddd, doublet of doublet of doublets; td, triplet of doublets; t, triplet; dt, doublet of triplets; ddt, doublet of doublet of triplets; q, quartet; m, multiplet. Mass spectrometry experiments were performed using a Q-ToF Premiere™ instrument (Waters, Co.®) equipped with an ESI source, or using a LTQ Orbitrap XL™ mass spectrometer (Thermo Scientific™). The reactions were monitored on silica gel 60 F254 plates (Merck) and the spots were visualized under UV light (λ = 254 nm, 365 nm). Analytical and semi-preparative reversed-phase HPLC was performed on Agilent Technologies, Inc.© 1200 Series high performance liquid chromatography using a Nucleodur© C8 reversed-phase column (100 x 2 mm, 4 μM, 80 Å, flow rate = 1 mL/min; 250 x 10.00 mm, 4 μM, 80 Å, flow rate = 4 mL/min respectively, Macherey-Nagel©). The binary solvent system (A/B) was as follows: 0.1% TFA in water (A) and 0.1% TFA in CH_3CN (B). The absorbance was detected at 240 nm. All biologically tested compounds were determined to be >98% pure by HPLC analysis and NMR data.

7.2 Quinazolinone derivatives (MO1-MO14)

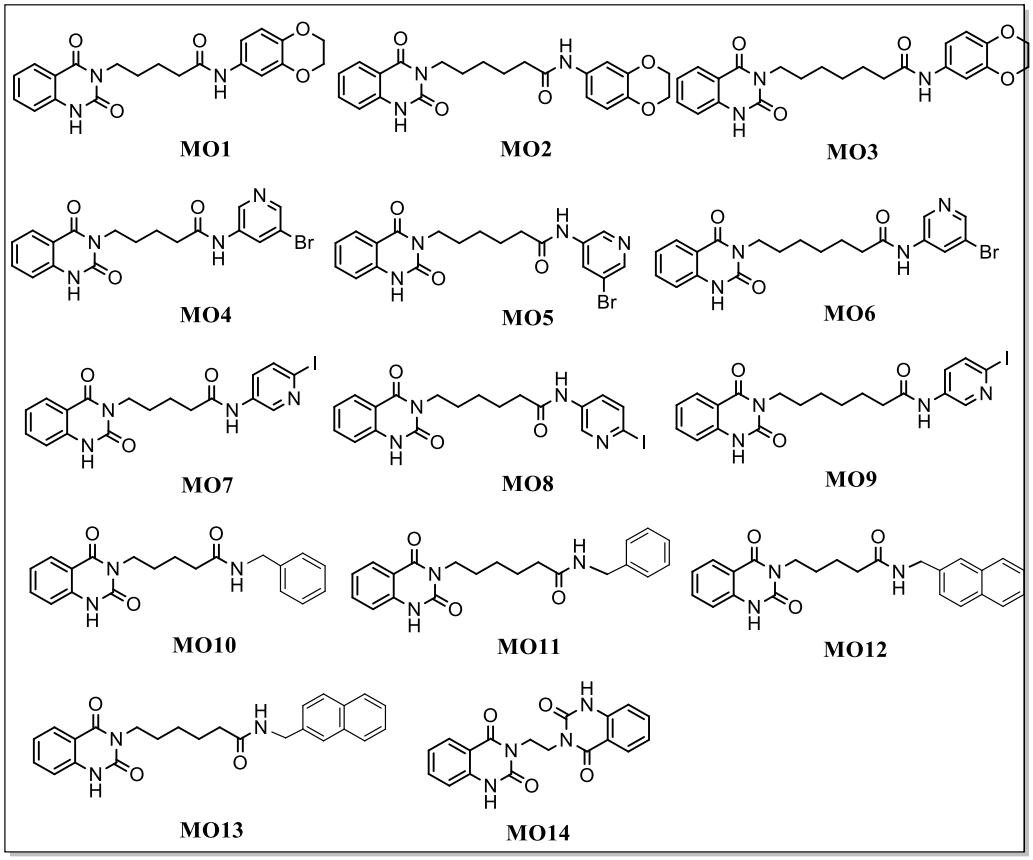

7.2.1 General procedure (A) for the synthesis of 3a-3c, and 4

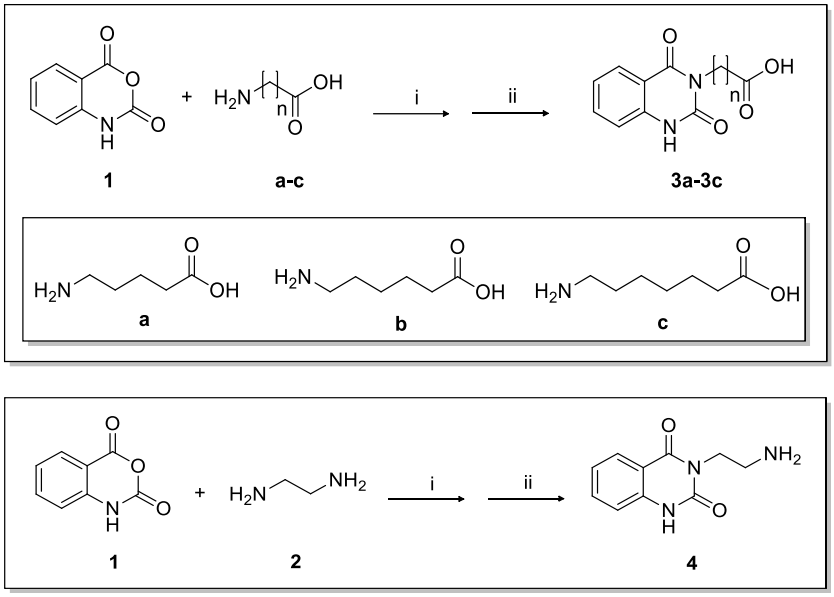

Synthetic scheme 1: i) Et_3N, H_2O, 2h, rt; ii) HCOOH, 7h, reflux.

Triethylamine (1.0 equiv) was added to a solution of **a-c** (1.0 equiv) or **2** (1.0 equiv.) in water (2.6 mL) followed by a portion wise addition of isatoic anhydride **1** (1.1 equiv). The reaction mixture was stirred for 2 hours at 30-40°C, cooled to room temperature and evaporated in vacuum. Then, the obtained oil residue was refluxed for 7 hours in formic acid (3.6 mL), cooled to room temperature and evaporated (**Synthetic scheme 1**). [246] The obtained powder was resuspended in water, extracted with DCM (3 x 25 mL), dried over anhydrous Na_2SO_4, filtered, and concentrated. The desired compounds **3a-3c**, **4** were confirmed by analytical RP-HPLC (Nucleodur© C8 reversed-phase column: 100 x 2 mm, 4 µM, 80 Å, flow rate = 1 mL/min) and ^{1}H NMR spectra. They were used without any further purification for the next step.

5-(2,4-dioxo-1,2-dihydroquinazolin-3(4*H*)-yl)pentanoic acid (3a)

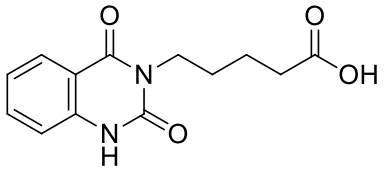

Compound **3a** was obtained by following the general procedure (**A**) as a brown solid (670 mg, 85% yield by HPLC analysis). RP-HPLC t_R = 14.9 min, gradient condition: from 5% B ending to 100% B 40 min, flow rate of 4 mL/min, λ = 240 nm. ^{1}H NMR (400 MHz, CD_3OD): δ_H = 8.55 (s, 1H), 8.29 (d, *J* = 8.0 Hz, 1H), 7.89 (t, *J* = 7.7 Hz, 1H), 7.73 (d, *J* = 8.2 Hz, 1H), 7.62 (t, *J* = 7.6 Hz, 1H), 4.13 (t, *J* = 7.3 Hz, 2H), 2.40 (t, *J* = 7.3 Hz, 2H), 1.88 (quint, *J* = 7.4 Hz, 2H), 1.71 (quint, *J* = 7.4 Hz, 2H).

6-(2,4-dioxo-1,2-dihydroquinazolin-3(4*H*)-yl)hexanoic acid (3b)

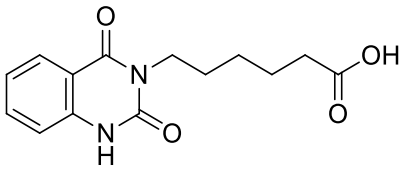

Compound **3b** was obtained by following the general procedure (**A**) as a brown solid (680 mg, 90% yield by HPLC analysis). RP-HPLC t_R = 15.6 min, gradient condition: from 5% B ending to 100% B 40 min, flow rate of 4 mL/min, λ = 240 nm. ^{1}H NMR (400 MHz, CD_3OD): δ_H = 8.27 (d, *J* = 8.0 Hz, 1H), 7.85 (t, *J* = 7.7 Hz, 1H), 7.72 (d, *J* = 8.1 Hz, 1H), 7.59 (t, *J* = 7.6 Hz, 1H), 4.09 (t, *J* = 7.3 Hz, 2H), 2.42 (t, *J* = 7.5 Hz, 2H), 1.85 (quint, *J* = 7.5 Hz, 2H), 1.45 (quint, *J* = 7.4 Hz, 2H), 1.29 (quint, J = 7.5 Hz, 2H).

7-(2,4-dioxo-1,2-dihydroquinazolin-3(4*H*)-yl)heptanoic acid (3c)

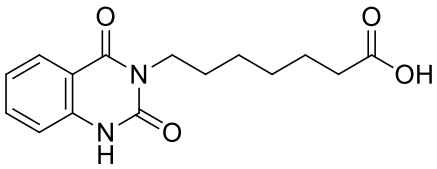

Compound **3c** was obtained by following the general procedure (**A**) as a brown solid (720 mg, 75% yield by HPLC analysis). RP-HPLC t_R = 17.9 min, gradient condition: from 5% B ending to 100% B 40 min, flow rate of 4 mL/min, λ = 240 nm. ^{1}H NMR (400 MHz, CD_3OD): δ_H = 8.25 (d, *J* = 8.0 Hz, 1H), 7.88 (t, *J* = 7.7 Hz, 1H), 7.69 (d, *J* = 8.1 Hz, 1H), 7.57 (t, *J* = 7.6 Hz, 1H), 4.10 (t, *J* = 7.3 Hz, 2H), 2.40 (t, *J* = 7.5 Hz, 2H), 1.87 (quint, *J* = 7.5 Hz, 2H), 1.44 (quint, *J* = 7.4 Hz, 2H), 1.40-1.27 (m, 4H).

3-(2-aminoethyl)quinazoline-2,4(1*H*,3*H*)-dione (4)

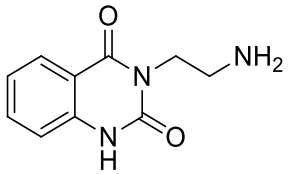

Compound **4** was obtained by following the general procedure (**A**) as a brown solid (800 mg, 70% yield by HPLC analysis). RP-HPLC t_R = 12.7 mg, gradient condition: from 5% B ending to 100% B 50 min, flow rate of 4 mL/min, λ = 240 nm. ^{1}H NMR (400 MHz, CD_3OD): δ_H = 8.37 (s, 1H), 8.30 (dd, *J* = 8.1, 1.5 Hz, 1H), 7.88 (ddd, *J* = 8.5, 7.2, 1.6 Hz, 1H), 7.72 (dd, *J* = 8.3, 1.1 Hz, 1H), 7.61 (ddd, *J* = 8.2, 7.1, 1.1 Hz, 1H), 4.22 (t, *J* = 5.8 Hz, 2H), 3.68 (*J* = 5.8 Hz, 2H).

7.2.2 Synthesis of 3,3'-(ethane-1,2-diyl)bis(quinazoline-2,4(1H,3H)-dione) (MO14)

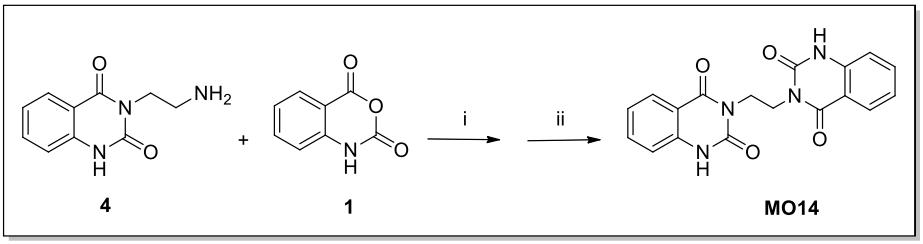

Synthetic scheme 2: i) Et_3N, H_2O, 2h, rt; ii) HCOOH, 7h, reflux.

Triethylamine (1.0 equiv) was added to a solution of **4** (1.0 equiv.) in water (2.6mL) by a portion wise addition of isatoic anhydride **1** (1.1 equiv). The reaction mixture was stirred for 2 hours at 30-40°C, cooled to room temperature and evaporated in vacuum. The obtained oil residue was refluxed then for 7 hours in formic acid (3.6 mL), cooled to room temperature and evaporated (**Synthetic scheme 2**). [246] The obtained powder was resuspended in water, extracted with DCM (3 x 25 mL), dried over anhydrous Na_2SO_4, filtered, and concentrated. The desired compound, **MO14,** was confirmed by analytical RP-HPLC (Nucleodur© C8 reversed-phase column: 100 x 2 mm, 4 µM, 80 Å, flow rate = 1 mL/min) and ^{1}H NMR spectra.

Compound **MO14** was obtained as a brown solid (165 mg, 60% yield after HPLC purification). RP-HPLC t_R = 20.8 min, gradient condition: from 5% B ending to 100% B 40 min, flow rate of 4 mL/min, λ = 240 nm. ^{1}H NMR (400 MHz, CD_3OD): δ_H = 8.35 (s, 2H), 8.17 (ddd, *J* = 8.0, 1.5, 0.6 Hz, 2H), 7.89 – 7.83 (m, 2H), 7.69 (ddd, *J* = 8.3, 1.1, 0.6, 2H), 7.60-7.55 (m, 2H), 4.54 (s, 4H). ^{13}C NMR (100 MHz, $(CD_3)_2SO$): δ = 158.8 (2C), 146.1 (2C), 137.7 (2C), 132.7 (2C), 125.5 (2C), 125.4 (2C), 124.4 (2C), 119.7 (2C), 43.3 (2C).

7.2.3 General procedure (B) for the synthesis of MO1-MO13

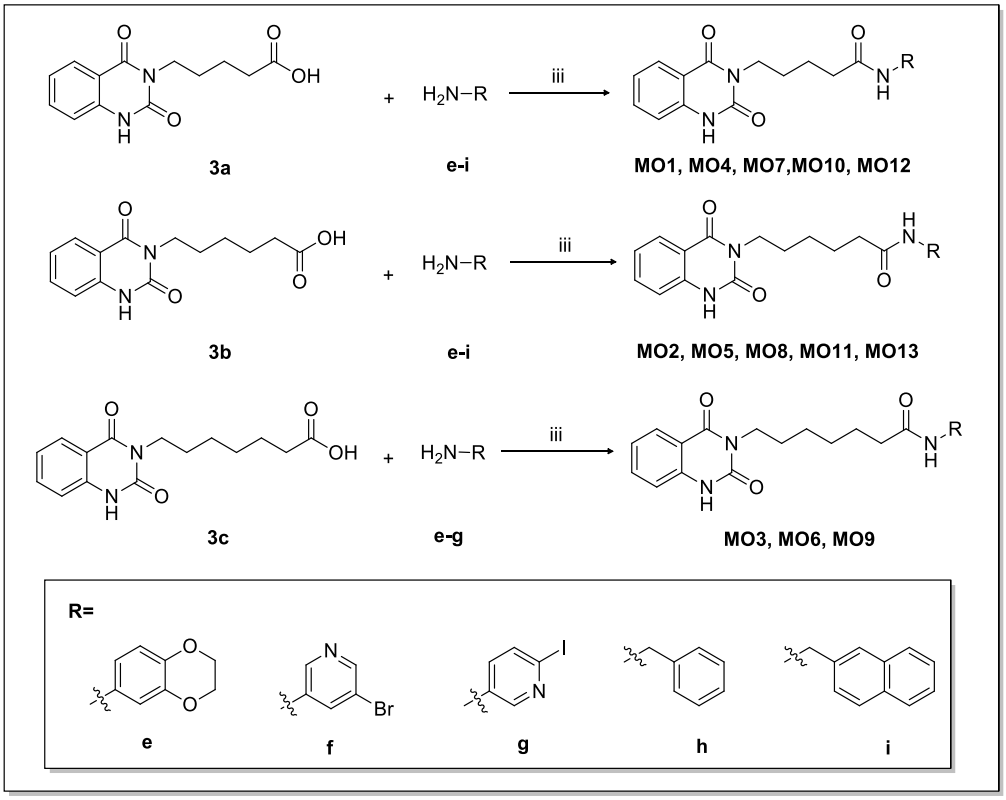

Synthetic scheme 3: iii) HOBt, DIC, DMF, 16h, rt.

In a flask containing **3a-3c** (1.0 equiv) in DMF (2 mL), 1-hydroxybenzotriazole (2.0 equiv) and *N,N'*-diisopropylcarbodiimide (1.5 equiv) were added. The mixture was left under magnetic stirring at room temperature for 1 hour, then the appropriate aniline **e-i** (2.0 equiv.) was added and the reaction mixture stirred for 16 hours at room temperature (**Synthetic scheme 3**). [212] After completion, the mixture was poured into water and extracted with AcOEt (3 x 25 mL). The combined organic phases were washed with a saturated solution of $NaHCO_3$, brine and finally dried under vacuum. HPLC purification was performed by semi-preparative reversed-phase HPLC (Nucleodur© C8 reversed-phase column: 250 x 10.00 mm, 4 μM, 80

Å, flow rate = 4 mL/min) and the final products, **MO1-MO13**, were characterized by NMR (^{1}H and ^{13}C) spectra as reported below.

_N_-(2,3-dihydrobenzo[_b_][1,4]dioxin-6-yl)-5-(2,4-dioxo-1,2 dihydroquinazolin-3(4_H_)-yl) pentanamide (MO1)

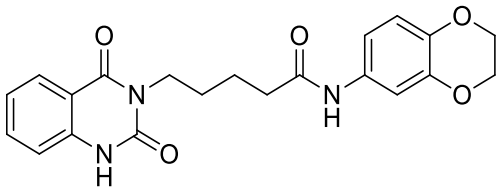

Compound **MO1** was obtained by following the general procedure (**B**), from the reaction between **3a** and 1,4-benzodioxan-6-amine (**e)**, as a brown solid (330 mg, 50% yield after HPLC purification). RP-HPLC t_R = 26.2 min, gradient condition: from 5% B ending to 100% B 40 min, flow rate of 4 mL/min, λ = 240 nm. ^{1}H NMR (400 MHz, $CDCl_3$): δ_H = 8.27 (d, *J* = 8.0 Hz, 1H), 7.82 – 7.74 (m, 2H), 7.58 – 7.53 (m, 2H), 6.82 (dd, *J* = 8.7, 2.4 Hz, 1H), 6.69 (d, *J* = 8.6, 1H), 4.20 – 4.16 (m, 4H), 4.08 (t, *J* = 7.1 Hz, 2H), 2.38 (t, *J* = 7.2 Hz, 2H), 1.86 (quint, *J* = 7.2 Hz, 2H), 1.75 (quint, *J* = 7.3 Hz, 2H). ^{13}C NMR (100 MHz, CD_3OD): δ = 173.7, 162.6, 149.6, 148.4, 144.9, 141.9, 136.0, 133.6, 129.0, 127.8, 127.4, 123.0, 118.0, 114.7, 110.9, 65.9, 65.7, 48.0, 37.2, 29.9, 23.9.

N-(2,3-dihydrobenzo[b][1,4]dioxin-6-yl)-6-(2,4-dioxo-1,2-dihydroquinazolin-3(4H)-yl)hexanamide (MO2)

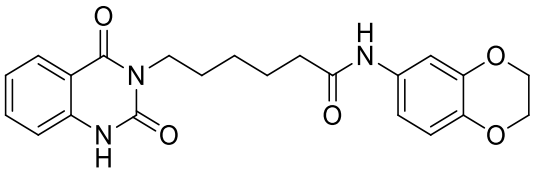

Compound **MO2** was obtained by following the general procedure (**B**), from the reaction between **3b** and 1,4-benzodioxan-6-amine **(e),** as a brown solid (145 mg, 75% yield after HPLC purification). RP-HPLC t_R = 23.6 min, gradient condition: from 5% B ending to 100% B 40 min, flow rate of 4 mL/min, λ = 240 nm. ^{1}H NMR (400 MHz, $CDCl_3$): δ_H = 8.33 (dd, *J* = 8.0, 1.4 Hz, 1H), 8.14 (s, 1H), 7.82 – 7.73 (m, 2H), 7.57 – 7.52 (m, 1H), 7.17 (d, *J* = 2.5 Hz, 1H), 6.91 (dd, *J* = 8.7, 2.5 Hz, 1H), 6.80 (d, *J* = 8.7 Hz, 1H), 4.25 (s, 4H), 4.04 (t, *J* = 7.4 Hz, 2H), 2.36 (t, *J* = 7.4 Hz, 2H), 1.93 – 1.76 (m, 4H), 1.49 (p, *J* = 7.7 Hz, 2H). ^{13}C NMR (100 MHz, $CDCl_3$): δ = 170.7, 160.9, 147.5, 146.8, 143.5, 140.4, 134.4, 131.6, 127.5, 127.0, 126.8, 122.0, 117.1, 113.5, 109.8, 64.4, 64.3, 46.9, 37.00, 28.9, 26.0, 24.8.

***N*-(2,3-dihydrobenzo[*b*][1,4]dioxin-6-yl)-7-(2,4-dioxo-1,2-dihydroquinazolin-3(4*H*)-yl)heptanamide (MO3)**

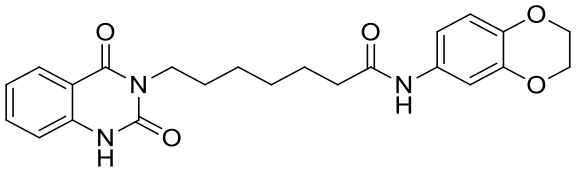

Compound **MO3** was obtained by following the general procedure (**B**), from the reaction between **3c** and 1,4-benzodioxan-6-amine (**e)**, as a brown solid (145 mg, 70% yield after HPLC purification). RP-HPLC t_R = 23.2 min, gradient condition: from 5% B ending to 100% B 40 min, flow rate of 4 mL/min, λ = 240 nm. ^{1}H NMR (400 MHz, CD_3OD): δ_H = 8.52 (s, 1H), 8.29 (dd, *J* = 8.1, 1.7 Hz, 1H), 7.90 – 7.85

(m, 1H), 7.73 (d, *J* = 8.2 Hz, 1H), 7.62 (t, *J* = 8.0 Hz, 1H), 7.16 (d, *J* = 2.6 Hz, 1H), 6.93 – 6.88 (m, 1H), 6.76 (dd, *J* = 7.1, 3.5, 1H), 4.25 – 4.19 (m, 4H), 4.10 (t, *J* = 7.5 Hz, 2H), 2.35 (t, *J* = 7.5 Hz, 2H), 1.88 – 1.81 (m, 2H), 1.75 – 1.69 (m, 2H), 1.50 – 1.44 (m, 4H). ^{13}C NMR (125 MHz, CD_3OD): δ = 172.8, 160.9, 147.9, 147.1, 143.4, 140.2, 134.8, 134.3, 132.00, 127.2, 126.1, 121.5, 116.4, 113.3, 109.4, 64.3, 64.1, 46,7, 36.2, 28.7, 28.4, 26.0, 25.3.

_N_-(5-bromopyridin-3-yl)-5-(2,4-dioxo-1,2-dihydroquinazolin-3(4*H*)-yl)pentanamide (MO4)

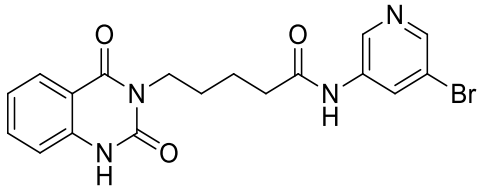

Compound **MO4** was obtained by following the general procedure (**B**), from the reaction between **3a** and 3-amino-5-bromopyridine (**f**), as a brown solid (235 mg, 45% yield after HPLC purification). RP-HPLC t_R = 21.3 min, gradient condition: from 5% B ending to 100% B 40 min, flow rate of 4 mL/min, λ = 240 nm. ^{1}H NMR (400 MHz, CD_3OD): δ_H = 8.70 (s, 1H), 8.59 (s, 1H), 8.45 (s, 1H), 8.39 (s, 1H), 8.29 (dd, *J* = 8.1, 1.4 Hz, 1H), 7.89 (ddd, *J* = 8.5, 7.2, 1.5 Hz, 1H), 7.73 (d, *J* = 8.2 Hz, 1H), 7.63 (t, *J* = 7.6 Hz, 1H), 4.16 (t, *J* = 7.1 Hz, 2H), 2.53 (t, *J* = 7.1 Hz, 2H), 1.92 (quint, *J* = 7.3 Hz, 2H), 1.82 (quint, *J* = 7.3Hz, 2H). ^{13}C NMR (100 MHz, CD_3OD): δ = 173.0, 160.9, 148.2, 146.3, 143.9, 138.0, 137.0, 134.6, 131.3, 129.7, 127.5, 126.1, 125.5, 121.4, 46.5, 35.3, 28.2, 21.8.

_N_-(5-bromopyridin-3-yl)-6-(2,4-dioxo-1,2-dihydroquinazolin-3(4_H_)-yl)hexanamide (MO5)

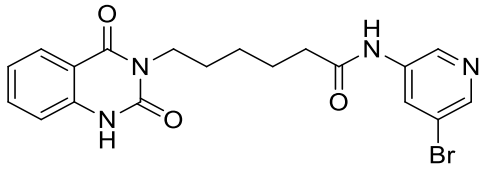

Compound **MO5** was obtained by following the general procedure (**B**), from the reaction between **3b** and 3-amino-5-bromopyridine (**f**), as a brown solid (230 mg, 65% yield after HPLC purification). RP-HPLC t_R = 23.3 min, gradient condition: from 5% B ending to 100% B 40 min, flow rate of 4 mL/min, λ = 240 nm. ^{1}H NMR (400 MHz, CD_3OD): δ_H = 8.72 (s, 1H), 8.65 (s, 1H), 8.46-8.39 (m, 2H), 8.27 (dd, *J* = 8.0, 1.5 Hz, 1H), 7.91 – 7.87 (m, 1H), 7.72 (d, *J* = 8.1 Hz, 1H), 7.65 – 7.61 (m, 1H), 4.13 (t, *J* = 7.3 Hz, 2H), 2.46 (t, *J* = 7.3 Hz, 2H), 1.89 (quint, *J* = 7.6 Hz, 2H), 1.80 (quint, *J* = 7.3 Hz, 2H), 1.54 -1.45 (m, 2H). ^{13}C NMR (100 MHz, CD_3OD): δ = 174.7, 162.2, 149.7, 147.4, 145.1, 139.4, 137.9, 135.9, 131.2, 129.9, 128.9, 127.6, 122.7, 48.2, 37.3, 29.7, 27.0, 25.8.

_N_-(5-bromopyridin-3-yl)-7-(2,4-dioxo-1,2-dihydroquinazolin-3(4_H_)-yl)heptanamide (MO6)

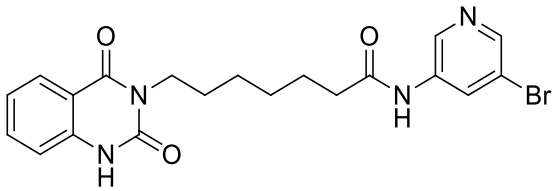

Compound **MO6** was obtained by following the general procedure (**B**), from the reaction between **3c** and 3-amino-5-bromopyridine (**f**), as a brown solid (150 mg, 60% yield after HPLC purification). RP-HPLC t_R = 22.8 min, gradient condition: from 5% B ending to 100% B 40 min, flow rate of 4 mL/min, λ = 240 nm. ^{1}H NMR (400 MHz, CD_3OD): δ_H = 8.66 (s, 1H), 8.48 – 8.44 (m, 2H), 8.38 (s, 1H), 8.28 (dd,

J = 8.0, 4.2 Hz, 1H), 7.88 (t, *J* = 7.6 Hz, 1H), 7.73 (dd, *J* = 8.1, 2.7 Hz, 1H), 7.61 (td, *J* = 7.7, 2.9 Hz, 1H), 4.13-4.07 (m, 2H), 2.35 (t, *J* = 7.4 Hz, 2H), 1.84 (quint, J = 7.7 Hz, 2H), 1.68 -1.63 (m, 2H), 1.50 – 1.41 (m, 4H). ^{13}C NMR (125 MHz, CD_3OD): δ = 173.6, 160.9, 148.0, 146.7, 144.0, 138.3, 137.1, 134.4, 129.7, 128.7, 127.4, 126.2, 125.7, 121.5, 46.8, 36.2, 28.6, 28.3, 25.9, 24.8.

5-(2,4-dioxo-1,2-dihydroquinazolin-3(4*H*)-yl)-*N*-(6-iodopyridin-3-yl)pentanamide (MO7)

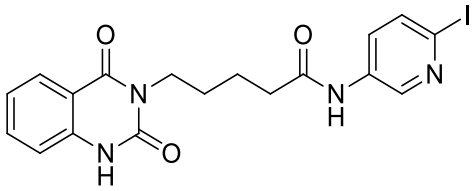

Compound **MO7** was obtained by following the general procedure (**B**), from the reaction between **3a** and 5-amino-2-iodopyridine (**g**), as a brown solid (265 mg, 40% yield after HPLC purification). RP-HPLC t_R = 22.8 min, gradient condition: from 5% B ending to 100% B 40 min, flow rate of 4 mL/min, λ = 240 nm. ^{1}H NMR (400 MHz, CD_3OD): δ_H = 8.57 (s, 1H), 8.51 (s, 1H), 8.28 (d, *J* = 8.3 Hz, 1H), 7.87 (d, *J* = 7.9 Hz, 1H), 7.82 – 7.70 (m, 2H), 7.69 – 7.53 (m, 2H), 4.14 (t, *J* = 7.0 Hz, 2H), 2.50 (t, *J* = 7.2 Hz, 2H), 1.90 (quint, *J* = 7.6 Hz, 2H), 1.80 (quint, *J* = 7.5 Hz, 2H). ^{13}C NMR (100 MHz, CD_3OD): δ = 172.8, 161.0, 147.9, 146.9, 141.6, 135.9, 134.8, 134.5, 129.0, 127.4, 126.2, 125.5, 121.5, 108.2 46.4, 35.7, 28.2, 21.9.

6-(2,4-dioxo-1,2-dihydroquinazolin-3(4*H*)-yl)-*N*-(6-iodopyridin-3-yl)hexanamide (MO8)

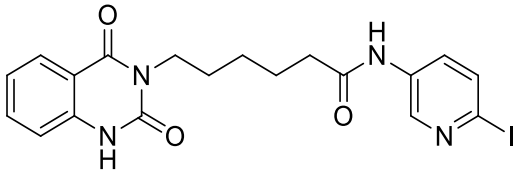

Compound **MO8** was obtained by following the general procedure (**B**), from the reaction between **3b** and 5-amino-2-iodopyridine (**g**), as a brown solid (255 mg, 45% yield after HPLC purification). RP-HPLC t_R = 22.7 min, gradient condition: from 5% B ending to 100% B 40 min, flow rate of 4 mL/min, λ = 240 nm. ^{1}H NMR (400 MHz, CD_3OD): δ_H = 8.59-8.55 (m, 2H), 8.26 (dd, *J* = 8.1, 1.6 Hz, 1H), 7.91 – 7.87 (m, 1H), 7.80 – 7.75 (m, 2H), 7.71 (d, *J* = 8.1 Hz, 1H), 7.62 (t, *J* = 7.7 Hz, 1H), 4.13 (t, *J* = 7.3 Hz, 2H), 2.44 (t, *J* = 7.3 Hz, 2H), 1.88 (quint, *J* = 7.4 Hz, 2H), 1.78 (quint, *J* = 7.3 Hz, 2H), 1.52 – 1.44 (m, 2H). ^{13}C NMR (100 MHz, CD_3OD): δ = 173.3, 161.1, 148.0, 147.0, 141.6, 136.0, 134.7, 134.4, 128.9, 127.3, 126.1, 126.0, 121.4, 108.3, 46.6, 36.0, 28.4, 26.6, 24.6.

7-(2,4-dioxo-1,2-dihydroquinazolin-3(4*H*)-yl)-*N*-(6-iodopyridin-3-yl)heptanamide (MO9)

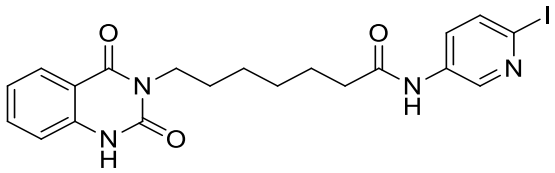

Compound **MO9** was obtained by following the general procedure (**B**), from the reaction between **3c** and 5-amino-2-iodopyridine (**g**), as a brown solid (170 mg, 60% yield after HPLC purification). RP-HPLC t_R = 23.5 min, gradient condition: from 5% B ending to 100% B 40 min, flow rate of 4 mL/min, λ = 240 nm. ^{1}H NMR (400 MHz, CD_3OD): δ_H = 8.64 (s, 1H), 8.58 (s, 1H), 8.29 (dd, *J* = 8.1, 1.5 Hz, 1H),

7.92-7.88 (m, 1H), 7.81 – 7.75 (m, 2H), 7.73 (d, *J* = 8.2 Hz, 1H), 7.64 (t, *J* = 7.6 Hz, 1H), 4.12 (t, *J* = 7.4 Hz, 2H), 2.42 (t, *J* = 7.4 Hz, 2H), 1.87 (quint, *J* = 7.5 Hz, 2H), 1.73 (quint, *J* = 7.1 Hz, 2H), 1.47 (quint, *J* = 3.5, 4H). ^{13}C NMR (100 MHz, CD_3OD): δ = 173.4, 161.1, 148.0, 147.0, 141.7, 136.0, 134.8, 134.4, 129.0, 127.3, 126.1, 126.0, 121.5, 108.2, 46.8, 36.2, 28.6, 28.4, 25.9, 24.9.

_N_-benzyl-5-(2,4-dioxo-1,2-dihydroquinazolin-3(4*H*)-yl)pentanamide (MO10)

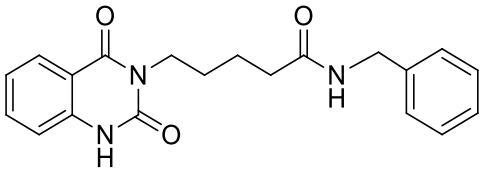

Compound **MO10** was obtained by following the general procedure (**B**), from the reaction between **3a** and benzylamine (**h**), as a brown solid (135 mg, 50% yield after HPLC purification). RP-HPLC t_R = 20.1 min, gradient condition: from 5% B ending to 100% B 40 min, flow rate of 4 mL/min, λ = 240 nm. ^{1}H NMR (400 MHz, CD_3OD): δ_H = 8.52 (s, 1H), 8.28 (dd, *J* = 8.0, 1.5, 1H), 7.91 – 7.86 (m, 1H), 7.73 (d, *J* = 8.1 Hz, 1H), 7.62 (t, *J* = 7.7 Hz, 1H), 7.32 – 7.23 (m, 5H), 4.36 (s, 2H), 4.10 (t, *J* = 7.1 Hz 2H), 2.33 (t, *J* = 7.2 Hz, 2H), 1.88 – 1.79 (m, 2H), 1.78 – 1.70 (m, 2H). ^{13}C NMR (100 MHz, CD_3OD): δ = 174.0, 160.8, 148.2, 146.2, 138.6, 134.6, 128.1 (2C), 127.5, 127.2 (2C), 126.8, 126.3, 125.5, 121.4, 46.6, 42.7, 34.9, 28.3, 22.6.

_N_-benzyl-6-(2,4-dioxo-1,2-dihydroquinazolin-3(4*H*)-yl)hexanamide (MO11)

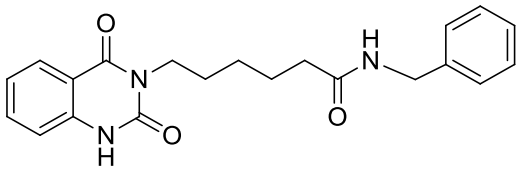

Compound **MO11** was obtained by following the general procedure (**B**), from the reaction between **3b** and benzylamine (**h**), as a brown solid (170 mg, 55% yield after HPLC purification). RP-HPLC t_R = 23.2 min, gradient condition: from 5% B ending to 100% B 40 min, flow rate of 4 mL/min, λ = 240 nm. ^{1}H NMR (400 MHz, CD_3OD): δ_H = 8.56 (s, 1H), 8.30 (dd, *J* = 8.1, 1.5 Hz, 1H), 7.90-7.85 (m, 1H), 7.73 (d, *J* = 8.3 Hz, 1H), 7.66 – 7.61 (m, 1H), 7.34 – 7.21 (m, 5H), 4.36 (s, 2H), 4.10 (t, *J* = 7.4 Hz, 2H), 2.28 (t, *J* = 7.3 Hz, 2H), 1.85 (quint, *J* = 7.5 Hz, 2H), 1.73 (quint, *J* = 7.4 Hz, 2H), 1.48 – 1.39 (m, 2H). ^{13}C NMR (100 MHz, CD_3OD): δ = 174.3, 161.0, 148.1, 146.8, 138.6, 134.4, 128.1 (2C), 127.4, 127.2 (2C), 126.8, 126.2, 125.9, 121.5, 46.7, 42.7, 35.3, 28.4, 25.7, 25.0.

5-(2,4-dioxo-1,2-dihydroquinazolin-3(4*H*)-yl)-*N*-(naphthalen-2-ylmethyl)pentanamide (MO12)

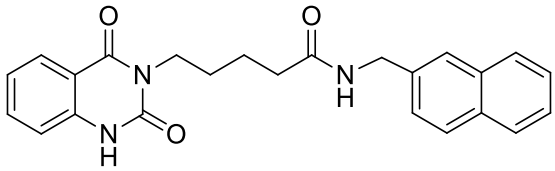

Compound **MO12** was obtained by following the general procedure (**B**), from the reaction between **3a** and 2-aminomethylnaphthalene (**i**), as a brown solid (150 mg, 55% yield after HPLC purification). RP-HPLC t_R = 25.7 min, gradient condition: from 5% B ending to 100% B 40 min, flow rate of 4 mL/min, λ = 240 nm. ^{1}H NMR (400 MHz, CD_3OD): δ_H = 8.51 (s, 1H), 8.26 (dd, *J* = 8.1, 1.5 Hz, 1H), 8.03 (d, *J* = 8.4 Hz, 1H), 7.92 – 7.87 (m, 1H), 7.84 (d, *J* = 8.1 Hz, 1H), 7.80 (d, *J* = 7.8 Hz, 1H),

7.73 (dd, *J* = 8.3, 4.2 Hz, 1H), 7.66 – 7.61 (m, 1H), 7.52 – 7.40 (m, 5H), 4.83 (s, 2H), 4.07 (t, *J* = 7.0 Hz, 2H), 2.33 (t, *J* = 6.9 Hz, 2H), 1.83 – 1.68 (m, 4H). ^{13}C NMR (100 MHz, CD_3OD): δ = 173.8, 160.8, 148.2, 146.4, 135.2, 134.5, 133.9, 133.6, 128.3, 127.9, 127.5, 126.2, 126.0, 125.9, 125.6, 125.4, 125.0, 123.1, 121.4, 46.5, 40.9, 34.9, 28.2, 22.5.

6-(2,4-dioxo-1,2-dihydroquinazolin-3(4*H*)-yl)-*N*-(naphthalen-2-ylmethyl)hexanamide (MO13)

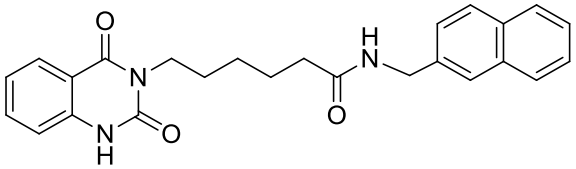

Compound **MO13** was obtained by following the general procedure (**B**), from the reaction between **3b** and 2-aminomethylnaphthalene (**i**), as a brown solid (170 mg, 65% yield after HPLC purification). RP-HPLC t_R = 26.1 min, gradient condition: from 5% B ending to 100% B 40 min, flow rate of 4 mL/min, λ = 240 nm. ^{1}H NMR (400 MHz, CD_3OD): δ_H = 8.56 (s, 1H), 8.28 (dd, *J* = 8.1, 1.5 Hz, 1H), 8.08 – 8.04 (m, 1H), 7.92 – 7.87 (m, 2H), 7.81 (dd, *J* = 7.6, 1.9 Hz, 1H), 7.72 (d, *J* = 8.2 Hz, 1H), 7.66 – 7.61 (m, 1H), 7.57 – 7.49 (m, 2H), 7.48 – 7.41 (m, 2H), 4.83 (s, 2H), 4.04 (t, *J* = 7.4 Hz, 2H), 2.28 (t, *J* = 7.3 Hz, 2H), 1.81 (quint, J = 7.7 Hz, 2H), 1.73 (quint, J = 7.7 Hz, 2H), 1.45 – 1.38 (m, 2H). ^{13}C NMR (100 MHz, CD_3OD): δ = 174.2, 160.7, 148.3, 146.0, 134.6, 134.0, 133.7, 131.3, 128.3, 127.9, 127.5, 126.3, 125.9, 125.9, 125.5, 125.3, 125.0, 123.1, 121.3, 46.8, 40.8, 35.2, 28.3, 25.7, 25.0.

7.3 Pyrimidine derivatives (BR1-BR7)

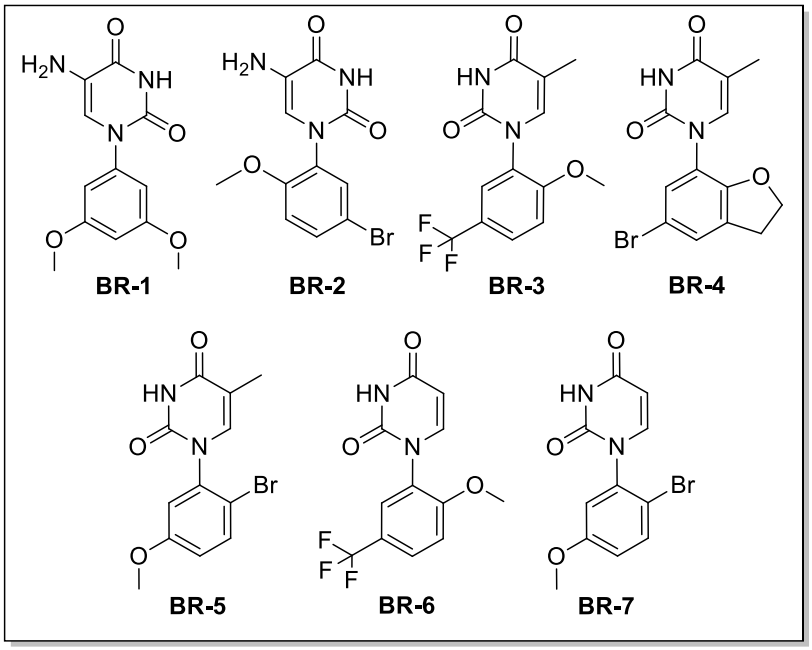

7.3.1 General procedure (C) for the synthesis of BR1-BR7

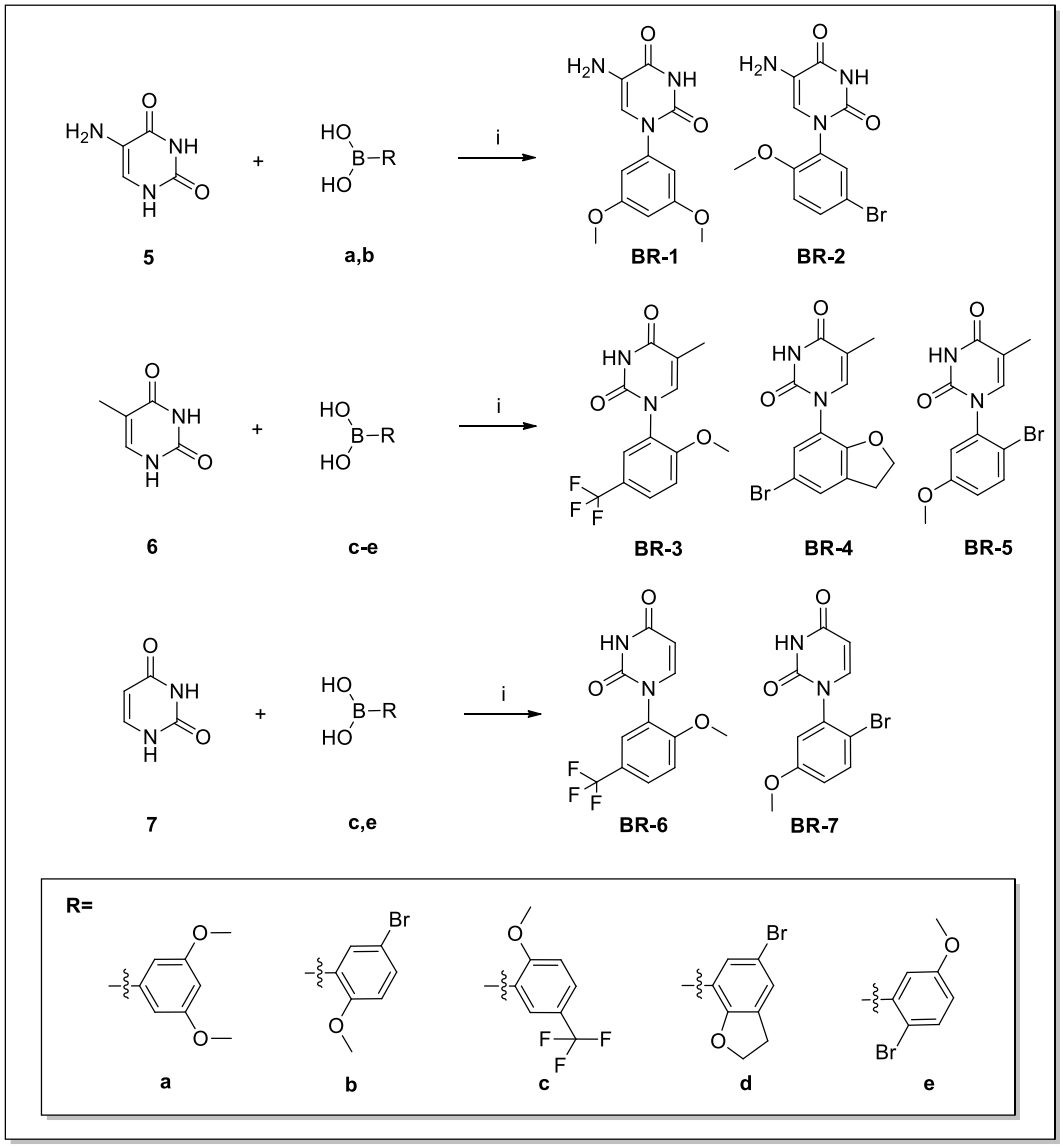

Synthetic scheme 4: i) $Cu(OAc)_2 \cdot H_2O$, dry TMEDA, MeOH/H_2O (4:1), rt overnight.

5, 6, or **7** (1.0 equiv), the appropriate boronic acid **a-e** (2.0 equiv), $Cu(OAc)_2 \cdot H_2O$ (1.0 equiv), TMEDA (2.0 equiv), MeOH/H_2O (40.0 mL and 10.0 mL; ratio 4:1) were placed in a 100 mL flask. The mixture was vigorously stirred at room temperature overnight (**Synthetic scheme 4**). [215] The solvent was evaporated and

the crude product was purified by semi-preparative reversed-phase HPLC (Nucleodur© C8 reversed-phase column: 250 x 10.00 mm, 4 μM, 80 Å, flow rate = 4 mL/min). The final products **BR1-BR7** were characterized by NMR spectra and ESI-MS.

5-amino-1-(3,5-dimethoxyphenyl)pyrimidine-2,4(1*H*,3*H*)-dione (BR1)

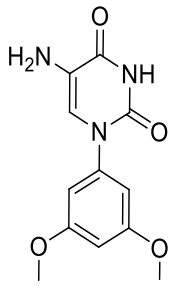

Compound **BR1** was obtained by following the general procedure (**C**), from the reaction between **5** and 3,5-dimethoxyphenylboronic acid (**a**), as a blue solid (125 mg, 30% yield after HPLC purification). RP-HPLC t_R = 27.5 min, gradient condition: from 5% B ending to 100% B 50 min, flow rate of 4 mL/min, λ = 240 nm. ^{1}H NMR (400 MHz, CD_3OD): δ_H = 6.99 (s, 1H), 6.52 (d, *J* = 2.3 Hz, 2H), 6.48-6.44 (m, 1H), 3.70 (s, 6H). ESI-MS: calculated for $C_{12}H_{13}N_3O_4$ 263.25; found m/z = 264.07 $[M+H]^+$.

5-amino-1-(5-bromo-2-methoxyphenyl)pyrimidine-2,4(1*H*,3*H*)-dione (BR2)

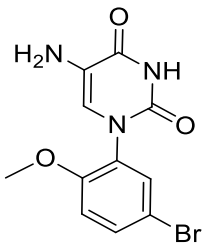

Compound **BR2** was obtained by following the general procedure (**C**), from the reaction between **5** and 5-bromo-2-methoxyphenylboronic acid (**b**), as a blue solid (145 mg, 35% yield after HPLC purification). RP-HPLC t_R = 19.7 min, gradient condition: from 5% B ending to 100% B 50 min, flow rate of 4 mL/min, λ = 240 nm. ^{1}H NMR (400 MHz, CD_3OD): δ_H = 7.50 (d, *J* = 8.7 Hz, 1H), 7.43 (d, *J* = 2.4 Hz, 1H), 7.03 (d, *J* = 8.7 Hz, 1H), 6.92 (s, 1H), 3.75 (s, 3H). ESI-MS: calculated for $C_{11}H_{10}BrN_3O_3$ 310.99; found m/z = 311.99 $[M+H]^+$, 313.98 $[M+H+2]^+$.

1-(2-methoxy-5-(trifluoromethyl)phenyl)-5-methylpyrimidine-2,4(1*H*,3*H*)-dione (BR3)

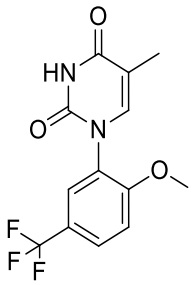

Compound **BR3** was obtained by following the general procedure (**C**), from the reaction between **6** and 2-methoxy-5-(trifluoromethyl) benzeneboronic acid (**c**), as a blue solid (145 mg, 70% yield after HPLC purification). RP-HPLC t_R = 25.1 min, gradient condition: from 5% B ending to 100% B 50 min, flow rate of 4 mL/min, λ = 240 nm. ^{1}H NMR (400 MHz, CD_3OD): δ_H = 7.68 (dd, *J* = 8.8, 2.4 Hz, 1H), 7.60

(d, *J* = 2.3 Hz, 1H), 7.27 – 7.23 (m, 2H), 3.84 (s, 3H), 1.80 (s, 3H). ^{13}C NMR (100 MHz, CD_3OD): δ = 165.0, 158.1, 150.6, 142.1, 128.2, 128.1, 127.3, 125.8, 121.6, 113.6, 109.3, 56.9, 12.0. ESI-MS calculated for $C_{13}H_{11}F_3N_2O_3$ 300.23; found m/z = 301.04 $[M+H]^+$.

1-(5-bromo-2,3-dihydrobenzofuran-7-yl)-5-methylpyrimidine-2,4(1*H*,3*H*)-dione (BR4)

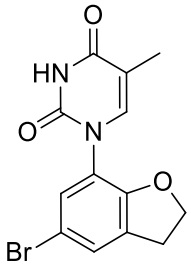

Compound **BR4** was obtained by following the general procedure (**C**), from the reaction between **6** and (5-bromo-2,3-dihydrobenzofuran-7-yl)boronic acid (**d**), as a blue solid (155 mg, 55% yield after HPLC purification). RP-HPLC t_R = 27.8 min, gradient condition: from 5% B ending to 100% B 50 min, flow rate of 4 mL/min, λ = 240 nm. ^{1}H NMR (400 MHz, CD_3OD): δ_H = 7.44 (dt, *J* = 2.2, 1.2 Hz, 1H), 7.39 (d, *J* = 2.3 Hz, 1H), 7.33 (dt, J = 1.8, 0.9 Hz, 1H), 4.67 (t, *J* = 8.8 Hz, 2H), 2.96 – 2.94 (m, 2H), 1.90 (s, 3H). ^{13}C NMR (100 MHz, CD_3OD): δ = 164.1, 160.3, 149.3, 141.4, 128.9, 128.4, 127.7, 120.9, 117.2, 109.4, 72.6, 29.1, 10.5. ESI-MS: calculated for $C_{13}H_{11}BrN_2O_3$ 322.00; found m/z = 323.00 $[M+H]^+$, 324.01 $[M+H+2]^+$.

1-(2-bromo-5-methoxyphenyl)-5-methylpyrimidine-2,4(1*H*,3*H*)-dione (BR5)

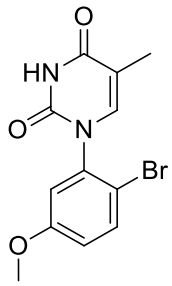

Compound **BR5** was obtained by following the general procedure (**C**), from the reaction between **6** and 2-bromo-5-methoxybenzene boronic acid (**e**), as a blue solid (150 mg, 50% yield after HPLC purification). RP-HPLC t_R = 25.2 min, gradient condition: from 5% B ending to 100% B 50 min, flow rate of 4 mL/min, λ = 240 nm. ^{1}H NMR (400 MHz, CD_3OD): δ_H = 7.56-7.50 (m, 1H), 7.25-7.20 (m, 1H), 7.01 (d, *J* = 3.1 Hz, 1H), 6.91 (dd, *J* = 8.9, 3.1 Hz, 1H), 3.73 (s, 3H), 1.82 (s, 3H). ^{13}C NMR (100 MHz, CD_3OD): δ = 164.8, 160.1, 141.1, 138.2, 133.1, 119.9, 116.8, 115.3, 112.1, 110.4, 55.7, 10.5. ESI-MS: calculated for $C_{12}H_{11}BrN_2O_3$ 310.00; found m/z = 311.00 $[M+H]^+$, 313.02 $[M+H+2]^+$.

1-(2-methoxy-5-(trifluoromethyl)phenyl)pyrimidine-2,4(1*H*,3*H*)-dione (BR6)

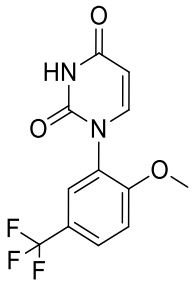

Compound **BR6** was obtained by following the general procedure (**C**), from the reaction between **7** and 2-methoxy-5-(trifluoromethyl)benzeneboronic acid (**c**), as a blue solid (155 mg, 50% yield after HPLC purification). RP-HPLC t_R = 24.3 min,

gradient condition: from 5% B ending to 100% B 50 min, flow rate of 4 mL/min, λ = 240 nm. ^{1}H NMR (400 MHz, CD_3OD): δ_H = 7.69 (dd, *J* = 8.9, 2.3 Hz, 1H), 7.62 (d, *J* = 2.3 Hz, 1H), 7.39 (d, *J* = 7.9 Hz, 1H), 7.26 (d, *J* = 8.8 Hz, 1H), 5.67 (d, *J* = 7.9 Hz, 1H), 3.84 (s, 3H). ^{13}C NMR (100 MHz, CD_3OD): δ = 165.1, 157.7, 150.8, 146.1, 127.9, 127.2, 126.3, 125.2, 122.5, 112.6, 101.4, 55.6. ESI-MS: calculated for $C_{12}H_9F_3N_2O_3$ 286.21; found m/z = 287.01 $[M+H]^+$.

1-(2-bromo-5-methoxyphenyl)pyrimidine-2,4(1H,3H)-dione (BR-7)

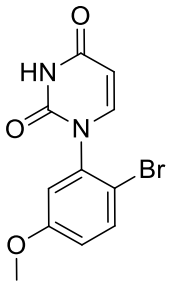

Compound **BR7** was obtained by following the general procedure (**C**), from the reaction between **7** and 2-bromo-5-methoxybenzene boronic acid (**e**), as a blue solid (160 mg, 45% yield after HPLC purification). RP-HPLC t_R = 24.7 min, gradient condition: from 5% B ending to 100% B 50 min, flow rate of 4 mL/min, λ = 240 nm. ^{1}H NMR (400 MHz, CD_3OD): δ_H = 7.54 (d, *J* = 8.9 Hz, 1H), 7.37 (d, *J* = 7.9 Hz, 1H), 7.03 (d, *J* = 3.0 Hz, 1H), 6.92 (dd, *J* = 9.0, 3.0 Hz, 1H), 5.71 (d, *J* = 7.9 Hz, 1H), 3.73 (s, 3H). ^{13}C NMR (100 MHz, CD_3OD): δ = 165.1, 160.2, 150.4, 145.4, 138.1, 133.5, 116.9, 115.2, 111.8, 101.5, 55.0. ESI-MS: calculated for $C_{11}H_9BrN_2O_3$ 295.98; found m/z = 296.96 $[M+H]^+$, 298.97 $[M+H+2]^+$.

7.4 Pyrimidinone derivatives (LAM1-LAM28)

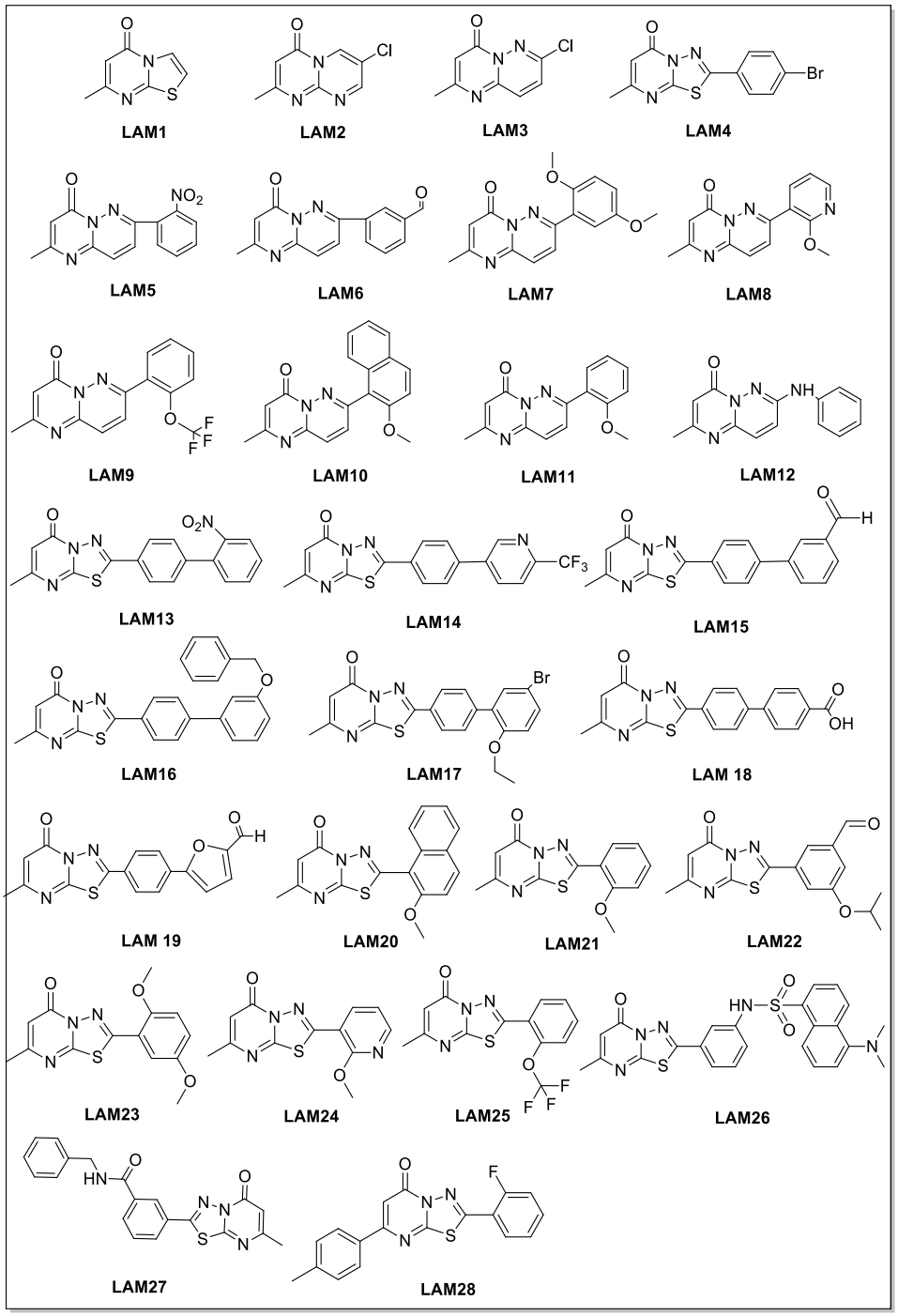

7.4.1 General procedure (D) for the synthesis of LAM1-LAM4, 14, and 16

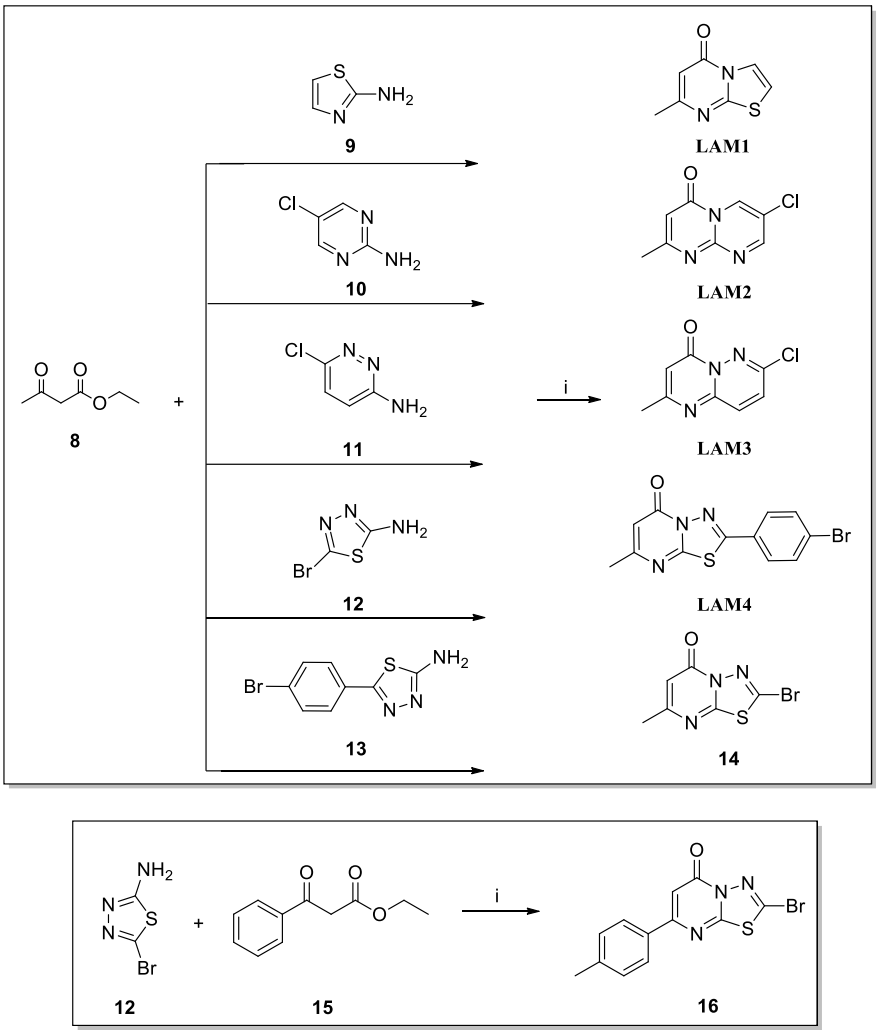

Synthetic scheme 5: i) PPA, 150°C, 1.5 h.

A mixture of aromatic amines **9-13** (1.0 equiv), β- ketoesters **8** or **15** (1.3 equiv) and PPA (6.5 equiv) was heated on an oil bath at 140~160 °C for 1.5 h. The reaction mixture was poured into water and extracted with $CHCl_3$ (3 x 25 mL) (**Synthetic scheme 5**). The combined organic phases were washed with water (25 mL), dried over anhydrous Na_2SO_4, filtered, and concentrated in vacuum. [217] The desired compounds **LAM1-LAM4, 14** and **16** were confirmed by analytical RP-HPLC

(Nucleodur© C8 reversed-phase column: 100 x 2 mm, 4 μM, 80 Å, flow rate = 1 mL/min), NMR and ESI-MS spectra.

7-methyl-5*H*-thiazolo[3,2-*a*]pyrimidin-5-one (LAM1)

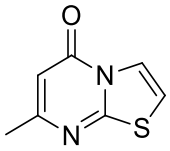

Compound **LAM1** was obtained by following the general procedure (**D**), from the reaction between **8** and **9,** as a brown solid (85 mg, 90% yield after HPLC purification). RP-HPLC t_R = 13.4 min, gradient condition: from 5% B ending to 100% B 50 min, flow rate of 4 mL/min, λ = 240 nm. ^{1}H NMR (400 MHz, CD_3OD): δ_H = 8.03 (d, *J* = 4.9 Hz, 1H), 7.44 (d, *J* = 4.9 Hz, 1H), 6.22 (s, 1H), 2.40 (s, 3H). ^{13}C NMR (100 MHz, $(CD_3)_2SO$): δ = 164.2, 163.0, 158.0, 122.1, 113.3, 103.3, 24.0. ESI-MS: calculated for $C_7H_6N_2OS$ 166.20; found m/z = 167.04 $[M+H]^+$.

7-chloro-2-methyl-4*H*-pyrimido[1,2-*a*]pyrimidin-4-one (LAM2)

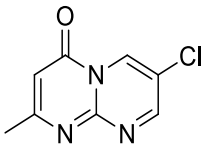

Compound **LAM2** was obtained by following the general procedure (**D**), from the reaction between **8** and **10**, as a brown solid (225 mg, 85% yield after HPLC purification). RP-HPLC t_R = 13.7 min, gradient condition: from 5% B ending to 100% B 50 min, flow rate of 4 mL/min, λ = 240 nm. ^{1}H NMR (400 MHz, CD_3OD): δ_H = 7.43 (s, 1H), 6.37 (s, 1H), 5.61 (s, 1H), 2.02 (s, 3H). ESI-MS: calculated for $C_8H_6ClN_3O$ 195.02; found m/z = 196.06 $[M+H]^+$, 198.08 $[M+H+2]^+$.

7-chloro-2-methyl-4*H*-pyrimido[1,2-*b*]pyridazin-4-one (LAM3)

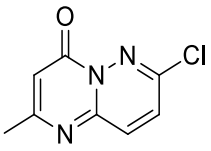

Compound **LAM3** was obtained by following the general procedure (**D**), from the reaction between **8** and **11**, as a brown solid (120 mg, 80% yield by HPLC analysis). RP-HPLC t_R = 12.5 min, gradient condition: from 5% B ending to 100% B 50 min, flow rate of 4 mL/min, λ = 240 nm. ^{1}H NMR (400 MHz, CD_3OD): δ = 7.81 (d, *J* = 9.4 Hz, 1H), 7.65 (d, *J* = 9.4 Hz, 1H), 6.49 (s, 1H), 2.37 (s, 3H). ESI-MS: calculated for $C_8H_6ClN_3O$ 195.02; found m/z = 196.09 $[M+H]^+$, 198.07 $[M+H+2]^+$.

2-(4-bromophenyl)-7-methyl-5*H*-[1,3,4]thiadiazolo[3,2-*a*]pyrimidin-5-one (LAM4)

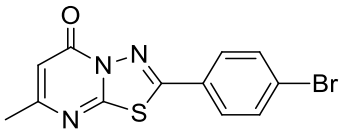

Compound **LAM4** was obtained by following the general procedure (**D**), from the reaction between **8** and **12,** as a brown solid (125 mg, 75% yield by HPLC analysis). RP-HPLC t_R = 30.1 min, gradient condition: from 5% B ending to 100% B 50 min, flow rate of 4 mL/min, λ = 240 nm. ^{1}H NMR (400 MHz, CD_3OD): δ_H = 7.99 (d, *J* = 8.3, 2H), 7.80 (d, *J* = 8.3 Hz, 2H), 6.42 (s, 1H). 2.43 (s, 3H). ESI-MS: calculated for $C_{12}H_8BrN_3OS$ 320.96; found m/z = 322.02 $[M+H]^+$, 324.02 $[M+H+2]^+$.

2-bromo-7-methyl-5*H*-[1,3,4]thiadiazolo[3,2-*a*]pyrimidin-5-one (14)

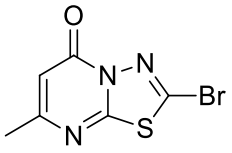

Compound **14** was obtained by following the general procedure (**D**), from the reaction between **8** and **13,** as a brown solid (325 mg, 85% yield by HPLC analysis). RP-HPLC t_R = 15.7 min, gradient condition: from 5% B ending to 100% B 50 min, flow rate of 4 mL/min, λ = 240 nm. ^{1}H NMR (400 MHz, CD_3OD): δ_H = 6.22 (s, 1H), 2.26 (s, 3H). ESI-MS: calculated for $C_6H_4BrN_3OS$ 244.93; found m/z = 246.05 $[M+H]^+$, 248.06 $[M+H+2]^+$.

2-bromo-7-(p-tolyl)-5*H*-[1,3,4]thiadiazolo[3,2-*a*]pyrimidin-5-one (16)

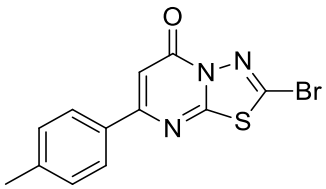

Compound **16** was obtained by following the general procedure (**D**), from the reaction between **12** and **15**, as a brown solid (270 mg, 70% yield by HPLC analysis). RP-HPLC t_R = 34.5 min, gradient condition: from 5% B ending to 100% B 50 min, flow rate of 4 mL/min, λ = 240 nm. ^{1}H NMR (400 MHz, $CDCl_3$): δ_H = 7.79 (d, *J* = 7.9 Hz, 2H), 7.30 (d, *J* = 8.1 Hz, 2H), 6.77 (s, 1H), 2.30 (s, 3H). ESI-MS: calculated for $C_{12}H_8BrN_3OS$ 320.96; found m/z = 322.02 $[M+H]^+$, 324.02 $[M+H+2]^+$.

7.4.2 General procedure (E) for the synthesis of LAM5-LAM11 and LAM13-LAM19

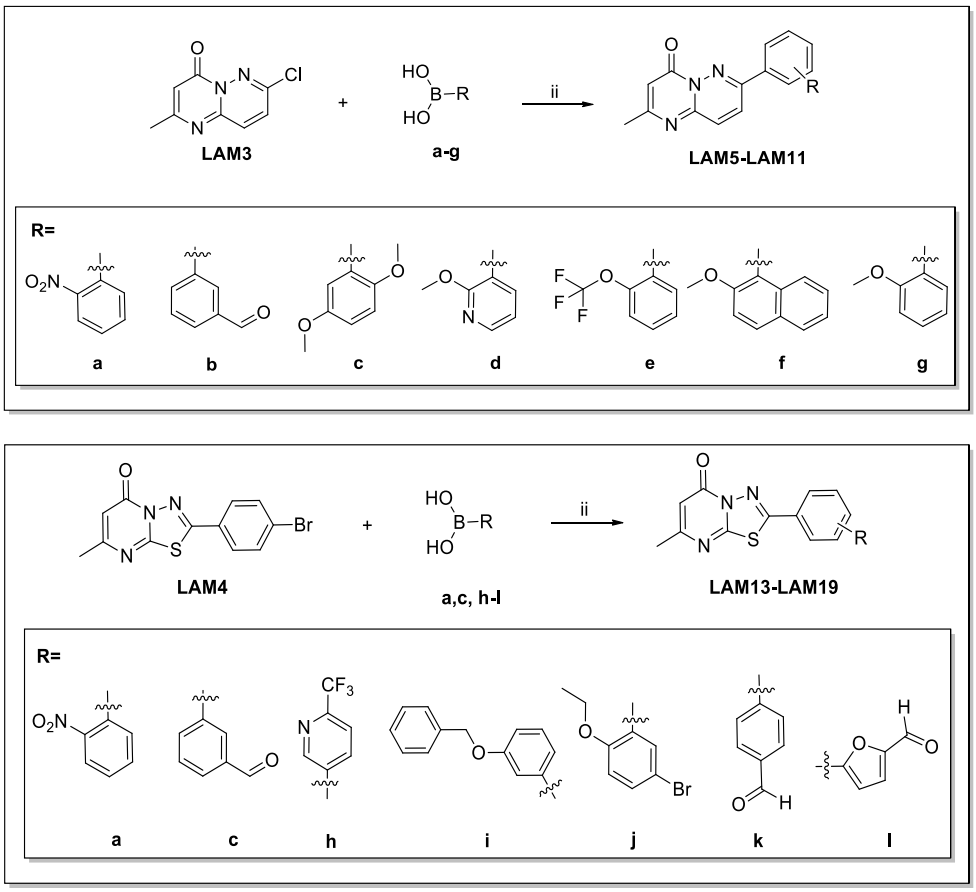

Synthetic scheme 6: ii) $Pd(PPh_3)_4$, K_2CO_3, dioxane/H_2O (2:1), reflux, overnight

LAM3 or **LAM4** (1.0 equiv), the appropriate boronic acid (**a-l**) (1.2 equiv), K_2CO_3 (2 equiv) and $Pd(PPh_3)_4$ (0.05 equiv) were placed in a two-neck round-bottom flask, equipped with a stir bar, and fitted with a condenser. The system was evacuated and refilled with N_2 five times. A mixture of dioxane/H_2O (3.0 mL and 1.5 mL; rate 2:1) was placed in a 25 ml round-bottom flask, it was evacuated and refilled with N_2 five times. Finally, dioxane/H_2O were added by syringe in the flask with the powders. The reaction flask was immersed in an oil bath and refluxed overnight (**Synthetic scheme 6**). [242] The reaction mixture was cooled, diluted with acidified

water (20 mL) and filtered. The filtered was dried over anhydrous Na_2SO_4 and concentrate under reduced pressure. The desired compounds **LAM5-LAM11** and **LAM13-LAM19** were confirmed by analytical RP-HPLC (Nucleodur© C8 reversed-phase column: 100 x 2mm, 4μM, 80 Å, flow rate = 1 mL/min). HPLC purification was performed by semi-preparative reversed-phase HPLC (Nucleodur© C8 reversed-phase column: 250 x 10.00 mm, 4μ M, 80 Å, flow rate = 4 mL/min). The final products were obtained with high purity (>98%) as detected by HPLC analysis and were fully characterized by ESI-MS and NMR spectra.

2-methyl-7-(2-nitrophenyl)-4*H*-pyrimido[1,2-*b*]pyridazin-4-one (LAM5)

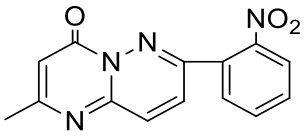

Compound **LAM5** was obtained by following the general procedure (**E**), from the reaction between **LAM3** and 2-nitrophenylboronic acid (**a**), as a brown solid (75 mg, 45% yield after HPLC purification). RP-HPLC t_R = 26.1 min, gradient condition: from 5% B ending to 100% B 50 min, flow rate of 4 mL/min, λ = 240 nm. ^{1}H NMR (400 MHz, CD_3OD): δ_H = 8.20 (d, *J* = 7.9 Hz, 1H), 7.88 – 7.83 (m, 1H), 7.81 (dd, *J* = 7.5, 1.3 Hz, 1H), 7.76 – 7.70 (m, 3H), 6.52 (s, 1H), 2.41 (s, 3H). ^{13}C NMR (100 MHz, $(CD_3)_2SO$): δ = 163.6, 156.6, 152.6, 147.7, 147.4, 134.3, 133.9, 131.9, 131.6, 130.3, 129.4, 125.0, 107.7, 23.6. ESI-MS: calculated for $C_{14}H_{10}N_4O_3$ 282.25; found m/z = 283.15 $[M+H]^+$.

3-(2-methyl-4-oxo-4*H*-pyrimido[1,2-*b*]pyridazin-7-yl)benzaldehyde (LAM6)

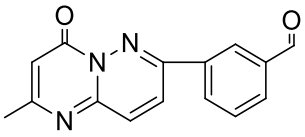

Compound **LAM6** was obtained by following the general procedure (**E**), from the reaction between **LAM3** and 3-formylphenylboronic acid (**b**), as a brown solid (50 mg, 40% yield after HPLC purification). RP-HPLC t_R = 21.1 min, gradient condition: from 5% B ending to 100% B 50 min, flow rate of 4 mL/min, λ = 240 nm. ^{1}H NMR (400 MHz, $CDCl_3$): δ_H = 10.08 (d, *J* = 3.1 Hz, 1H), 8.48 (s, *J* = 6.2 Hz, 1H), 8.40 (d, *J* = 7.4 Hz, 1H), 8.03 (t, *J* = 8.3 Hz, 1H), 7.93 (d, *J* = 2.5 Hz, 1H), 7.73 – 7.67 (m, 2H), 6.55 (s, 1H), 2.60 (s, 3H). ^{3}C NMR (100 MHz, $(CD_3)_2SO$): δ = 193.4, 165.1, 162.5, 148.2, 148.2, 137.8, 135.6, 133.5, 132.4, 131.6, 130.7 (2C), 127.8, 108.2, 24.1. ESI-MS: calculated for $C_{15}H_{11}N_3O_2$ 265.27; found m/z = 266.21 $[M+H]^+$.

7-(2,5-dimethoxyphenyl)-2-methyl-4*H*-pyrimido[1,2-*b*]pyridazin-4-one (LAM7)

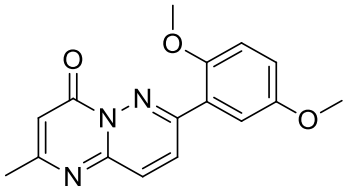

Compound **LAM7** was obtained by following the general procedure (**E**), from the reaction between **LAM3** and 2,5-dimethoxyphenylboronic acid (**c**), as a brown solid (70 mg, 60% yield after HPLC purification). RP-HPLC t_R = 25.3 min, gradient condition: from 5% B ending to 100% B 50 min, flow rate of 4 mL/min, λ = 240 nm. ^{1}H NMR (400 MHz, CD_3OD): δ = 8.11 (d, *J* = 9.4 Hz, 1H), 7.79 (d, *J* = 9.4 Hz, 1H), 7.33 (dt, *J* = 2.5, 1.3 Hz, 1H), 7.02-7.07 (m, 2H), 6.49 (d, *J* = 1.0 Hz, 1H), 3.77

(s, 3H), 3.74 (s, 3H), 2.40 (s, 3H). ^{13}C NMR (100 MHz, CH_3OD): δ = 164.1, 158.9, 154.2, 154.0, 152.0, 148.2, 131.8, 131.3, 123.6, 118.1, 115.5, 112.8, 107.2, 55.4, 54.9, 22.3. ESI-MS: calculated for $C_{16}H_{15}N_3O_3$ 297.31 found m/z = 298.12 $[M+H]^+$, 320.09 $[M+Na]^+$.

7-(2-methoxypyridin-3-yl)-2-methyl-4*H*-pyrimido[1,2-*b*]pyridazin-4-one (LAM8)

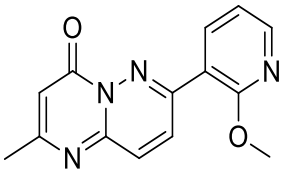

Compound **LAM8** was obtained by following the general procedure (**E**), from the reaction between **LAM3** and 2-methoxy-3-pyridinylboronic acid (**d**), as a brown solid (70 mg, 50% yield after HPLC purification). RP-HPLC t_R = 23.7 min, gradient condition: from 5% B ending to 100% B 50 min, flow rate of 4 mL/min, λ = 240 nm. ^{1}H NMR (400 MHz, CD_3OD): δ_H = 8.27-8.22 (m, 2H), 8.15 (d, *J* = 9.5 Hz, 1H), 7.83 (d, *J* = 9.5 Hz, 1H), 7.08 (dd, *J* = 7.5, 5.0 Hz, 1H), 6.50 (s, 1H), 3.96 (s, 3H), 2.40 (s, 3H). ^{13}C NMR (100 MHz, CD_3OD): δ = 164.2, 161.4, 158.8, 152.6, 149.5, 148.2, 140.2, 132.0, 130.8, 117.7, 117.4, 107.3, 52.9, 22.8. ESI-MS: calculated for $C_{14}H_{12}N_4O_2$ 268.10 found m/z = 269.10 $[M+H]^+$, 291.08 $[M+Na]^+$.

2-methyl-7-(2-(trifluoromethoxy)phenyl)-4*H*-pyrimido[1,2-*b*]pyridazin-4-one (LAM9)

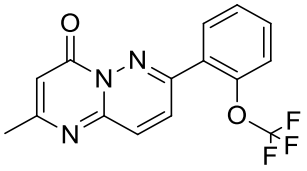

Compound **LAM9** was obtained by following the general procedure (**E**), from the reaction between **LAM3** and 2-(trifluoromethoxy)phenylboronic acid (**e**), as a brown solid (80 mg, 55% yield after HPLC purification). RP-HPLC t_R = 28.6 min, gradient condition: from 5% B ending to 100% B 50 min, flow rate of 4 mL/min, λ = 240 nm. ^{1}H NMR (400 MHz, CD_3OD): δ_H = 7.98–7.90 (m, 2H), 7.88 (dd, *J* = 7.7, 1.8 Hz, 1H), 7.61 (td, *J* = 7.9, 1.8 Hz, 1H), 7.52-7.43 (m, 2H), 6.53 (s, 1H), 2.41 (s, 3H)**.** ^{13}C NMR (100 MHz, CD_3OD): δ = 164.7, 158.8, 152.3, 148.0, 146.7, 133.2, 132.3, 131.9, 130.2, 128.5, 127.7, 121.3, 119.1, 107.7, 22.7**.** ESI-MS: calculated for $C_{15}H_{10}F_3N_3O_2$ 321.25 found m/z = 322.07 $[M+H]^+$, 344.05 $[M+Na]^+$.

7-(2-methoxynaphthalen-1-yl)-2-methyl-4*H*-pyrimido[1,2-*b*]pyridazin-4-one (LAM10)

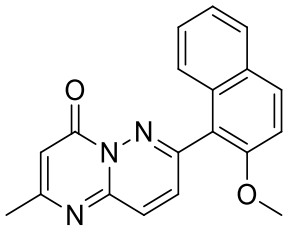

Compound **LAM10** was obtained by following the general procedure (**E**), from the reaction between **LAM3** and 2-methoxy-1-naphthaleneboronic acid (**f**), as a brown solid (105 mg, 45% yield after HPLC purification). RP-HPLC t_R = 28.2 min, gradient condition: from 5% B ending to 100% B 50 min, flow rate of 4 mL/min, λ = 240 nm. ^{1}H NMR (400 MHz, CD_3OD): δ_H = 8.01 (d, *J* = 9.2 Hz, 1H), 7.91 (d, *J* = 9.2 Hz, 1H), 7.81 (dd, *J* = 7.9, 1.6 Hz, 1H), 7.73 (d, *J* = 9.2 Hz, 1H), 7.55 (d, *J* =

8.3 Hz, 1H), 7.46 (d, *J* = 9.2 Hz, 1H), 7.37 – 7.27 (m, 2H), 6.51 (s, 1H), 3.85 (s, 3H), 2.43 (s, 3H). ^{13}C NMR (100 MHz, $(CD_3)_2SO$): δ = 163.9, 157.6, 155.3, 152.5, 148.5, 134.3, 132.7, 132.5, 132.3, 128.8, 128.6, 127.9, 124.5, 124.4, 118.2, 114.1, 108.0, 57.1, 24.2. ESI-MS: calculated for $C_{19}H_{15}N_3O_2$ 317.34 found m/z = 318.12 $[M+H]^+$, 340.10 $[M+Na]^+$.

7-(2-methoxyphenyl)-2-methyl-4*H*-pyrimido[1,2-*b*]pyridazin-4-one (LAM 11)

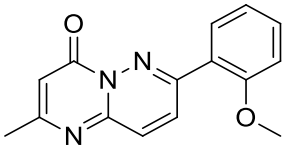

Compound **LAM11** was obtained by following the general procedure (**E**), from the reaction between **LAM3** and 2-methoxyphenylboronic acid (**g**), as a brown solid (85 mg, 55% yield after HPLC purification). RP-HPLC t_R = 23.6 min, gradient condition: from 5% B ending to 100% B 50 min, flow rate of 4 mL/min, λ = 240 nm. ^{1}H NMR (400 MHz, CD_3OD): δ_H = 8.12 (d, *J* = 9.4 Hz, 1H), 7.81 (d, *J* = 9.4 Hz, 1H), 7.72 (dd, *J* = 7.6, 1.8 Hz, 1H), 7.45 (ddt, *J* = 8.9, 7.5, 2.0 Hz, 1H), 7.09 (dd, *J* = 8.5, 1.0 Hz, 1H), 7.02 (td, *J* = 7.6, 1.0 Hz, 1H), 6.49 (s, 1H), 3.82 (s, 3H), 2.40 (s, 3H). ^{13}C NMR (100 MHz, $(CD_3)_2SO$): δ = 163.6, 157.8, 157.4, 153.1, 148.4, 133.1, 132.8, 131.3, 131.2, 124.0, 121.4, 112.7, 107.8, 56.3, 24.00. ESI-MS: calculated for $C_{15}H_{13}N_3O_2$ 267.28 found m/z = 268.11 $[M+H]^+$, 290.08 $[M+Na]^+$.

7-methyl-2-(2'-nitro-[1,1'-biphenyl]-4-yl)-5*H*-[1,3,4]thiadiazolo[3,2-*a*]pyrimidin-5-one (LAM13)

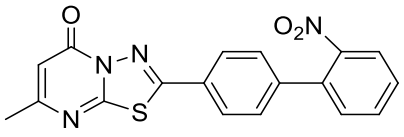

Compound **LAM13** was obtained by following the general procedure (**E**), from the reaction between **LAM4** and 2-nitrophenylboronic acid (**a**), as a brown solid (100 mg, 45% yield after HPLC purification). RP-HPLC t_R = 32.2 min, gradient condition: from 5% B ending to 100% B 50 min, flow rate of 4 mL/min, λ = 240 nm. ^{1}H NMR (400 MHz, CD_3OD): δ_H = 8.04 (d, *J* = 8.1 Hz, 2H), 7.89 (dd, *J* = 12.9, 8.4 Hz, 2H), 7.68 (t, *J* = 7.7 Hz, 2H), 7.55 (t, *J* = 7.7 Hz, 1H), 7.47 (d, *J* = 7.6 Hz, 1H), 6.31 (s, 1H), 2.44 (s, 3H). ^{13}C NMR (101 MHz, $(CD_3)_2SO$): δ = 163.5, 161.7, 157.9, 156.5, 148.9, 141.9, 134.5, 133.8, 132.2, 130.2, 129.5 (2C), 128.5, 128.1 (2C), 124.9, 107.3, 23.8. ESI-MS: calculated for $C_{18}H_{12}N_4O_3S$ 364.38; found m/z = 365.10 $[M+H]^+$.

7-methyl-2-(4-(6-(trifluoromethyl)pyridin-3-yl)phenyl)-5*H*-[1,3,4]thiadiazolo[3,2-*a*]pyrimidin-5-one (LAM14)

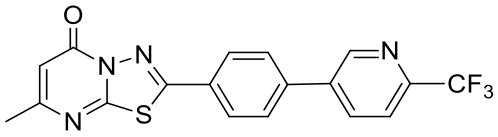

Compound **LAM14** was obtained by following the general procedure (**E**), from the reaction between **LAM4** and 6-(trifluoromethyl)pyridine-3-boronic acid (**h**), as a brown solid (100 mg, 70% yield after HPLC purification). RP-HPLC t_R = 41.9 min, gradient condition: from 5% B ending to 100% B 50 min, flow rate of 4 mL/min, λ = 240 nm. ^{1}H NMR (400 MHz, $CDCl_3$): δ_H = 8.93 (s, 1H), 8.08 – 8.03 (m, 3H), 7.78-7.70 (m, 3H), 6.31 (s, 1H), 2.50 (s, 3H). ^{13}C NMR (100 MHz, $(CD_3)_2SO$): δ =

164.5, 158.3, 154.9, 143.7, 142.8, 142.0, 137.0, 133.5, 132.7, 130.6 129.0 (2C), 128.7 (2C), 124.3, 121.5, 107.3, 23.7. ESI-MS: calculated for $C_{18}H_{11}F_3N_4OS$ 388.37; found m/z = 389.06 $[M+H]^+$.

4'-(7-methyl-5-oxo-5*H*-[1,3,4]thiadiazolo[3,2-*a*]pyrimidin-2-yl)-[1,1'-biphenyl]-3-carbaldehyde (LAM15)

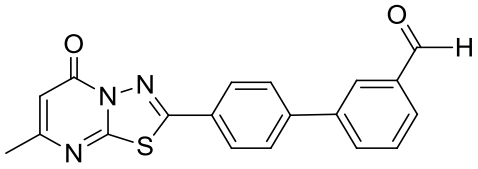

Compound **LAM15** was obtained by following the general procedure (**E**), from the reaction between **LAM4** and 3-formylphenylboronic acid (**b**), as a brown solid (60 mg, 45% yield after HPLC purification). RP-HPLC t_R = 36.4 min, gradient condition: from 5% B ending to 100% B 50 min, flow rate of 4 mL/min, λ = 240 nm. ^{1}H NMR (400 MHz, $CDCl_3$): δ_H = 8.34 (s, 1H), 8.18 – 8.11 (m, 3H), 8.05 (d, *J* = 8.2 Hz, 2H), 7.99 (d, *J* = 7.6 Hz, 1H), 7.77 (t, *J* = 7.7 Hz, 1H), 6.36 (s, 1H), 2.33 (s, 3H). ^{13}C NMR (100 MHz, $(CD_3)_2SO$): δ = 193.7, 163.5, 161.7, 158.0, 156.5, 143.3, 139.9, 137.4, 133.3, 130.6, 129.5, 128.7, 128.7 (2C), 128.4 (2C), 128.3, 107.5, 23.7. ESI-MS: calculated for $C_{19}H_{13}N_3O_2S$ 347.07; found m/z = 348.13 $[M+H]^+$.

2-(3'-(benzyloxy)-[1,1'-biphenyl]-4-yl)-7-methyl-5*H*-[1,3,4]thiadiazolo[3,2-*a*]pyrimidin-5-one (LAM16)

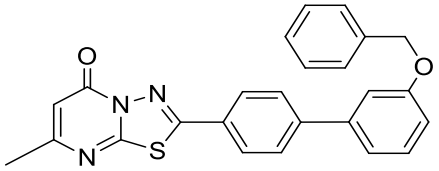

Compound **LAM16** was obtained by following the general procedure (**E**), from the reaction between **LAM4** and 3-(benzyloxy)phenylboronic acid (**i**), as a brown solid (70 mg, 65% yield after HPLC purification). RP-HPLC t_R = 45.3 min, gradient condition: from 5% B ending to 100% B 50 min, flow rate of 4 mL/min, λ = 240 nm. ^{1}H NMR (400 MHz, $CDCl_3$): δ_H = 7.95 (d, *J* = 7.7 Hz, 2H), 7.66 (d, *J* = 7.8 Hz, 2H), 7.42-7.27 (m, 8H), 6.97 (d, *J* = 8.2, 1H), 6.31 (s, 1H), 5.08 (s, 2H), 2.35 (s, 3H). ^{13}C NMR (100 MHz, $(CD_3)_2SO$): δ = 163.5, 159.4, 158.9, 158.6, 156.6, 144.5, 140.4, 137.5, 131.7, 130.5 (2C), 128.9 (2C), 128.4, 128.2 (2C), 127.2, 122.3 (2C), 119.9, 115.5, 113.8, 107.4, 69.8, 20.9. ESI-MS: calculated for $C_{25}H_{19}N_3O_2S$ 425.50; found m/z = 426.22 $[M+H]^+$, 851.48 $[M+M+H]^+$.

2-(5'-bromo-2'-ethoxy-[1,1'-biphenyl]-4-yl)-7-methyl-5*H*-[1,3,4]thiadiazolo[3,2-*a*]pyrimidin-5-one (LAM 17)

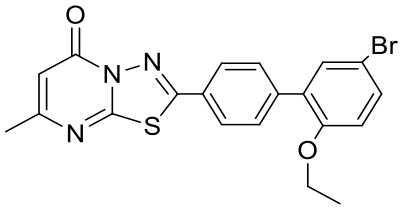

Compound **LAM17** was obtained by following the general procedure (**E**), from the reaction between **LAM4** and (5-bromo-2-ethoxyphenyl)boronic acid (**j**), as a brown solid (135 mg, 30% yield after HPLC purification). RP-HPLC t_R = 38.8 min, gradient condition: from 5% B ending to 100% B 50 min, flow rate of 4 mL/min, λ

= 240 nm. ^{1}H NMR (400 MHz, CD_3OD): δ_H = 7.98 (dt, *J* = 8.7, 2.1 Hz, 2H), 7.67-7.62 (m, 2H), 7.42 – 7.36 (m, 2H), 6.94 (d, *J* = 8.6 Hz, 1H), 6.30 (s, 1H), 3.97 (q, *J* = 7.0 Hz, 2H), 2.36 (s, 3H), 1.29 (t, *J* = 7.0 Hz, 3H). ^{13}C NMR (100 MHz, $(CD_3)_2SO$): δ = 163.5, 161.8, 158.1, 156.5, 155.3, 141.5, 132.8, 132.6, 130.9, 130.8 (2C), 127.6 (2C), 127.5, 115.7, 112.7, 107.3, 64.6, 23.7, 14.9. ESI-MS: calculated for $C_{20}H_{16}BrN_3O_2S$ 441.01; found m/z = 442.09 $[M+H]^+$, 444.09 $[M+H+2]^+$.

4'-(7-methyl-5-oxo-5*H*-[1,3,4]thiadiazolo[3,2-*a*]pyrimidin-2-yl)-[1,1'-biphenyl]-4-carboxylic acid (LAM18)

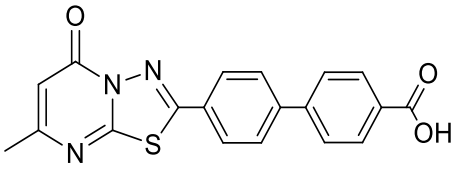

Compound **LAM18** was obtained by following the general procedure (**E**), from the reaction between **LAM4** and 4-carboxyphenylboronic acid (**k**), as a brown solid (80 mg, 60% yield after HPLC purification). RP-HPLC t_R = 22.3 min, gradient condition: from 5% B ending to 100% B 50 min, flow rate of 4 mL/min, λ = 240 nm. ^{1}H NMR (400 MHz, $(CD_3)_2SO$): δ_H = 8.05 (d, *J* = 8.0 Hz, 2H), 7.98 (d, *J* = 8,1 Hz, 2H), 7.93 – 7.86 (m, 4H), 5.63 (s, 1H), 2.13 (s, 3H). ^{13}C NMR (100 MHz, $(CD_3)_2SO$): δ = 198.8, 167.5, 160.3, 152.9, 149.6, 143.3, 142.3, 138.1, 130.7, 130.5 (2C), 129.0 (2C), 127.5 (2C), 127.3 (2C), 98.9, 18.7. ESI-MS: calculated for $C_{19}H_{13}N_3O_3S$ 363.39; found m/z = 364.16 $[M+H]^+$.

5-(4-(7-methyl-5-oxo-5*H*-[1,3,4]thiadiazolo[3,2-*a*]pyrimidin-2-yl)phenyl)furan-2-carbaldehyde (LAM19)

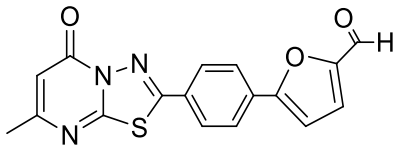

Compound **LAM19** was obtained by following the general procedure (**E**), from the reaction between **LAM4** and 5-Formyl-2-furanylboronic acid (**l**), as a brown solid (80 mg, 50% yield after HPLC purification). RP-HPLC t_R = 31.2 min, gradient condition: from 5% B ending to 100% B 50 min, flow rate of 4 mL/min, λ = 240 nm. ^{1}H NMR (400 MHz, $CDCl_3$): δ_H = 9.65 (s, 1H), 7.98 (dd, *J* = 8.5, 1.7 Hz, 2H), 7.90 (dd, *J* = 8.5, 1.7 Hz, 2H), 7.30 (dd, *J* = 3.8, 1.6 Hz, 1H), 6.95 (dd, 3.7, 1.6 Hz, 1H), 6.33 (s, 1H), 2.35 (s, 3H). ^{13}C NMR (100 MHz, $(CD_3)_2SO$): δ = 178.7, 163.6, 158.7, 158.4, 157.7, 156.5, 152.8, 132.7, 129.2, 128.8 (2C), 126.4 (2C), 125.5, 111.4, 107.3, 23.7. ESI-MS: calculated for $C_{17}H_{11}N_3O_3S$ 337.35; found m/z = 338.13 $[M+H]^+$.

7.4.3 Synthesis of 2-methyl-7-(phenylamino)-4*H*-pyrimido[1,2-*b*]pyridazin-4-one (LAM-12)

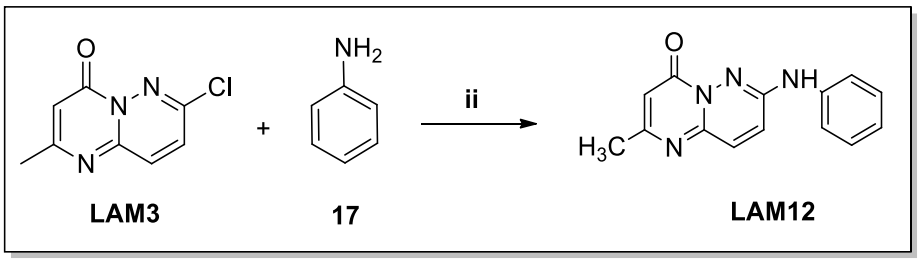

Synthetic scheme 7: ii) EtOH, reflux, overnight.

A mixture of **LAM3** (1.0 equiv) and aniline **17** (1.0 equiv) was dissolved in ethanol (2 mL) and refluxed for 24 h (**Synthetic scheme 7**). The reaction mixture was

cooled, diluted with acidified water (10 mL), and filtered. The filtered was dried over anhydrous Na_2SO_4 and concentrate under reduced pressure. The desired compound **LAM12** was confirmed by analytical RP-HPLC (Nucleodur© C8 reversed-phase column: 100 x 2 mm, 4 μM, 80 Å, flow rate = 1 mL/min). HPLC purification was performed by semi-preparative reversed-phase HPLC (Nucleodur© C8 reversed-phase column: 250 x 10.00 mm, 4 μM, 80 Å, flow rate = 4 mL/min). The final product was obtained with high purity (>98%) as detected by HPLC analysis and was fully characterized by ESI-MS and NMR spectra.

Compound **LAM12** was obtained as a brown solid (50 mg, 75% yield after HPLC purification). RP-HPLC t_R = 20.4 min, gradient condition: from 5% B ending to 100% B 50 min, flow rate of 4 mL/min, λ = 240 nm. ^{1}H NMR (400 MHz, $(CD_3)_2SO$): δ_H = 9.86 (s, 1H), 8.01 (d, *J* = 8.1 Hz, 2H), 7.73 (d, *J* = 9.5 Hz, 1H), 7.45 (d, *J* = 9.5 Hz, 1H), 7.37 (t, *J* = 7.8 Hz, 2H), 7.04 (t, *J* = 7.2 Hz, 1H), 6.39 (s, 1H), 2.33 (s, 3H). ^{13}C NMR (100 MHz, $(CD_3)_2SO$): δ = 161.6, 157.2, 150.4, 146.9, 140.4, 133.9, 129.4 (2C), 125.2, 122.7, 119.0 (2C), 107.8, 23.4. ESI-MS: calculated for $C_{14}H_{12}N_4O$ 252.27; found m/z = 253.16 $[M+H]^+$

7.4.4 General procedure (F) for the synthesis of LAM20-LAM28

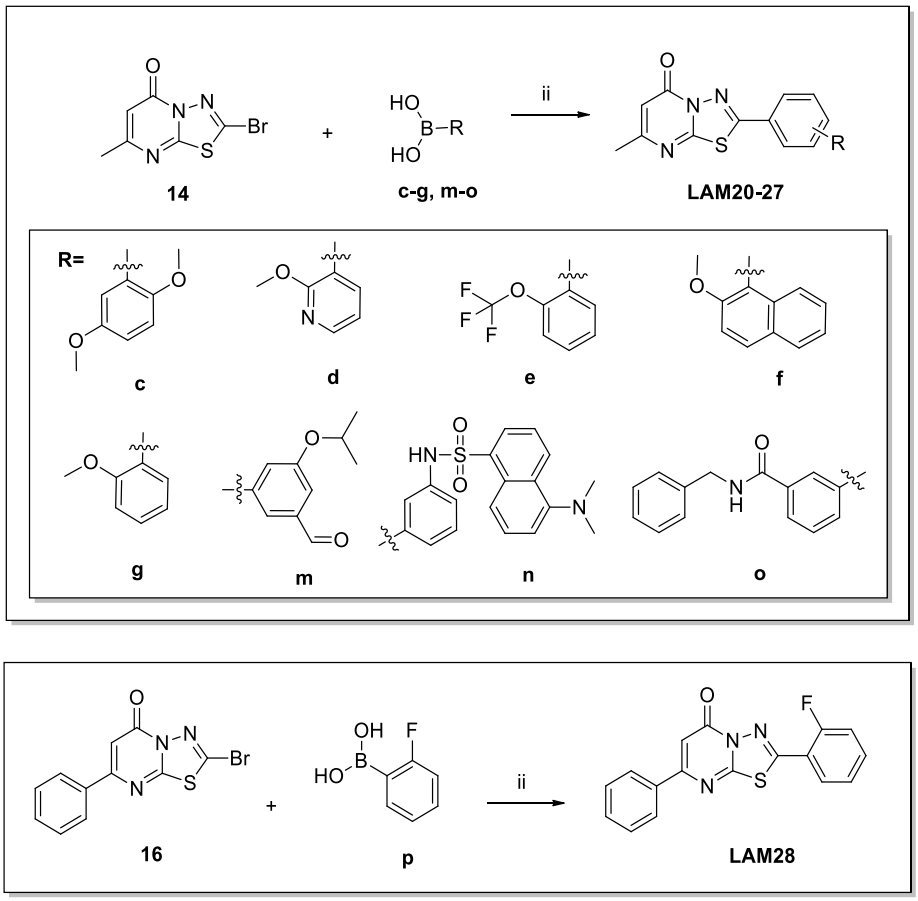

Synthetic scheme 8: ii) $Pd(AcO)_2$, K_2CO_3, xantphos, dry 1,4-dioxane, 100°C, 16h.

A mixture of **14** (1.0 equiv), the appropriate arylboronic acids **c-g**, **m-o** (1.1 equiv), palladium(II)acetate (0.1 equiv), xantphos (0.2 equiv), and potassium carbonate (2.0 equiv) was vigorously stirred and heated in dry 1,4-dioxane (2 mL) at 100°C for 16 h. Compound **16** was placed to react with (2-fluorophenyl)boronic acid (**p**) in the same experimental conditions (**Synthetic scheme 8**). [220] After cooling to room temperature, the reaction mixture was diluted with water and extracted with ethyl acetate. The organic layer was dried with Na_2SO_4 and the solvent was evaporated. The desired compounds **LAM20-LAM28** were confirmed by

analytical RP-HPLC (Nucleodur© C8 reversed-phase column: 100 x 2 mm, 4 μM, 80 Å, flow rate = 1 mL/min). HPLC purification was performed by semi-preparative reversed-phase HPLC (Nucleodur© C8 reversed-phase column: 250 x 10.00 mm, 4 μM, 80 Å, flow rate = 4 mL/min). The final products were obtained with high purity (>98%) as detected by HPLC analysis and were fully characterized by ESI-MS and NMR spectra.

2-(2-methoxynaphthalen-1-yl)-7-methyl-5*H*-[1,3,4]thiadiazolo[3,2-*a*]pyrimidin-5-one (LAM20)

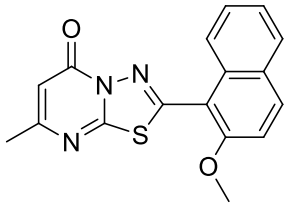

Compound **LAM20** was obtained by following the general procedure (**F**), from the reaction between **14** and 2-methoxy-1-naphthaleneboronic acid (**f**), as a brown solid (80 mg, 40% yield after HPLC purification). RP-HPLC t_R = 34.3 min, gradient condition: from 5% B ending to 100% B 50 min, flow rate of 4 mL/min, λ = 240 nm. ^{1}H NMR (400 MHz, $CDCl_3$): δ = 8.37 (dd, *J* = 8.7, 1.0 Hz, 1H), 7.99 (d, *J* = 9.1 Hz, 1H), 7.79-7.76 (m, 1H), 7.53 (ddd, *J* = 8.5, 6.8, 1.4 Hz, 1H), 7.38 (ddd, *J* = 8.0, 6.8, 1.1 Hz, 1H), 7.28 (d, *J* = 9.1 Hz, 1H), 6.29 (s, 1H), 3.97 (s, 3H), 2.36 (s, 3H). ^{13}C NMR (100 MHz, $CDCl_3$): δ = 163.6, 162.2, 157.3, 156.7, 154.9, 134.6, 132.0, 129.2, 128.8, 128.4, 124.8, 124.4, 112.1, 110.4, 107.0, 56.6, 24.0. ESI-MS: calculated for $C_{17}H_{13}N_3O_2S$ 323.07; found m/z = 324.08 $[M+H]^+$, 346.06 $[M+Na]^+$.

2-(2-methoxyphenyl)-7-methyl-5*H*-[1,3,4]thiadiazolo[3,2-*a*]pyrimidin-5-one (LAM21)

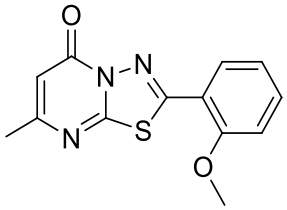

Compound **LAM21** was obtained by following the general procedure (**F**), from the reaction between **14** and 2-methoxyphenylboronic acid (**g**), as a brown solid (65 mg, 60% yield after HPLC purification). RP-HPLC t_R = 28.8 min, gradient condition: from 5% B ending to 100% B 50 min, flow rate of 4 mL/min, λ = 240 nm. ^{1}H NMR (400 MHz, CD_3OD): δ_H = 8.46 (dd, *J* = 8.0, 1.7 Hz, 1H), 7.67 (ddd, *J* = 8.7, 7.3, 1.7 Hz, 1H), 7.31 (d, *J* = 8.5 Hz, 1H), 7.24 – 7.19 (m, 1H), 6.39 (s, 1H), 4.11 (s, 3H), 2.43 (s, 3H). ^{13}C NMR (100 MHz, $(CD_3)_2SO$): δ = 163.2, 162.0, 157.2, 156.2, 153.2, 134.5, 127.4, 121.7, 116.8, 113.1, 106.3, 56.7, 23.6. ESI-MS: calculated for $C_{13}H_{11}N_3O_2S$ 273.06 found m/z = 274.07 $[M+H]^+$, 296.04 $[M+Na]^+$.

3-isopropoxy-5-(7-methyl-5-oxo-5*H*-[1,3,4]thiadiazolo[3,2-*a*]pyrimidin-2-yl)benzaldehyde (LAM22)

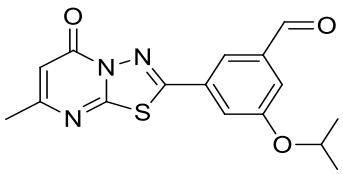

Compound **LAM22** was obtained by following the general procedure (**F**), from the reaction between **14** and 3-formyl-5-isopropoxyphenylboronic acid (**m**), as a brown solid (90 mg, 45% yield after HPLC purification). RP-HPLC t_R = 32.4 min, gradient condition: from 5% B ending to 100% B 50 min, flow rate of 4 mL/min, λ = 240 nm. ^{1}H NMR (400 MHz, CD_3OD): δ_H = 7.95 (t, *J* = 1.5 Hz, 1H), 7.82 (t, *J* = 2.1

Hz, 1H), 7.58 (dd, *J* = 2.6, 1.3 Hz, 1H), 6.32 (s, 1H), 4.69-4.64 (m, 1H), 2.32 (s, 3H), 1.31 (s, 3H), 1.30 (s, 3H). ^{13}C NMR (100 MHz, $(CD_3)_2SO$): δ = 191.0, 164.5, 158.3, 158.0, 154.9, 143.7, 137.6, 131.7, 120.7, 119.2, 118.3, 103.8, 75.8, 23.8, 22.0 (2C) ESI-MS: calculated $C_{16}H_{15}N_3O_3S$ 329.37 found m/z = 330.09 $[M+H]^+$, 352.07 $[M+Na]^+$.

2-(2,5-dimethoxyphenyl)-7-methyl-5*H*-[1,3,4]thiadiazolo[3,2-*a*]pyrimidin-5-one (LAM23)

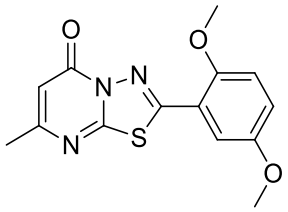

Compound **LAM23** was obtained by following the general procedure (**F**), from the reaction between **14** and 2,5-dimethoxyphenylboronic acid (**c**), as a brown solid (65 mg, 50% yield after HPLC purification). RP-HPLC t_R = 31.8 min, gradient condition: from 5% B ending to 100% B 50 min, flow rate of 4 mL/min, λ = 240 nm. ^{1}H NMR (400 MHz, $CDCl_3$): δ_H = 7.86 (d, *J* = 3.1 Hz, 1H), 7.07 (dd, *J* = 9.1, 3.1 Hz, 1H), 6.95 (d, *J* = 9.1 Hz, 1H), 6.31 (s, 1H), 3.94 (s, 3H), 3.81 (s, 3H), 2.35 (s, 3H). ^{13}C NMR (100 MHz, $(CD_3)_2SO$): δ = 163.6, 162.3, 156,4, 153.9, 153.3, 152.1, 121.4, 117.4, 115.2, 110.8, 106.7, 57.4, 56.2, 23.8. ESI-MS: calculated for $C_{14}H_{13}N_3O_3S$ 303.34 found m/z = 304.07 $[M+H]^+$, 326.06 $[M+Na]^+$.

2-(2-methoxypyridin-3-yl)-7-methyl-5*H*-[1,3,4]thiadiazolo[3,2-*a*]pyrimidin-5-one (LAM24)

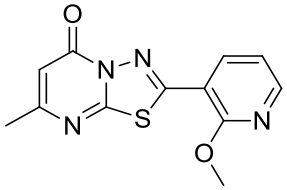

Compound **LAM24** was obtained by following the general procedure (**F**), from the reaction between **14** and 2-methoxy-3-pyridinylboronic acid (**d**), as a brown solid (60 mg, 65% yield after HPLC purification). RP-HPLC t_R = 26.6 min, gradient condition: from 5% B ending to 100% B 50 min, flow rate of 4 mL/min, λ = 240 nm. ^{1}H NMR (400 MHz, $(CD_3)_2SO$): δ_H= 8.59 (d, *J* = 7.7 Hz, 1H), 8.51 (d, *J* = 4.7 Hz, 1H), 7.33 (dd, *J* = 7.7, 4.8 Hz, 1H), 6.33 (s, 1H), 4.12 (s, 3H), 2.33 (s, 3H). ^{13}C NMR (100 MHz, $(CD_3)_2SO$): δ = 163.7, 158.4, 158.1, 156.4, 152.0, 151.7, 137.5, 118.8, 114.0, 106.7, 55.1, 23.7. ESI-MS: calculated for $C_{12}H_{10}N_4O_2S$ 274.30 found m/z = 275.06 $[M+H]^+$, 297.04 $[M+Na]^+$.

7-methyl-2-(2-(trifluoromethoxy)phenyl)-5*H*-[1,3,4]thiadiazolo[3,2-*a*]pyrimidin-5-one (LAM25)

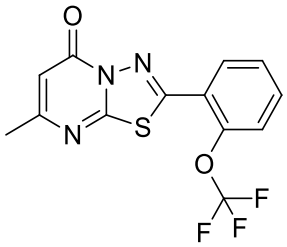

Compound **LAM25** was obtained by following the general procedure (**F**). from the reaction between **14** and 2-(trifluoromethoxy)phenylboronic acid (**e**), as a brown solid (70 mg, 75% yield after HPLC purification). RP-HPLC t_R = 34.8 min, gradient condition: from 5% B ending to 100% B 50 min, flow rate of 4 mL/min, λ = 240

nm. ^{1}H NMR (400 MHz, $CDCl_3$): δ = 8.41 (dd, *J* = 8.0, 1.7 Hz, 1H), 7.58 (ddd, *J* = 8.3, 7.4, 1.7 Hz, 1H), 7.44 -7.36 (m, 2H), 6.29 (s, 1H), 2.34 (s, 3H). ^{13}C NMR (100 MHz, $(CD_3)_2SO$): δ = 163.8, 161.8, 156.4, 152.5, 146.3, 135.0, 130.4, 128.9, 121.9, 121.7, 119.0, 107.2, 23.7. ESI-MS: calculated for $C_{13}H_8F_3N_3O_2S$ 327.28 found m/z = 328.04 $[M+H]^+$, 350.02 $[M+Na]^+$.

5-(dimethylamino)-*N*-(3-(7-methyl-5-oxo-5*H*-[1,3,4]thiadiazolo[3,2-*a*]pyrimidin-2-yl)phenyl)naphthalene-1-sulfonamide (LAM26)

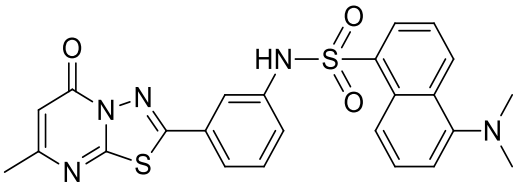

Compound **LAM26** was obtained by following the general procedure (**F**), from the reaction between **14** and 3-(dansylamino)phenylboronic acid (**n**), as a brown solid (105 mg, 55% yield after HPLC purification). RP-HPLC t_R = 34.8 min, gradient condition: from 5% B ending to 100% B 50 min, flow rate of 4 mL/min, λ = 240 nm. ^{1}H NMR (400 MHz, $(CD_3)_2SO$): δ_H = 11.10 (s, 1H), 8.47 (dd, *J* = 8.4, 2.8 Hz, 1H), 8.38 (dd, *J* = 8.7, 2.7 Hz, 1H), 8.30 (dd, *J* = 7.4, 2.8 Hz, 1H), 7.68-7.62 (m, 3H), 7.49 (d, *J* = 7.5, 1H), 7.42 (d, *J* = 7.7 Hz, 1H), 7.36 (d, *J* = 8.0 Hz, 1H), 7.28 (dd, *J* = 7.7, 2.8 Hz, 1H). 6.32 (s, 1H), 2.81 (s, 6H), 2.30 (s, 3H). ^{13}C NMR (100 MHz, $(CD_3)_2SO$): δ = 163.5, 161.5, 157.7, 156.4, 151.9, 139.3, 134.7, 131.2, 131.0, 130.5, 129.5, 129.5, 129.4, 128.9, 124.1, 123.1, 122.5, 118.9, 116.5, 115.9, 107.3, 45.5 (2C), 23.7. ESI-MS: calculated for $C_{24}H_{21}N_5O_3S_2$ 491.11; found m/z = 492.11 $[M+H]^+$, 514.10 $[M+Na]^+$.

N-benzyl-3-(7-methyl-5-oxo-5*H*-[1,3,4]thiadiazolo[3,2-*a*]pyrimidin-2-yl)benzamide (LAM27)

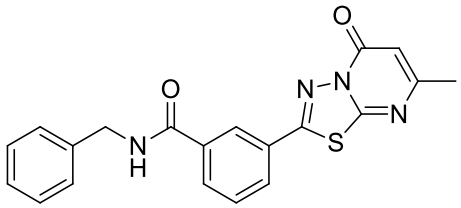

Compound **LAM27** was obtained by following the general procedure (**F**), from the reaction between **14** and 3-[(benzylamino)carbonyl]phenylboronic acid (**o**), as a brown solid (75 mg, 50% yield after HPLC purification). RP-HPLC t_R = 31.3 min, gradient condition: from 5% B ending to 100% B 50 min, flow rate of 4 mL/min, λ = 240 nm. ^{1}H NMR (400 MHz, $(CD_3)_2SO$): δ_H = 9.38 (t, *J* = 6.0 Hz, 1H), 8.45 (d, *J* = 1.9 Hz, 1H), 8.21-8.13 (m, 2H), 7.75 (t, *J* = 7.8 Hz, 1H), 7.38-7.34 (m, 4H), 7.27 (td, *J* = 5.3, 2.7 Hz, 1H), 6.36 (s, 1H), 4.54 (d, *J* = 5.9 Hz, 2H), 2.33 (s, 3H). ^{13}C NMR (100 MHz, $(CD_3)_2SO$): δ = 165.4, 163.6, 161.8, 158.0, 156.5, 139.8, 135.9, 131.9, 130.5, 130.3, 128.9, 128.81 (2C), 127.7 (2C), 127.3, 126.5, 107.4, 43.3, 23.8. ESI-MS: calculated for $C_{20}H_{16}N_4O_2S$ 376.10; found m/z = 377.11 $[M+H]^+$, 399.09 $[M+Na]^+$.

2-(2-fluorophenyl)-7-(p-tolyl)-5*H*-[1,3,4]thiadiazolo[3,2-*a*]pyrimidin-5-one (LAM28)

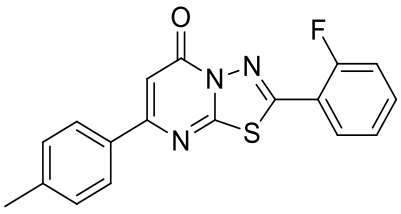

Compound **LAM28** was obtained by following the general procedure (**F**), from the reaction between **16** and 2-fluorophenylboronic acid (**p**), as a brown solid (100 mg,

35% yield after HPLC purification). RP-HPLC t_R = 45.4 min, gradient condition: from 5% B ending to 100% B 50 min, flow rate of 4 mL/min, λ = 240 nm. ^{1}H NMR (400 MHz, $CDCl_3$): δ_H = 7.85 (d, *J* = 7.9 Hz, 2H), 7.54 (q, *J* = 7.3 Hz, 1H), 7.30 (t, *J* = 7.5 Hz, 1H), 7.23 (dd, *J* = 8.1, 3.4 Hz, 4H), 6.87 (s, 1H), 2.36 (s, 3H). ^{13}C NMR (100 MHz, $CDCl_3$): δ = 162.0, 161.7, 161.7, 161.3, 159.4, 153.3, 141.8, 134.6, 132.8, 129.7 (2C), 127.4 (2C), 126.7, 125.7, 116.5, 100.8, 21.4. ESI-MS: calculated for $C_{18}H_{12}FN_3OS$ 337.07 found m/z = 338.08 $[M+H]^+$, 360.06 $[M+Na]^+$.

7.5 Biophysical and biological assays

SPR assay

Recombinant Human Heat Shock Transcription Factor-1 (HSF1) full length was purchased from Prospec-Tany Technogene Ltd. Surface Plasmon Resonance Spectroscopy (SPR) analyses were performed on a Biacore 3000^{TM} optical biosensor equipped with research-grade CM5 sensor chips (GE Healthcare^{TM}). HSF1 was coupled to the surface of a CM5 sensor chip using standard amine-coupling protocol, according to the manufacturer's instructions; one unmodified reference surface was prepared for simultaneous analyses. The protein (20 µg µl^{-1} in 10 mM CH_3COONa, pH 4.5) was immobilized at a flow rate of 5 µL min^{-1} to obtain densities of 10–11 kRU. Compounds were dissolved to obtain 50 mM solution concentrations, in 100% DMSO and diluted 1:100 (v/v) in PBS (10 mM NaH_2PO_4, 150 mM NaCl, pH 7.4) to a final DMSO concentration of 1.0%. For each molecule a six-point concentration series were set up, including 0–0.25–1–10–50–100 µM, and the complete binding study was performed using triplicate aliquots. Binding experiments were performed at 25 °C, using a flow rate of 10 µL min^{-1}, with 60 s monitoring of association and 300 s monitoring of dissociation (**Figure 70-97**).

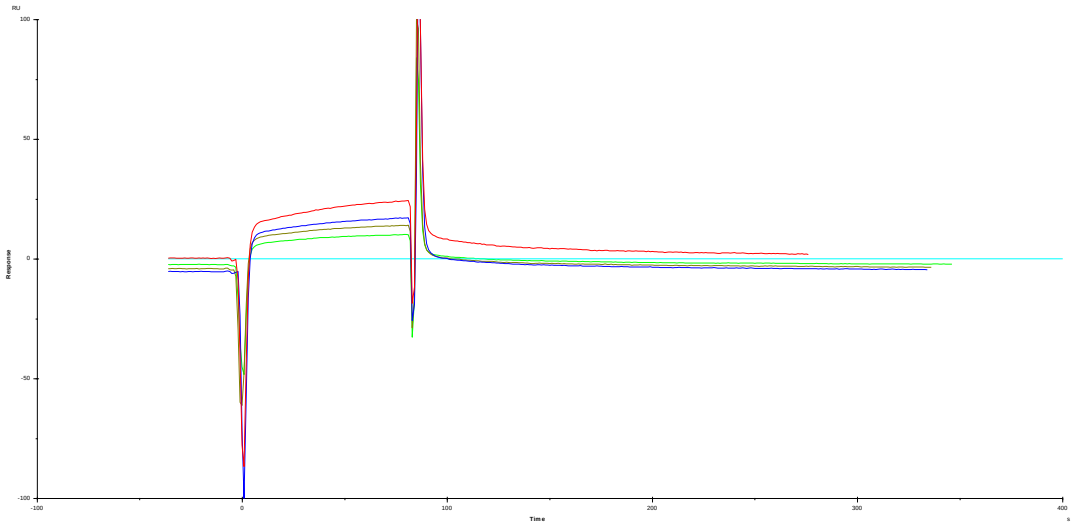

Figure 70: Surface Plasmon resonance sensorgram acquired for compound **HO-1** interacting with full-length HSF1.

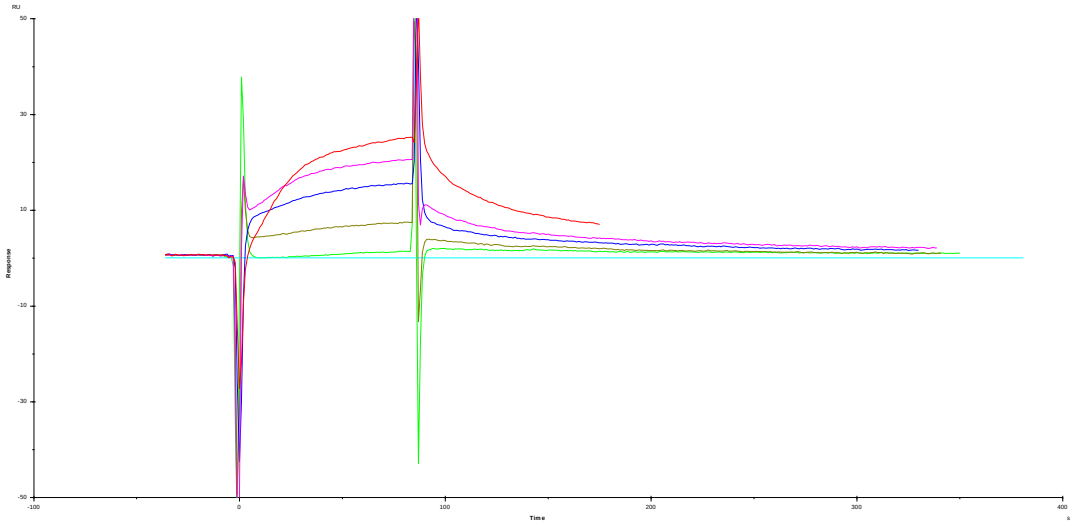

Figure 71: Surface Plasmon resonance sensorgram acquired for compound **HO-2** interacting with full-length HSF1.

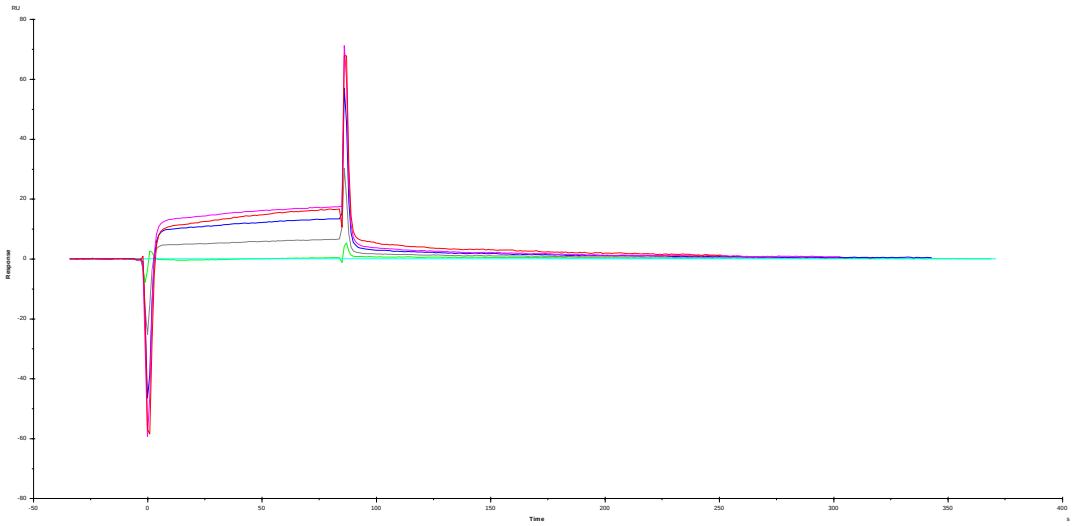

Figure 72: Surface Plasmon resonance sensorgram acquired for compound **HO-11** interacting with full-length HSF1.

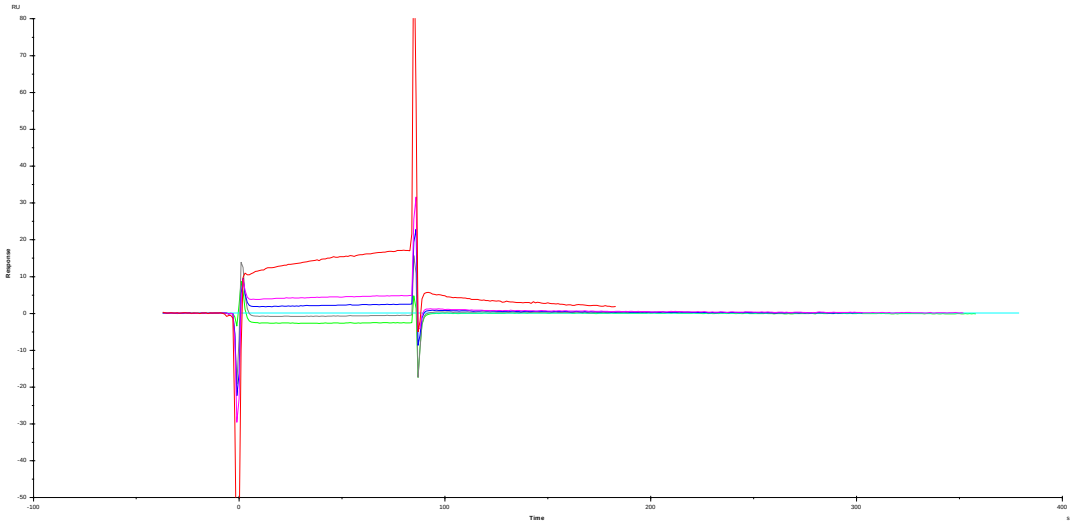

Figure 73: Surface Plasmon resonance sensorgram acquired for compound **HO-15** interacting with full-length HSF1.

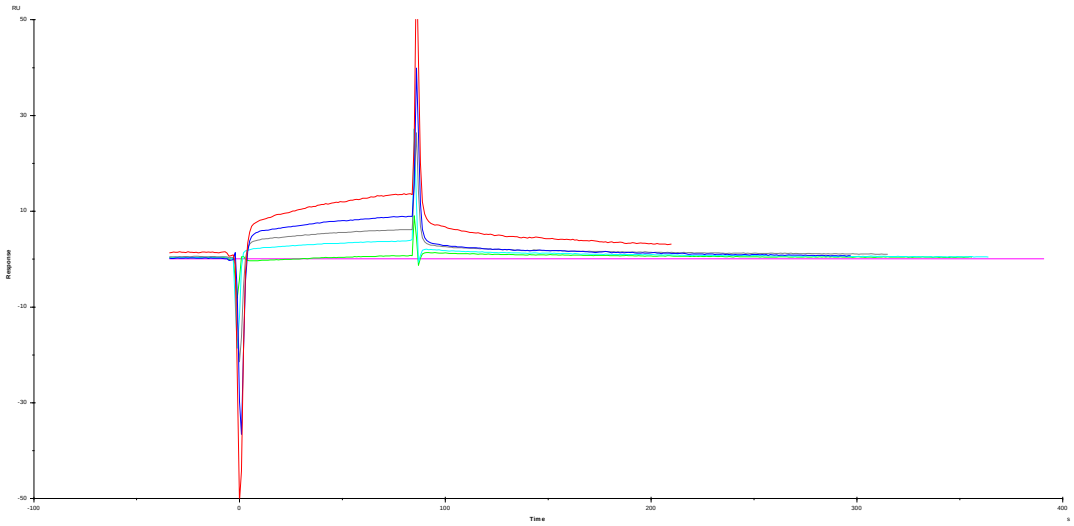

Figure 74: Surface Plasmon resonance sensorgram acquired for compound **HO-16** interacting with full-length HSF1.

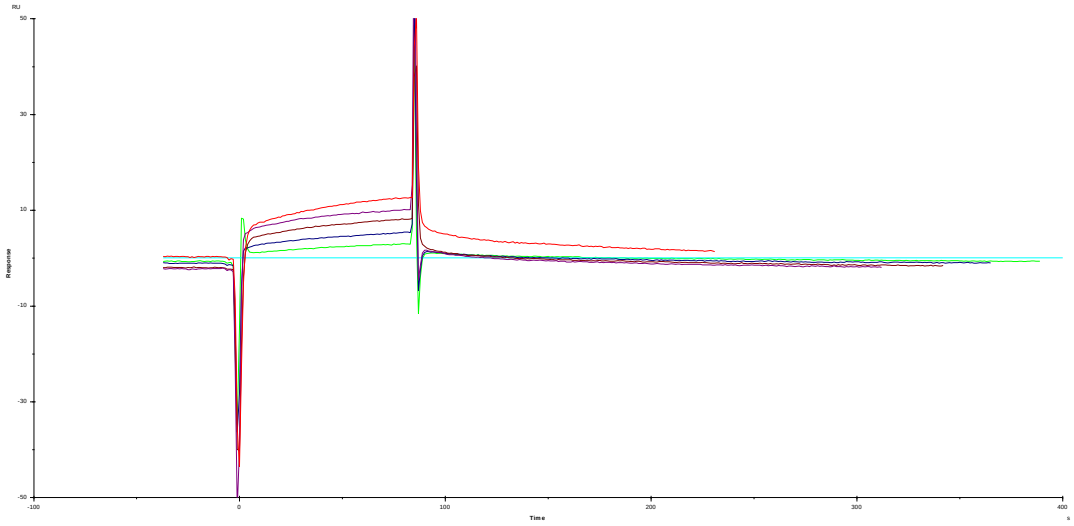

Figure 75: Surface Plasmon resonance sensorgram acquired for compound **HO-19** interacting with full-length HSF1.

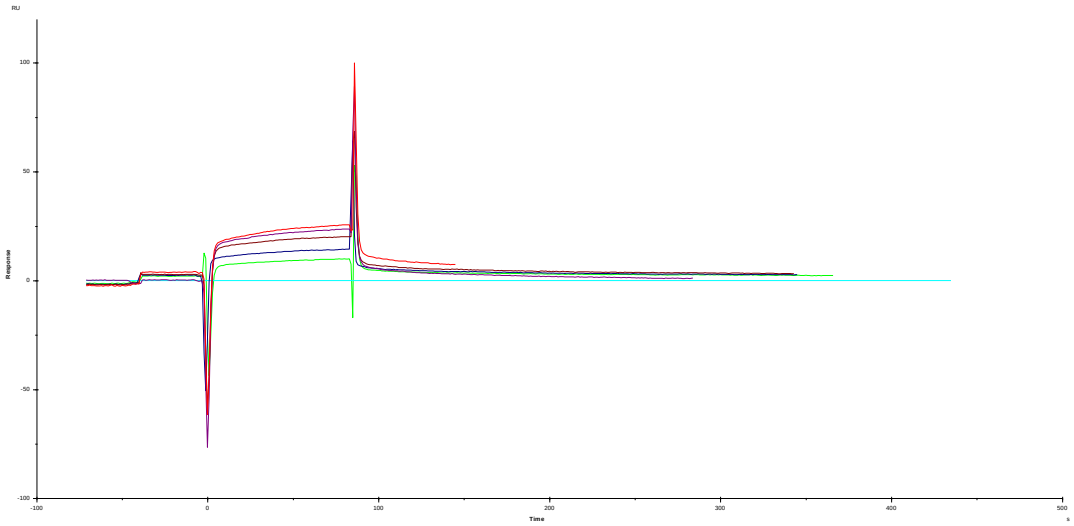

Figure 76: Surface Plasmon resonance sensorgram acquired for compound **HO-23** interacting with full-length HSF1.

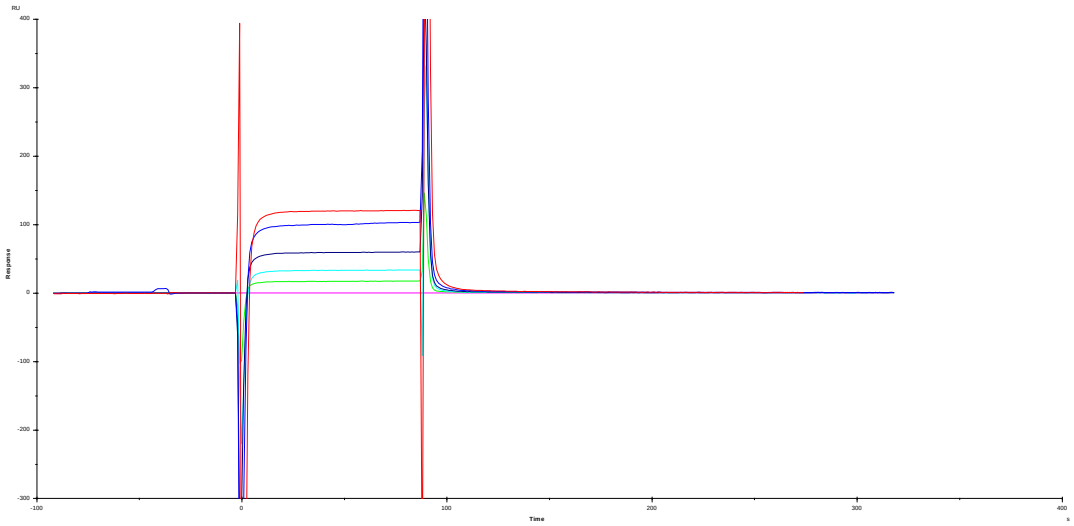

Figure 77: Surface Plasmon resonance sensorgram acquired for compound **HO-27** interacting with full-length HSF1.

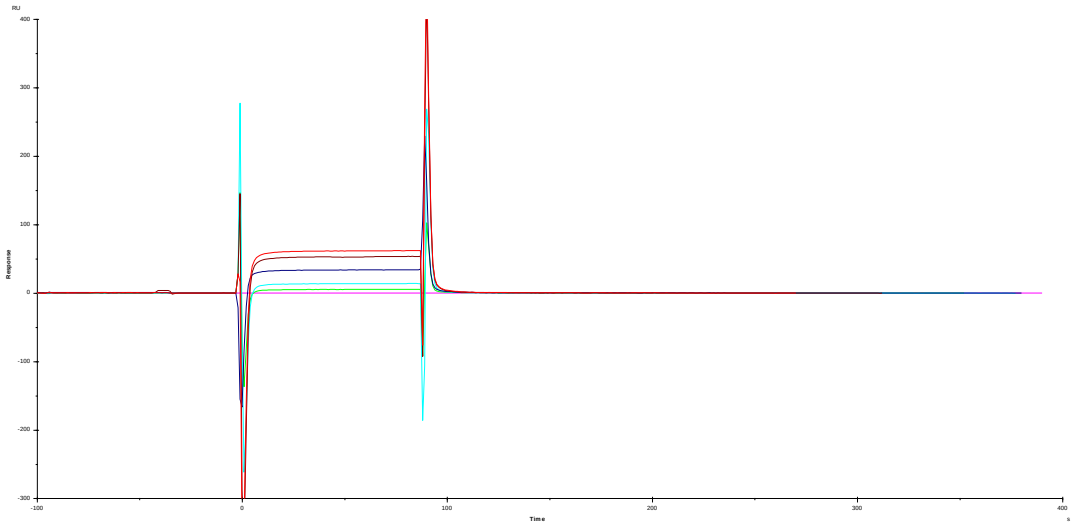

Figure 78: Surface Plasmon resonance sensorgram acquired for compound **HO-28** interacting with full-length HSF1.

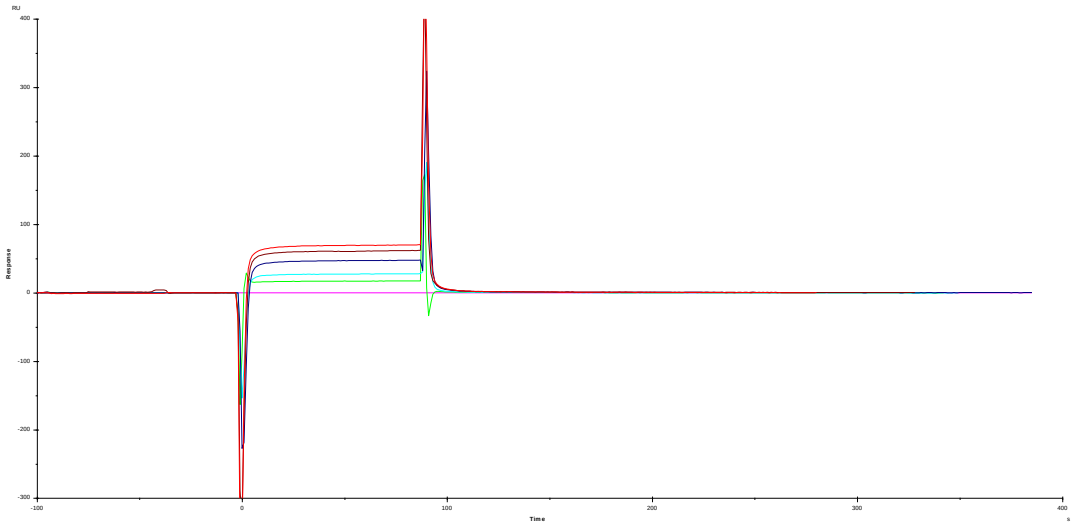

Figure 79: Surface Plasmon resonance sensorgram acquired for compound **HO-38** interacting with full-length HSF1.

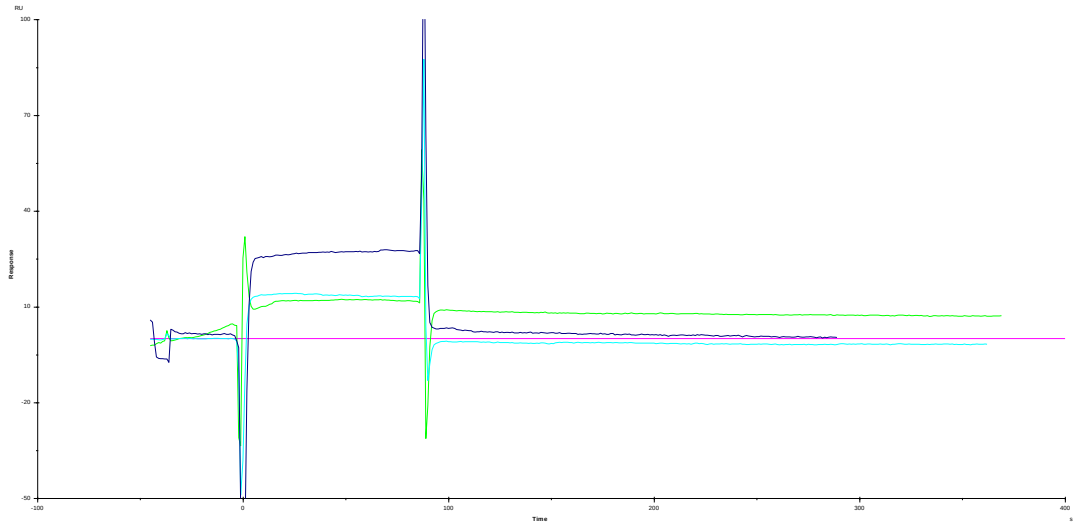

Figure 80: Surface Plasmon resonance sensorgram acquired for compound **HO-39** interacting with full-length HSF1.

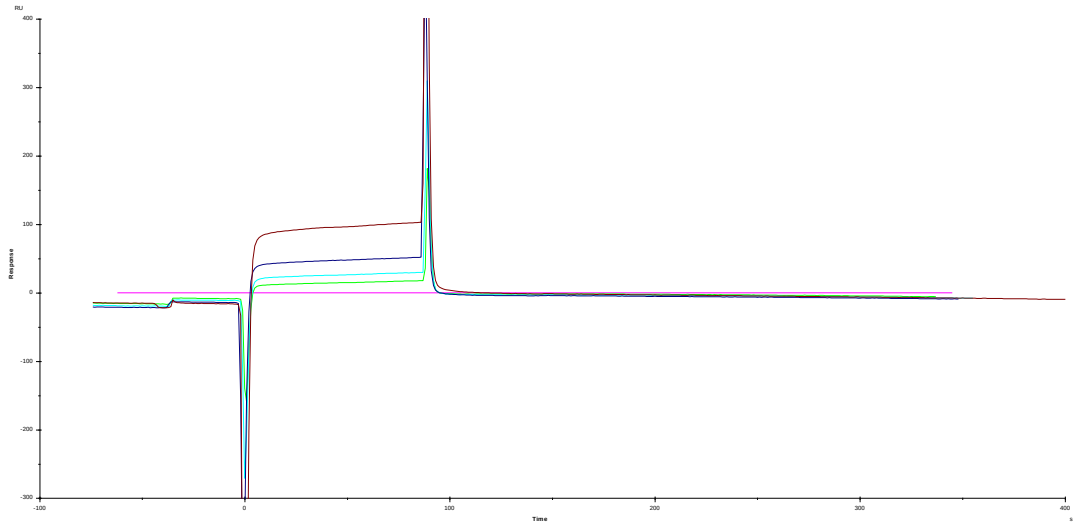

Figure 81: Surface Plasmon resonance sensorgram acquired for compound **SP7** interacting with full-length HSF1.

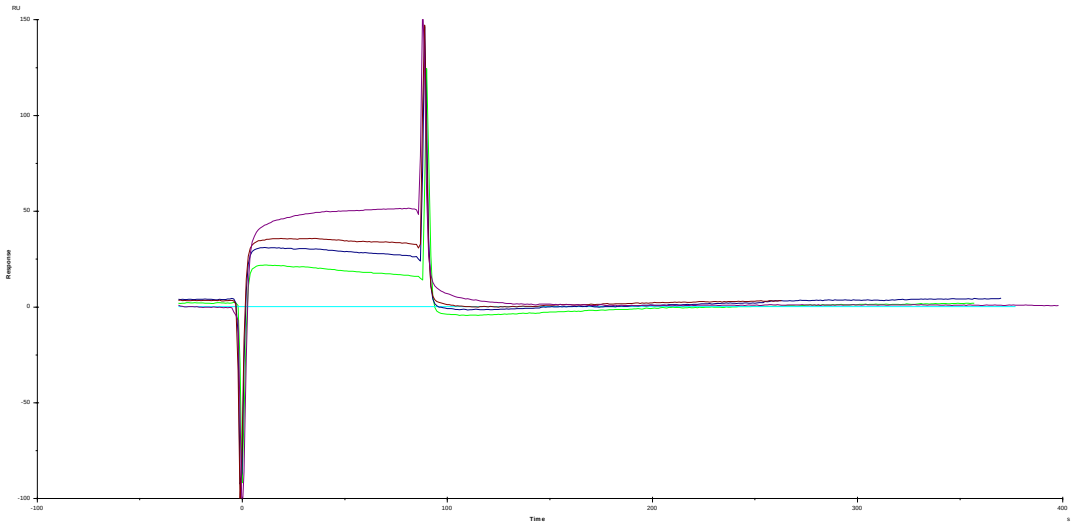

Figure 82: Surface Plasmon resonance sensorgram acquired for compound **BD-1** interacting with full-length HSF1.

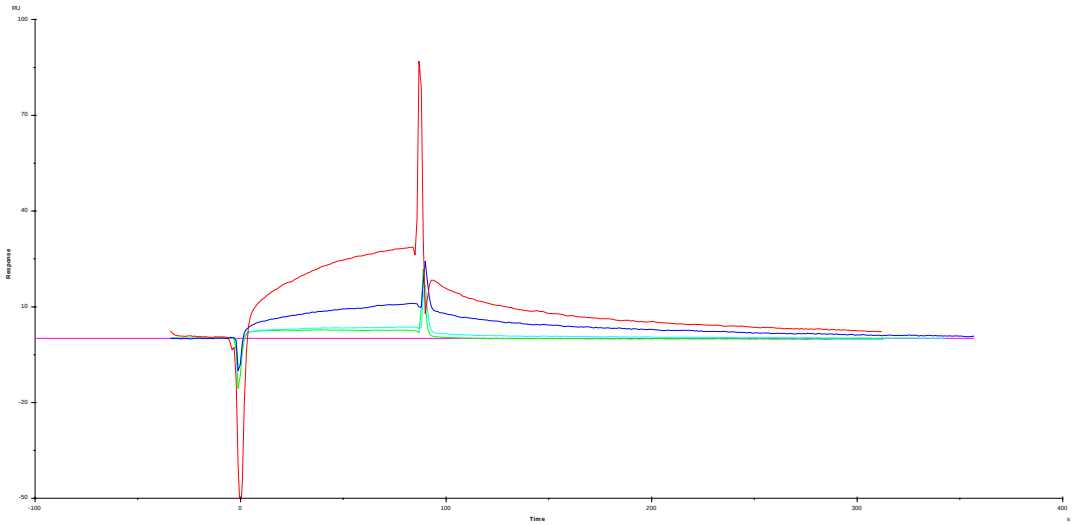

Figure 83: Surface Plasmon resonance sensorgram acquired for compound **BGN-JM4** interacting with full-length HSF1.

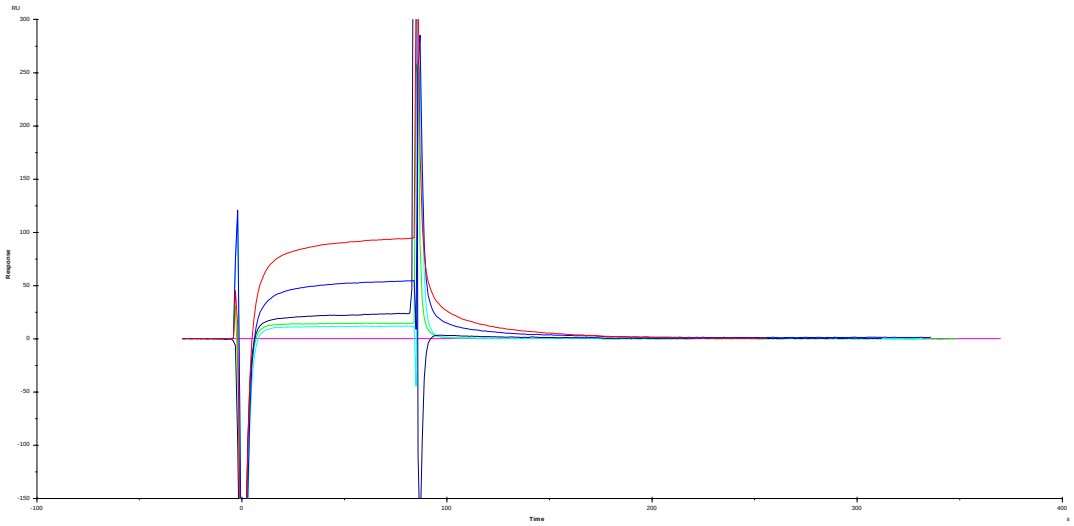

Figure 84: Surface Plasmon resonance sensorgram acquired for compound **MO-1** interacting with full-length HSF1.

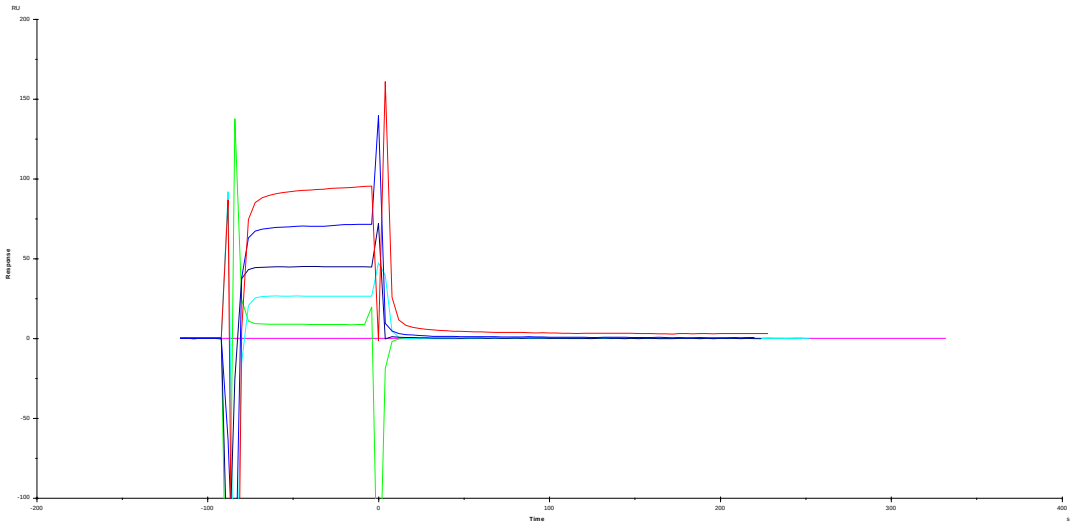

Figure 85: Surface Plasmon resonance sensorgram acquired for compound **MO-2** interacting with full-length HSF1.

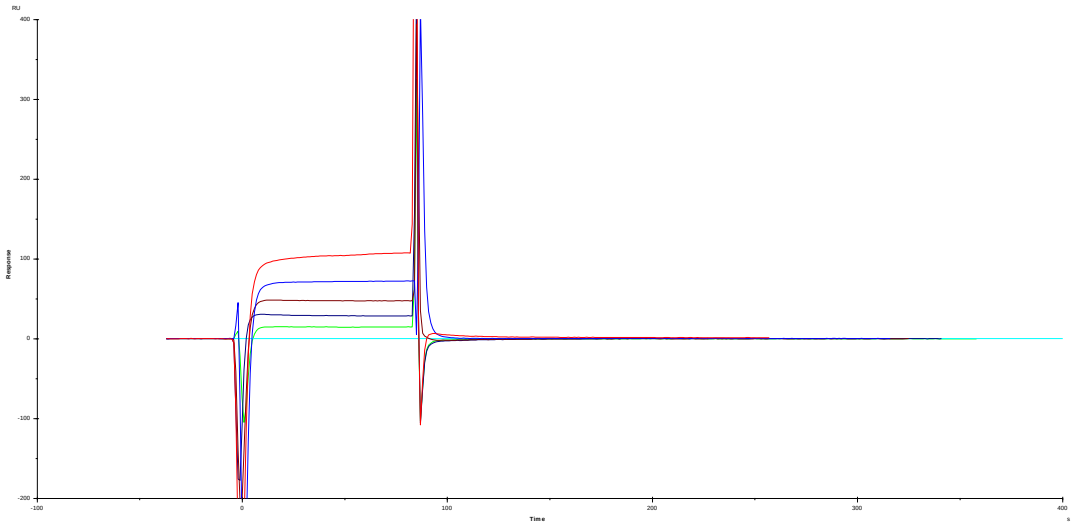

Figure 86: Surface Plasmon resonance sensorgram acquired for compound **MO-3** interacting with full-length HSF1.

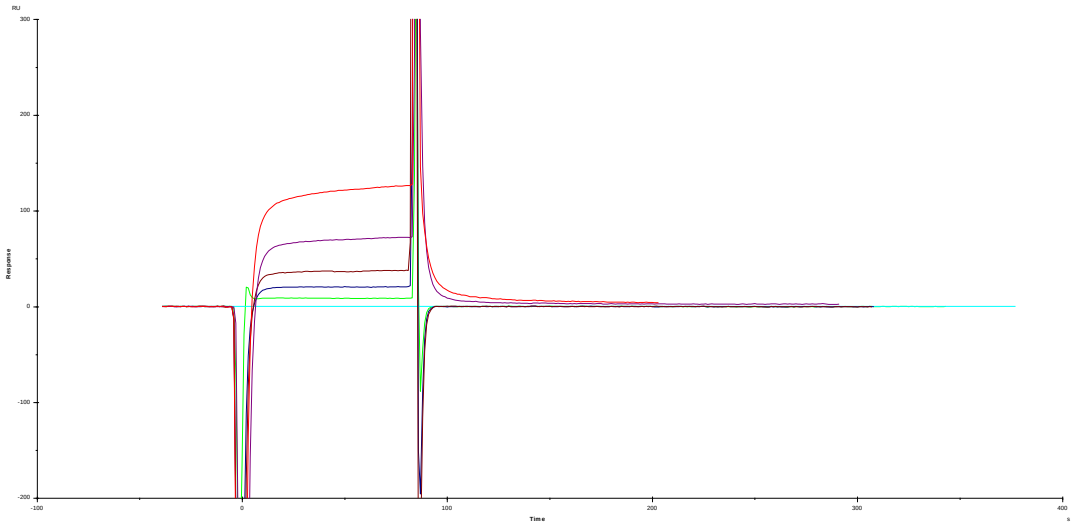

Figure 87: Surface Plasmon resonance sensorgram acquired for compound **MO-4** interacting with full-length HSF1.

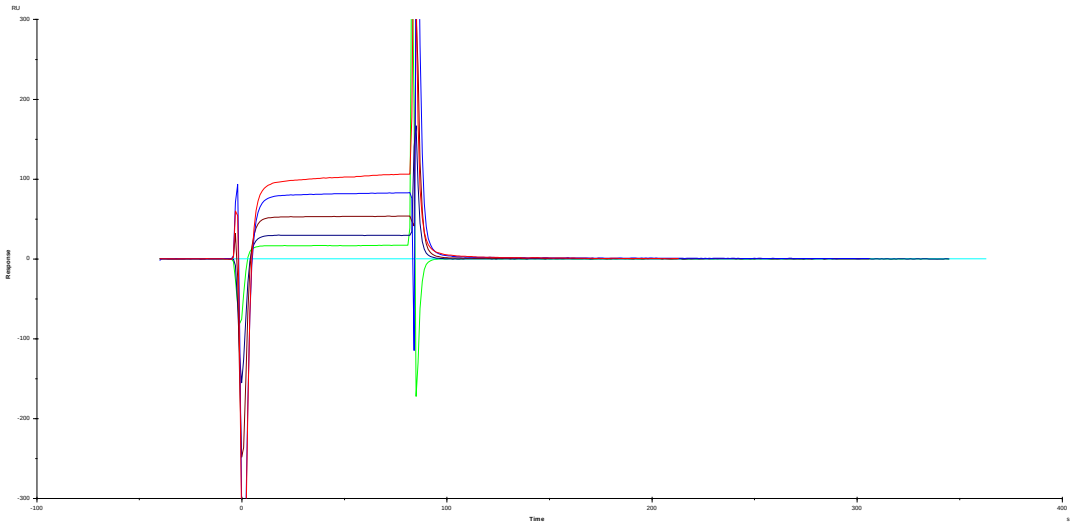

Figure 88: Surface Plasmon resonance sensorgram acquired for compound **MO-5** interacting with full-length HSF1.

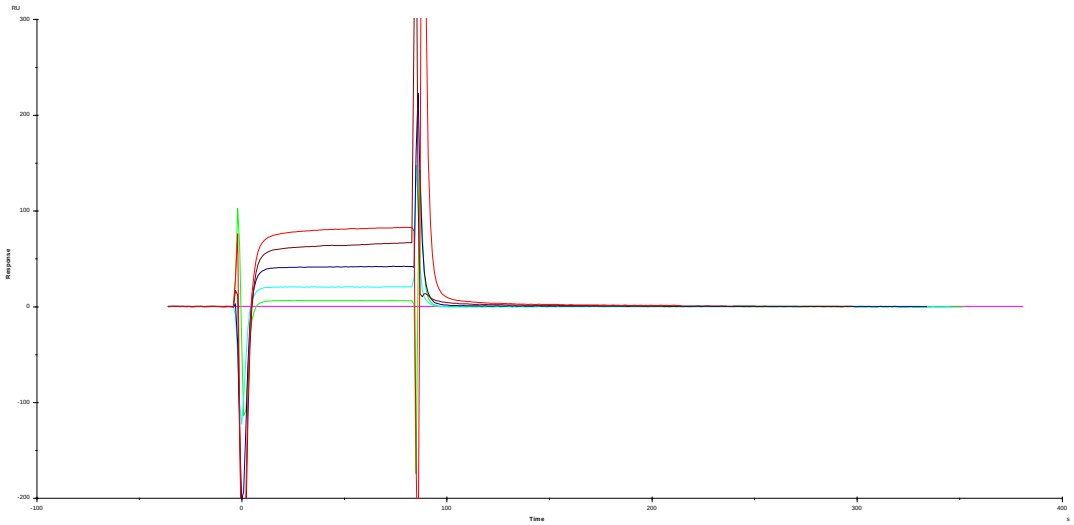

Figure 89: Surface Plasmon resonance sensorgram acquired for compound **MO-6** interacting with full-length HSF1.

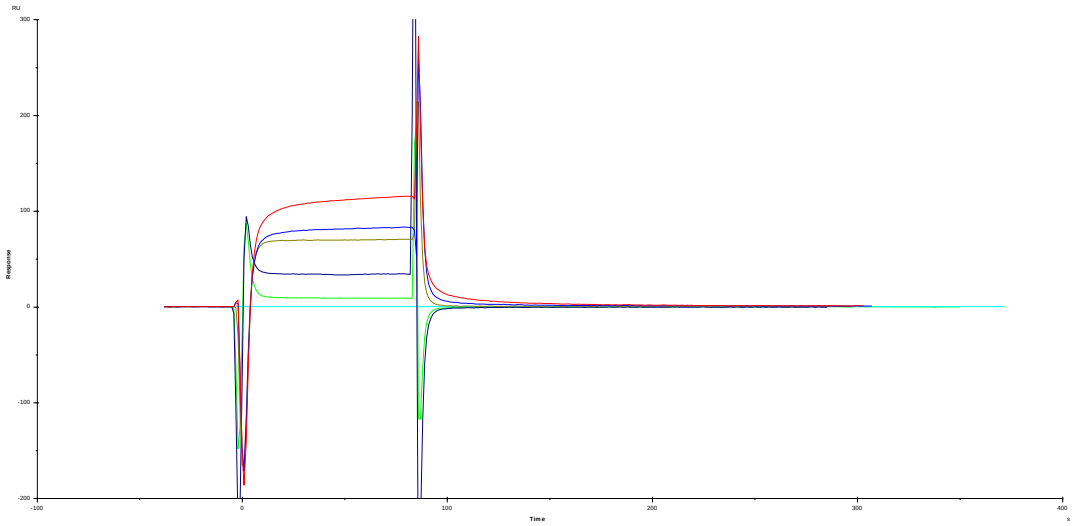

Figure 90: Surface Plasmon resonance sensorgram acquired for compound **MO-7** interacting with full-length HSF1.

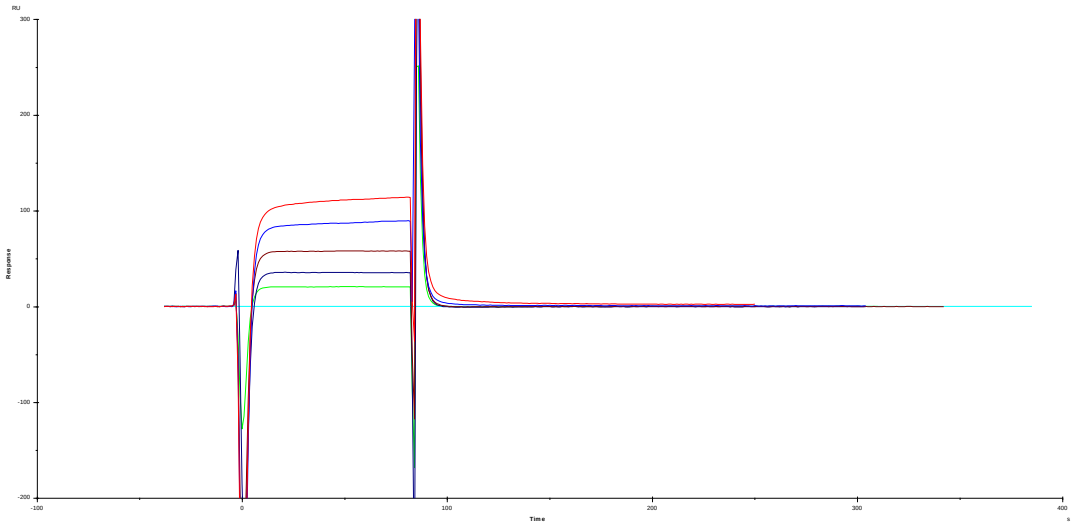

Figure 91: Surface Plasmon resonance sensorgram acquired for compound **MO-8** interacting with full-length HSF1.

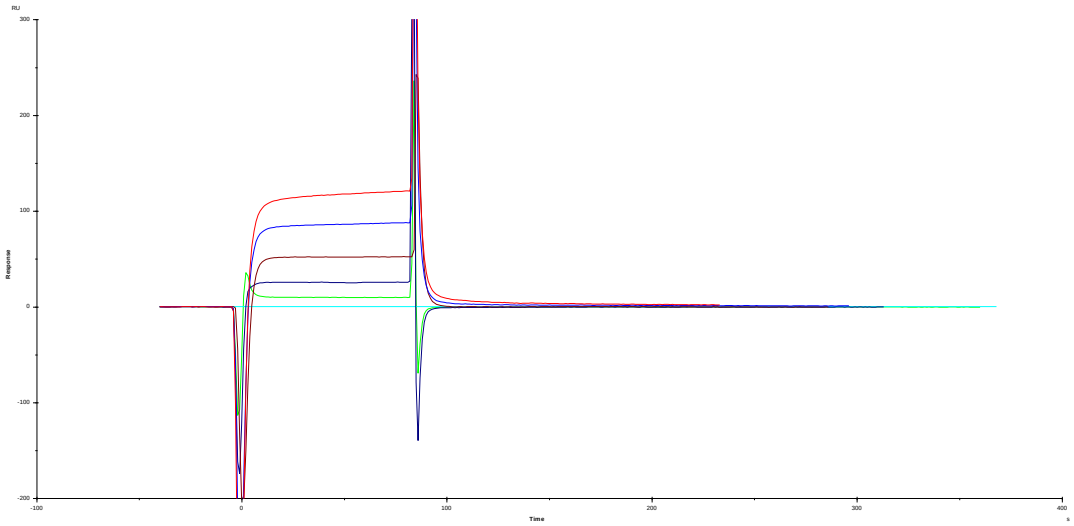

Figure 92: Surface Plasmon resonance sensorgram acquired for compound **MO-9** interacting with full-length HSF1.

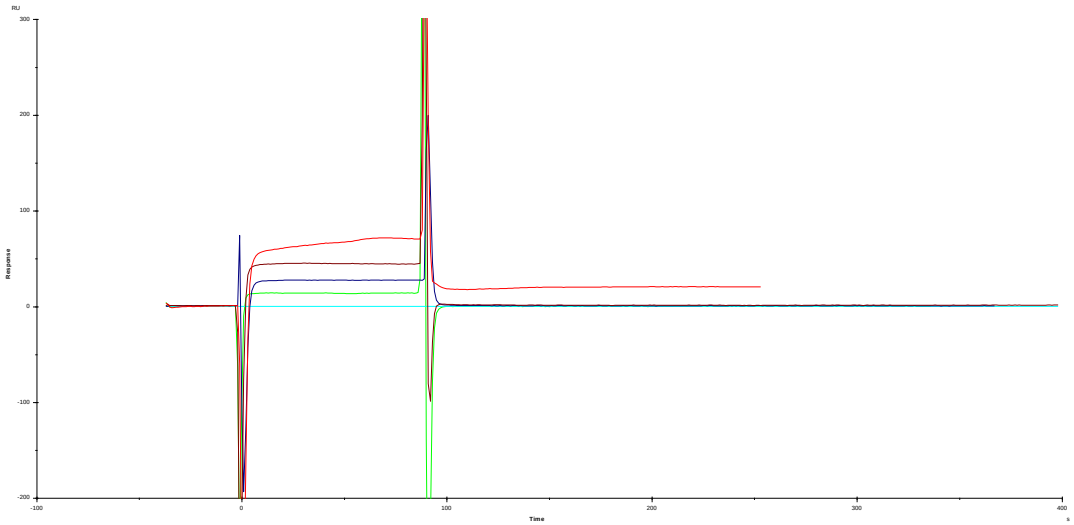

Figure 93: Surface Plasmon resonance sensorgram acquired for compound **MO-13** interacting with full-length HSF1.

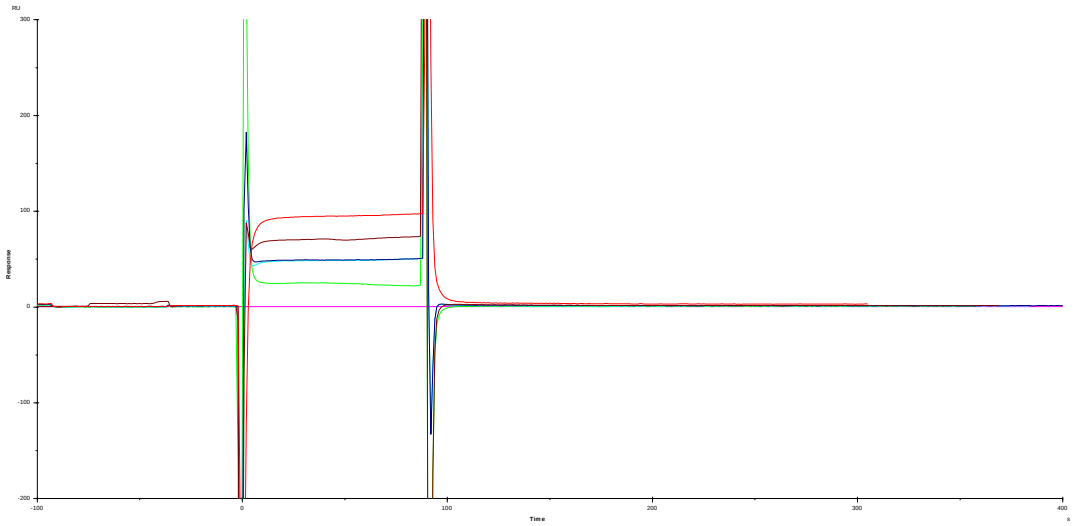

Figure 94: Surface Plasmon resonance sensorgram acquired for compound **MO-14** interacting with full-length HSF1.

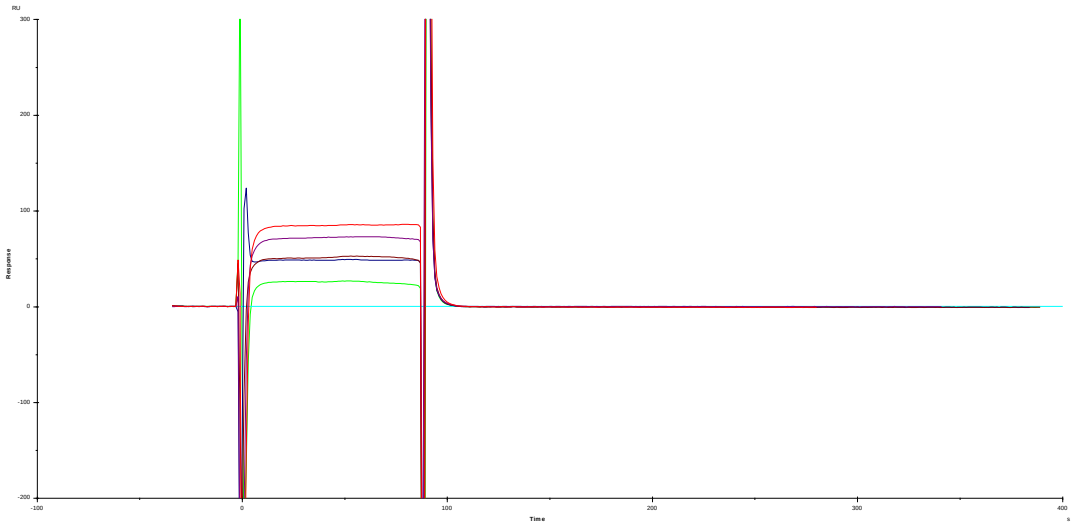

Figure 95: Surface Plasmon resonance sensorgram acquired for compound **LAM1** interacting with full-length HSF1.

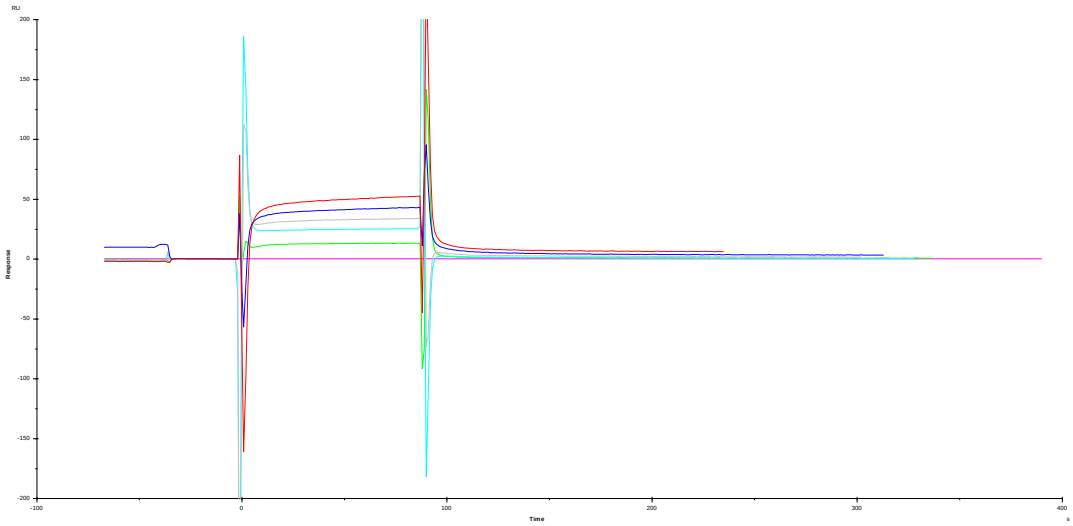

Figure 96: Surface Plasmon resonance sensorgram acquired for compound **LAM12** interacting with full-length HSF1.

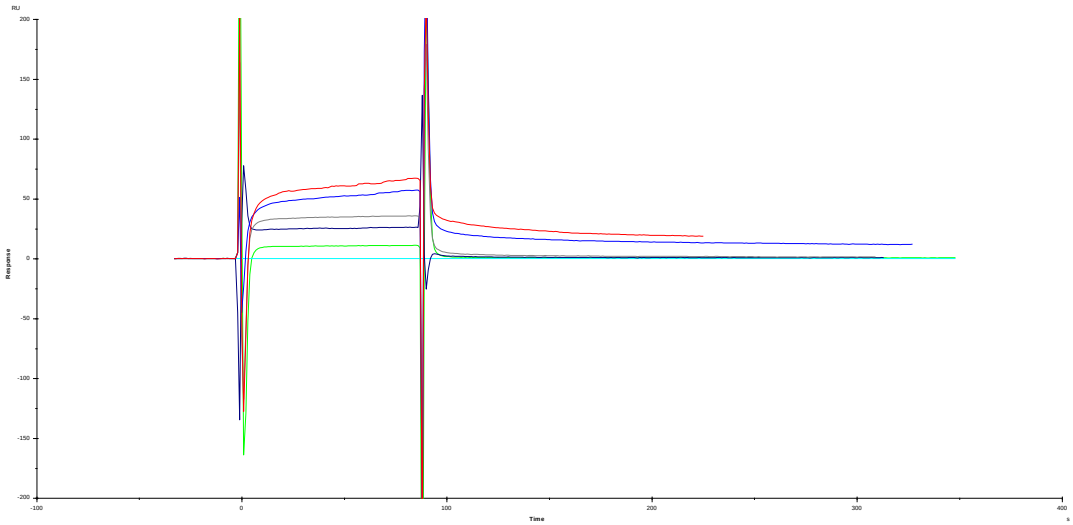

Figure 97: Surface Plasmon resonance sensorgram acquired for compound **LAM17** interacting with full-length HSF1.

Cell line

Human HeLa (ATCC® CCL-2™) cells were cultured in Dulbecco's modified Eagle's medium (DMEM; Lonza™). DMEM was supplemented with 10% (v/v) fetal bovine serum, supplemented with 10 U/ml penicillin and 0.01 mg/ml streptomycin. Cells were maintained in a humidified 5% CO_2 atmosphere at 37°C. To obtain cell line Z74 containing *HSP70B-RLUC, LEXA-FLUC,* and *CMV-LEXA-HSF1* genes, HeLa cells were co-transfected with *pHsp70BRen/LexA-Luc* and *pLexAHSF1* (5:1 molar ratio). Cell lines we isolated after selection with 1.3 g/ml puromycin. All transfections employed Lipofectamine reagent (Invitrogen ™).

Measurement of reporter gene activities in Z74 cells

Z74 cells (1×10^4) were seeded in 96-well plates and cultured for 24h. The cells were pre-incubated for 2h with the compounds to be tested or vehicle (DMSO), heated at 43°C for 30 min in a thermostatically controlled water bath, and then incubated for another 6h at 37°C. FLUC and RLUC activities were determined using the Dual-Glo™ Luciferase Assay System (Promega, Co.). Luciferase light counts were detected in a Wallac Microbeta™ Trilux-1450 Luminometer (PerkinElmer®).

Analysis of differential gene expression by reverse transcription (RT) and qPCR

Z74 cells (3×10^5) were seeded in 6-well plates and cultured for 24 h. The cells were pre-exposed to test compounds or DMSO for 2 h and then heat-treated at 43°C for 30 min in a thermostatically controlled water bath. After a further incubation for 1 h at 37°C, the cells were harvested. The total-RNA was prepared using TRI Reagent (Molecular Research Center, Inc.), following the manufacturer's instructions. To quantify the levels of *RLUC, FLUC, HSPA7* mRNA, cDNA was prepared from total RNA using transcriptor reverse transcriptase and an anchoredoligo (dT)18 primer (both purchased from Roche Applied Science©).

qPCR was performed using LightCycler FastStart DNA Master SYBR Green I and a LightCycler instrument (Roche Applied System©). Quantitative expression values were extrapolated from standard curves, and were normalized to *β2-microglobulin* (*B2M*) values. Specific oligonucleotide primers were: *RLUC*: 5_-ATGGGATGAATGGCCTGATA-3_ (F), 5_-TGTTGGACGACGAACTTCAC-3_ (R); *B2M*: 5_-CCAGCAGAGAATGGAAAGTC-3_ (F), 5_-GATGCTGCTTACATGTCTCG-3_ (R). The level of *HSPA7* mRNA was estimated using the Hs HSPA7 FAM 1 QuantiTect Primer Assay.

Alamar blue assay

Cell viability was investigated using an alamar blue assay (Invitrogen, Co.). HeLa cells (1×10^4) were seeded in 48-well plates, cultured for 24h and exposed to the test compounds or vehicle. The medium was removed, and the attached cells were incubated in culture medium containing 10% (v/v) alamar blue dye for 4h at 37°C. The medium was collected and, after a laser excitation at 530 nm, the emitted fluorescence at 590 nm was quantified using a BioTek Synergy4 multimode plate reader (BioTek Instruments, Inc.). The attached cells in the original plate were then stained with crystal violet and observed to a microscope with a magnification of 4X.

MTT assay

HeLa were seeded in triplicate in 96-well plates (3.5×10^3/well) and incubated for 72 h in the absence or presence of **LAM7-LAM11**, **LAM20-LAM28** at a final concentration of 50 and 10 µM. Stock solutions of compounds (50 mM in DMSO) were stored at -20 °C and diluted just before addition to the sterile culture medium. **KRIBB11** (purchased from Merck), was used in the same experimental condition at 10 and 1 µM. The number of viable cells was determined by using a [3-4,5-dimethyldiazol-2-yl]-2,5-diphenyl tetrazolium bromide (MTT, Merck) conversion

assay. The indicated percentages were all calculated using as 100% control cells treated with DMSO.

CHAPTER 8

Synthesis of 2,4-thiazolidinedione molecules as new BAG3 modulators

CHAPTER 8

Synthesis of 2,4-thiazolidinedione molecules as new BAG3 modulators

8.1 General synthetic methods

All commercially available starting materials were purchased from Merck and were used as received. Solvents used for the synthesis were of HPLC grade (Merck). NMR spectra (^{1}H, ^{13}C) were recorded on a Bruker Avance 400 MHz instrument at T = 298 K. Compounds were dissolved in 0.5 mL of CD_3OD, $CDCl_3$ or $(CD_3)_2SO$ (Merck, 99.8 Atom %D). The chemical shifts (δ) are expressed in parts per million (ppm) relative to the solvent peak as the internal reference; coupling constants (J) are expressed in Hertz. Multiplicities are reported as follows: s, singlet; d, doublet; dd, doublet of doublets; t, triplet; dt, doublet of triplets; q, quartet; m, multiplet. Mass spectrometry experiments were performed using a Q-ToF™ Premiere instrument (Waters, Co.®) equipped with an ESI source, or using a LTQ Orbitrap XL™ mass spectrometer (Thermo Scientific™). Chemical reactions were monitored on silica gel 60 F254 plates (Merck) and the spots were visualized under UV light (λ = 254nm, 365nm). Analytical and semi-preparative reversed-phase HPLC were performed on Agilent Technologies, Inc.© 1200 Series high performance liquid chromatography using a Nucleodur© C8 reversed-phase column (100 x 2mm, 4μM, 80 Å, flow rate = 1 mL/min; 250 x 10.00mm, 4μM, 80 Å, flow rate = 4 mL/min respectively, Macherey-Nagel©). The binary solvent system (A/B) was as follows: 0.1% TFA in water (A) and 0.1% TFA in CH_3CN (B). The absorbance was detected at λ = 240 nm. All biologically tested compounds were determined to be >98% pure by HPLC analysis and NMR data.

8.2 2,4-thiazolidinendione derivatives (LK2-LK9)

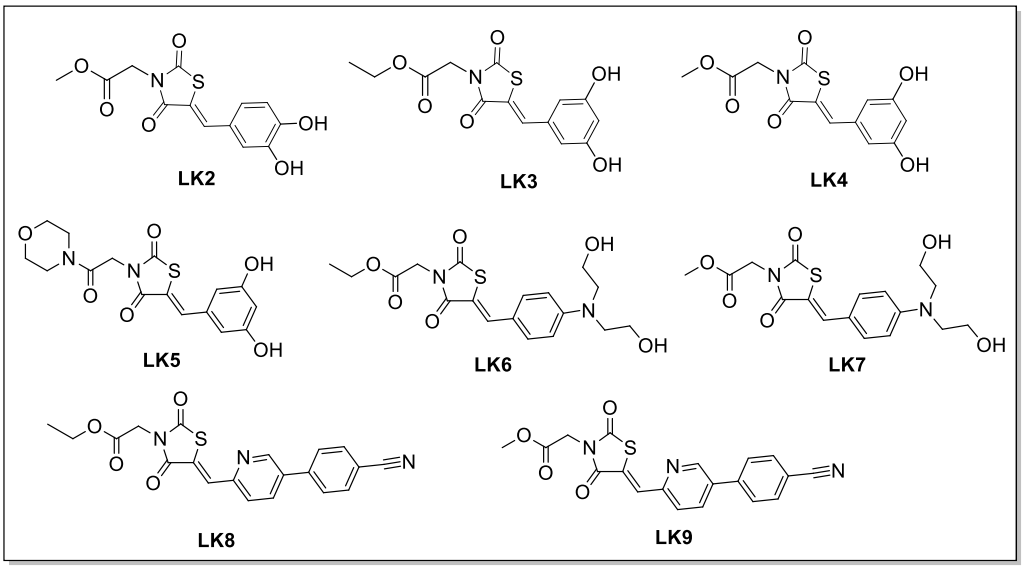

8.2.1 General procedure (G) for the synthesis of 20a-20d

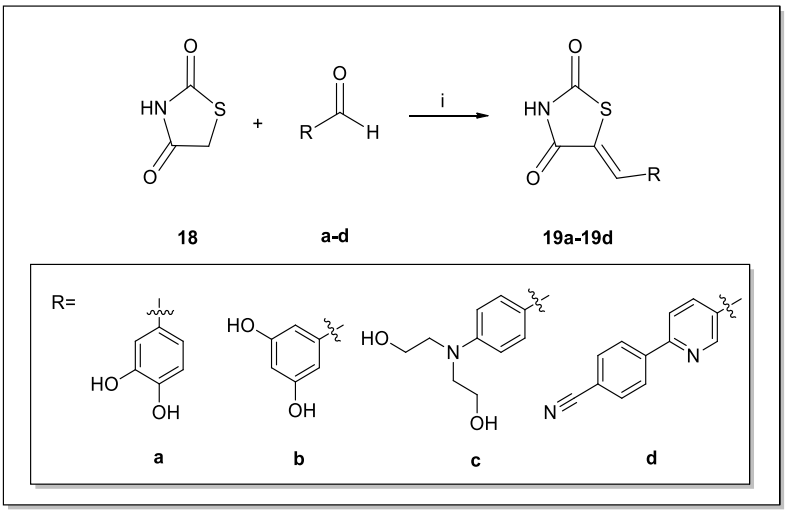

Synthetic scheme 9: i) piperidine, EtOH, reflux 16-24h.

Thiazolidine-2,4-dione **18** (1.0 equiv), the appropriate aromatic aldehydes **a-d** (1.0 equiv), piperidine (0.8 equiv), and ethanol (5 mL) were placed in a 25 ml round-

bottom flask. The reaction mixture was continuously stirred and refluxed for 16-24h (**Synthetic scheme 9**). [228] The crude product was poured into water and extracted with AcOEt (3 x 25 mL). The combined organic phases were washed with water (3 x 25.0 mL), dried over anhydrous Na_2SO_4, filtered, and concentrated in vacuum. The desired compounds **19a-19d** were confirmed by analytical RP-HPLC (Nucleodur© C8 reversed-phase column: 100 x 2 mm, 4 μM, 80 Å, flow rate = 1 mL/min) and ^{1}H NMR spectra. **19a-19d** were used without any further purification in the next step.

(Z)-5-(3,4-dihydroxybenzylidene)thiazolidine-2,4-dione (19a)

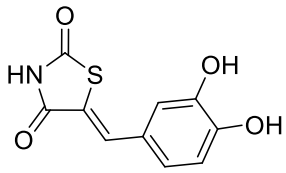

Compound **19a** was obtained by following the general procedure (**G**), from the reaction between **18** and 3,4-dihydroxybenzaldehyde (**a**), as a brown solid (230mg, 85% yield by HPLC analysis). RP-HPLC t_R = 21.5, gradient condition: from 5% B ending to 100% B 50 min, flow rate of 4 mL/min, λ = 240 nm. ^{1}H NMR (400 MHz, CD_3OD): δ_H = 7.55 (s, 1H), 6.91 (d, *J* = 2.2 Hz, 1H), 6.86 (dd, *J* = 8.3, 2.2 Hz, 1H), 6.77 (d, *J* = 8.3 Hz, 1H). ESI-MS: calculated for $C_{10}H_7NO_4S$ 237.01 found m/z = 238.00 $[M+H]^+$.

(Z)-5-(3,5-dihydroxybenzylidene)thiazolidine-2,4-dione (19b)

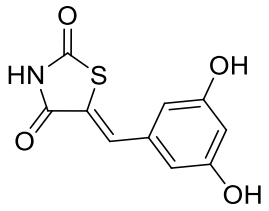

Compound **19b** was obtained by following the general procedure (**G**), from the reaction between **18** and 3,5-dihydroxybenzaldehyde (**b**), as a brown solid (350 mg, 80% yield by HPLC analysis). RP-HPLC t_R = 21.5, gradient condition: from 5% B ending to 100% B 50 min, flow rate of 4 mL/min, λ = 240 nm. ^{1}H NMR (400 MHz, CD_3OD): δ_H = 7.51 (s, 1H), 6.39 (d, *J* = 2.1 Hz, 2H), 6.25 (t, *J* = 2.1 Hz, 1H). ESI-MS: calculated for $C_{10}H_7NO_4S$ 237.01 found m/z = 238.02 $[M+H]^+$.

(Z)-5-(4-(bis(2-hydroxyethyl)amino)benzylidene)thiazolidine-2,4-dione (19c)

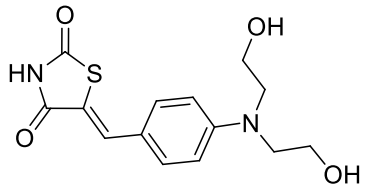

Compound **19c** was obtained by following the general procedure (**G**), from the reaction between **18** and 4-[*N*,*N*-Bis(2-hydroxyethyl)amino]benzaldehyde (**c**), as a brown solid (230 mg, 80% yield by HPLC analysis). RP-HPLC t_R = 20.4, gradient condition: from 5% B ending to 100% B 50 min, flow rate of 4 mL/min, λ = 240 nm. ^{1}H NMR (400 MHz, CD_3OD): δ_H = 7.53(s, 1H), 7.30 (d, *J* = 8.9 Hz, 2H), 6.76 (dd, *J* = 7.4, 5.6 Hz, 2H), 3.66 (t, *J* = 5.7 Hz, 4H), 3.53 (t, *J* = 6.0 Hz, 4H). ESI-MS: calculated for $C_{14}H_{16}N_2O_4S$ 308.08 found m/z = 309.13 $[M+H]^+$.

(Z)-4-(6-((2,4-dioxothiazolidin-5-ylidene)methyl)pyridin-3-yl)benzonitrile (19d)

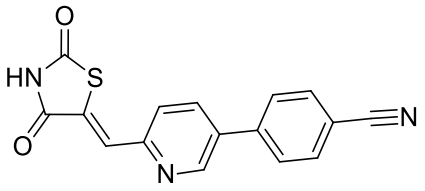

Compound **19d** was obtained by following the general procedure (**G**), from the reaction between **18** and 4-(6-formylpyridin-2-yl)benzonitrile **(d)**, as a brown solid (210 mg, 85% yield by HPLC analysis). RP-HPLC t_R = 32.5, gradient condition: from 5% B ending to 100% B 50 min, flow rate of 4 mL/min, λ = 240 nm. ^{1}H NMR (400 MHz, CD_3OD): δ_H = 8.43 (d, *J* = 8.1 Hz, 2H), 7.98 – 7.87 (m, 4H), 7.69 – 7.61 (m, 2H). ESI-MS: calculated for $C_{16}H_9N_3O_2S$ 307.04 found m/z = 308.11 $[M+H]^+$.

8.2.2 General procedure (H) for the synthesis of 20 bg, LK2-LK4, and LK6-LK9

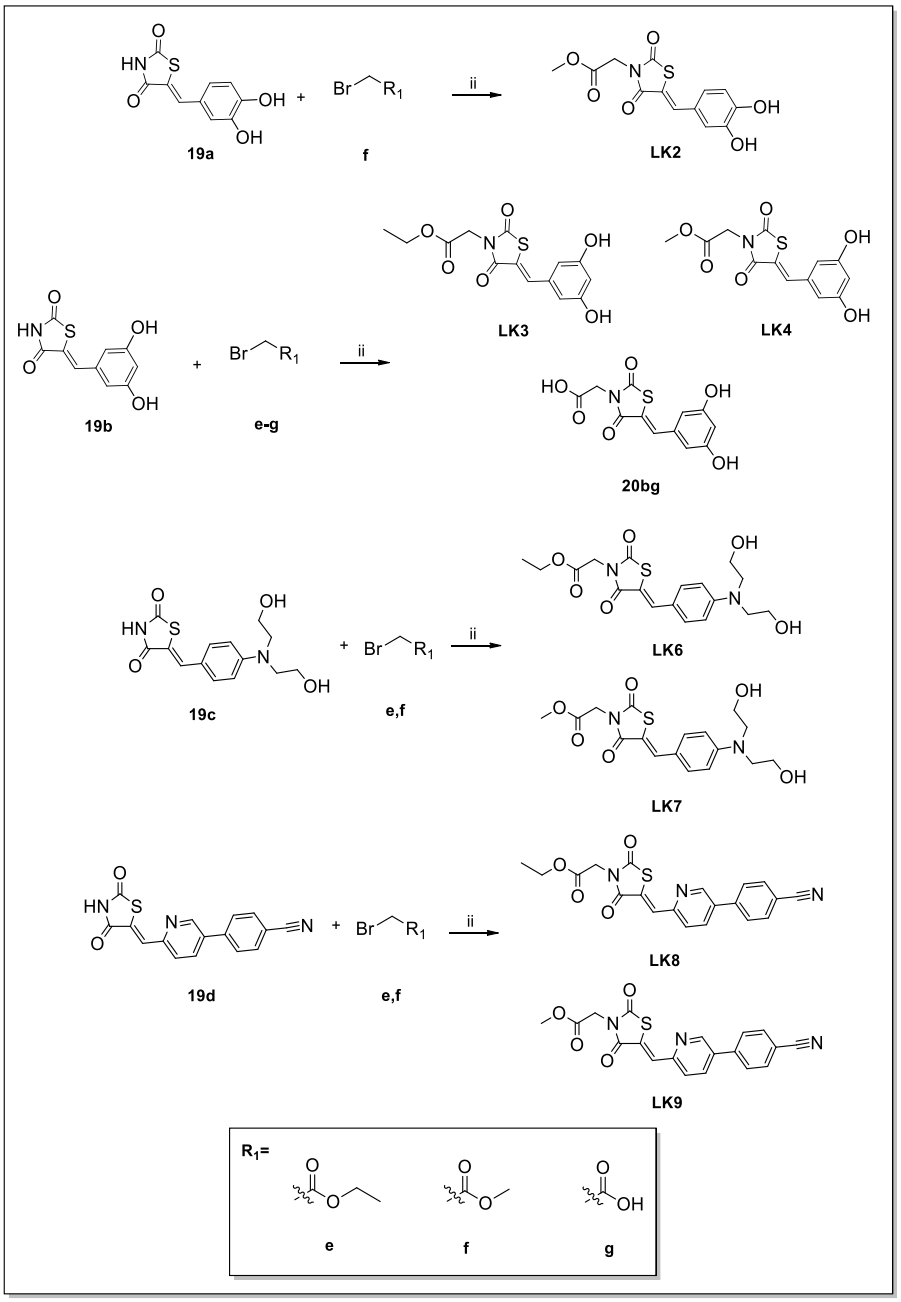

Synthetic scheme 10: ii) NaH, DMF dry, 80°C 16-20h.

In a two-neck round-bottom flask, sodium hydride NaH (1.2 equiv) was added portion-wise to a solution of **19a**-**19d** (1.0 equiv) in dry DMF (3.5 mL). The reaction mixture was stirred for 1.5 h at 80°C and it was allowed to return to room temperature. Then, ethyl bromoacetate (**e**) (1.5 equiv) for the compounds **LK3, LK6, LK8**, methyl bromoacetate (**f**) (1.5 equiv) **LK2, LK4, LK7, LK9**, and bromoacetic acid (1.5 equiv) (**g**) for the synthesis of **20bg** was added and the mixture was stirred at 80 °C for 16-20 h. The reaction was monitored by TLC (**Synthetic scheme 10**). [228] The suspension was poured into ice-cold water and the solid product filtered and recovered. HPLC purification was performed by semi-preparative reversed-phase HPLC (Nucleodur© C8 reversed-phase column: 250 x 10.00 mm, 4 μM, 80 Å, flow rate = 4 mL/min) and the final products were characterized by ESI-MS and NMR spectra.

(Z)-methyl 2-(5-(3,4-dihydroxybenzylidene)-2,4-dioxothiazolidin-3-yl) acetate (LK2)

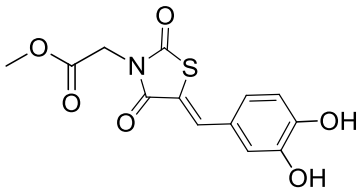

Compound **LK2** was obtained by following the general procedure (**H**), from the reaction between **19a** and methyl bromoacetate (**f**), as a brown solid (75 mg, 50% yield after HPLC purification). RP-HPLC t_R = 28.9 min, gradient condition: from 5% B ending to 100% B 50 min, flow rate of 4 mL/min, λ = 240 nm. ^{1}H NMR (400 MHz, CD_3OD): δ_H = 7.82 (s, 1H), 7.07 (d, *J* = 2.2 Hz, 1H), 7.02 (dd, *J* = 8.4, 2.2, 1H), 6.91 (d, *J* = 8.2 Hz, 1H), 4.52 (s, 2H), 3,79 (s, 3H). ^{13}C NMR (100 MHz, CD_3OD): δ = 168.79, 168.71, 166.95, 150.05, 146.97, 136.02, 126.10, 125.51, 117.55, 117.33, 116.74, 53.00, 42.52. ESI-MS: calculated for $C_{13}H_{11}NO_6S$, 309.03; found m/z = 332.02 $[M+Na]^+$.

(Z)-ethyl 2-(5-(3,5-dihydroxybenzylidene)-2,4-dioxothiazolidin-3-yl) acetate (LK3)

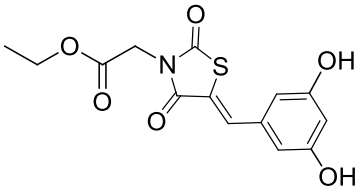

Compound **LK3** was obtained by following the general procedure (**H**), from the reaction between **19b** and ethyl bromoacetate (**e**), as a brown solid (80 mg, 60% yield after HPLC purification). RP-HPLC t_R = 28.1 min, gradient condition: from 5% B ending to 100% B 50 min, flow rate of 4 mL/min, λ = 240 nm. ^{1}H NMR (400 MHz, $(CD_3)_2SO$): δ_H = 9.72 (s, 2H), 7.80 (s, 1H), 6.52 (d, *J* = 6.9 Hz, 2H), 6.38 (d, *J* = 7.2 Hz, 1H), 4.49 (s, 2H), 4.18 (q, *J* = 7.3 Hz, 2H), 1.23 (t, *J* = 7.3 Hz, 3H). ^{13}C NMR (100 MHz, CD_3OD): δ = 167.38, 166.89, 165.54, 159.09 (2C), 134.67, 134.44, 120.59, 108.13 (2C), 105.00, 61.69, 41.60, 13.04. ESI-MS: calculated for $C_{14}H_{13}NO_6S$, 323.05; found m/z = 346.03 $[M+Na]^+$.

(Z)-methyl 2-(5-(3,5-dihydroxybenzylidene)-2,4-dioxothiazolidin-3-yl) acetate (LK4)

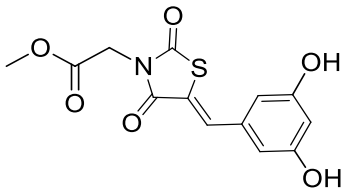

Compound **LK4** was obtained by following the general procedure (**H**), from the reaction between **19b** and methyl bromoacetate (**f**), as a brown solid (75 mg, 75% yield after HPLC purification). RP-HPLC t_R = 29.5 min, gradient condition: from 5% B ending to 100% B 50 min, flow rate of 4 mL/min, λ = 240 nm. ^{1}H NMR (400 MHz, CD_3OD): δ_H = 7.78 (s, 1H), 6.54 (d, *J* = 2.1 Hz, 2H), 6.39 (t, *J* = 2.1 Hz, 1H),

4.53 (s, 2H), 3.80 (s, 3H). ^{13}C NMR (100 MHz, CD_3OD): δ = 167.42, 167.38, 165.50, 159.07 (2C), 134.66, 134.45, 120.52, 108.24 (2C), 104.95, 51.85, 41.37. ESI-MS: calculated for $C_{13}H_{11}NO_6S$, 309.03; found m/z = 332.02 $[M+Na]^+$.

(Z)-ethyl 2-(5-(4-(bis(2-hydroxyethyl) amino) benzylidene)-2,4-dioxothiazolidin-3-yl) acetate (LK6)

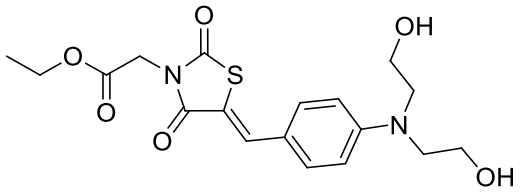

Compound **LK6** was obtained by following the general procedure (**H)**, from the reaction between **19c** and ethyl bromoacetate (**e**), as a yellow solid (60 mg, 45% yield after HPLC purification). RP-HPLC t_R = 26.2 min, gradient condition: from 5% B ending to 100% B 50 min, flow rate of 4 mL/min, λ = 240 nm. ^{1}H NMR (400 MHz, CD_3OD): δ_H = 7.84 (s, 1H), 7.49-7.45 (m, 2H), 6.93-6.90 (m, 2H), 4.49 (s, 2H), 4.28-4.22 (m, 2H), 3.79 (t, *J* = 6.0, 4H), 3.67 (t, *J* = 6.0 Hz, 4H), 1.33-1.28 (m, 3H). ^{13}C NMR (100 MHz, CD_3OD): δ = 167.8, 167.1, 166.0, 150.4, 134.9, 132.5 (2C), 120.3, 113.0, 111.8 (2C), 61.6, 58.8 (2C), 53.3 (2C), 41.4, 12.88. ESI-MS: calculated for $C_{18}H_{22}N_2O_6S$, 394.12; found m/z = 395.23 $[M+H]^+$.

(Z)-methyl 2-(5-(4-(bis(2-hydroxyethyl) amino) benzylidene)-2,4-dioxothiazolidin-3-yl) acetate (LK7)

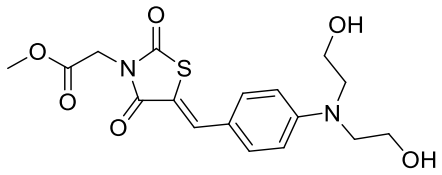

Compound **LK7** was obtained by following the general procedure (**H**), from the reaction between **19c** and methyl bromoacetate (**f**), as a yellow solid (70 mg, 40% yield after HPLC purification). RP-HPLC t_R = 24.2 min, gradient condition: from 5% B ending to 100% B 50 min, flow rate of 4 mL/min, λ = 240 nm. ^{1}H NMR (400 MHz, CD_3OD): δ_H = 7.84 (s, 1H), 7.47 (d, *J* = 8.6 Hz, 2H), 6.91 (d, *J* = 8.6 Hz, 2H), 4.51 (s, 2H), 3.81-3.77 (m, 7H), 3.67 (t, *J* = 5.7 Hz, 4H), 1.31 (s, 2H). ^{13}C NMR (100 MHz, CD_3OD): δ = 169.0, 168.8, 167.1, 151.6, 136.2, 133.7 (2C), 121.6, 114.2, 113.1 (2C), 60.0 (2C), 54.5 (2C), 53.0, 42.5. ESI-MS: calculated for $C_{17}H_{20}N_2O_6S$, 380.10; found m/z = 381.20 $[M+H]^+$.

(Z)-ethyl 2-(5-((5-(4-cyanophenyl) pyridin-2-yl) methylene)-2,4-dioxothiazolidin-3-yl) acetate (LK8)

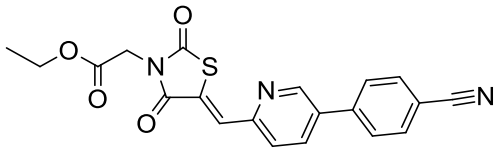

Compound **LK8** was obtained by following the general procedure (**H**), from the reaction between **19d** and ethyl bromoacetate (**e**), as a yellow solid (100 mg, 50% yield after HPLC purification). RP-HPLC t_R = 42.3 min, gradient condition: from 5% B ending to 100% B 50 min, flow rate of 4 mL/min, λ = 240 nm. ^{1}H NMR (400 MHz, $CDCl_3$): δ_H = 8.24 (d, *J* = 8.3 Hz, 2H), 7.97-7.92 (m, 2H), 7.87 (d, *J* = 8.2 Hz, 2H), 7.80 (d, *J* = 8.0 Hz, 1H), 7.58 (d, *J* = 7.6 Hz, 1H), 4.52 (s, 2H), 4.27 (q, *J*

= 7.1 Hz, 2H), 1.32 (t, *J* = 7.1 Hz, 3H). ^{13}C NMR (100 MHz, $CDCl_3$): δ = 170.8, 166.3, 165.8, 155.9, 151.8, 142.3, 138.3, 132.8 (2C), 129.3, 127.8 (2C), 126.9, 126.6, 121.1, 118.6, 113.3, 62.2, 41.7, 14.06. ESI-MS: calculated for $C_{20}H_{15}N_3O_4S$, 393.08; found m/z = 416.03 $[M+Na]^+$.

(Z)-methyl 2-(5-((5-(4-cyanophenyl) pyridin-2-yl) methylene)-2,4-dioxothiazolidin-3-yl) acetate (LK9)

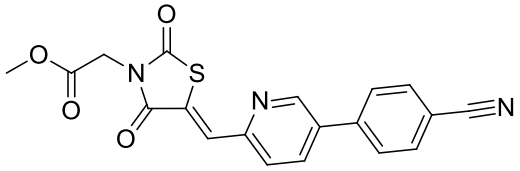

Compound **LK9** was obtained by following the general procedure (**H**), from the reaction between **19d** and methyl bromoacetate (**f**), as a dark brown solid (75 mg, 45% yield after HPLC purification). RP-HPLC t_R = 43.2 min, gradient condition: from 5% B ending to 100% B 50 min, flow rate of 4 mL/min, λ = 240 nm. ^{1}H NMR (400 MHz, $CDCl_3$): δ_H = 8.17-8.14 (m, 2H), 7.89-7.84 (m, 2H), 7.80-7.76 (m, 2H), 7.73 (dd, *J* = 8.0, 0.9 Hz, 1H), 7.50 (dd, *J* = 7.7, 0.9 Hz, 1H), 4.45 (s, 2H), 3.73 (s, 3H). ^{13}C NMR (100 MHz, $(CD_3)_2SO$): δ = 170.5, 167.7, 165.5, 155.2, 151.5, 142.2, 139.5, 133.3 (2C), 130.4, 128.5, 128.1 (2C), 125.3, 122.6, 119.1, 112.6, 53.1, 42.0. ESI-MS: calculated for $C_{19}H_{13}N_3O_4S$, 379.06; found m/z = 380.21 $[M+H]^+$.

(Z)-2-(5-(3,5-dihydroxybenzylidene)-2,4-dioxothiazolidin-3-yl) acetic acid (20bg)

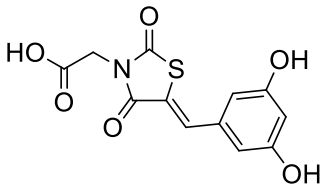

Compound **20bg** was obtained by following the general procedure (**H**), from the reaction between **19a** and bromoacetic acid (**g**), as a brown solid (90 mg, 70% yield after HPLC purification). RP-HPLC t_R = 16.3 gradient condition: from 5% B ending to 100% B 50 min, flow rate of 4 mL/min, λ = 240 nm. ^{1}H NMR (400 MHz, CD_3OD): δ_H = 7.79 (s, 1H), 6.62 (d, *J* = 2.0 Hz, 2H), 6.26 (t, *J* = 1.9 Hz, 1H), 4.63 (s, 2H). ESI-MS: calculated for $C_{12}H_9NO_6S$, 295.02; found m/z = 296.00 $[M+Na]^+$. The desired compound was directly used for the following step.

8.2.3 Synthesis of (Z)-5-(3,5-dihydroxybenzylidene)-3-(2-morpholino-2-oxoethyl) thiazolidine-2,4-dione (LK5)

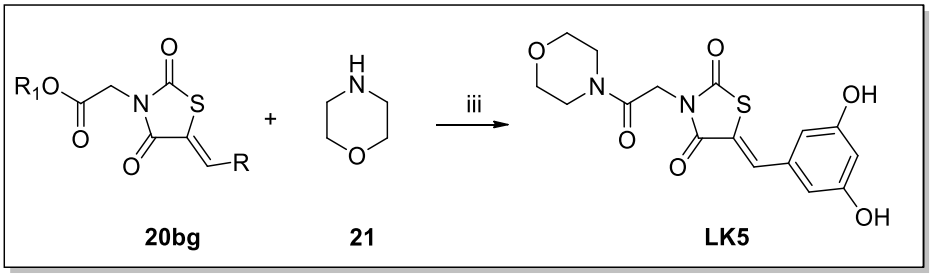

Synthetic scheme 11: iii) HOBt, DIC, DMF, rt, overnight.

1-Hydroxybenzotriazole (2.0 equiv) and *N*,*N*′-diisopropylcarbodiimide (1.5 equiv) were added to a solution of **20bg** (1.0 equiv) in DMF (3 mL). The mixture was stirred for 1h at room temperature and then morpholine (**21**) (2.0 equiv) was added.

The reaction mixture was stirred overnight at room temperature to obtain **LK5** (**Synthetic scheme 11**). [246] After completion, the suspension was diluted with 10 mL of water and extracted with AcOEt (3 x 20 mL). The combined organic layers were dried over Na_2SO_4 and evaporated under vacuum. A portion of the crude product was purified by semi-preparative reversed-phase HPLC (Nucleodur© C8 reversed-phase column: 250 x 10.00 mm, 4 μM, 80 Å, flow rate = 4 mL/min). The desired **LK5** compound was characterized by ESI-MS and NMR spectra.

Compound **LK5** was obtained as a pale brown solid (85 mg, 55% yield after HPLC purification). RP-HPLC t_R = 17.5 min, gradient condition: from 5% B ending to 100% B 50 min, flow rate of 4 mL/min, λ = 240 nm. ^{1}H NMR (400 MHz, CD_3OD): δ_H = 7.71 (s, 1H), 6.57 (s, 2H), 6.40-6.37 (m, 2H), 6.26 (dt, *J* = 6.1, 2.2 Hz, 1H), 5.34 (s, 2H), 3.61 – 3.54 (m, 4H), 3.52 – 3.45 (m, 4H). ^{13}C NMR (100 MHz, CD_3OD): δ = 171.9, 170.7, 169.3, 159.0 (2C), 132.9, 132.2, 120.5, 108.2 (2C), 104.9, 75.9 (2C), 66.2 (2C), 29.4. ESI-MS: calculated for $C_{16}H_{16}N_2O_6S$, 364.07; found m/z = 362.90 $[M-H]^+$.

8.3 Biophysical and biological assay

SPR assay

The SPR analysis were performed on Biacore 3000™ equipped with research-grade CM5 sensor chip (GE Healthcare™). Human recombinant BAG3 (rBAG3) protein was purchased from MyBioSource©, BAG3 domain (rBAG3-BD) was purchased from ARETA International S.r.l. and human recombinant BAG4 protein was purchased from Abnova, Co.©. Our previously synthesized compound (E)-ethyl 2-(5-(3,4-dihydroxybenzylidene)-2,4-dioxothiazolidin-3-yl)acetate was used as positive control in the same experimental conditions. [146] The proteins were coupled to the surface of a CM5 sensor chip using standard amine-coupling protocols, according to the manufacturer's instructions. Three separates recombinant rBAG proteins surfaces and one unmodified reference surface were prepared for

simultaneous analyses. rBAG proteins (BAG3 and BAG4) and rBAG3-BD (100 µg mL^{-1} in 10 mM CH_3COONa, pH 4.5) were immobilized on the sensor chip surface at a flow rate of 5 µL min^{-1} to obtain densities of 5–9 kRU. Compounds **LK2-LK9** and the (E)-ethyl 2-(5-(3,4-dihydroxybenzylidene)-2,4-dioxothiazolidin-3-yl)acetate were dissolved in 100% DMSO to obtain 50 mM solutions and diluted 1:100 (v/v) in PBS (Phosphate buffered saline: 10 mM NaH_2PO_4, 150 mM NaCl, pH 7.4) to a final DMSO concentration of 1.0%. For each molecule a six-point concentration series in triplicate were set up (0–0.25–1–10–20–100µM). SPR experiments were performed at 25 °C, using a flow rate of 10 µL min^{-1}, with 60 s monitoring of association and 300 s monitoring of dissociation. Sensorgram elaborations were performed using the BIAevaluation software provided by GE Healthcare™. Simple interactions were suitably fitted to a single-site bimolecular interaction model (A+B = AB), yielding a single K_D (**Figure 98-106**).

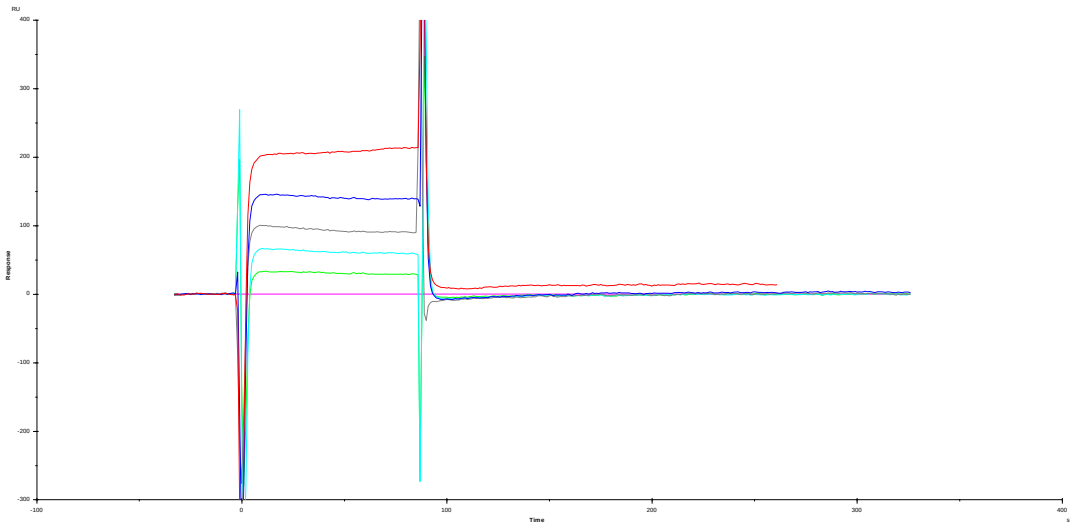

Figure 98: Surface Plasmon Resonance sensorgram acquired for compound **LK2** interacting with BAG3 full length protein.

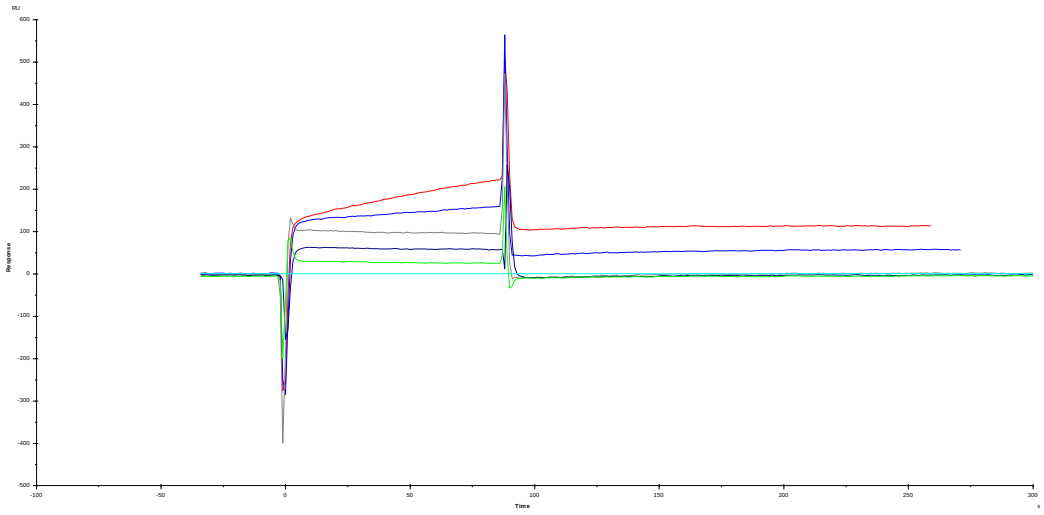

Figure 99: Surface Plasmon Resonance sensorgram acquired for compound **LK5** interacting with BAG3 full-length protein.

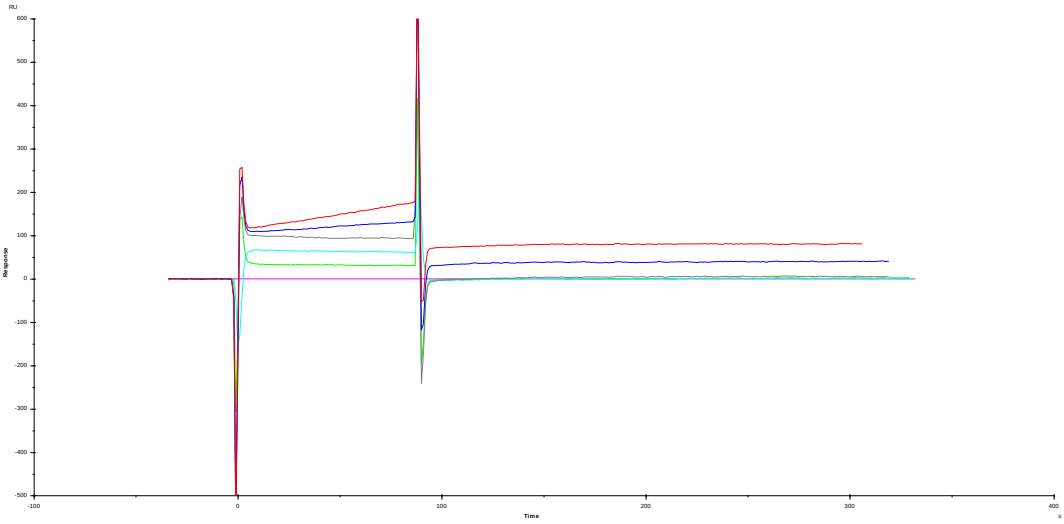

Figure 100: Surface Plasmon Resonance sensorgram acquired for compound **LK6** interacting with BAG3 full-length protein.

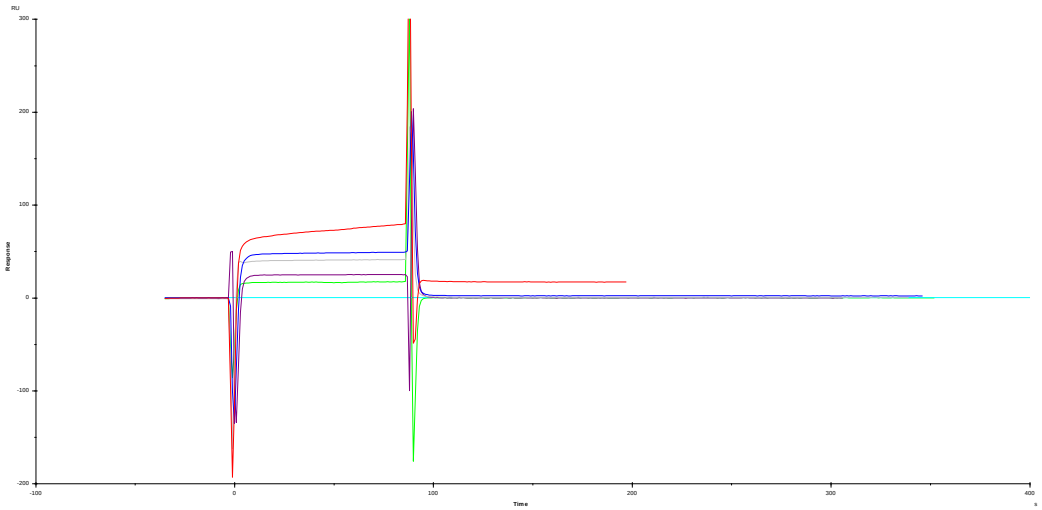

Figure 101: Surface Plasmon Resonance sensorgram acquired for compound **LK7** interacting with BAG3 full-length protein.

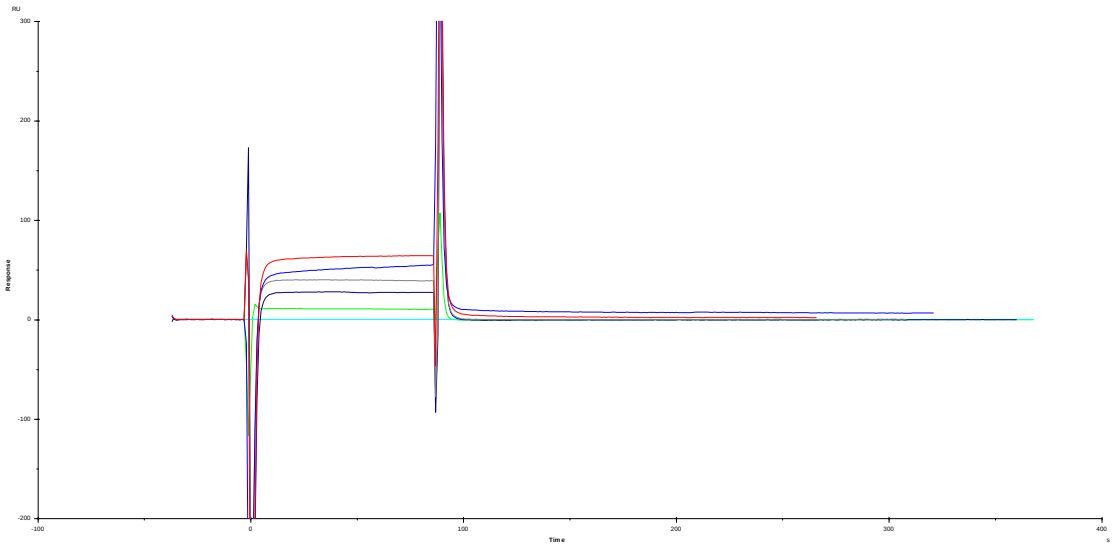

Figure 102: Surface Plasmon Resonance sensorgram acquired for compound **LK8** interacting with BAG3 full-length protein.

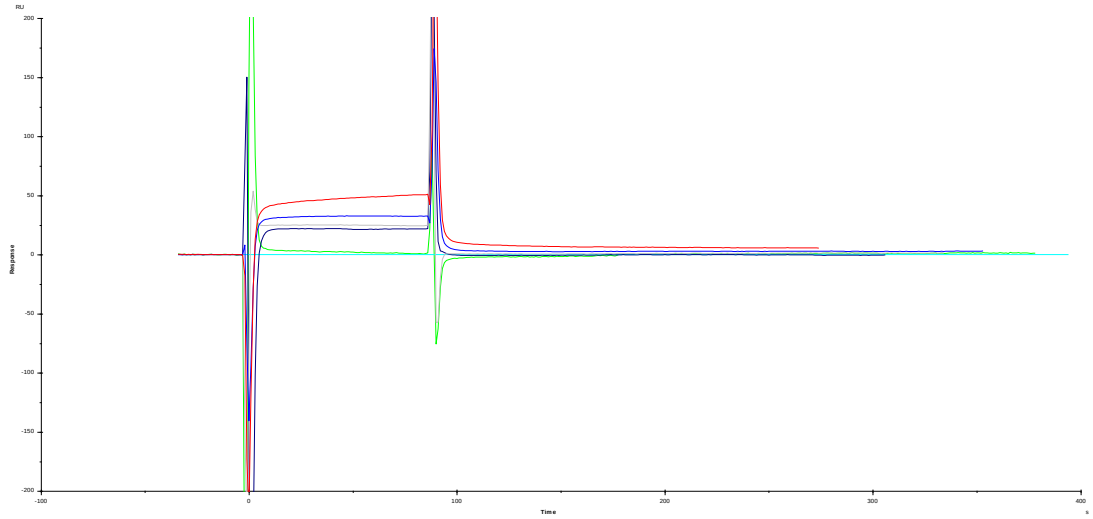

Figure 103: Surface Plasmon Resonance sensorgram acquired for compound **LK9** interacting with BAG3 full-length protein.

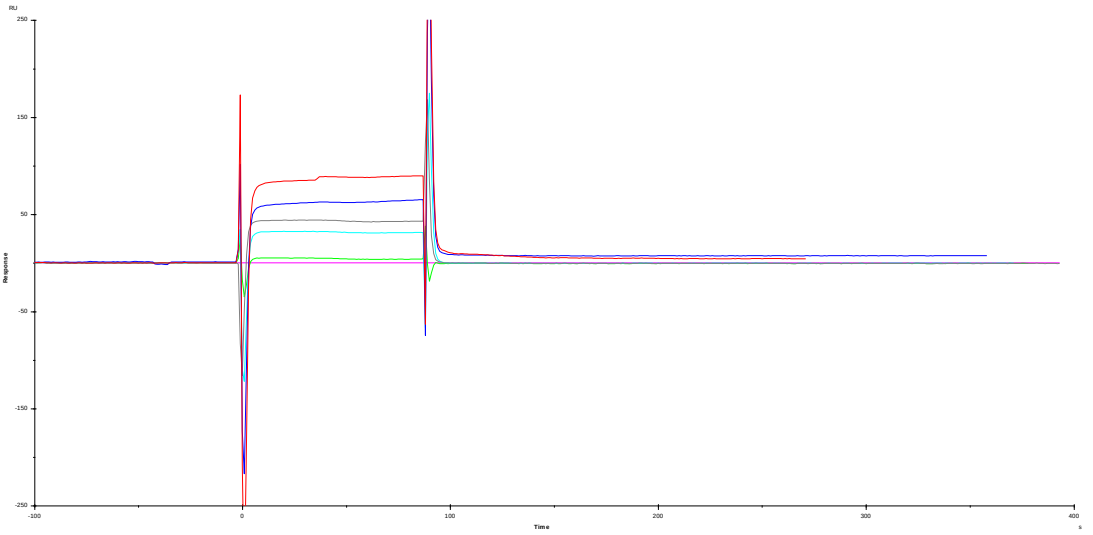

Figure 104: Surface Plasmon resonance sensorgram acquired for compound **LK6** interacting with BAG3-BD.

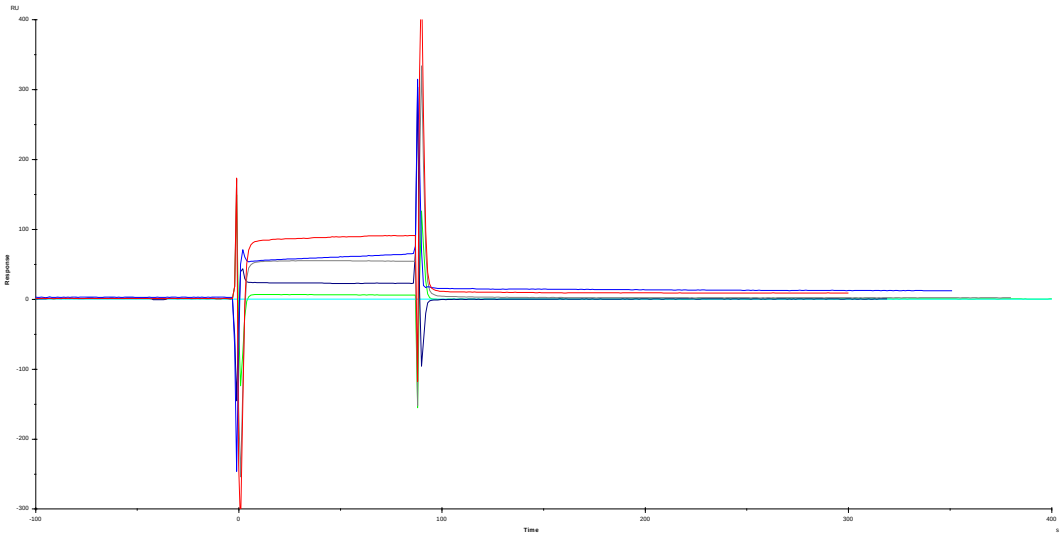

Figure 105: Surface Plasmon resonance sensorgram acquired for compound **LK7** interacting with BAG3-BD.

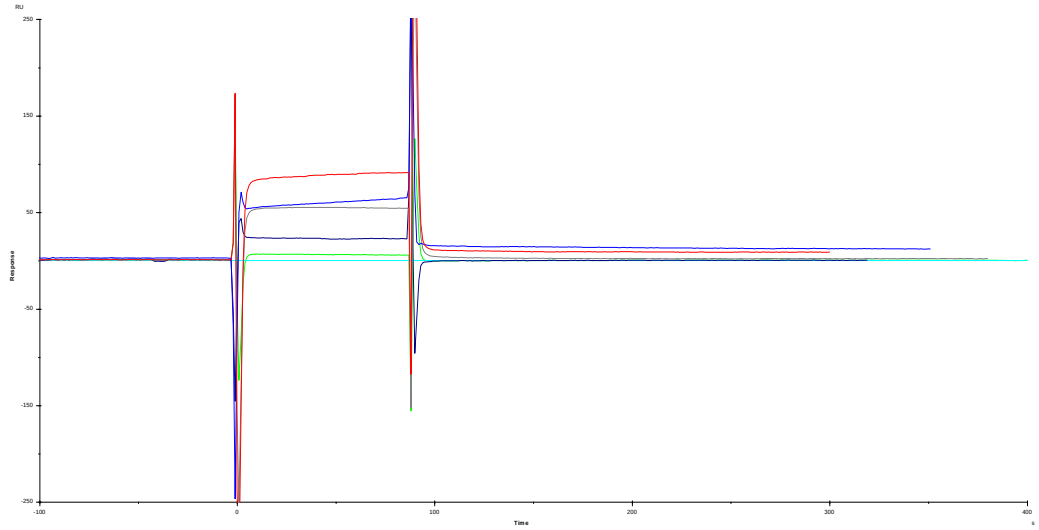

Figure 106: Surface Plasmon resonance sensorgram acquired for compound **LK9** interacting with BAG3-BD.

Cell culture

Cell lines of human cervical carcinoma (HeLa) and human malignant melanoma (A375) (ATCC® CCL-2 ™) were cultured in Dulbecco's modified Eagle's medium (DMEM; Euroclone S.p.A.) containing 10% fetal bovine serum (FBS), supplemented with 100 U/mL each of penicillin and streptomycin, and 2 mM/L glutamine and were grown at 37°C under 5% CO_2 air humidified atmosphere.

MTT assay

HeLa and A375 were seeded in triplicate in 96-well plates (3.5 x 10^3/well) and incubated for 48 h in the absence or presence of **LK1-LK9** at a final concentration of 5-10-25-50μM. Stock solutions of compounds (50 mM in DMSO) were stored at -20°C and diluted just before addition to the sterile culture medium. Following the treatment, 20 μL of MTT solution (5 mg/mL in PBS) [3-4,5-dimethyldiazol-2-yl]-2,5-diphenyl tetrazolium bromide reagent (Merck), was added and the cells were incubated for additional 3 h at 37 °C. The formazan crystals thus formed were dissolved in 100 μl of buffer containing 50% (v/v) *N*,*N*'-dimethylformamide, 20% SDS (pH 4.5). The absorbance was measured at 570 nm with a Multiskan™ GO Microplate Spectrophotometer (Thermo Fisher Scientific, USA).

CHAPTER 9

Synthesis of a small collections of mPGES-1 inhibitors

CHAPTER 9

Synthesis of a small collections of mPGES-1 inhibitors

9.1 General synthetic methods

All commercially available starting materials were purchased from Merck and used as received. All solvents used for the synthesis were of HPLC grade (Merck). NMR spectra (^{1}H, ^{13}C) were recorded on Bruker Avance 400 MHz, 500 MHz, 600 MHz instruments, T = 298 K. Compounds were dissolved in 0.5 mL of $(CD_3)_2SO$, CD_3OD, $CDCl_3$ (Merck, 99.8 Atom %D). Coupling constants (J) are reported in Hertz, and chemical shifts are expressed in parts per million (ppm) on the delta (δ) scale relative to the solvent peak as the internal reference. Multiplicities are reported as follows: s, singlet; d, doublet; dd, doublet of doublets; ddd, doublet of doublet of doublets; t, triplet; m, multiplet. Mass spectrometry experiments were performed using an HPLC–MS system Q-ToF Premiere™ instrument (Waters, Co.®) equipped with an ESI source and Waters pump system and a LCQ DECA TermoQuest (San Josè, California, USA) mass spectrometer. Reactions were monitored on silica gel 60 F254 plates (Merck) and the spots were visualized under UV light (λ = 254nm, 365nm). Analytical and semi-preparative reversed-phase HPLC was performed on Agilent Technologies, Inc.© 1200 Series high performance liquid chromatography using a Nucleodur© C8 reversed-phase column (100 x 2mm, 4μM, 80 Å, flow rate = 1 mL/min; 250 x 10.00mm, 4μM, 80 Å, flow rate = 4 mL/min respectively, Macherey-Nagel©) and Fusion-RP® C18 reversed-phase column (100 x 2mm, 4μM, 80 Å, flow rate = 1 mL/min; 250 x 10.00 mm, 4 μM, 80 Å, flow rate = 4 mL/min respectively, Phenomenex®). The binary solvent system (A/B) was as follows: 0.1% TFA in water (A) and 0.1% TFA in CH_3CN (B). The absorbance was detected at 220/240 nm. The purity of all tested compound (>98%) was determined by HPLC analysis and NMR spectra.

9.2 Synthesis of aryl halide molecules (SZK1-SZK12)

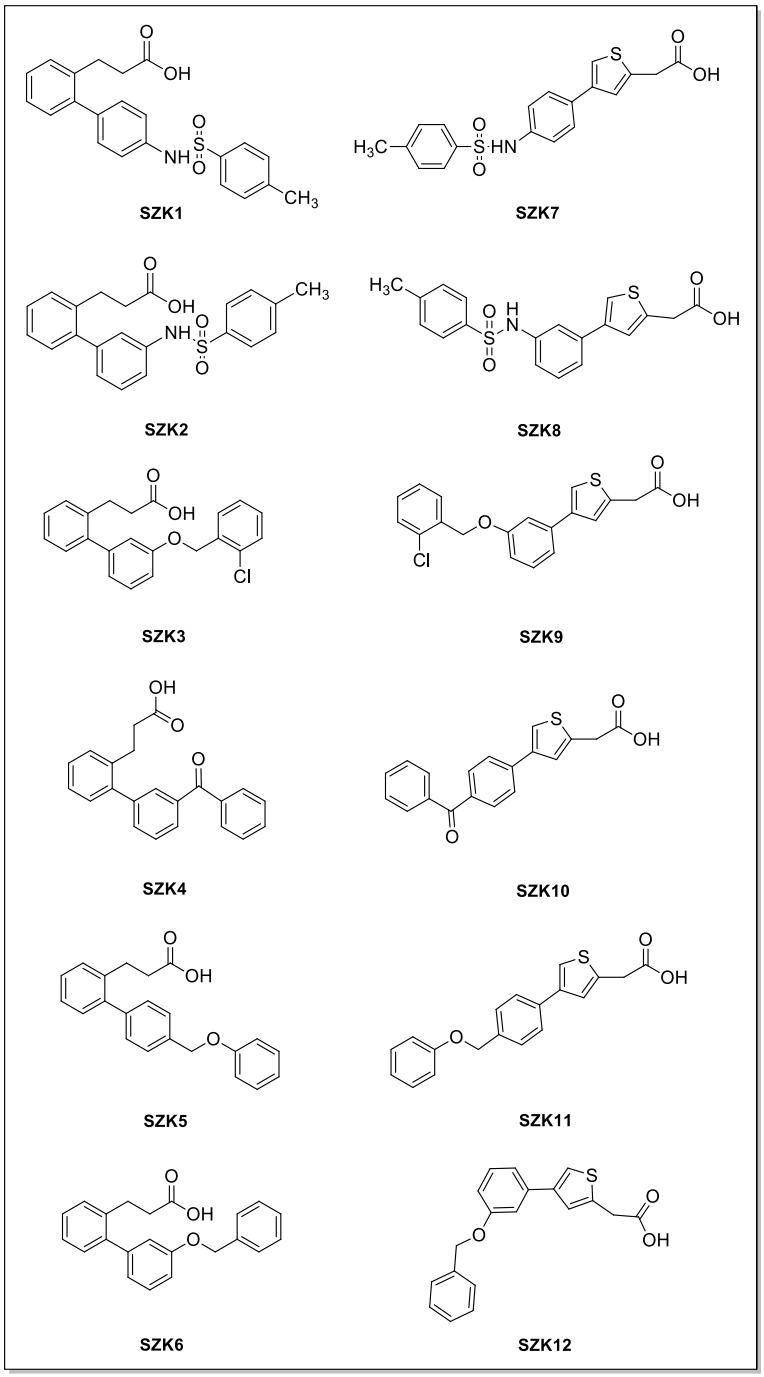

9.2.1 General procedure (I) for the synthesis of SZK1-SZK12

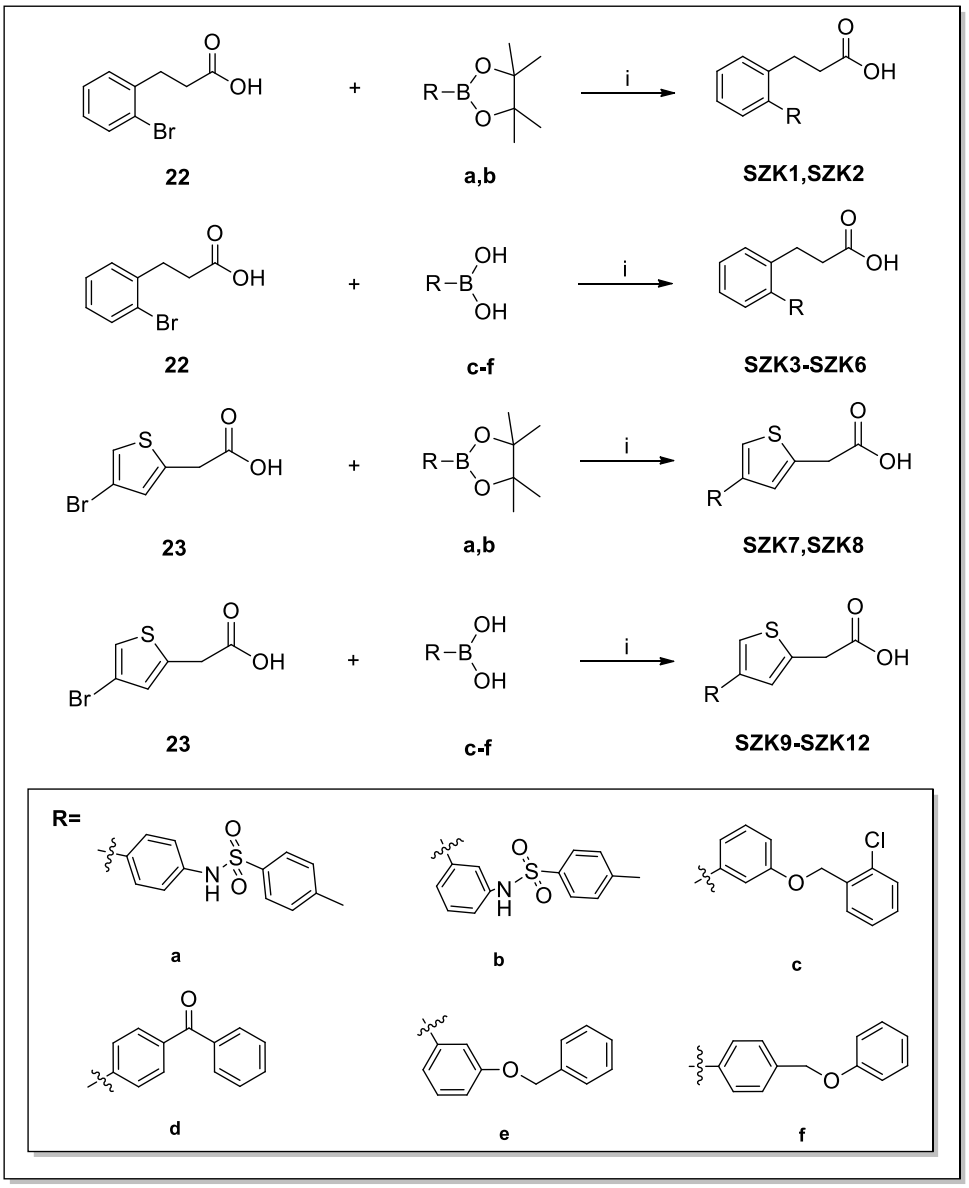

Synthetic scheme 12: i) $Pd(PPh_3)_4$, K_2CO_3, dioxane/H_2O (2:1), reflux, overnight

3-(2-bromophenyl)propanoic acid (**22**) (1.0 equiv) or 2-(4-bromothiophen-2-yl)acetic acid (**23**) (1.0 equiv), the appropriate substituted boronic acid/ester (**a-f**) (1.2 equiv), K_2CO_3 (2 equiv) and $Pd(PPh_3)_4$ (0.05 equiv) were placed in a two-neck

round-bottom flask, equipped with a stir bar. The system was evacuated and refilled with N_2 five times. A mixture of dioxane/H_2O (3.0 and 1.5 mL; rate 2:1) was placed in another 25 ml round-bottom flask and this latter too was evacuated and refilled with N_2 five times. Finally, dioxane/H_2O were added by syringe in the flask with the powders and the reaction mixture was refluxed overnight (**Synthetic scheme 12**). [242] The solution was, then, cooled and diluted with acidified water (20 mL); this process led to the formation of a precipitate. The filtrate was dried over anhydrous Na_2SO_4 and, finally, concentrated under reduced pressure. The desired compounds **SZK1-SZK12** were confirmed by analytical RP-HPLC (Nucleodur© C8 reversed-phase column: 100 x 2mm, 4μM, 80 Å, flow rate = 1 mL/min). HPLC purification was performed by semi-preparative reversed-phase HPLC (Nucleodur© C8 reversed-phase column: 250 x 10.00mm, 4μM, 80 Å, flow rate = 4 mL/min). The final products were obtained with high purity (>98%) as detected by HPLC analysis and were fully characterized by ESI-MS and NMR spectra.

3-(4'-(4-methylphenylsulfonamido)-[1,1'-biphenyl]-2-yl)propanoic acid (SZK1)

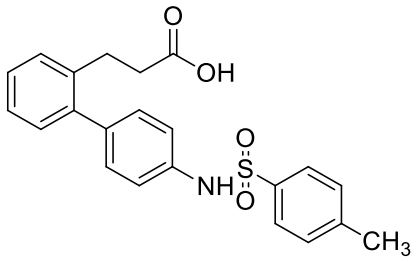

Compound **SZK1** was obtained by following the general procedure (**I**), from the reaction between **22** and *N*-4-(4,4,5,5-tetramethyl-1,3,2-dioxaborolan-2-yl)phenyltolylsulfonamide (**a**), as a brown solid (170mg, 30% yield after HPLC). RP-HPLC t_R = 31.8 min, gradient condition: from 5% B to 100% B in 60min, flow rate of 4 mL/min, λ = 240 nm. ^{1}H NMR (400 MHz, CD_3OD): δ_H = 7.55 (d, *J* = 8.2

Hz, 2H), 7.20 (d, *J* = 8.0 Hz, 2H), 7.16-7.13 (m, 2H), 7.10 (ddd, *J* = 8.8, 5.3, 3.7 Hz, 1H), 7.06 – 7.01 (m, 4H), 7.00 – 6.97 (m, 1H), 2.74 (t, *J* = 7.9 Hz, 2H), 2.26 (s, 3H), 2.24 (t, *J* = 7.9 Hz, 2H). ^{13}C NMR (100 MHz, CD_3OD): δ = 173.5, 143.6 (2C), 141.1, 138.0, 137.7, 136,7, 129.7, 129.4 (2C), 129.2 (2C), 128.8, 127.3, 126.9 (2C), 126.0, 120.9 (2C), 34.5, 28.0, 20.0. ESI-MS: calculated for $C_{22}H_{21}NO_4S$ 395.47; found m/z = 394.93 $[M-H]^-$.

3-(3'-(4-methylphenylsulfonamido)-[1,1'-biphenyl]-2-yl)propanoic acid (SZK2)

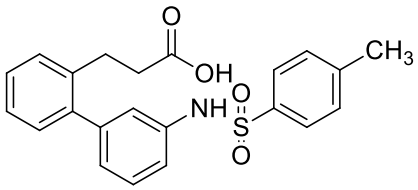

Compound **SZK2** was obtained by following the general procedure (**I**), from the reaction between **22** and 3-(p-toluenesulfonylamino)phenylboronic acid pinacol ester (**b**), as a dark brown solid (175mg, 60% yield after HPLC). RP-HPLC t_R = 35.3 min, gradient condition: from 5% B to 100% B in 60min, flow rate of 4 mL/min, λ = 240 nm. ^{1}H NMR (400 MHz, CD_3OD): δ_H = 7.67 – 7.64 (m, 2H), 7.32 –7.20 (m, 6H), 7.10 – 6.99 (m, 4H), 2.80 (t, *J* = 7.9 Hz, 2H), 2.39 (s, 3H), 2.32 (t, *J* = 7.9 Hz, 2H). ^{13}C NMR (101 MHz, CD_3OD): δ = 173.4, 143.6, 142.5, 141.2, 137.6, 137.5, 136.6, 129.5, 129.2 (2C), 128.9, 128.7, 127.5, 126.9 (2C), 126.0, 125.2, 121.9, 119.9, 34.6, 27.9, 20.0. ESI-MS: calculated for $C_{22}H_{21}NO_4S$ 395.47; found m/z = 394.12 $[M-H]^-$.

3-(3'-((2-chlorobenzyl)oxy)-[1,1'-biphenyl]-2-yl)propanoic acid (SZK3)

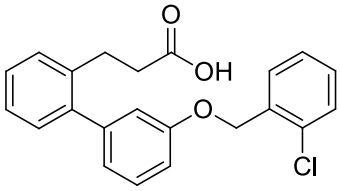

Compound **SZK3** was obtained by following the general procedure (**I**), from the reaction between **22** and 3-(2-chlorobenzyloxy)phenylboronic acid (**c**), as a yellow solid (160mg, 65% after HPLC). RP-HPLC t_R = 40.9 min, gradient condition: from 5% B to 100% B in 60min, flow rate of 4 mL/min, λ = 240 nm. ^{1}H NMR (400 MHz, CD_3OD): δ_H = 7.60 – 7.55 (m, 1H), 7.48 – 7.39 (m, 1H), 7.37 – 7.26 (m, 5H), 7.23 (t, *J* = 4.6 Hz, 1H), 7.17 (d, *J* = 7.1 Hz, 1H), 7.04 - 6.97 (m, 1H), 6.91 (d, *J* = 7.1Hz, 2H), 5.21 (s, 2H), 2.88 (t, *J* = 7.9 Hz, 2H), 2.38 (t, *J* = 7.9 Hz, 2H). ^{13}C NMR (125 MHz, CD_3OD): δ = 175.4, 158.4, 143.1, 141.6, 137.9, 134.7, 132.6, 129.6, 129.1, 129.2 (2C), 129.0, 128.8, 127.3, 126.8, 125.8, 121.8, 115.4, 113.3, 66.9, 34.9, 28.1. ESI-MS: calculated for $C_{22}H_{19}ClO_3$ 366.10; found m/z = 367.09 $[M+H]^+$, 369.10 $[M+H+2]^+$.

3-(3'-benzoyl-[1,1'-biphenyl]-2-yl)propanoic acid (SZK4)

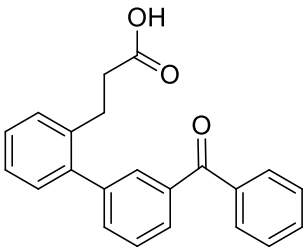

Compound **SZK4** was obtained by following the general procedure (**I**), from the reaction between **22** and 4-benzoylphenylboronic acid (**d**), as a dark brown solid (145mg, 45% after HPLC). RP-HPLC t_R = 36.5 min, gradient condition: from 5%

B to 100% B in 60min, flow rate of 4 mL/min, λ = 240 nm. ^{1}H NMR (400 MHz, CD_3OD): δ_H = δ 7.91 – 7.80 (m, 4H), 7.68 (dd, *J* = 8.4, 6.3 Hz, 1H), 7.57 (t, *J* = 7.7, 2H), 7.51 (dd, *J* = 8.3, 3.1 Hz, 2H), 7.41 – 7.33 (m, 3H), 7.24 (d, *J* = 7.2 Hz, 1H), 2.96 (t, *J* = 7.9 Hz, 2H), 2.45 (t, *J* = 7.9 Hz, 2H). ^{13}C NMR (150 MHz, CD_3OD): δ = 196.9, 175.0, 146.3, 140.9, 137.8, 137.5, 136.0, 132.4, 129.7 (2C), 129.6 (2C), 129.5, 129.0 (2C), 128.9, 128.1 (2C), 127.9, 126.1, 34.7, 28.0. ESI-MS: calculated for $C_{22}H_{18}O_3$ 330.13; found m/z = 331.09 $[M+H]^+$.

3-(4'-(phenoxymethyl)-[1,1'-biphenyl]-2-yl)propanoic acid (SZK5)

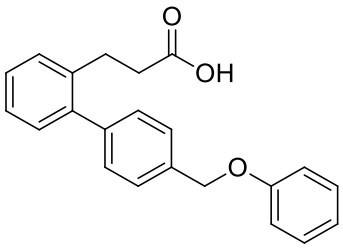

Compound **SZK5** was obtained by following the general procedure (**I**), from the reaction between **22** and 4-(phenoxymethyl)phenylboronic acid (**e**), as a red solid (50mg, 65% after HPLC). RP-HPLC t_R = 39.7 min, gradient condition: from 5% B to 100% B in 60min, flow rate of 4 mL/min, λ = 240 nm. ^{1}H NMR (400 MHz, CD_3OD): δ_H = 7.43 – 7.37 (m, 2H), 7.23 – 7.11 (m, 7H), 7.05 (d, *J* = 7.4 Hz, 1H), 6.91 (d, *J* = 8.0 Hz, 2H), 6.83 (t, *J* = 7.4 Hz, 1H), 4.75 (s, 2H), 2.79 (t, *J* = 8.0 Hz, 2H), 2.28 (t, *J* = 8.0 Hz, 2H). ^{13}C NMR (100 MHz, CD_3OD): δ = 173.5, 158.8, 141.6, 141.2, 137.7, 136.2, 129.8, 129.1 (2C), 128.9 (2C), 128.8, 127.3, 127.1 (2C), 126.0, 120.6, 114.6 (2C), 69.3, 34.5, 28.0. ESI-MS: calculated for $C_{22}H_{20}O_3$; found 332.14 m/z = 371.08 $[M+K]^+$.

3-(3'-(benzyloxy)-[1,1'-biphenyl]-2-yl)propanoic acid (SZK6)

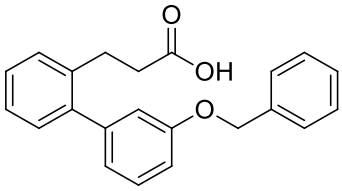

Compound **SZK6** was obtained by following the general procedure **(I)**, from the reaction between **22** and 3-(benzyloxy)phenylboronic acid (**f**), as a dark green solid (145 mg, 60% after HPLC). RP-HPLC t_R = 39.3 min, gradient condition: from 5% B to 100% B in 60min, flow rate of 4 mL/min, λ = 240 nm. ^{1}H NMR (400 MHz, CD_3OD): δ_H = 7.33 (d, *J* = 7.5 Hz, 2H), 7.25 (t, *J* = 7.4 Hz, 2H), 7.22 – 7.16 (m, 4H), 7.15 – 7.09 (m, 1H), 7.04 (d, *J* = 7.6 Hz, 1H), 6.89 (d, *J* = 8.5 Hz, 1H), 6.81 – 6.74 (m, 2H), 4.75 (s, 2H), 2.75 (t, *J* = 8.0 Hz, 2H), 2.25 (t, *J* = 8.0 Hz, 2H). ^{13}C NMR (100 MHz, CD_3OD): δ = 175.4, 158.6, 143.0, 141.7, 137.8, 137.3, 129.6, 128.9, 128.7, 128.1 (2C), 127.4, 127.2, 127.1 (2C), 125.8, 121.5, 115.4, 113.4, 69.6, 34.9, 28.1. ESI-MS: calculated for $C_{22}H_{20}O_3$; found 332.14 m/z = 333.17 $[M+H]^+$.

2-(4-(4-(4-methylphenylsulfonamido)phenyl)thiophen-2-yl)acetic acid (SZK7)

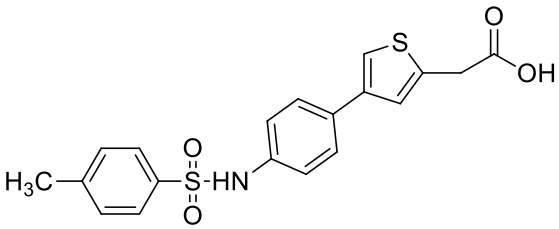

Compound **SZK7** was obtained by following the general procedure (**I**), from the reaction between **23** and N-4-(4,4,5,5-tetramethyl-1,3,2-dioxaborolan-2-yl)phenyltolylsulfonamide (**a**), as a brown solid (250mg, 55% after HPLC). RP-HPLC t_R = 39.3 min, gradient condition: from 5% B to 100% B in 60min, flow rate of 4 mL/min, λ = 240 nm. ^{1}H NMR (400 MHz, $CDCl_3$): δ_H = 7.67 (d, *J* = 7.9 Hz,

2H), 7.45 (d, *J* = 8.0 Hz, 2H), 7.27 – 7.21 (m, 3H), 7.09 (d, *J* = 8.1 Hz, 2H), 6.63 (s, 1H), 3.92 (s, 2H), 2.40 (s, 3H). ^{13}C NMR (100 MHz, CD_3OD): δ = 172.7, 143.6, 140.8, 136.8, 136.7, 136.5, 132.4, 129.1 (2C), 126.9 (2C), 126.3 (2C), 125.5, 121.3 (2C), 119.0, 34.7, 20.0. ESI-MS: calculated for $C_{19}H_{17}NO_4S_2$; found 387.06 m/z = 388.10 $[M+H]^+$.

2-(4-(3-(4-methylphenylsulfonamido)phenyl)thiophen-2-yl)acetic acid (SZK8)

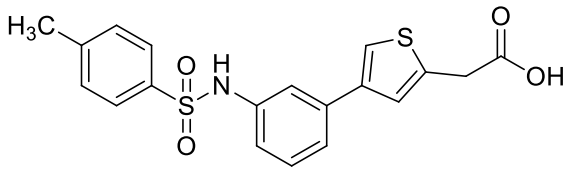

Compound **SZK8** was obtained by following the general procedure (**I**), from the reaction between **23** and 3-(p-toluenesulfonylamino)phenylboronic acid pinacol ester (**b**), as a dark brown solid (175mg, 40% after HPLC). RP-HPLC t_R = 26.9 min, gradient condition: from 5% B to 100% B in 60min, flow rate of 4 mL/min, λ = 240 nm. ^{1}H NMR (400 MHz, $CDCl_3$): δ_H = 7.59 (d, *J* = 8.0 Hz, 2H), 7.25 – 7.12 (m, 5H), 7.10 (s, 1H), 6.89 (d, *J* = 7.8 Hz, 1H), 6.55 (s, 1H), 3.83 (s, 2H), 2.30 (s, 3H). ^{13}C NMR (100 MHz, CD_3OD): δ = 172.7, 143.7, 140.9, 138.1, 137.0, 136.8, 136.6, 129.2 (2C), 129.1, 126.9 (2C), 125.5, 122.0, 119.7, 119.3, 118.4, 34.6, 20.0. ESI-MS: calculated for $C_{19}H_{17}NO_4S_2$; found 387.06 m/z = 388.08 $[M+H]^+$.

2-(4-(3-((2-chlorobenzyl)oxy)phenyl)thiophen-2-yl)acetic acid (SZK9)

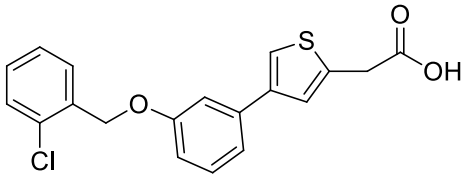

Compound **SZK9** was obtained by following the general procedure (**I**), from the reaction between **23** and 3-(2-chlorobenzyloxy)phenylboronic acid (**c**), as a dark brown solid (160mg, 45% after HPLC). RP-HPLC t_R = 27.9 min, gradient condition: from 5% B to 100% B in 60min, flow rate of 4 mL/min, λ = 240 nm. ^{1}H NMR (400 MHz, $(CD_3)_2SO$): δ_H = 7.76 (d, *J* = 1.5 Hz, 1H), 7.66-7.62 (m, 1H), 7.55-7.51 (m, 1H), 7.42-7.39 (m, 3H), 7.36-7.31 (m, 2H), 7.30-7.26 (m, 1H), 6.95 (dd, *J* = 8.0, 2.5 Hz, 1H), 5.22 (s, 2H), 3.85 (s, 2H). ^{13}C NMR (100 MHz, CD_3OD): δ = 171.0, 157.9, 145.1, 136.5, 135.2, 134.8, 132.6, 129.0, 128.9, 128.6, 128.3, 128.1, 126.7, 126.4, 125.8, 116.6, 115.9, 66.7, 39.0. ESI-MS: calculated for $C_{19}H_{15}ClO_3S$; found 358.04 m/z = 359.29 $[M+H]^+$.

2-(4-(4-benzoylphenyl)thiophen-2-yl)acetic acid (SZK10)

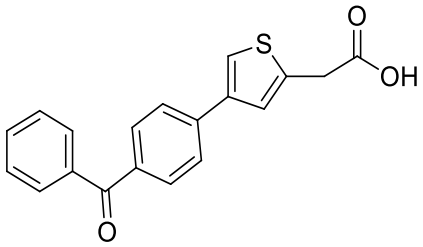

Compound **SZK10** was obtained by following the general procedure (**I**), from the reaction between **23** and 4-benzoylphenylboronic acid (**d**), as a dark brown solid (145mg, 40% after HPLC). RP-HPLC t_R = 35.3 min, gradient condition: from 5% B to 100% B in 60min, flow rate of 4 mL/min, λ = 240 nm. ^{1}H NMR (400 MHz, CD_3OD): δ_H = 7.85 – 7.78 (m, 6H), 7.74 – 7.72 (m, 1H), 7.67 (t, *J* = 7.5 Hz, 1H),

7.56 (t, *J* = 7.6 Hz, 2H), 7.43 (s, 1H), 3.96 (s, 2H). ^{13}C NMR (100 MHz, CD_3OD): δ = 196.6, 171.2, 140.4, 139.9, 137.7, 136.9, 135.6, 132.3, 130.5 (2C), 129.5 (2C), 128.1 (2C), 125.7, 125.6 (2C), 121.7, 34.5. ESI-MS: calculated for $C_{19}H_{14}O_3S$; found 322.38 m/z = 321.07 $[M-H]^-$.

2-(4-(4-(phenoxymethyl)phenyl)thiophen-2-yl)acetic acid (SZK11)

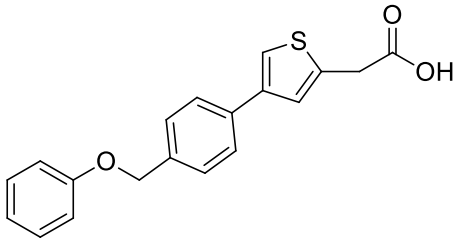

Compound **SZK11** was obtained by following the general procedure (**I**), from the reaction between **23** and 4-(phenoxymethyl)phenylboronic acid (**e**), as a dark brown solid (50mg, 55% after HPLC). RP-HPLC t_R = 37.8 min, gradient condition: from 5% B to 100% B in 60min, flow rate of 4 mL/min, λ = 240 nm. ^{1}H NMR (400 MHz, CD_3OD): δ_H = 7.56 – 7.52 (m, 2H), 7.40 (s, 1H), 7.36 (d, *J* = 7.7 Hz, 2H), 7.22 (s, 1H), 7.17 (t, *J* = 8.0 Hz, 2H), 6.89 (d, *J* = 8.0 Hz, 2H), 6.83 (t, *J* = 7.7 Hz, 1H), 4.97 (s, 2H), 3.76 (s, 2H). ^{13}C NMR (100 MHz, CD_3OD): δ = 179.3, 160.0, 145.5, 141.0, 141.9, 137.7, 129.6 (2C), 128.8 (2C), 128.2, 128.8 (2C), 127.7, 121.7, 115.8 (2C), 70.4, 40.3. ESI-MS: calculated for $C_{19}H_{16}O_3S$; found 324.08 m/z = 325.08 $[M+H]^+$.

2-(4-(3-(benzyloxy)phenyl)thiophen-2-yl)acetic acid (SZK12)

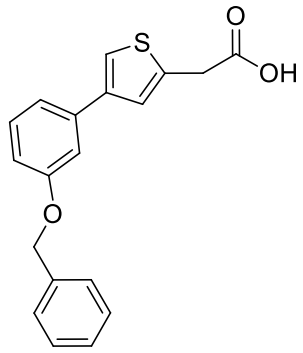

Compound **SZK12** was obtained by following the general procedure (**I**), from the reaction between **20** and 3-(benzyloxy)phenylboronic acid (**f**), as a dark brown solid (150mg, 40% after HPLC). RP-HPLC t_R = 36.3 min, gradient condition: from 5% B to 100% B in 60min, flow rate of 4 mL/min, λ = 240 nm. ^{1}H NMR (400 MHz, $CDCl_3$): δ_H = 7.38 (d, *J* = 7.0 Hz, 2H), 7.32 (t, *J* = 7.4 Hz, 2H), 7.28 – 7.24 (m, 2H), 7.21-7.16 (m, 2H), 7.11 – 7.07 (m, 2H), 6.83 (dd, *J* = 8.3, 2.5 Hz, 1H), 5.03 (s, 2H), 3.84 (s, 2H). ^{13}C NMR (150 MHz, CD_3OD): δ = 172.9, 159.2, 141.5, 137.4, 137.2, 136.7, 129.4, 128.1 (2C), 127.4, 127.2 (2C), 125.7, 119.5, 118.5, 113.1, 112,4, 69.6, 34.4. ESI-MS: calculated for $C_{19}H_{16}O_3S$; found 324.08 m/z = 325.20 $[M+H]^+$

9.3 Synthesis of 2,4-thiazolidinedione derivatives (TZ1-TZ9)

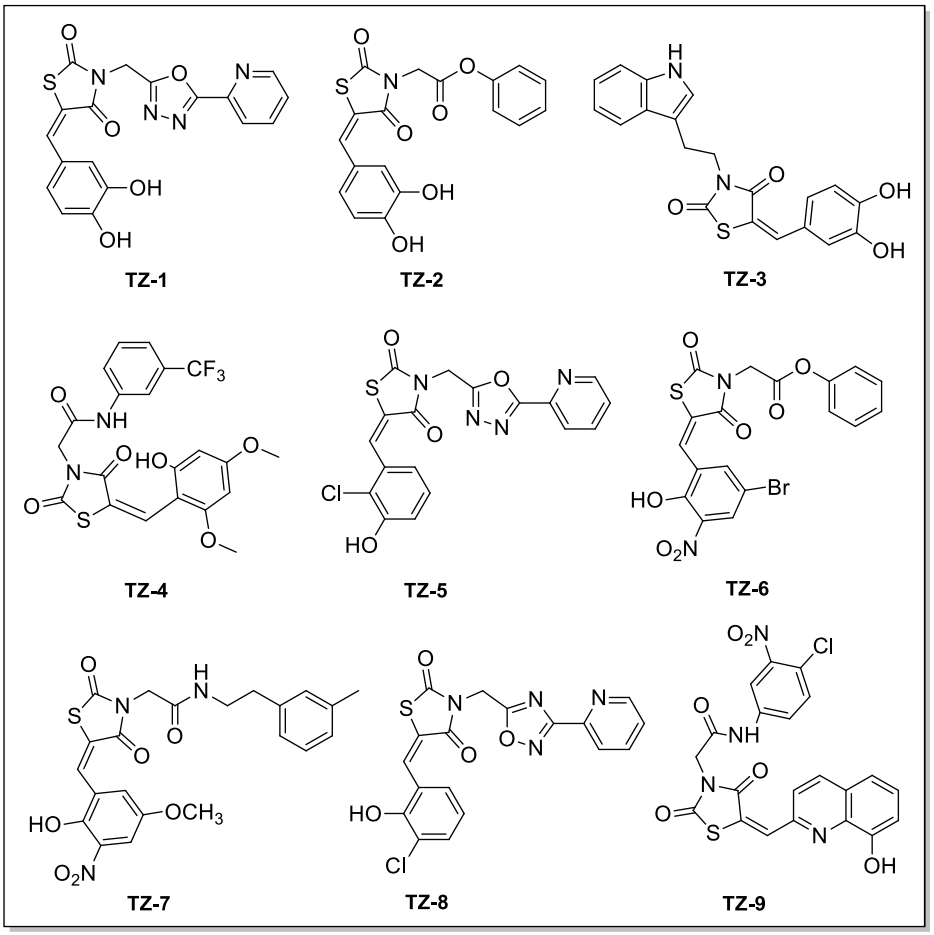

9.3.1 General Method (J) for synthesis of *N*-substituted thiazolidine-2,4-diones (25a-25d)

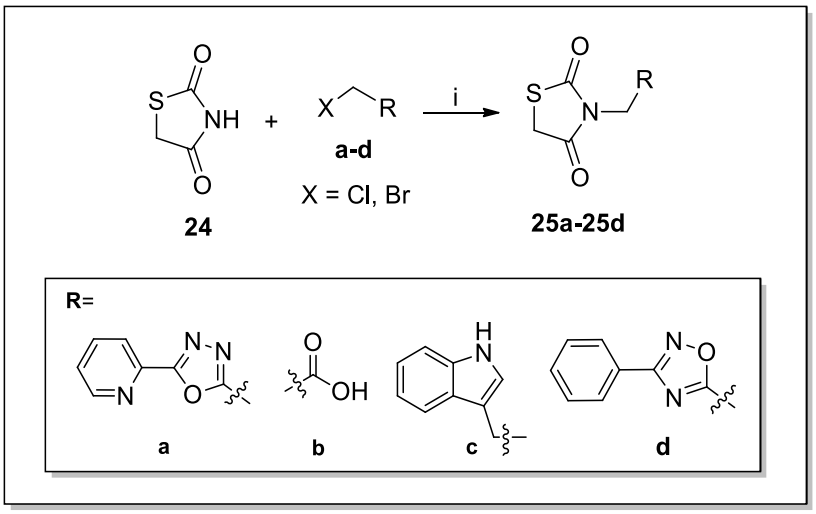

Synthetic scheme 13: i) NaH, THF dry, reflux, 24h.

To a solution of thiazolidine-2,4-dione (**24**) (1.0 equiv) in dry THF (3.0 mL), NaH (1.2 equiv) was added dropwise, and the mixture was stirred for 30 min at 80°C; then the reaction mixture was cooled to room temperature and halides **a-c** (1.5 equiv) were added. The solution was stirred at 80°C for 24, and poured into ice-cold water (**Synthetic scheme 13**). [228] The aqueous phase was extracted with AcOEt (3 x 20 mL), and the combined organic layers were dried over anhydrous $MgSO_4$, filtered, and concentrated in vacuum. The desired compounds **25a-25c** were used without any further purification in the next step.

3-((5-(pyridin-2-yl)-1,3,4-oxadiazol-2-yl)methyl)thiazolidine-2,4-dione (25a)

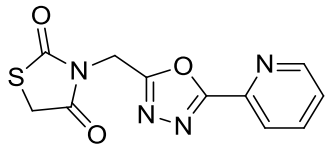

Compound **25a** was obtained by following the general procedure (**J**), from the reaction between **24** and 2-chloro-5-(pyridin-2-yl)-1,3,4-oxadiazole (**a**), as a brown solid (355 mg, 85% yield by HPLC analysis). RP-HPLC t_R = 12.6, gradient condition: from 5% B ending to 100% B 50 min, flow rate of 4 mL/min, λ = 240 nm. ^{1}H NMR (400 MHz, $CDCl_3$): δ_H = 8.76 (dd, *J* = 4.0, 1.7 Hz, 1H), 8.06 (dd, *J* = 9.7, 1.4 Hz, 1H), 7.85 (ddd, *J* = 9.7, 7.1, 1.6 Hz, 1H), 7.30 (ddd, *J* = 7.1, 4.0, 1.5 Hz, 1H), 5.23 (s, 2H), 3.89 (s, 2H). ESI-MS: calculated for $C_{11}H_8N_4O_3S$ 276.03 found m/z = 277.02 $[M+H]^+$.

2-(2,4-dioxothiazolidin-3-yl)acetic acid (25b)

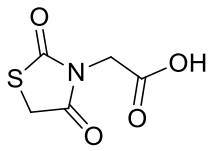

Compound **25b** was obtained by following the general procedure (**J**), from the reaction between **24** and carbonobromidic acid (**b**), as a brown solid (420 mg, 80% yield by HPLC analysis). RP-HPLC t_R = 14.1, gradient condition: from 5% B ending to 100% B 50 min, flow rate of 4 mL/min, λ = 240 nm. ^{1}H NMR (400 MHz, $CDCl_3$): δ_H = 4.92 (s, 2H), 3.88 (s, 2H). ESI-MS: calculated for $C_5H_5NO_4S$ 174.99 found m/z = 175.87 $[M+H]^+$.

3-(2-(1H-indol-3-yl)ethyl)thiazolidine-2,4-dione (25c)

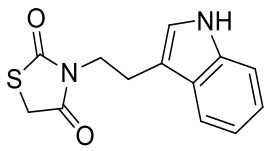

Compound **25c** was obtained by following the general procedure (**J**), from the reaction between **24** and 3-(bromomethyl)-1H-indole (**c**), as a brown solid (125 mg, 75% yield by HPLC analysis). RP-HPLC t_R = 31.9, gradient condition: from 5% B ending to 100% B 50 min, flow rate of 4 mL/min, λ = 240 nm. ^{1}H NMR (400 MHz, $CDCl_3$): δ_H = 7.60 – 7.55 (m, 1H), 7.35 (dt, *J* = 7.7, 0.8 Hz 1H), 7.15 (td, *J* = 7.6, 1.3 Hz, 1H), 7.12 – 7.05 (m, 2H), 4.19 (t, *J* = 5.7 Hz, 2H), 3.92 (s, 2H), 3.13 (dt, *J* = 13.9, 5.7 Hz, 1H), 3.01 (dt, *J* = 13.9, 5.7 Hz, 1H). ESI-MS: calculated for $C_{13}H_{12}N_2O_2S$ 260.06 found m/z = 261.05 $[M+H]^+$.

3-((3-(pyridin-2-yl)-1,2,4-oxadiazol-5-yl)methyl)thiazolidine-2,4-dione (25d)

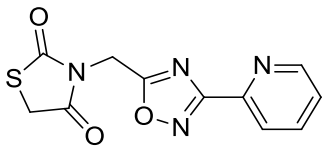

Compound **25d** was obtained by following the general procedure (**J**), from the reaction between **24** and 5-chloro-3-phenyl-1,2,4-oxadiazole (**d**), as a brown solid (320 mg, 85% yield by HPLC analysis). RP-HPLC t_R = 12.6, gradient condition: from 5% B ending to 100% B 50 min, flow rate of 4 mL/min, λ = 240 nm. ^{1}H NMR (400 MHz, $CDCl_3$): δ_H = 8.77 (dd, *J* = 4.0, 1.7 Hz, 1H), 8.17 (dd, *J* = 9.2, 1.5 Hz, 1H), 7.87 (ddd, *J* = 9.2, 7.2, 1.7 Hz, 1H), 7.29 (ddd, *J* = 7.1, 4.0, 1.5 Hz, 1H), 5.26 (d, *J* = 15.6 Hz, 1H), 5.19 (d, *J* = 15.7 Hz, 1H), 3.89 (s, 2H). ESI-MS: calculated for $C_{11}H_8N_4O_3S$ 276.03 found m/z = 277.04 $[M+H]^+$.

9.3.2 General Method (K) for the Synthesis of 5-arylidenethiazolidine-2,4-diones (TZ1, TZ3, TZ5, TZ8, 26be, 26bf, 26bh, 26bj, 26bk)

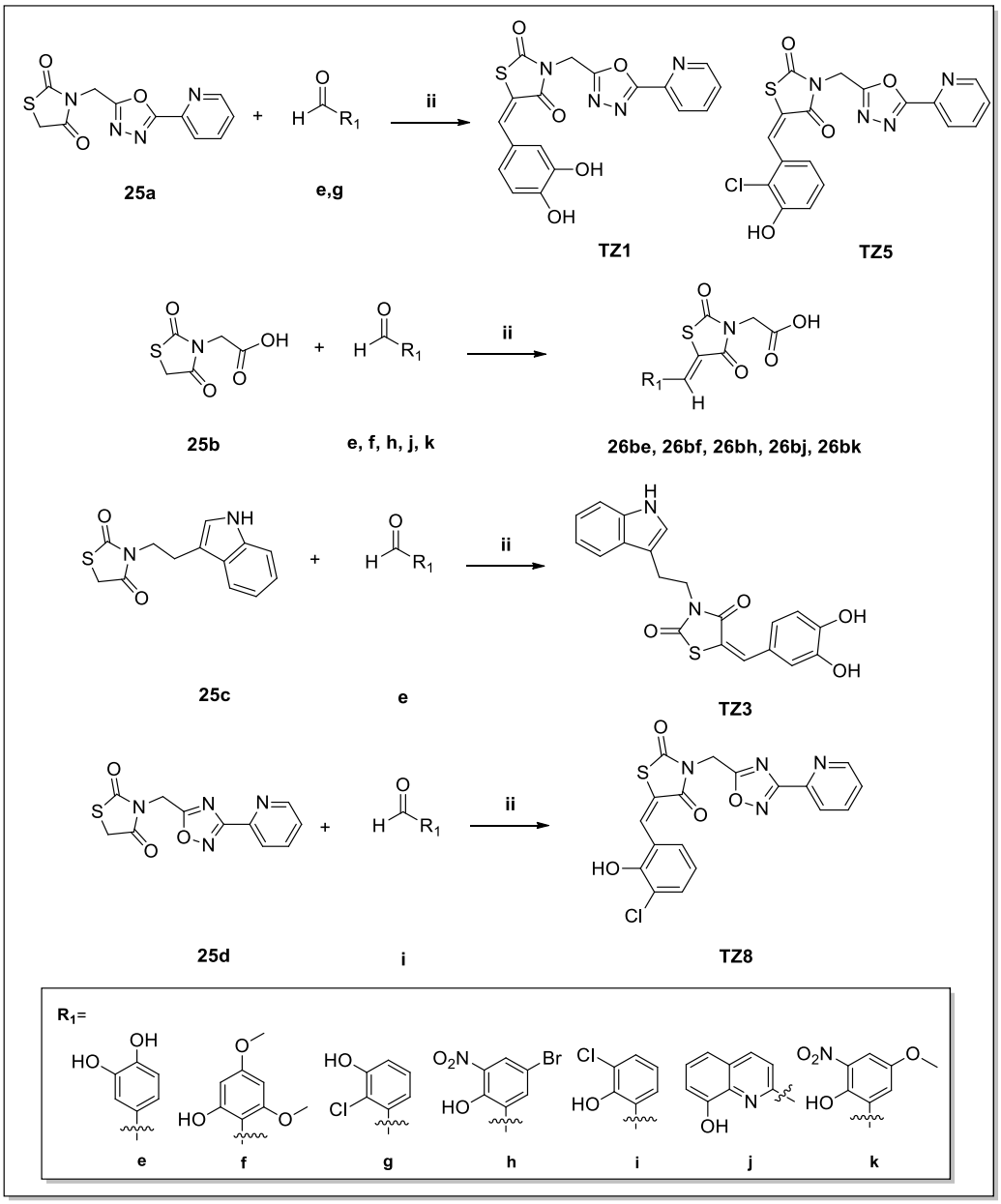

Synthetic scheme 14: ii) piperidine, EtOH, reflux, overnight.

A mixture of **25a-25d** (1.0 equiv), aromatic aldehydes **e-k** (1.0 equiv), piperidine (0.8 equiv), and ethanol (1.5mL) were placed in a 25mL bottom flask. The reaction mixture was continuously stirred and refluxed overnight (**Synthetic scheme 14**). [228] The mixture was allowed to cool down before acidified water and AcOEt were added. The aqueous phase was extracted with AcOEt (3 x 20 mL), the combined organic layers were dried over $MgSO_4$, filtered, and concentrated in vacuum. HPLC purification was performed by semi-preparative reversed-phase HPLC (Fusion-RP® C18 reversed-phase column: 250 x 10.00mm, 4μM, 80 Å, flow rate = 4mL/min) using the gradient conditions reported below. The final products **TZ1, TZ3, TZ5,** and **TZ8** were characterized by ESI-MS and NMR spectra as well as the intermediates **26be**, **26bf**, **26bh**, **26bj**, and **26bk**.

5-(3,4-dihydroxy-benzylidene)-3-(5-pyridin-2-yl-[1,3,4]oxadiazol-2-ylmethyl)-thiazolidine-2,4-dione) (TZ-1)

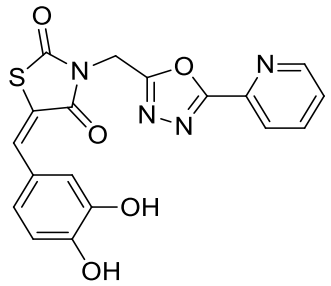

Compound **TZ1** was obtained by following the general procedure (**K**), from the reaction between **25a** and 3,4-dihydroxybenzaldehyde (**e**), as a pale yellow powdery solid (79.5 mg, 22% yield after HPLC purification); RP-HPLC t_R = 20.5 min, gradient condition: from 5% B to 100 % B over 50 min, flow rate of 4 mL/min, λ = 240 nm. ^{1}H NMR (400 MHz, CD_3OD): δ_H = 7.81 (s, 1H), 7.76 (s, 1H), 6.97-6.94 (m, 2H), 6.93-6.89 (m, 2H), 6.81 (d, *J* = 3.1 Hz, 1H), 6.79 (d, *J* = 3.1 Hz, 1H), 5.19 (s, 2H). ESI-MS: calculated for $C_{18}H_{12}N_4O_5S$ 396.05; found m/z = 395.05 $[M-H]^-$.

5-(3,4-dihydroxy-benzylidene)-3-[2-(1*H*-indol-3-yl)-ethyl]-thiazolidine-2,4-dione (TZ-3)

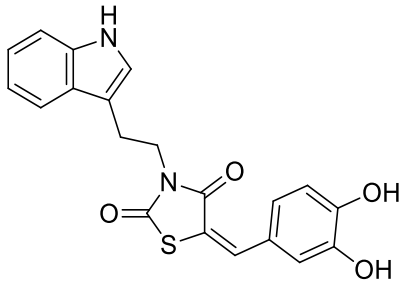

Compound **TZ3** was obtained by following the general procedure (**K**), from the reaction between **25c** and 3,4-dihydroxybenzaldehyde (**e**), as a pale-yellow solid (91.8 mg, 20% yield after HPLC purification); RP-HPLC t_R = 30.2 min, gradient condition: from 5% B ending to 100% B over 50 min, flow rate of 4 mL/min, λ = 240 nm. ^{1}H NMR (400 MHz, CD_3OD) δ_H = 7.63 (s, 1H), 7.53 (d, *J* = 7.9 Hz, 1H), 7.22 (d, *J* = 8.0 Hz, 1H), 7.01-6.95 (m, 2H), 6.93-6.85 (m, 3H), 6.77 (d, *J* = 8.2 Hz, 1H), 3.92-3.87 (m, 2H), 3.02-2.98 (m, 2H). ESI-MS, calculated for $C_{20}H_{16}N_2O_4S$ 380.08; found m/z = 381.10 $[M+H]^+$.

5-(2-chloro-3-hydroxy-benzylidene)-3-(5-pyridin-2-yl-[1,3,4]oxadiazol-2-ylmethyl) thiazolidine-2,4-dione (TZ-5)

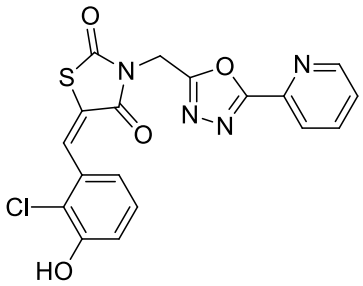

Compound **TZ5** was obtained by following the general procedure (**K**), from the reaction between **25a** and 2-chloro-3-hydroxybenzaldehyde (**g**), as pale-yellow

solid (60.6 mg, 15% yield after HPLC purification); RP-HPLC t_R = 23.9 min, gradient condition: from 5% B to 100 % B over 50 min, flow rate of 4 mL/min, λ = 240 nm. ^{1}H NMR (400 MHz, $CDCl_3$): δ_H = 8.94-8.86 (m, 2H), 8.74 (s, 1H), 8.20 (s, 1H), 8.03-7.96 (m, 1H), 7.19 (t, *J* = 8.0 Hz, 1H), 7.12-7.06 (m, 1H), 6.99 (d, *J* = 7.6 Hz, 1H), 4.27 (s, 2H). ESI-MS: calculated for $C_{18}H_{11}ClN_4O_4S$ 414.02; found m/z = 415.03 $[M+H]^+$.

5-(3-chloro-2-hydroxy-benzylidene)-3-(3-pyridin-2-yl-[1,2,4]oxadiazol-5-ylmethyl)-thiazolidine-2,4-dione (TZ-8)

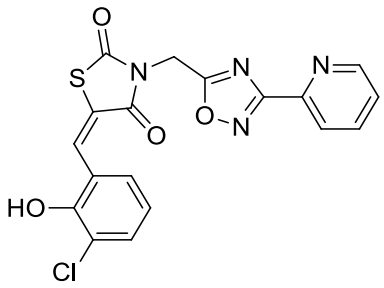

Compound **TZ8** was obtained by following the general procedure (**K**), from the reaction between **25d** and 3-chloro-2-hydroxybenzaldehyde (**i**) as a yellow solid (63.7 mg, 41% yield after HPLC purification); RP-HPLC t_R = 25.3 min, gradient condition: from 5% B to 100 % B over 50 min, flow rate of 4 mL/min, λ = 240 nm. ^{1}H NMR (400 MHz, $CDCl_3$): δ_H = 8.94-8.86 (m, 2H), 8.74 (s, 1H), 8.20 (s, 1H), 8.03- 7.96 (m, 1H), 7.19 (t, *J* = 8.0 Hz, 1H), 7.12-7.06 (m, 1H), 7.01 (t, *J* = 8.0 Hz, 1H), 4.40 (s, 2H). ESI-MS: calculated for $C_{18}H_{11}ClN_4O_4S$ 414.02; found m/z = 415.04 $[M+H]^+$.

(Z)-2-(5-(3,4-dihydroxybenzylidene)-2,4-dioxothiazolidin-3-yl)acetic acid (26be)

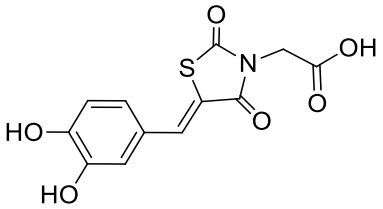

Compound **26be** was obtained by following the general procedure (**K**), from the reaction between **25b** and 3,4-dihydroxybenzaldehyde (**e**), as a pale brown powdery solid (225 mg, 70% yield after HPLC purification); RP-HPLC t_R = 18.3 min, gradient condition: from 5% B to 100 % B over 50 min, flow rate of 4 mL/min, λ = 240 nm. ^{1}H NMR (400 MHz, $CDCl_3$): δ_H = 7.86 (s, 1H), 7.19 (dd, *J* = 9.4, 1.9 Hz, 1H), 7.07 (d, *J* = 2.0 Hz, 1H), 6.74 (d, *J* = 9.4 Hz, 1H), 4.63 (s, 2H). ESI-MS: calculated for $C_{12}H_9NO_6S$ 295.02; found m/z = 296.04 $[M+H]^+$.

(Z)-2-(5-(2-hydroxy-4,6-dimethoxybenzylidene)-2,4-dioxothiazolidin-3-yl)acetic acid (26bf)

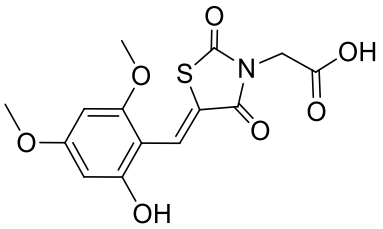

Compound **26be** was obtained by following the general procedure (**K**), from the reaction between **25b** and 2-hydroxy-4,6-dimethoxybenzaldehyde (**f**), as a pale brown powdery solid (240 mg, 75% yield after HPLC purification); RP-HPLC t_R = 22.5 min, gradient condition: from 5% B to 100 % B over 50 min, flow rate of 4 mL/min, λ = 240 nm. ^{1}H NMR (400 MHz, $CDCl_3$): δ_H = 8.27 (s, 1H), 6.31 – 6.25

(m, 2H), 4.63 (s, 2H), 3.91 (s, 3H), 3.84 (s, 3H). ESI-MS: calculated for $C_{14}H_{13}NO_7S$ 339.04; found m/z = 340.05 $[M+H]^+$.

(Z)-2-(5-(5-bromo-2-hydroxy-3-nitrobenzylidene)-2,4-dioxothiazolidin-3-yl)acetic acid (26bh)

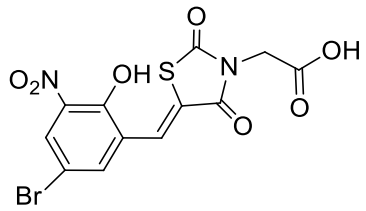

Compound **26bh** was obtained by following the general procedure (**K**), from the reaction between **25b** and 5-bromo-2-hydroxy-3-nitrobenzaldehyde (**h**), as a brown powdery solid (255 mg, 82% yield after HPLC purification); RP-HPLC t_R = 30.3 min, gradient condition: from 5% B to 100 % B over 50 min, flow rate of 4 mL/min, λ = 240 nm. ^{1}H NMR (400 MHz, $CDCl_3$): δ_H = 8.13 (d, *J* = 2.0 Hz, 1H), 8.02 (s, 1H), 7.92 (d, *J* = 2.2 Hz, 1H), 4.63 (s, 2H). ESI-MS: calculated for $C_{12}H_7BrN_2O_7S$ 401.92; found m/z = 402.85 $[M+H]^+$.

(Z)-2-(5-((8-hydroxyquinolin-2-yl)methylene)-2,4-dioxothiazolidin-3-yl)acetic acid (26bj)

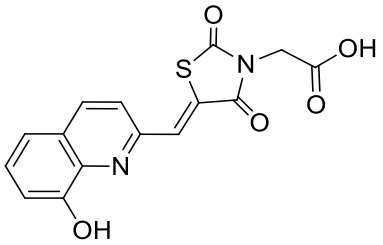

Compound **26bh** was obtained by following the general procedure (**K**), from the reaction between **25b** and 8-hydroxyquinoline-2-carbaldehyde (**j**), as a brown powdery solid (270 mg, 80% yield after HPLC purification); RP-HPLC t_R = 20.5 min, gradient condition: from 5% B to 100 % B over 50 min, flow rate of 4 mL/min, λ = 240 nm. ^{1}H NMR (400 MHz, $CDCl_3$): δ_H = 8.07 (dd, *J* = 8.1, 0.8 Hz, 1H), 7.83 (s, 1H), 7.68 (d, *J* = 8.0 Hz, 1H), 7.41 – 7.34 (m, 2H), 7.05 (dd, *J* = 8.7, 1.7 Hz, 1H), 4.62 (s, 2H). ESI-MS: calculated for $C_{15}H_{10}N_2O_5S$ 330.03; found m/z = 331.02 $[M+H]^+$.

(Z)-2-(5-(2-hydroxy-5-methoxy-3-nitrobenzylidene)-2,4-dioxothiazolidin-3-yl)acetic acid (26bk)

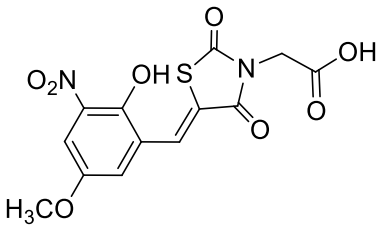

Compound **26bk** was obtained by following the general procedure (**K**), from the reaction between **25b** and 2-hydroxy-5-methoxy-3-nitrobenzaldehyde (**k**), as a brown solid (245 mg, 85% yield after HPLC purification); RP-HPLC t_R = 32.6 min, gradient condition: from 5% B to 100 % B over 50 min, flow rate of 4 mL/min, λ

= 240 nm. ^{1}H NMR (400 MHz, $CDCl_3$): δ_H = 8.04 (s, 1H), 7.57 (d, *J* = 2.2 Hz, 1H), 7.29 (d, *J* = 2.4 Hz, 1H), 4.63 (s, 2H), 3.85 (s, 3H). ESI-MS: calculated for $C_{13}H_{10}N_2O_8S$ 354.02; found m/z = 355.03 $[M+H]^+$.

9.4.3 General synthetic procedure (L) for the synthesis of TZ2 and TZ6

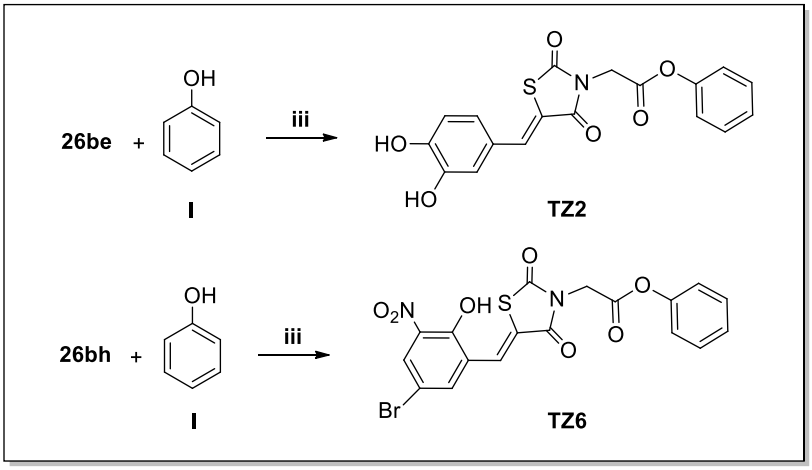

Synthetic scheme 15: **iii)** DMAP, DIC, DCM, rt, overnight.

1.0 equiv of **26be** or **26bh** was dissolved in DCM (4 mL), and DMAP (1.0 equiv), phenol (1.0 equiv), and DIC (1.0 equiv) were added. The mixture was stirred overnight at room temperature and the reaction was monitored by TLC (**Synthetic scheme 15**). [246] The mixture was diluted with 10 mL of H_2O, extracted with AcOEt (3 x 20 mL), and the combined organic layers were dried over Na_2SO_4.

A portion of the crude product was purified by semi-preparative reversed-phase HPLC (Fusion-RP® C18 reversed-phase column, using the gradient conditions reported below). The final products were characterized by ESI-MS and NMR spectra.

[5-(3,4-dihydroxy-benzylidene)-2,4-dioxo-thiazolidin-3-yl]-acetic acid phenyl ester (TZ-2)

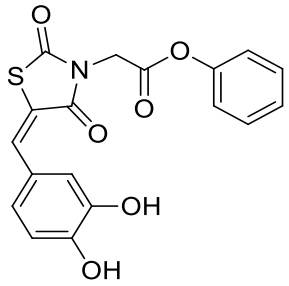

Compound **TZ2** was obtained following the general synthetic procedure (**L**), from the reaction between **26be** and phenol (**l**), as white powdery solid (153.7 mg, 33% yield after HPLC purification); RP-HPLC t_R = 20.1 min, gradient condition: from 5% B ending to 100% B over 50 min, flow rate of
4 mL/min, λ = 240 nm. ^{1}H NMR (400 MHz, $CDCl_3$): δ_H = 8.30-8.24 (m, 1H), 8.03 (s, 1H), 7.83-7.77 (m, 1H), 7.50-7.43 (m, 2H), 7.37-7.35 (m, 3H), 3.59 (s, 2H). ESI-MS: calculated for $C_{18}H_{13}NO_6S$ 371.05; found m/z = 395.10 $[M+Na]^+$.

[5-(5-bromo-2-hydroxy-3-nitro-benzylidene)-2,4-dioxothiazolidin-3-yl]-acetic acid phenyl ester (TZ-6)

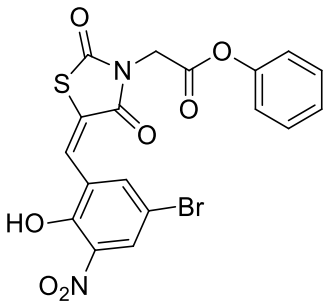

Compound **TZ6** was obtained following the general synthetic procedure (**L**), from the reaction between **26bh** and phenol (**l**), as white solid (48.5 mg, 25% yield after

HPLC purification); RP-HPLC t_R = 32.4 min, gradient condition: from 5% B to 100 % B over 50 min, flow rate of 4 mL/min, λ = 240 nm. ^{1}H NMR (400 MHz, CD_3OD): δ_H = 8.18 (d, *J* = 8.8 Hz, 1H), 7.91 (s, 1H), 7.80- 7.74 (m, 1H), 7.51-7.44 (m, 2H), 7.34 (d, *J* = 7.3 HZ, 1H), 7.28-7.23 (m, 2H), 5.19 (s, 2H). ESI-MS: calculated for $C_{18}H_{11}BrN_2O_7S$ 477.95; found m/z = 517.12 $[M+K]^+$.

9.4.4 General method (M) for synthesis of compounds TZ4, TZ7, and TZ9

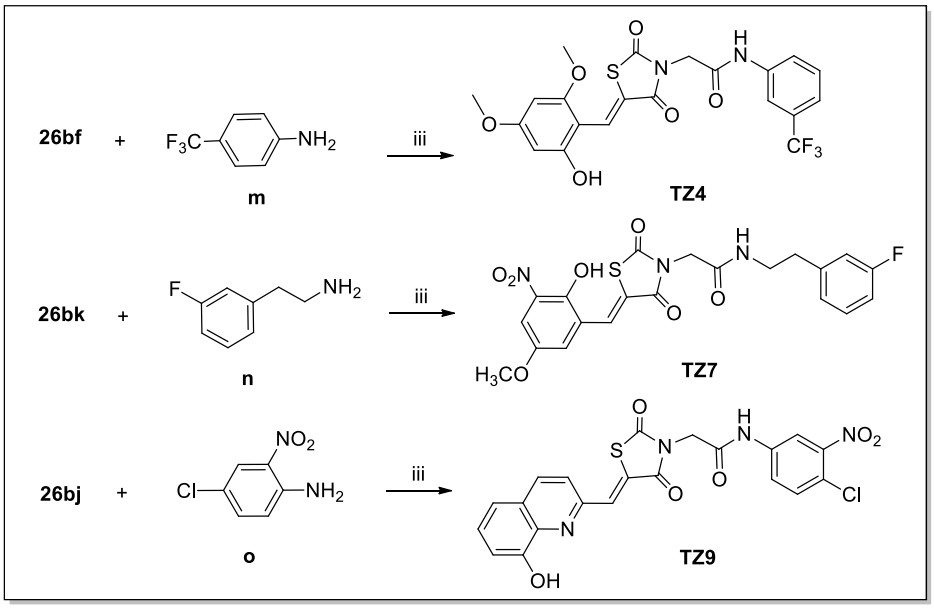

Synthetic scheme 16: iii) HOBt, DIC, DMF, rt, overnight.

26bf, **26bk** or **26bj** (1.0 equiv), amines **m-o** (2.0 equiv.), HOBt (1.0 equiv), and DIC (1.5 equiv) were dissolved in DCM (4 mL) (**Scheme 18**). [246] The resulting mixture was stirred overnight at room temperature and the reaction was monitored by TLC. After completion, the reaction mixture was extracted with AcOEt (3 x 20mL), and the organic phase was dried over Na_2SO_4 and then evaporated under vacuum to give the desired products **TZ4**, **TZ7**, and **TZ9**. HPLC purification was performed by semi-preparative reversed-phase HPLC (Fusion-RP® C18 reversed-

phase column, using the gradient conditions reported below) and the final products were characterized by ESI-MS and NMR spectra.

2-[5-(2-hydroxy-4,6-dimethoxy-benzylidene)-2,4-dioxothiazolidin-3-yl]-N-(3 trifluoromethyl-phenyl)-acetamide (TZ-4)

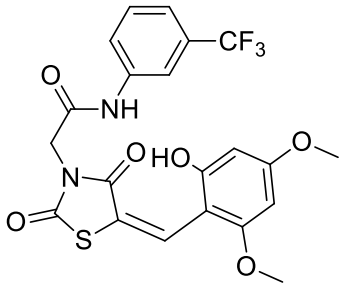

Compound **TZ4** was obtained by following the general procedure (**M**), from the reaction between **26bf** and 4-(trifluoromethyl)aniline (**m**), as a pale yellow solid (48.6 mg, 24% yield after HPLC purification); RP-HPLC t_R = 24.1 min, gradient condition: from 5% B to 100 % B over 50 min, flow rate of 4 mL/min, λ = 240 nm. ^{1}H NMR (400 MHz, CD_3OD): δ_H = 8.66 (s, 1H), 8.00-7.87 (m, 2H), 7.63 (t, *J* = 7.7Hz, 1H), 7.53-7.45 (m, 1H), 6.63 (s, 1H), 6.58 (s, 1H), 5.47 (s, 2H), 3.99 (s, 3H), 3.95 (s, 3H). ^{13}C NMR (100 MHz, CD_3OD): δ = 174.9, 172.7, 172.1, 168.5, 167.3, 152.1, 137.5, 136.8, 134.3, 132.5, 131.7, 129.2, 128.6, 120.0, 116.8, 112.2, 103.0, 99.4, 54.1, 51.3, 33.0. ESI-MS: calculated for $C_{21}H_{17}F_3N_2O_6S$ 482.08; found m/z = 505.4 $[M+Na]^+$.

_N_-[2-(3-fluoro-phenyl)-ethyl]-2-[5-(2-hydroxy-5-methoxy-3-nitro-benzylidene)-2,4-dioxo-thiazolidin-3-yl]-acetamide (TZ-7)

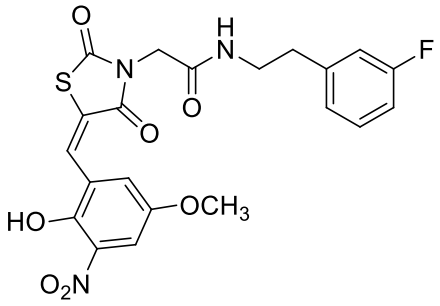

Compound **TZ7** was obtained by following the general procedure (**M**), from the reaction between **26bk** and 3-fluorophenethylamine (**n**), as a pale-yellow solid (122.0 mg, 60% yield after HPLC purification); RP-HPLC t_R = 35.9 min, gradient condition: from 5% B to 100 % B over 50 min, flow rate of 4mL/min, λ = 240nm. ^{1}H NMR (400 MHz, $CDCl_3$): δ_H = 7.87 (s, 1H), 7.77 (s, 1H), 7.32 (s, 1H), 6.98-6.84 (m, 4H), 3.94 (s, 3H), 3.70-3.64 (m, 2H), 3.43 (s, 2H) 2.89 (q, *J* = 6.8 Hz, 2H). ESI-MS: calculated for $C_{21}H_{18}FN_3O_7S$ 475.45; found m/z = 476.50 $[M+H]^+$.

_N_-(4-chloro-3-nitro-phenyl)-2-[5-(8-hydroxy-quinolin-2-ylmethylene)-2,4-dioxo-thiazolidin-3-yl]-acetamide (TZ-9)

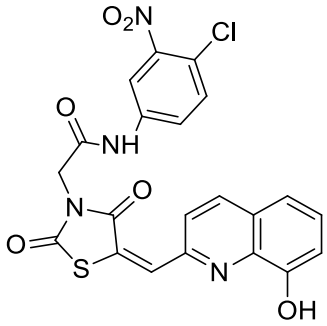

Compound **TZ9** was obtained by following the general procedure (**M**), from the reaction between **26bj** and 4-chloro-2-nitroaniline (**o**), as a yellow solid (116.1 mg, 72% yield after HPLC purification); RP-HPLC t_R = 23.6 min, gradient condition: from 5% B to 100 % B over 50 min, flow rate of 4 mL/min, λ = 240 nm. ^{1}H NMR (400 MHz, $CDCl_3$): δ_H = 8.23 (s, 1H), 8.19-8.06 (m, 1H), 7.81 (d, *J* = 8.6 Hz, 1H), 7.62 (d, *J* = 8.6 Hz, 1H), 7.22-7.14 (m, 4H), 6.81 (d, *J* = 8.6 Hz, 1H), 3.84 (s, 2H). ESI-MS, calcd for $C_{21}H_{13}ClN_4O_6S$ 484.02; found m/z = 507.20 $[M+Na]^+$.

References

1. Naidu, S. D.; Dinkova-Kostova, A. T., Regulation of the mammalian heat shock factor 1. *The FEBS journal* **2017,** *284* (11), 1606-1627.
2. Baudisch, W., Balbiani ring pattern and biochemical activities in the salivary gland of Acricotopus lucidus (Chironomidae). In *Biochemical Differentiation in Insect Glands*, Springer: 1977; pp 197-212.
3. Ritossa, F. M.; Von Borstel, R. C., Chromosome puffs in Drosophila induced by ribonuclease. *Science* **1964,** *145* (3631), 513-514.
4. Tissiéres, A.; Mitchell, H. K.; Tracy, U. M., Protein synthesis in salivary glands of Drosophila melanogaster: relation to chromosome puffs. *Journal of molecular biology* **1974,** *84* (3), 389-398.
5. Ritossa, F., Discovery of the heat shock response. *Cell stress & chaperones* **1996,** *1* (2), 97.
6. Richter, K.; Haslbeck, M.; Buchner, J., The heat shock response: life on the verge of death. *Molecular cell* **2010,** *40* (2), 253-266.
7. Nakai, A.; Tanabe, M.; Kawazoe, Y.; Inazawa, J.; Morimoto, R. I.; Nagata, K., HSF4, a new member of the human heat shock factor family which lacks properties of a transcriptional activator. *Molecular and cellular biology* **1997,** *17* (1), 469-481.
8. Schuetz, T. J.; Gallo, G. J.; Sheldon, L.; Tempst, P.; Kingston, R. E., Isolation of a cDNA for HSF2: evidence for two heat shock factor genes in humans. *Proceedings of the National Academy of Sciences* **1991,** *88* (16), 6911-6915.
9. Nakai, A.; Kawazoe, Y.; Tanabe, M.; Nagata, K.; Morimoto, R. I., The DNA-binding properties of two heat shock factors, HSF1 and HSF3, are induced in the avian erythroblast cell line HD6. *Molecular and cellular biology* **1995,** *15* (10), 5268-5278.
10. Pirkkala, L.; Alastalo, T.-P.; NykäNen, P. I.; Seppä, L.; Sistonen, L. E. A., Differentiation lineage-specific expression of human heat shock transcription factor 2. *The FASEB journal* **1999,** *13* (9), 1089-1098.
11. Alastalo, T.-P.; Hellesuo, M.; Sandqvist, A.; Hietakangas, V.; Kallio, M.; Sistonen, L., Formation of nuclear stress granules involves HSF2 and coincides with the nucleolar localization of Hsp70. *Journal of cell science* **2003,** *116* (17), 3557-3570.
12. Mathew, A.; Mathur, S. K.; Morimoto, R. I., Heat shock response and protein degradation: regulation of HSF2 by the ubiquitin-proteasome pathway. *Molecular and Cellular Biology* **1998,** *18* (9), 5091-5098.
13. Nakai, A.; Ishikawa, T., A nuclear localization signal is essential for stress-induced dimer-to-trimer transition of heat shock transcription factor 3. *Journal of Biological Chemistry* **2000,** *275* (44), 34665-34671.
14. Tanabe, M.; Nakai, A.; Kawazoe, Y.; Nagata, K., Different thresholds in the responses of two heat shock transcription factors, HSF1 and HSF3. *Journal of Biological Chemistry* **1997,** *272* (24), 15389-15395.
15. Prakasam, R.; Fujimoto, M.; Takii, R.; Hayashida, N.; Takaki, E.; Tan, K.; Wu, F.; Inouye, S.; Nakai, A., Chicken IL-6 is a heat-shock gene. *FEBS letters* **2013,** *587* (21), 3541-3547.
16. Rabindran, S. K.; Haroun, R. I.; Clos, J.; Wisniewski, J.; Wu, C., Regulation of heat shock factor trimer formation: role of a conserved leucine zipper. *Science* **1993,** *259* (5092), 230-234.
17. Shi, Y.; Mosser, D. D.; Morimoto, R. I., Molecularchaperones as HSF1-specific transcriptional repressors. *Genes & development* **1998,** *12* (5), 654-666.
18. Ali, A.; Bharadwaj, S.; O'Carroll, R.; Ovsenek, N., HSP90 interacts with and regulates the activity of heat shock factor 1 in Xenopus oocytes. *Molecular and cellular biology* **1998,** *18* (9), 4949-4960.
19. Neef, D. W.; Jaeger, A. M.; Gomez-Pastor, R.; Willmund, F.; Frydman, J.; Thiele, D. J., A direct regulatory interaction between chaperonin TRiC and stress-responsive transcription factor HSF1. *Cell reports* **2014,** *9* (3), 955-966.
20. Trinklein, N. D.; Murray, J. I.; Hartman, S. J.; Botstein, D.; Myers, R. M., The role of heat shock transcription factor 1 in the genome-wide regulation of the mammalian heat shock response. *Molecular biology of the cell* **2004,** *15* (3), 1254-1261.
21. Jaeger, A. M.; Makley, L. N.; Gestwicki, J. E.; Thiele, D. J., Genomic heat shock element sequences drive cooperative human heat shock factor 1 DNA binding and selectivity. *Journal of Biological Chemistry* **2014,** *289* (44), 30459-30469.
22. Biamonti, G.; Vourc'h, C., Nuclear stress bodies. *Cold Spring Harbor perspectives in biology* **2010,** *2* (6), a000695.
23. Biamonti, G., Nuclear stress bodies: a heterochromatin affair? *Nature reviews Molecular cell biology* **2004,** *5* (6), 493-498.
24. Neudegger, T.; Verghese, J.; Hayer-Hartl, M.; Hartl, F. U.; Bracher, A., Structure of human heat-shock transcription factor 1 in complex with DNA. *Nature structural & molecular biology* **2016,** *23* (2), 140.

25. Cicero, M. P.; T. Hubl, S.; Harrison, C. J.; Littlefield, O.; Hardy, J. A.; Nelson, H. C. M., The wing in yeast heat shock transcription factor (HSF) DNA-binding domain is required for full activity. *Nucleic acids research* **2001,** *29* (8), 1715-1723.
26. Peteranderl, R.; Nelson, H. C. M., Trimerization of the heat shock transcription factor by a triple-stranded. alpha.-helical coiled-coil. *Biochemistry* **1992,** *31* (48), 12272-12276.
27. Liu, P. C. C.; Thiele, D. J., Modulation of human heat shock factor trimerization by the linker domain. *Journal of Biological Chemistry* **1999,** *274* (24), 17219-17225.
28. Newton, E. M.; Knauf, U.; Green, M.; Kingston, R. E., The regulatory domain of human heat shock factor 1 is sufficient to sense heat stress. *Molecular and cellular biology* **1996,** *16* (3), 839-846.
29. Brown, S. A.; Weirich, C. S.; Newton, E. M.; Kingston, R. E., Transcriptional activation domains stimulate initiation and elongation at different times and via different residues. *The EMBO journal* **1998,** *17* (11), 3146-3154.
30. Sullivan, E. K.; Weirich, C. S.; Guyon, J. R.; Sif, S. d.; Kingston, R. E., Transcriptional activation domains of human heat shock factor 1 recruit human SWI/SNF. *Molecular and cellular biology* **2001,** *21* (17), 5826-5837.
31. Asano, Y.; Kawase, T.; Okabe, A.; Tsutsumi, S.; Ichikawa, H.; Tatebe, S.; Kitabayashi, I.; Tashiro, F.; Namiki, H.; Kondo, T., IER5 generates a novel hypo-phosphorylated active form of HSF1 and contributes to tumorigenesis. *Scientific reports* **2016,** *6*, 19174.
32. Olsen, J. V.; Vermeulen, M.; Santamaria, A.; Kumar, C.; Miller, M. L.; Jensen, L. J.; Gnad, F.; Cox, J.; Jensen, T. S.; Nigg, E. A., Quantitative phosphoproteomics reveals widespread full phosphorylation site occupancy during mitosis. *Science signaling* **2010,** *3* (104), ra3-ra3.
33. Soncin, F.; Zhang, X.; Chu, B.; Wang, X.; Asea, A.; Stevenson, M. A.; Sacks, D. B.; Calderwood, S. K., Transcriptional activity and DNA binding of heat shock factor-1 involve phosphorylation on threonine 142 by CK2. *Biochemical and biophysical research communications* **2003,** *303* (2), 700-706.
34. Calderwood, S. K.; Wang, Y.; Xie, X.; Khaleque, M. A.; Chou, S. D.; Murshid, A.; Prince, T.; Zhang, Y., Signal transduction pathways leading to heat shock transcription. *Signal transduction insights* **2010,** *2*, STI-S3994.
35. Lee, Y.-J.; Kim, E.-H.; Lee, J. S.; Jeoung, D.; Bae, S.; Kwon, S. H.; Lee, Y.-S., HSF1 as a mitotic regulator: phosphorylation of HSF1 by Plk1 is essential for mitotic progression. *Cancer research* **2008,** *68* (18), 7550-7560.
36. Holmberg, C. I.; Hietakangas, V.; Mikhailov, A.; Rantanen, J. O.; Kallio, M.; Meinander, A.; Hellman, J.; Morrice, N.; MacKintosh, C.; Morimoto, R. I., Phosphorylation of serine 230 promotes inducible transcriptional activity of heat shock factor 1. *The EMBO journal* **2001,** *20* (14), 3800-3810.
37. Budzyński, M. A.; Puustinen, M. C.; Joutsen, J.; Sistonen, L., Uncoupling stress-inducible phosphorylation of heat shock factor 1 from its activation. *Molecular and cellular biology* **2015,** *35* (14), 2530-2540.
38. Hietakangas, V.; Ahlskog, J. K.; Jakobsson, A. M.; Hellesuo, M.; Sahlberg, N. M.; Holmberg, C. I.; Mikhailov, A.; Palvimo, J. J.; Pirkkala, L.; Sistonen, L., Phosphorylation of serine 303 is a prerequisite for the stress-inducible SUMO modification of heat shock factor 1. *Molecular and cellular biology* **2003,** *23* (8), 2953-2968.
39. Guettouche, T.; Boellmann, F.; Lane, W. S.; Voellmy, R., Analysis of phosphorylation of human heat shock factor 1 in cells experiencing a stress. *BMC biochemistry* **2005,** *6* (1), 4.
40. Murshid, A.; Chou, S.-D.; Prince, T.; Zhang, Y.; Bharti, A.; Calderwood, S. K., Protein kinase A binds and activates heat shock factor 1. *PloS one* **2010,** *5* (11), e13830.
41. Sourbier, C.; Scroggins, B. T.; Ratnayake, R.; Prince, T. L.; Lee, S.; Lee, M.-J.; Nagy, P. L.; Lee, Y. H.; Trepel, J. B.; Beutler, J. A., Englerin A stimulates PKCθ to inhibit insulin signaling and to simultaneously activate HSF1: pharmacologically induced synthetic lethality. *Cancer cell* **2013,** *23* (2), 228-237.
42. Chu, B.; Zhong, R.; Soncin, F.; Stevenson, M. A.; Calderwood, S. K., Transcriptional Activity of Heat Shock Factor 1 at 37 oC Is Repressed through Phosphorylation on Two Distinct Serine Residues by Glycogen Synthase Kinase 3α and Protein Kinases Cα and Cζ. *Journal of Biological Chemistry* **1998,** *273* (29), 18640-18646.
43. Zelin, E.; Freeman, B. C., Lysine deacetylases regulate the heat shock response including the age-associated impairment of HSF1. *Journal of molecular biology* **2015,** *427* (7), 1644-1654.
44. Westerheide, S. D.; Anckar, J.; Stevens, S. M.; Sistonen, L.; Morimoto, R. I., Stress-inducible regulation of heat shock factor 1 by the deacetylase SIRT1. *Science* **2009,** *323* (5917), 1063-1066.

45. Raychaudhuri, S.; Loew, C.; Körner, R.; Pinkert, S.; Theis, M.; Hayer-Hartl, M.; Buchholz, F.; Hartl, F. U., Interplay of acetyltransferase EP300 and the proteasome system in regulating heat shock transcription factor 1. *Cell* **2014,** *156* (5), 975-985.
46. Hendriks, I. A.; Lyon, D.; Young, C.; Jensen, L. J.; Vertegaal, A. C. O.; Nielsen, M. L., Site-specific mapping of the human SUMO proteome reveals co-modification with phosphorylation. *Nature structural & molecular biology* **2017,** *24* (3), 325.
47. Kline, M. P.; Morimoto, R. I., Repression of the heat shock factor 1 transcriptional activation domain is modulated by constitutive phosphorylation. *Molecular and cellular biology* **1997,** *17* (4), 2107-2115.
48. Wang, X.; Grammatikakis, N.; Siganou, A.; Calderwood, S. K., Regulation of molecular chaperone gene transcription involves the serine phosphorylation, 14-3-3ε binding, and cytoplasmic sequestration of heat shock factor 1. *Molecular and cellular biology* **2003,** *23* (17), 6013-6026.
49. Hay, R. T., SUMO: a history of modification. *Molecular cell* **2005,** *18* (1), 1-12.
50. Geiss-Friedlander, R.; Melchior, F., Concepts in sumoylation: a decade on. *Nature reviews Molecular cell biology* **2007,** *8* (12), 947-956.
51. Hietakangas, V.; Anckar, J.; Blomster, H. A.; Fujimoto, M.; Palvimo, J. J.; Nakai, A.; Sistonen, L., PDSM, a motif for phosphorylation-dependent SUMO modification. *Proceedings of the National Academy of Sciences* **2006,** *103* (1), 45-50.
52. Anckar, J.; Sistonen, L., SUMO: getting it on. Portland Press Ltd.: 2007.
53. Vujanac, M.; Fenaroli, A.; Zimarino, V., Constitutive Nuclear Import and Stress-Regulated Nucleocytoplasmic Shuttling of Mammalian Heat-Shock Factor 1. *Traffic* **2005,** *6* (3), 214-229.
54. Mendillo, M. L.; Santagata, S.; Koeva, M.; Bell, G. W.; Hu, R.; Tamimi, R. M.; Fraenkel, E.; Ince, T. A.; Whitesell, L.; Lindquist, S., HSF1 drives a transcriptional program distinct from heat shock to support highly malignant human cancers. *Cell* **2012,** *150* (3), 549-562.
55. Santagata, S.; Mendillo, M. L.; Tang, Y.-c.; Subramanian, A.; Perley, C. C.; Roche, S. P.; Wong, B.; Narayan, R.; Kwon, H.; Koeva, M., Tight coordination of protein translation and HSF1 activation supports the anabolic malignant state. *Science* **2013,** *341* (6143), 1238303.
56. Li, D.; Marchenko, N. D.; Schulz, R.; Fischer, V.; Velasco-Hernandez, T.; Talos, F.; Moll, U. M., Functional inactivation of endogenous MDM2 and CHIP by HSP90 causes aberrant stabilization of mutant p53 in human cancer cells. *Molecular Cancer Research* **2011,** *9* (5), 577-588.
57. Moses, M. A.; Kim, Y. S.; Rivera-Marquez, G. M.; Oshima, N.; Watson, M. J.; Beebe, K. E.; Wells, C.; Lee, S.; Zuehlke, A. D.; Shao, H., Targeting the Hsp40/Hsp70 chaperone axis as a novel strategy to treat castration-resistant prostate cancer. *Cancer research* **2018,** *78* (14), 4022-4035.
58. Wang, X.; Zhang, D.; Cao, M.; Ba, J.; Wu, B.; Liu, T.; Nie, C., A study on the biological function of heat shock factor 1 proteins in breast cancer. *Oncology letters* **2018,** *16* (3), 3821-3825.
59. Fujimoto, M.; Takii, R.; Takaki, E.; Katiyar, A.; Nakato, R.; Shirahige, K.; Nakai, A., The HSF1–PARP13–PARP1 complex facilitates DNA repair and promotes mammary tumorigenesis. *Nature communications* **2017,** *8* (1), 1-16.
60. Björk, J. K.; Ahonen, I.; Mirtti, T.; Erickson, A.; Rannikko, A.; Bützow, A.; Nordling, S.; Lundin, J.; Lundin, M.; Sistonen, L., Increased HSF1 expression predicts shorter disease-specific survival of prostate cancer patients following radical prostatectomy. *Oncotarget* **2018,** *9* (58), 31200.
61. Fok, J. H. L.; Hedayat, S.; Zhang, L.; Aronson, L. I.; Mirabella, F.; Pawlyn, C.; Bright, M. D.; Wardell, C. P.; Keats, J. J.; De Billy, E., HSF1 is essential for myeloma cell survival and a promising therapeutic target. *Clinical Cancer Research* **2018,** *24* (10), 2395-2407.
62. Desai, S.; Liu, Z.; Yao, J.; Patel, N.; Chen, J.; Wu, Y.; Ahn, E. E.-Y.; Fodstad, O.; Tan, M., Heat shock factor 1 (HSF1) controls chemoresistance and autophagy through transcriptional regulation of autophagy-related protein 7 (ATG7). *Journal of Biological Chemistry* **2013,** *288* (13), 9165-9176.
63. Schilling, D.; Kühnel, A.; Konrad, S.; Tetzlaff, F.; Bayer, C.; Yaglom, J.; Multhoff, G., Sensitizing tumor cells to radiation by targeting the heat shock response. *Cancer letters* **2015,** *360* (2), 294-301.
64. Chuma, M.; Sakamoto, N.; Nakai, A.; Hige, S.; Nakanishi, M.; Natsuizaka, M.; Suda, G.; Sho, T.; Hatanaka, K.; Matsuno, Y., Heat shock factor 1 accelerates hepatocellular carcinoma development by activating nuclear factor-κB/mitogen-activated protein kinase. *Carcinogenesis* **2014,** *35* (2), 272-281.
65. Santagata, S.; Hu, R.; Lin, N. U.; Mendillo, M. L.; Collins, L. C.; Hankinson, S. E.; Schnitt, S. J.; Whitesell, L.; Tamimi, R. M.; Lindquist, S., High levels of nuclear heat-shock factor 1 (HSF1) are associated with poor prognosis in breast cancer. *Proceedings of the National Academy of Sciences* **2011,** *108* (45), 18378-18383.
66. Engerud, H.; Tangen, I. L.; Berg, A.; Kusonmano, K.; Halle, M. K.; Øyan, A. M.; Kalland, K. H.; Stefansson, I.; Trovik, J.; Salvesen, H. B., High level of HSF1 associates with aggressive endometrial carcinoma and suggests potential for HSP90 inhibitors. *British journal of cancer* **2014,** *111* (1), 78-84.

67. Ishiwata, J.; Kasamatsu, A.; Sakuma, K.; Iyoda, M.; Yamatoji, M.; Usukura, K.; Ishige, S.; Shimizu, T.; Yamano, Y.; Ogawara, K., State of heat shock factor 1 expression as a putative diagnostic marker for oral squamous cell carcinoma. *International journal of oncology* **2012,** *40* (1), 47-52.
68. Hoang, A. T.; Huang, J.; Rudra-Ganguly, N.; Zheng, J.; Powell, W. C.; Rabindran, S. K.; Wu, C.; Roy-Burman, P., A novel association between the human heat shock transcription factor 1 (HSF1) and prostate adenocarcinoma. *The American journal of pathology* **2000,** *156* (3), 857-864.
69. Cen, H.; Zheng, S.; Fang, Y.-M.; Tang, X.-P.; Dong, Q., Induction of HSF1 expression is associated with sporadic colorectal cancer. *World journal of gastroenterology: WJG* **2004,** *10* (21), 3122.
70. Scherz-Shouval, R.; Santagata, S.; Mendillo, M. L.; Sholl, L. M.; Ben-Aharon, I.; Beck, A. H.; Dias-Santagata, D.; Koeva, M.; Stemmer, S. M.; Whitesell, L., The reprogramming of tumor stroma by HSF1 is a potent enabler of malignancy. *Cell* **2014,** *158* (3), 564-578.
71. El Fatimy, R.; Miozzo, F.; Le Mouël, A.; Abane, R.; Schwendimann, L.; Sabéran-Djoneidi, D.; De Thonel, A.; Massaoudi, I.; Paslaru, L.; Hashimoto-Torii, K., Heat shock factor 2 is a stress-responsive mediator of neuronal migration defects in models of fetal alcohol syndrome. *EMBO molecular medicine* **2014,** *6* (8), 1043-1061.
72. Hooper, P. L.; Durham, H. D.; Török, Z.; Hooper, P. L.; Crul, T.; Vígh, L., The central role of heat shock factor 1 in synaptic fidelity and memory consolidation. *Cell Stress and Chaperones* **2016,** *21* (5), 745-753.
73. Anckar, J.; Sistonen, L., Regulation of HSF1 function in the heat stress response: implications in aging and disease. *Annual review of biochemistry* **2011,** *80*, 1089-1115.
74. Neef, D. W.; Jaeger, A. M.; Thiele, D. J., Heat shock transcription factor 1 as a therapeutic target in neurodegenerative diseases. *Nature reviews Drug discovery* **2011,** *10* (12), 930-944.
75. Havel, L. S.; Li, S.; Li, X.-J., Nuclear accumulation of polyglutamine disease proteins and neuropathology. *Molecular brain* **2009,** *2* (1), 1-7.
76. Auluck, P. K.; Chan, H. Y. E.; Trojanowski, J. Q.; Lee, V. M. Y.; Bonini, N. M., Chaperone suppression of α-synuclein toxicity in a Drosophila model for Parkinson's disease. *Science* **2002,** *295* (5556), 865-868.
77. Mavroudis, I. A.; Fotiou, D. F.; Adipepe, L. F.; Manani, M. G.; Njau, S. D.; Psaroulis, D.; Costa, V. G.; Baloyannis, S. J., Morphological changes of the human purkinje cells and deposition of neuritic plaques and neurofibrillary tangles on the cerebellar cortex of Alzheimer's disease. *American Journal of Alzheimer's Disease & Other Dementias®* **2010,** *25* (7), 585-591.
78. Lin, P.-Y.; Simon, S. M.; Koh, W. K.; Folorunso, O.; Umbaugh, C. S.; Pierce, A., Heat shock factor 1 over-expression protects against exposure of hydrophobic residues on mutant SOD1 and early mortality in a mouse model of amyotrophic lateral sclerosis. *Molecular neurodegeneration* **2013,** *8* (1), 1-17.
79. Yoon, Y. J.; Kim, J. A.; Shin, K. D.; Shin, D.-S.; Han, Y. M.; Lee, Y. J.; Lee, J. S.; Kwon, B.-M.; Han, D. C., KRIBB11 inhibits HSP70 synthesis through inhibition of heat shock factor 1 function by impairing the recruitment of positive transcription elongation factor b to the hsp70 promoter. *Journal of Biological Chemistry* **2011,** *286* (3), 1737-1747.
80. Vilaboa, N.; Boré, A.; Martin-Saavedra, F.; Bayford, M.; Winfield, N.; Firth-Clark, S.; Kirton, S. B.; Voellmy, R., New inhibitor targeting human transcription factor HSF1: effects on the heat shock response and tumor cell survival. *Nucleic acids research* **2017,** *45* (10), 5797-5817.
81. Mallikaratchy, P., Evolution of complex target SELEX to identify aptamers against mammalian cell-surface antigens. *Molecules* **2017,** *22* (2), 215.
82. Salamanca, H. H.; Antonyak, M. A.; Cerione, R. A.; Shi, H.; Lis, J. T., Inhibiting heat shock factor 1 in human cancer cells with a potent RNA aptamer. *PloS one* **2014,** *9* (5).
83. Nagai, N.; Nakai, A.; Nagata, K., Quercetin suppresses heat shock response by down-regulation of HSF1. *Biochemical and biophysical research communications* **1995,** *208* (3), 1099-1105.
84. Yang, W.; Cui, M.; Lee, J.; Gong, W.; Wang, S.; Fu, J.; Wu, G.; Yan, K., Heat shock protein inhibitor, quercetin, as a novel adjuvant agent to improve radiofrequency ablation-induced tumor destruction and its molecular mechanism. *Chinese Journal of Cancer Research* **2016,** *28* (1), 19.
85. Westerheide, S. D.; Kawahara, T. L. A.; Orton, K.; Morimoto, R. I., Triptolide, an inhibitor of the human heat shock response that enhances stress-induced cell death. *Journal of biological chemistry* **2006,** *281* (14), 9616-9622.
86. Titov, D. V.; Gilman, B.; He, Q.-L.; Bhat, S.; Low, W.-K.; Dang, Y.; Smeaton, M.; Demain, A. L.; Miller, P. S.; Kugel, J. F., XPB, a subunit of TFIIH, is a target of the natural product triptolide. *Nature chemical biology* **2011,** *7* (3), 182.

87. Yoon, T.; Kang, G.-Y.; Han, A.-R.; Seo, E.-K.; Lee, Y.-S., 2, 4-Bis (4-hydroxybenzyl) phenol inhibits heat shock transcription factor 1 and sensitizes lung cancer cells to conventional anticancer modalities. *Journal of natural products* **2014,** *77* (5), 1123-1129.
88. Kim, J. A.; Kim, Y.; Kwon, B.-M.; Han, D. C., The natural compound cantharidin induces cancer cell death through inhibition of heat shock protein 70 (HSP70) and Bcl-2-associated athanogene domain 3 (BAG3) expression by blocking heat shock factor 1 (HSF1) binding to promoters. *Journal of Biological Chemistry* **2013,** *288* (40), 28713-28726.
89. Nikotina, A. D.; Koludarova, L.; Komarova, E. Y.; Mikhaylova, E. R.; Aksenov, N. D.; Suezov, R.; Kartzev, V. G.; Margulis, B. A.; Guzhova, I. V., Discovery and optimization of cardenolides inhibiting HSF1 activation in human colon HCT-116 cancer cells. *Oncotarget* **2018,** *9* (43), 27268.
90. Koishi, M.; Yokota, S. i.; Mae, T.; Nishimura, Y.; Kanamori, S.; Horii, N.; Shibuya, K.; Sasai, K.; Hiraoka, M., The effects of KNK437, a novel inhibitor of heat shock protein synthesis, on the acquisition of thermotolerance in a murine transplantable tumor in vivo. *Clinical cancer research* **2001,** *7* (1), 215-219.
91. Yokota, S.-i.; Kitahara, M.; Nagata, K., Benzylidene lactam compound, KNK437, a novel inhibitor of acquisition of thermotolerance and heat shock protein induction in human colon carcinoma cells. *Cancer research* **2000,** *60* (11), 2942-2948.
92. Zhang, D.; Zhang, B., Selective killing of cancer cells by small molecules targeting heat shock stress response. *Biochemical and biophysical research communications* **2016,** *478* (4), 1509-1514.
93. Zaarur, N.; Gabai, V. L.; Porco, J. A.; Calderwood, S.; Sherman, M. Y., Targeting heat shock response to sensitize cancer cells to proteasome and Hsp90 inhibitors. *Cancer research* **2006,** *66* (3), 1783-1791.
94. Maira, S.-M.; Stauffer, F.; Brueggen, J.; Furet, P.; Schnell, C.; Fritsch, C.; Brachmann, S.; Chene, P.; De Pover, A.; Schoemaker, K., Identification and characterization of NVP-BEZ235, a new orally available dual phosphatidylinositol 3-kinase/mammalian target of rapamycin inhibitor with potent in vivo antitumor activity. *Molecular cancer therapeutics* **2008,** *7* (7), 1851-1863.
95. Sondermann, H.; Scheufler, C.; Schneider, C.; Höhfeld, J.; Hartl, F. U.; Moarefi, I., Structure of a Bag/Hsc70 complex: convergent functional evolution of Hsp70 nucleotide exchange factors. *Science* **2001,** *291* (5508), 1553-1557.
96. Sondermann, H.; Ho, A. K.; Listenberger, L. L.; Siegers, K.; Moarefi, I.; Wente, S. R.; Hartl, F. U.; Young, J. C., Prediction of novel Bag-1 homologs based on structure/function analysis identifies Snl1p as an Hsp70 co-chaperone in Saccharomyces cerevisiae. *Journal of biological chemistry* **2002,** *277* (36), 33220-33227.
97. Colvin, T. A.; Gabai, V. L.; Gong, J.; Calderwood, S. K.; Li, H.; Gummuluru, S.; Matchuk, O. N.; Smirnova, S. G.; Orlova, N. V.; Zamulaeva, I. A., Hsp70–Bag3 interactions regulate cancer-related signaling networks. *Cancer research* **2014,** *74* (17), 4731-4740.
98. Salah, Z.; Alian, A.; Aqeilan, R. I., WW domain-containing proteins: retrospectives and the future. *Front Biosci* **2012,** *17*, 331-348.
99. Bimston, D.; Song, J.; Winchester, D.; Takayama, S.; Reed, J. C.; Morimoto, R. I., BAG-1, a negative regulator of Hsp70 chaperone activity, uncouples nucleotide hydrolysis from substrate release. *The EMBO Journal* **1998,** *17* (23), 6871-6878.
100. Lüders, J.; Demand, J.; Höhfeld, J., The ubiquitin-related BAG-1 provides a link between the molecular chaperones Hsc70/Hsp70 and the proteasome. *Journal of Biological Chemistry* **2000,** *275* (7), 4613-4617.
101. Arndt, V.; Daniel, C.; Nastainczyk, W.; Alberti, S.; Hohfeld, J., BAG-2 acts as an inhibitor of the chaperone-associated ubiquitin ligase CHIP. *Molecular biology of the cell* **2005,** *16* (12), 5891-5900.
102. Carrettiero, D. C.; Hernandez, I.; Neveu, P.; Papagiannakopoulos, T.; Kosik, K. S., The cochaperone BAG2 sweeps paired helical filament-insoluble tau from the microtubule. *Journal of Neuroscience* **2009,** *29* (7), 2151-2161.
103. Jiang, Y.; Woronicz, J. D.; Liu, W.; Goeddel, D. V., Prevention of constitutive TNF receptor 1 signaling by silencer of death domains. *Science* **1999,** *283* (5401), 543-546.
104. Kalia, S. K.; Lee, S.; Smith, P. D.; Liu, L.; Crocker, S. J.; Thorarinsdottir, T. E.; Glover, J. R.; Fon, E. A.; Park, D. S.; Lozano, A. M., BAG5 inhibits parkin and enhances dopaminergic neuron degeneration. *Neuron* **2004,** *44* (6), 931-945.
105. Desmots, F.; Russell, H. R.; Lee, Y.; Boyd, K.; McKinnon, P. J., The reaper-binding protein scythe modulates apoptosis and proliferation during mammalian development. *Molecular and cellular biology* **2005,** *25* (23), 10329-10337.

106. Desmots, F.; Russell, H. R.; Michel, D.; McKinnon, P. J., Scythe regulates apoptosis-inducing factor stability during endoplasmic reticulum stress-induced apoptosis. *Journal of Biological Chemistry* **2008,** *283* (6), 3264-3271.
107. Corduan, A.; Lecomte, S.; Martin, C.; Michel, D.; Desmots, F., Sequential interplay between BAG6 and HSP70 upon heat shock. *Cellular and molecular life sciences* **2009,** *66* (11-12), 1998-2004.
108. Franceschelli, S.; Rosati, A.; Lerose, R.; De Nicola, S.; Turco, M. C.; Pascale, M., Bag3 gene expression is regulated by heat shock factor 1. *Journal of cellular physiology* **2008,** *215* (3), 575-577.
109. Homma, S.; Iwasaki, M.; Shelton, G. D.; Engvall, E.; Reed, J. C.; Takayama, S., BAG3 deficiency results in fulminant myopathy and early lethality. *The American journal of pathology* **2006,** *169* (3), 761-773.
110. Youn, D.-Y.; Lee, D.-H.; Lim, M.-H.; Yoon, J.-S.; Lim, J. H.; Jung, S. E.; Yeum, C. E.; Park, C. W.; Youn, H.-J.; Lee, J.-S., Bis deficiency results in early lethality with metabolic deterioration and involution of spleen and thymus. *American Journal of Physiology-Endocrinology and Metabolism* **2008,** *295* (6), E1349-E1357.
111. Bruno, A. P.; Festa, M.; Dal Piaz, F.; Rosati, A.; Turco, M. C.; Giuditta, A.; Marzullo, L., Identification of a synaptosome-associated form of BAG3 protein. *Cell Cycle* **2008,** *7* (19), 3104-3105.
112. Gentilella, A.; Khalili, K., BAG3 expression in glioblastoma cells promotes accumulation of ubiquitinated clients in an Hsp70-dependent manner. *Journal of Biological Chemistry* **2011,** *286* (11), 9205-9215.
113. Gamerdinger, M.; Hajieva, P.; Kaya, A. M.; Wolfrum, U.; Hartl, F. U.; Behl, C., Protein quality control during aging involves recruitment of the macroautophagy pathway by BAG3. *The EMBO journal* **2009,** *28* (7), 889-901.
114. Jin, Y.-H.; Ahn, S.-G.; Kim, S.-A., BAG3 affects the nucleocytoplasmic shuttling of HSF1 upon heat stress. *Biochemical and biophysical research communications* **2015,** *464* (2), 561-567.
115. Doong, H.; Vrailas, A.; Kohn, E. C., What's in the 'BAG'?–a functional domain analysis of the BAG-family proteins. *Cancer letters* **2002,** *188* (1-2), 25-32.
116. Carra, S.; Seguin, S. J.; Lambert, H.; Landry, J., HspB8 chaperone activity toward poly (Q)-containing proteins depends on its association with Bag3, a stimulator of macroautophagy. *Journal of Biological Chemistry* **2008,** *283* (3), 1437-1444.
117. Iwasaki, M.; Tanaka, R.; Hishiya, A.; Homma, S.; Reed, J. C.; Takayama, S., BAG3 directly associates with guanine nucleotide exchange factor of Rap1, PDZGEF2, and regulates cell adhesion. *Biochemical and biophysical research communications* **2010,** *400* (3), 413-418.
118. Doong, H.; Price, J.; Kim, Y. S.; Gasbarre, C.; Probst, J.; Liotta, L. A.; Blanchette, J.; Rizzo, K.; Kohn, E., CAIR-1/BAG-3 forms an EGF-regulated ternary complex with phospholipase C-γ and Hsp70/Hsc70. *Oncogene* **2000,** *19* (38), 4385-4395.
119. Virador, V. M.; Davidson, B.; Czechowicz, J.; Mai, A.; Kassis, J.; Kohn, E. C., The anti-apoptotic activity of BAG3 is restricted by caspases and the proteasome. *PLoS One* **2009,** *4* (4).
120. Babu, M. M., The contribution of intrinsically disordered regions to protein function, cellular complexity, and human disease. *Biochemical Society Transactions* **2016,** *44* (5), 1185-1200.
121. Ge, F.; Xiao, C.-L.; Bi, L.-J.; Tao, S.-C.; Xiong, S.; Yin, X.-F.; Li, L.-P.; Lu, C.-H.; Jia, H.-T.; He, Q.-Y., Quantitative phosphoproteomics of proteasome inhibition in multiple myeloma cells. *PLoS One* **2010,** *5* (9).
122. Chen, Y.; Yang, L.-N.; Cheng, L.; Tu, S.; Guo, S.-J.; Le, H.-Y.; Xiong, Q.; Mo, R.; Li, C.-Y.; Jeong, J.-S., Bcl2-associated athanogene 3 interactome analysis reveals a new role in modulating proteasome activity. *Molecular & Cellular Proteomics* **2013,** *12* (10), 2804-2819.
123. Jacobs, A. T.; Marnett, L. J., HSF1-mediated BAG3 expression attenuates apoptosis in 4-hydroxynonenal-treated colon cancer cells via stabilization of anti-apoptotic Bcl-2 proteins. *Journal of Biological Chemistry* **2009,** *284* (14), 9176-9183.
124. Wang, H. Q.; Liu, B. Q.; Gao, Y. Y.; Meng, X.; Guan, Y.; Zhang, H. Y.; Du, Z. X., Inhibition of the JNK signalling pathway enhances proteasome inhibitor-induced apoptosis of kidney cancer cells by suppression of BAG3 expression. *British journal of pharmacology* **2009,** *158* (5), 1405-1412.
125. Ammirante, M.; Rosati, A.; Arra, C.; Basile, A.; Falco, A.; Festa, M.; Pascale, M.; d'Avenia, M.; Marzullo, L.; Belisario, M. A., IKKγ protein is a target of BAG3 regulatory activity in human tumor growth. *Proceedings of the National Academy of Sciences* **2010,** *107* (16), 7497-7502.
126. Rosati, A.; Ammirante, M.; Gentilella, A.; Basile, A.; Festa, M.; Pascale, M.; Marzullo, L.; Belisario, M. A.; Tosco, A.; Franceschelli, S., Apoptosis inhibition in cancer cells: a novel molecular pathway that involves BAG3 protein. *The international journal of biochemistry & cell biology* **2007,** *39* (7-8), 1337-1342.

127. Du, Z.-X.; Meng, X.; Zhang, H.-Y.; Guan, Y.; Wang, H.-Q., Caspase-dependent cleavage of BAG3 in proteasome inhibitors-induced apoptosis in thyroid cancer cells. *Biochemical and biophysical research communications* **2008,** *369* (3), 894-898.
128. Festa, M.; Del Valle, L.; Khalili, K.; Franco, R.; Scognamiglio, G.; Graziano, V.; De Laurenzi, V.; Turco, M. C.; Rosati, A., BAG3 protein is overexpressed in human glioblastoma and is a potential target for therapy. *The American journal of pathology* **2011,** *178* (6), 2504-2512.
129. Behl, C., Breaking BAG: the co-chaperone BAG3 in health and disease. *Trends in pharmacological sciences* **2016,** *37* (8), 672-688.
130. Bukau, B.; Weissman, J.; Horwich, A., Molecular chaperones and protein quality control. *Cell* **2006,** *125* (3), 443-451.
131. Rosati, A.; Graziano, V.; De Laurenzi, V.; Pascale, M.; Turco, M. C., BAG3: a multifaceted protein that regulates major cell pathways. *Cell death & disease* **2011,** *2* (4), e141-e141.
132. Ma, J.; Grant, C. E.; Plagens, R. N.; Barrett, L. N.; Guisbert, K. S. K.; Guisbert, E., Cellular proteomes drive tissue-specific regulation of the heat shock response. *G3: Genes, Genomes, Genetics* **2017,** *7* (3), 1011-1018.
133. Kassis, J. N.; Guancial, E. A.; Doong, H.; Virador, V.; Kohn, E. C., CAIR-1/BAG-3 modulates cell adhesion and migration by downregulating activity of focal adhesion proteins. *Experimental cell research* **2006,** *312* (15), 2962-2971.
134. Iwasaki, M.; Homma, S.; Hishiya, A.; Dolezal, S. J.; Reed, J. C.; Takayama, S., BAG3 regulates motility and adhesion of epithelial cancer cells. *Cancer research* **2007,** *67* (21), 10252-10259.
135. Xiao, H.; Cheng, S.; Tong, R.; Lv, Z.; Ding, C.; Du, C.; Xie, H.; Zhou, L.; Wu, J.; Zheng, S., Bag3 regulates epithelial–mesenchymal transition and angiogenesis in human hepatocellular carcinoma. *Laboratory investigation* **2014,** *94* (3), 252-261.
136. Chiappetta, G.; Ammirante, M.; Basile, A.; Rosati, A.; Festa, M.; Monaco, M.; Vuttariello, E.; Pasquinelli, R.; Arra, C.; Zerilli, M., The antiapoptotic protein BAG3 is expressed in thyroid carcinomas and modulates apoptosis mediated by tumor necrosis factor-related apoptosis-inducing ligand. *The Journal of Clinical Endocrinology & Metabolism* **2007,** *92* (3), 1159-1163.
137. Staibano, S.; Mascolo, M.; Di Benedetto, M.; Vecchione, M. L.; Ilardi, G.; Di Lorenzo, G.; Autorino, R.; Salerno, V.; Morena, A.; Rocco, A., BAG3 protein delocalisation in prostate carcinoma. *Tumor Biology* **2010,** *31* (5), 461-469.
138. Franco, R.; Scognamiglio, G.; Salerno, V.; Sebastiani, A.; Cennamo, G.; Ascierto, P. A.; Botti, G.; Turco, M. C.; Rosati, A., Expression of the anti-apoptotic protein BAG3 in human melanomas. **2012**.
139. Yang, X.; Tian, Z.; Gou, W.-f.; Takahashi, H.; Xing, Y.-n.; Takano, Y.; Zheng, H.-C., Bag-3 expression is involved in pathogenesis and progression of colorectal carcinomas. **2013**.
140. Nymoen, D. A.; Falkenthal, T. E. H.; Holth, A.; Ow, G. S.; Ivshina, A. V.; Tropé, C. G.; Kuznetsov, V. A.; Staff, A. C.; Davidson, B., Expression and clinical role of chemoresponse-associated genes in ovarian serous carcinoma. *Gynecologic oncology* **2015,** *139* (1), 30-39.
141. Chiappetta, G.; Basile, A.; Barbieri, A.; Falco, A.; Rosati, A.; Festa, M.; Pasquinelli, R.; Califano, D.; Palma, G.; Costanzo, R., The anti-apoptotic BAG3 protein is expressed in lung carcinomas and regulates small cell lung carcinoma (SCLC) tumor growth. *Oncotarget* **2014,** *5* (16), 6846.
142. Nourashrafeddin, S.; Aarabi, M.; Modarressi, M. H.; Rahmati, M.; Nouri, M., The evaluation of WBP2NL-related genes expression in breast cancer. *Pathology & Oncology Research* **2015,** *21* (2), 293-300.
143. Esposito, V.; Baldi, C.; Zeppa, P.; Festa, M.; Guerriero, L.; d'Avenia, M.; Chetta, M.; Zullo, F.; De Laurenzi, V.; Turco, M. C., BAG3 protein is over-expressed in endometrioid endometrial adenocarcinomas. *Journal of cellular physiology* **2017,** *232* (2), 309-311.
144. Rosati, A.; Basile, A.; Falco, A.; d'Avenia, M.; Festa, M.; Graziano, V.; De Laurenzi, V.; Arra, C.; Pascale, M.; Turco, M. C., Role of BAG3 protein in leukemia cell survival and response to therapy. *Biochimica et Biophysica Acta (BBA)-Reviews on Cancer* **2012,** *1826* (2), 365-369.
145. Li, X.; Colvin, T.; Rauch, J. N.; Acosta-Alvear, D.; Kampmann, M.; Dunyak, B.; Hann, B.; Aftab, B. T.; Murnane, M.; Cho, M., Validation of the Hsp70–Bag3 protein–protein interaction as a potential therapeutic target in cancer. *Molecular cancer therapeutics* **2015,** *14* (3), 642-648.
146. Terracciano, S.; Lauro, G.; Russo, A.; Vaccaro, M. C.; Vassallo, A.; De Marco, M.; Ranieri, B.; Rosati, A.; Turco, M. C.; Riccio, R., Discovery and synthesis of the first selective BAG domain modulator of BAG3 as an attractive candidate for the development of a new class of chemotherapeutics. *Chemical Communications* **2018,** *54* (55), 7613-7616.
147. Funk, C. D., Prostaglandins and leukotrienes: advances in eicosanoid biology. *science* **2001,** *294* (5548), 1871-1875.

148. Dennis, E. A.; Norris, P. C., Eicosanoid storm in infection and inflammation. *Nature Reviews Immunology* **2015,** *15* (8), 511-523.
149. Nakanishi, M.; Rosenberg, D. W. In *Multifaceted roles of PGE 2 in inflammation and cancer*, 2013; Springer: pp 123-137.
150. Montrose, D. C.; Nakanishi, M.; Murphy, R. C.; Zarini, S.; McAleer, J. P.; Vella, A. T.; Rosenberg, D. W., The role of PGE2 in intestinal inflammation and tumorigenesis. *Prostaglandins & other lipid mediators* **2015,** *116*, 26-36.
151. Kawahara, K.; Hohjoh, H.; Inazumi, T.; Tsuchiya, S.; Sugimoto, Y., Prostaglandin E2-induced inflammation: Relevance of prostaglandin E receptors. *Biochimica et Biophysica Acta (BBA)-Molecular and Cell Biology of Lipids* **2015,** *1851* (4), 414-421.
152. Tang, X.; Edwards, E. M.; Holmes, B. B.; Falck, J. R.; Campbell, W. B., Role of phospholipase C and diacylglyceride lipase pathway in arachidonic acid release and acetylcholine-induced vascular relaxation in rabbit aorta. *American Journal of Physiology-Heart and Circulatory Physiology* **2006,** *290* (1), H37-H45.
153. Bell, R. L.; Kennerly, D. A.; Stanford, N.; Majerus, P. W., Diglyceride lipase: a pathway for arachidonate release from human platelets. *Proceedings of the National Academy of Sciences* **1979,** *76* (7), 3238-3241.
154. Park, J. Y.; Pillinger, M. H.; Abramson, S. B., Prostaglandin E2 synthesis and secretion: the role of PGE2 synthases. *Clinical immunology* **2006,** *119* (3), 229-240.
155. Tanioka, T.; Nakatani, Y.; Semmyo, N.; Murakami, M.; Kudo, I., Molecular identification of cytosolic prostaglandin E2 synthase that is functionally coupled with cyclooxygenase-1 in immediate prostaglandin E2biosynthesis. *Journal of Biological Chemistry* **2000,** *275* (42), 32775-32782.
156. Hara, S.; Kamei, D.; Sasaki, Y.; Tanemoto, A.; Nakatani, Y.; Murakami, M., Prostaglandin E synthases: understanding their pathophysiological roles through mouse genetic models. *Biochimie* **2010,** *92* (6), 651-659.
157. Koeberle, A.; Werz, O., Perspective of microsomal prostaglandin E2 synthase-1 as drug target in inflammation-related disorders. *Biochemical pharmacology* **2015,** *98* (1), 1-15.
158. Murakami, M.; Nakashima, K.; Kamei, D.; Masuda, S.; Ishikawa, Y.; Ishii, T.; Ohmiya, Y.; Watanabe, K.; Kudo, I., Cellular prostaglandin E2 production by membrane-bound prostaglandin E synthase-2 via both cyclooxygenases-1 and-2. *Journal of Biological Chemistry* **2003,** *278* (39), 37937-37947.
159. Tanikawa, N.; Ohmiya, Y.; Ohkubo, H.; Hashimoto, K.; Kangawa, K.; Kojima, M.; Ito, S.; Watanabe, K., Identification and characterization of a novel type of membrane-associated prostaglandin E synthase. *Biochemical and biophysical research communications* **2002,** *291* (4), 884-889.
160. Wallace, J. L., Prostaglandian biology in inflammatory bowel disease. *Gastroenterology Clinics* **2001,** *30* (4), 971-980.
161. Levy, B. D.; Clish, C. B.; Schmidt, B.; Gronert, K.; Serhan, C. N., Lipid mediator class switching during acute inflammation: signals in resolution. *Nature immunology* **2001,** *2* (7), 612-619.
162. Mancini, A. D.; Di Battista, J. A., The cardinal role of the phospholipase A 2/cyclooxygenase-2/prostaglandin E synthase/prostaglandin E 2 (PCPP) axis in inflammostasis. *Inflammation Research* **2011,** *60* (12), 1083-1092.
163. Forsberg, L.; Leeb, L.; Thorén, S.; Morgenstern, R.; Jakobsson, P.-J., Human glutathione dependent prostaglandin E synthase: gene structure and regulation. *FEBS letters* **2000,** *471* (1), 78-82.
164. Samuelsson, B.; Morgenstern, R.; Jakobsson, P.-J., Membrane prostaglandin E synthase-1: a novel therapeutic target. *Pharmacological reviews* **2007,** *59* (3), 207-224.
165. Rådmark, O.; Samuelsson, B., Microsomal prostaglandin E synthase-1 and 5-lipoxygenase: potential drug targets in cancer. *Journal of internal medicine* **2010,** *268* (1), 5-14.
166. Jegerschöld, C.; Pawelzik, S.-C.; Purhonen, P.; Bhakat, P.; Gheorghe, K. R.; Gyobu, N.; Mitsuoka, K.; Morgenstern, R.; Jakobsson, P.-J.; Hebert, H., Structural basis for induced formation of the inflammatory mediator prostaglandin E2. *Proceedings of the National Academy of Sciences* **2008,** *105* (32), 11110-11115.
167. Jakobsson, P.-J.; Thorén, S.; Morgenstern, R.; Samuelsson, B., Identification of human prostaglandin E synthase: a microsomal, glutathione-dependent, inducible enzyme, constituting a potential novel drug target. *Proceedings of the National Academy of Sciences* **1999,** *96* (13), 7220-7225.
168. Sjögren, T.; Nord, J.; Ek, M.; Johansson, P.; Liu, G.; Geschwindner, S., Crystal structure of microsomal prostaglandin E2 synthase provides insight into diversity in the MAPEG superfamily. *Proceedings of the National Academy of Sciences* **2013,** *110* (10), 3806-3811.
169. Schiffler, M. A.; Antonysamy, S.; Bhattachar, S. N.; Campanale, K. M.; Chandrasekhar, S.; Condon, B.; Desai, P. V.; Fisher, M. J.; Groshong, C.; Harvey, A., Discovery and characterization of 2-acylaminoimidazole microsomal prostaglandin E synthase-1 inhibitors. *Journal of medicinal chemistry* **2016,** *59* (1), 194-205.

170. Li, D.; Howe, N.; Dukkipati, A.; Shah, S. T. A.; Bax, B. D.; Edge, C.; Bridges, A.; Hardwicke, P.; Singh, O. M. P.; Giblin, G., Crystallizing membrane proteins in the lipidic mesophase. Experience with human prostaglandin E2 synthase 1 and an evolving strategy. *Crystal growth & design* **2014,** *14* (4), 2034-2047.
171. Hamza, A.; AbdulHameed, M. D. M.; Zhan, C.-G., Understanding microscopic binding of human microsomal prostaglandin E synthase-1 with substrates and inhibitors by molecular modeling and dynamics simulation. *The Journal of Physical Chemistry B* **2008,** *112* (24), 7320-7329.
172. Pawelzik, S.-C.; Uda, N. R.; Spahiu, L.; Jegerschöld, C.; Stenberg, P.; Hebert, H.; Morgenstern, R.; Jakobsson, P.-J., Identification of key residues determining species differences in inhibitor binding of microsomal prostaglandin E synthase-1. *Journal of Biological Chemistry* **2010,** *285* (38), 29254-29261.
173. Prage, E. B.; Pawelzik, S.-C.; Busenlehner, L. S.; Kim, K.; Morgenstern, R.; Jakobsson, P.-J.; Armstrong, R. N., Location of inhibitor binding sites in the human inducible prostaglandin E synthase, MPGES1. *Biochemistry* **2011,** *50* (35), 7684-7693.
174. Luz, J. G.; Antonysamy, S.; Kuklish, S. L.; Condon, B.; Lee, M. R.; Allison, D.; Yu, X.-P.; Chandrasekhar, S.; Backer, R.; Zhang, A., Crystal structures of mPGES-1 inhibitor complexes form a basis for the rational design of potent analgesic and anti-inflammatory therapeutics. *Journal of medicinal chemistry* **2015,** *58* (11), 4727-4737.
175. Cheng, Y.; Austin, S. C.; Rocca, B.; Koller, B. H.; Coffman, T. M.; Grosser, T.; Lawson, J. A.; FitzGerald, G. A., Role of prostacyclin in the cardiovascular response to thromboxane A2. *Science* **2002,** *296* (5567), 539-541.
176. Hanaka, H.; Pawelzik, S.-C.; Johnsen, J. I.; Rakonjac, M.; Terawaki, K.; Rasmuson, A.; Sveinbjörnsson, B.; Schumacher, M. C.; Hamberg, M.; Samuelsson, B., Microsomal prostaglandin E synthase 1 determines tumor growth in vivo of prostate and lung cancer cells. *Proceedings of the National Academy of Sciences* **2009,** *106* (44), 18757-18762.
177. Gudis, K.; Tatsuguchi, A.; Wada, K.; Hiratsuka, T.; Futagami, S.; Fukuda, Y.; Kiyama, T.; Tajiri, T.; Miyake, K.; Sakamoto, C., Clinical significance of prostaglandin E synthase expression in gastric cancer tissue. *Human pathology* **2007,** *38* (12), 1826-1835.
178. Hasan, S.; Satake, M.; Dawson, D. W.; Funahashi, H.; Angst, E.; Go, V. L. W.; Reber, H. A.; Hines, O. J.; Eibl, G., Expression analysis of the prostaglandin E2 production pathway in human pancreatic cancers. *Pancreas* **2008,** *37* (2), 121-127.
179. Elinav, E.; Nowarski, R.; Thaiss, C. A.; Hu, B.; Jin, C.; Flavell, R. A., Inflammation-induced cancer: crosstalk between tumours, immune cells and microorganisms. *Nature Reviews Cancer* **2013,** *13* (11), 759-771.
180. Virchow, R., An address on the value of pathological experiments. *British medical journal* **1881,** *2* (1075), 198.
181. de Visser, K. E.; Coussens, L. M., The inflammatory tumor microenvironment and its impact on cancer development. In *Infection and Inflammation: Impacts on Oncogenesis*, Karger Publishers: 2006; Vol. 13, pp 118-137.
182. Mantovani, A.; Allavena, P.; Sica, A.; Balkwill, F., Cancer-related inflammation. *nature* **2008,** *454* (7203), 436-444.
183. Porta, C.; Larghi, P.; Rimoldi, M.; Totaro, M. G.; Allavena, P.; Mantovani, A.; Sica, A., Cellular and molecular pathways linking inflammation and cancer. *Immunobiology* **2009,** *214* (9-10), 761-777.
184. Mantovani, A., Inflaming metastasis. *Nature* **2009,** *457* (7225), 36-37.
185. De Marzo, A. M.; Platz, E. A.; Sutcliffe, S.; Xu, J.; Grönberg, H.; Drake, C. G.; Nakai, Y.; Isaacs, W. B.; Nelson, W. G., Inflammation in prostate carcinogenesis. *Nature Reviews Cancer* **2007,** *7* (4), 256-269.
186. Rius, J.; Guma, M.; Schachtrup, C.; Akassoglou, K.; Zinkernagel, A. S.; Nizet, V.; Johnson, R. S.; Haddad, G. G.; Karin, M., NF-κB links innate immunity to the hypoxic response through transcriptional regulation of HIF-1α. *Nature* **2008,** *453* (7196), 807-811.
187. Yu, H.; Kortylewski, M.; Pardoll, D., Crosstalk between cancer and immune cells: role of STAT3 in the tumour microenvironment. *Nature Reviews Immunology* **2007,** *7* (1), 41-51.
188. Igney, F. H.; Krammer, P. H., Immune escape of tumors: apoptosis resistance and tumor counterattack. *Journal of leukocyte biology* **2002,** *71* (6), 907-920.
189. Mellman, I.; Coukos, G.; Dranoff, G., Cancer immunotherapy comes of age. *Nature* **2011,** *480* (7378), 480-489.
190. Koeberle, A.; Northoff, H.; Werz, O., Curcumin blocks prostaglandin E2 biosynthesis through direct inhibition of the microsomal prostaglandin E2 synthase-1. *Molecular cancer therapeutics* **2009,** *8* (8), 2348-2355.

191. Koeberle, A.; Bauer, J.; Verhoff, M.; Hoffmann, M.; Northoff, H.; Werz, O., Green tea epigallocatechin-3-gallate inhibits microsomal prostaglandin E2 synthase-1. *Biochemical and biophysical research communications* **2009,** *388* (2), 350-354.
192. Koeberle, A.; Rossi, A.; Bauer, J.; Dehm, F.; Verotta, L.; Northoff, H.; Sautebin, L.; Werz, O., Hyperforin, an anti-inflammatory constituent from St. John's wort, inhibits microsomal prostaglandin E.
193. Koeberle, A.; Northoff, H.; Werz, O., Identification of 5-lipoxygenase and microsomal prostaglandin E2 synthase-1 as functional targets of the anti-inflammatory and anti-carcinogenic garcinol. *Biochemical pharmacology* **2009,** *77* (9), 1513-1521.
194. Bauer, J.; Kuehnl, S.; Rollinger, J. M.; Scherer, O.; Northoff, H.; Stuppner, H.; Werz, O.; Koeberle, A., Carnosol and carnosic acids from Salvia officinalis inhibit microsomal prostaglandin E2 synthase-1. *Journal of Pharmacology and Experimental Therapeutics* **2012,** *342* (1), 169-176.
195. Schaible, A. M.; Traber, H.; Temml, V.; Noha, S. M.; Filosa, R.; Peduto, A.; Weinigel, C.; Barz, D.; Schuster, D.; Werz, O., Potent inhibition of human 5-lipoxygenase and microsomal prostaglandin E2 synthase-1 by the anti-carcinogenic and anti-inflammatory agent embelin. *Biochemical pharmacology* **2013,** *86* (4), 476-486.
196. Riendeau, D.; Aspiotis, R.; Ethier, D.; Gareau, Y.; Grimm, E. L.; Guay, J.; Guiral, S.; Juteau, H.; Mancini, J. A.; Méthot, N., Inhibitors of the inducible microsomal prostaglandin E2 synthase (mPGES-1) derived from MK-886. *Bioorganic & medicinal chemistry letters* **2005,** *15* (14), 3352-3355.
197. Giroux, A.; Boulet, L.; Brideau, C.; Chau, A.; Claveau, D.; Côté, B.; Ethier, D.; Frenette, R.; Gagnon, M.; Guay, J., Discovery of disubstituted phenanthrene imidazoles as potent, selective and orally active mPGES-1 inhibitors. *Bioorganic & medicinal chemistry letters* **2009,** *19* (20), 5837-5841.
198. Chau, A.; Cote, B.; Ducharme, Y.; Frenette, R.; Friesen, R.; Gagnon, M.; Giroux, A.; Martins, E.; Yu, H.; Hamel, P., 2-(Phenyl or heterocyclic)-1H-phenanthro [9, 10-D] imidazoles. Google Patents: 2009.
199. Guerrero, M. D.; Aquino, M.; Bruno, I.; Terencio, M. C.; Paya, M.; Riccio, R.; Gomez-Paloma, L., Synthesis and pharmacological evaluation of a selected library of new potential anti-inflammatory agents bearing the γ-hydroxybutenolide scaffold: A new class of inhibitors of prostanoid production through the selective modulation of microsomal prostaglandin e synthase-1 expression. *Journal of medicinal chemistry* **2007,** *50* (9), 2176-2184.
200. Wu, T. Y. H.; Juteau, H.; Ducharme, Y.; Friesen, R. W.; Guiral, S.; Dufresne, L.; Poirier, H.; Salem, M.; Riendeau, D.; Mancini, J., Biarylimidazoles as inhibitors of microsomal prostaglandin E2 synthase-1. *Bioorganic & medicinal chemistry letters* **2010,** *20* (23), 6978-6982.
201. Singh Bahia, M.; Silakari, O., Exploring the biological potential of urea derivatives against mPGES-1: a combination of quantum mechanics, pharmacophore modelling and QSAR analyses. *Medicinal Chemistry* **2013,** *9* (1), 138-151.
202. Shiro, T.; Takahashi, H.; Kakiguchi, K.; Inoue, Y.; Masuda, K.; Nagata, H.; Tobe, M., Synthesis and SAR study of imidazoquinolines as a novel structural class of microsomal prostaglandin E2 synthase-1 inhibitors. *Bioorganic & medicinal chemistry letters* **2012,** *22* (1), 285-288.
203. Arhancet, G. B.; Walker, D. P.; Metz, S.; Fobian, Y. M.; Heasley, S. E.; Carter, J. S.; Springer, J. R.; Jones, D. E.; Hayes, M. J.; Shaffer, A. F., Discovery and SAR of PF-4693627, a potent, selective and orally bioavailable mPGES-1 inhibitor for the potential treatment of inflammation. *Bioorganic & medicinal chemistry letters* **2013,** *23* (4), 1114-1119.
204. Walker, D. P.; Arhancet, G. B.; Lu, H.-F.; Heasley, S. E.; Metz, S.; Kablaoui, N. M.; Franco, F. M.; Hanau, C. E.; Scholten, J. A.; Springer, J. R., Synthesis and biological evaluation of substituted benzoxazoles as inhibitors of mPGES-1: use of a conformation-based hypothesis to facilitate compound design. *Bioorganic & medicinal chemistry letters* **2013,** *23* (4), 1120-1126.
205. Banerjee, A.; Pawar, M. Y.; Patil, S.; Yadav, P. S.; Kadam, P. A.; Kattige, V. G.; Deshpande, D. S.; Pednekar, P. V.; Pisat, M. K.; Gharat, L. A., Development of 2-aryl substituted quinazolin-4 (3H)-one, pyrido [4, 3-d] pyrimidin-4 (3H)-one and pyrido [2, 3-d] pyrimidin-4 (3H)-one derivatives as microsomal prostaglandin E2 synthase-1 inhibitors. *Bioorganic & medicinal chemistry letters* **2014,** *24* (20), 4838-4844.
206. Jin, Y.; Smith, C. L.; Hu, L.; Campanale, K. M.; Stoltz, R.; Huffman Jr, L. G.; McNearney, T. A.; Yang, X. Y.; Ackermann, B. L.; Dean, R., Pharmacodynamic comparison of LY3023703, a novel microsomal prostaglandin e synthase 1 inhibitor, with celecoxib. *Clinical Pharmacology & Therapeutics* **2016,** *99* (3), 274-284.
207. Darnell, J. E., Transcription factors as targets for cancer therapy. *Nature Reviews Cancer* **2002,** *2* (10), 740-749.
208. Bunnett, J. F.; Naff, M. B., Kinetics of reactions of amines with isatoic anhydride. *Journal of the American Chemical Society* **1966,** *88* (17), 4001-4008.

209. Staiger, R. P.; Wagner, E. C., Isatoic anhydride. III. Reactions with primary and secondary amines. *The Journal of Organic Chemistry* **1953,** *18* (10), 1427-1439.
210. Williams, A.; Ibrahim, I. T., Carbodiimide chemistry: recent advances. *Chemical Reviews* **1981,** *81* (6), 589-636.
211. König, W.; Geiger, R., Eine neue methode zur synthese von peptiden: aktivierung der carboxylgruppe mit dicyclohexylcarbodiimid unter zusatz von 1-hydroxy-benzotriazolen. *Chemische Berichte* **1970,** *103* (3), 788-798.
212. Carpino, L. A.; El-Faham, A., The diisopropylcarbodiimide/1-hydroxy-7-azabenzotriazole system: segment coupling and stepwise peptide assembly. *Tetrahedron* **1999,** *55* (22), 6813-6830.
213. Evans, B. E.; Rittle, K. E.; Bock, M. G.; DiPardo, R. M.; Freidinger, R. M.; Whitter, W. L.; Lundell, G. F.; Veber, D. F.; Anderson, P. S.; Chang, R. S. L., Methods for drug discovery: development of potent, selective, orally effective cholecystokinin antagonists. *Journal of medicinal chemistry* **1988,** *31* (12), 2235-2246.
214. Lam, P. Y. S.; Clark, C. G.; Saubern, S.; Adams, J.; Averill, K. M.; Chan, D. M. T.; Combs, A., Copper promoted aryl/saturated heterocyclic CN bond cross-coupling with arylboronic acid and arylstannane. *Synlett* **2000,** *2000* (05), 0674-0676.
215. Tao, L.; Yue, Y.; Zhang, J.; Chen, S. Y.; Yu, X. Q., A Mild and Efficient Method for N-Arylnucleobase Synthesis via the Cross-Coupling Reactions of Nucleobases with Arylboronic Acids Catalyzed by Simple Copper Salts. *Helvetica Chimica Acta* **2008,** *91* (6), 1008-1014.
216. Okabe, T.; Maekawa, K.; Taniguchi, E., Syntheses of thiadiazolopyrimidine and related compounds. *Agricultural and Biological Chemistry* **1973,** *37* (5), 1197-1201.
217. Jafari, B.; Ospanov, M.; Ejaz, S. A.; Yelibayeva, N.; Khan, S. U.; Amjad, S. T.; Safarov, S.; Abilov, Z. A.; Turmukhanova, M. Z.; Kalugin, S. N., 2-Substituted 7-trifluoromethyl-thiadiazolopyrimidones as alkaline phosphatase inhibitors. Synthesis, structure activity relationship and molecular docking study. *European Journal of Medicinal Chemistry* **2018,** *144*, 116-127.
218. Miyaura, N.; Yamada, K.; Suzuki, A., A new stereospecific cross-coupling by the palladium-catalyzed reaction of 1-alkenylboranes with 1-alkenyl or 1-alkynyl halides. *Tetrahedron Letters* **1979,** *20* (36), 3437-3440.
219. Di Micco, S.; Pulvirenti, L.; Bruno, I.; Terracciano, S.; Russo, A.; Vaccaro, M. C.; Ruggiero, D.; Muccilli, V.; Cardullo, N.; Tringali, C., Identification by Inverse Virtual Screening of magnolol-based scaffold as new tankyrase-2 inhibitors. *Bioorganic & medicinal chemistry* **2018,** *26* (14), 3953-3957.
220. Jafari, B.; Yelibayeva, N.; Ospanov, M.; Ejaz, S. A.; Afzal, S.; Khan, S. U.; Abilov, Z. A.; Turmukhanova, M. Z.; Kalugin, S. N.; Safarov, S., Synthesis of 2-arylated thiadiazolopyrimidones by Suzuki–Miyaura cross-coupling: a new class of nucleotide pyrophosphatase (NPPs) inhibitors. *RSC advances* **2016,** *6* (109), 107556-107571.
221. Kabbage, M.; Dickman, M. B., The BAG proteins: a ubiquitous family of chaperone regulators. *Cellular and Molecular Life Sciences* **2008,** *65* (9), 1390-1402.
222. Takayama, S.; Reed, J. C., Molecular chaperone targeting and regulation by BAG family proteins. *Nature cell biology* **2001,** *3* (10), E237-E241.
223. Stürner, E.; Behl, C., The role of the multifunctional BAG3 protein in cellular protein quality control and in disease. *Frontiers in molecular neuroscience* **2017,** *10*, 177.
224. Rauch, J. N.; Tse, E.; Freilich, R.; Mok, S.-A.; Makley, L. N.; Southworth, D. R.; Gestwicki, J. E., BAG3 is a modular, scaffolding protein that physically links heat shock protein 70 (Hsp70) to the small heat shock proteins. *Journal of molecular biology* **2017,** *429* (1), 128-141.
225. Arakawa, A.; Handa, N.; Ohsawa, N.; Shida, M.; Kigawa, T.; Hayashi, F.; Shirouzu, M.; Yokoyama, S., The C-terminal BAG domain of BAG5 induces conformational changes of the Hsp70 nucleotide-binding domain for ADP-ATP exchange. *Structure* **2010,** *18* (3), 309-319.
226. Sastry, G. M.; Inakollu, V. S. S.; Sherman, W., Boosting virtual screening enrichments with data fusion: coalescing hits from two-dimensional fingerprints, shape, and docking. *Journal of chemical information and modeling* **2013,** *53* (7), 1531-1542.
227. Pala, D.; Beuming, T.; Sherman, W.; Lodola, A.; Rivara, S.; Mor, M., Structure-based virtual screening of MT2 melatonin receptor: influence of template choice and structural refinement. *Journal of chemical information and modeling* **2013,** *53* (4), 821-835.
228. Bruno, G.; Costantino, L.; Curinga, C.; Maccari, R.; Monforte, F.; Nicolo, F.; Ottana, R.; Vigorita, M. G., Synthesis and aldose reductase inhibitory activity of 5-arylidene-2, 4-thiazolidinediones. *Bioorganic & medicinal chemistry* **2002,** *10* (4), 1077-1084.
229. Leonova, E. S.; Makarov, M. V.; Rybalkina, E. Y.; Nayani, S. L.; Tongwa, P.; Fonari, A.; Timofeeva, T. V.; Odinets, I. L., Structure–cytotoxicity relationship in a series of N-phosphorus substituted E,

E-3, 5-bis (3-pyridinylmethylene)-and E, E-3, 5-bis (4-pyridinylmethylene) piperid-4-ones. *European journal of medicinal chemistry* **2010,** *45* (12), 5926-5934.
230. Dalessandro, E. V.; Collin, H. P.; Guimarães, L. G. L.; Valle, M. S.; Pliego Jr, J. R., Mechanism of the piperidine-catalyzed Knoevenagel condensation reaction in methanol: the role of iminium and Enolate ions. *The Journal of Physical Chemistry B* **2017,** *121* (20), 5300-5307.
231. De Marco, M.; Basile, A.; Iorio, V.; Festa, M.; Falco, A.; Ranieri, B.; Pascale, M.; Sala, G.; Remondelli, P.; Capunzo, M. In *Role of BAG3 in cancer progression: A therapeutic opportunity*, 2018; Elsevier: pp 85-92.
232. Luchetti, F.; Canonico, B.; Biagiarelli, L.; Bucci, L.; Valentini, M.; Papa, S., Indagini citofluorimetriche nella vitalità e morte cellulare. I. Necrosi, apoptosi e proliferazione cellulare. *biochimica clinica* **2009,** *33* (2), 83.
233. Wang, H. Q.; Meng, X.; Gao, Y. Y.; Liu, B. Q.; Niu, X. F.; Zhang, H. Y.; Du, Z. X., Characterization of BAG3 cleavage during apoptosis of pancreatic cancer cells. *Journal of cellular physiology* **2010,** *224* (1), 94-100.
234. Gentilella, A.; Khalili, K., Autoregulation of co-chaperone BAG3 gene transcription. *Journal of cellular biochemistry* **2009,** *108* (5), 1117-1124.
235. Trebino, C. E.; Stock, J. L.; Gibbons, C. P.; Naiman, B. M.; Wachtmann, T. S.; Umland, J. P.; Pandher, K.; Lapointe, J.-M.; Saha, S.; Roach, M. L., Impaired inflammatory and pain responses in mice lacking an inducible prostaglandin E synthase. *Proceedings of the National Academy of Sciences* **2003,** *100* (15), 9044-9049.
236. Di Micco, S.; Spatafora, C.; Cardullo, N.; Riccio, R.; Fischer, K.; Pergola, C.; Koeberle, A.; Werz, O.; Chalal, M.; Vervandier-Fasseur, D., 2, 3-Dihydrobenzofuran privileged structures as new bioinspired lead compounds for the design of mPGES-1 inhibitors. *Bioorganic & medicinal chemistry* **2016,** *24* (4), 820-826.
237. Bergqvist, F.; Morgenstern, R.; Jakobsson, P.-J., A review on mPGES-1 inhibitors: From preclinical studies to clinical applications. *Prostaglandins & other lipid mediators* **2020,** *147*, 106383.
238. Di Micco, S.; Terracciano, S.; Cantone, V.; Fischer, K.; Koeberle, A.; Foglia, A.; Riccio, R.; Werz, O.; Bruno, I.; Bifulco, G., Discovery of new potent molecular entities able to inhibit mPGES-1. *European journal of medicinal chemistry* **2018,** *143*, 1419-1427.
239. Lauro, G.; Tortorella, P.; Bertamino, A.; Ostacolo, C.; Koeberle, A.; Fischer, K.; Bruno, I.; Terracciano, S.; Gomez-Monterrey, I. M.; Tauro, M., Structure-Based Design of Microsomal Prostaglandin E2 Synthase-1 (mPGES-1) Inhibitors using a Virtual Fragment Growing Optimization Scheme. *ChemMedChem* **2016,** *11* (6), 612-619.
240. Giordano, A.; Forte, G.; Terracciano, S.; Russo, A.; Sala, M.; Scala, M. C.; Johansson, C.; Oppermann, U.; Riccio, R.; Bruno, I., Identification of the 2-Benzoxazol-2-yl-phenol scaffold as new hit for JMJD3 inhibition. *ACS medicinal chemistry letters* **2019,** *10* (4), 601-605.
241. Vass, M.; Keserű, G. M., Fragments to link. A multiple docking strategy for second site binders. *MedChemComm* **2013,** *4* (3), 510-514.
242. Miyaura, N.; Suzuki, A., Palladium-catalyzed cross-coupling reactions of organoboron compounds. *Chemical reviews* **1995,** *95* (7), 2457-2483.
243. Tomasic, T.; Masic, L. P., Rhodanine as a privileged scaffold in drug discovery. *Current medicinal chemistry* **2009,** *16* (13), 1596-1629.
244. Naim, M. J.; Alam, M. J.; Ahmad, S.; Nawaz, F.; Shrivastava, N.; Sahu, M.; Alam, O., Therapeutic journey of 2, 4-thiazolidinediones as a versatile scaffold: An insight into structure activity relationship. *European journal of medicinal chemistry* **2017,** *129*, 218-250.
245. Mendgen, T.; Steuer, C.; Klein, C. D., Privileged scaffolds or promiscuous binders: a comparative study on rhodanines and related heterocycles in medicinal chemistry. *Journal of medicinal chemistry* **2012,** *55* (2), 743-753.
246. Vaisburg, A.; Bernstein, N.; Frechette, S.; Allan, M.; Abou-Khalil, E.; Leit, S.; Moradei, O.; Bouchain, G.; Wang, J.; Woo, S. H., (2-Amino-phenyl)-amides of ω-substituted alkanoic acids as new histone deacetylase inhibitors. *Bioorganic & medicinal chemistry letters* **2004,** *14* (1), 283-287.

List of abbreviations

2-AG	2-arachidonoyl glycerol
5-HPETE	5-hydroperoxyeicosatetraenoic acid
5-LO	5-Lipoxygenase
11β-PGE_2	11β-Prostaglandin E_2
12-HTT	12-hydroxyheptadecatrienoic acid
AA	Arachidonic acid
AcOEt	Ethyl acetate
AcOH	Acetic acid
ADME	Absorption, distribution, metabolism, and excretion
ALS	Amyotrophic lateral sclerosis
AKT	RAC-alpha serine/threonine-protein kinase
AR	Androgen receptor
ATF1	Activating transcription factor 1
ATP	Adenosine triphosphate
BAG1/RAP46/HAP46	Bcl-2-associated athanogene 1
BAG2	Bcl-2-associated athanogene 2
BAG3/CAIR-1/B	Bcl-2 associated athanogene 3
BAG4/SODD	Bcl-2-associated athanogene 4
BAG5	Bcl-2-associated athanogene 5
BAG6/BAT3/Scythe	Bcl-2-associated athanogene 6
BAX	Bcl-2-associated X protein
Bcl-2	B-cell lymphoma 2 protein
Bcl-xL	B-cell lymphoma-extra large protein
BD	BAG domain
BH3	BH3 interacting-domain death agonist
BRAF	Serine/threonine-protein kinase B-raf
BRG1	Brahma-related gene-1
$CHCl_3$	Chloroform
CHIP or STUB1	C-terminus of the Hsc70-interacting protein
CK2	Casein kinase 2
COX-1/2	Cyclooxygenase-1/2
cPGES	Cytosolic prostaglandin E_2 synthase
DAG	Diacylglycerol
DBD	DNA binding domain
DCM	Dichloromethane
DIC	*N,N′*-diisopropylcarbodiimide
DMAP	4-Dimethylaminopyridine
DMEM	Dulbecco's Modified Eagle Medium
DMF	Dimethylformamide
DMSO	Dimethyl sulfoxide
EDTA	Ethylenediamine tetraacetic acid
EP-1/2/3/4	Prostaglandin E2 receptors
ESI-MS	Electrospray ionization mass spectrometry

FACS	Fluorescence-activated cell sorting
FAK	Focal adhesion kinase
FBS	Fetal bovine serum
FLAP	5-lipoxygenase activating protein
FLUC	Firefly luciferase
GSH	Glutathione
HOBt	1-Hydroxybenzotriazole
HR-A/B/C	Heptad repeat regions
HSF1	Heat shock factor 1
HSE	Heat shock element
HSP	Heat shock protein
HSR	Heat shock response
IC_{50}	Half maximal inhibitory concentration
IL-1β	Interleukin-1β
IL-8	Interleukin-8
IL-10	Interleukin-10
IL-17	Interleukin-17
IPV	Isoleucine-proline-valine motif
IKK-γ	Inhibitor of nuclear factor kappa-B kinase subunit γ
K_D	Dissociation constant
LC3	Microtubule-associated protein 1A/1B-light chain 3
LPS	Lipopolysaccharide
LTA_4	Leukotriene A_4
LTB_4	Leukotriene B_4
LTC_4	Leukotriene C_4
LTD_4	Leukotriene D_4
LTE_4	Leukotriene E_4
LTC4S	Leukotriene C4 synthase
LTQ	Linear Trap Quadropole
LZ	Leucine zipper domain
MAPEG	Membrane-associated proteins in eicosanoid and glutathione metabolism
MAPK	Mitogen-activated protein kinase
Mcl-1	Induced myeloid leukemia cell differentiation protein
MeOH/CH_3OH	Methanol
MGST-1	Microsomal glutathione S-transferase 1
MGST-2	Microsomal glutathione S-transferase 2
MGST-3	Microsomal glutathione S-transferase 3
MPGES-1	Microsomal prostaglandin E2 synthase-1
MSGT1-L1	Microsomal glutathione-S-transferase-1-like-1
MTT	3-(4,5-Dimethyl-2-thiazolyl)-2,5-diphenyl-2H-tetrazolium bromide
NaH	Sodium hydride

NF-κB	Nuclear factor kappa-light-chain-enhancer of activated B cells
NMR	Nuclear magnetic resonance
NSAIDs	Nonsteroidal anti-inflammatory drugs
nSBs	nuclear Stress Bodies
OD	Optical density
P62	Sequestosome-1 protein
PBS	Phosphate buffered saline
PDB	Protein data bank
PDZGEF2	Guanine nucleotide exchange factor 2 containing a PDZ domain
PDSM	Phosphorylation-dependent SUMOylation
PGB_1	Prostaglandin B_1
PGD_2	Prostaglandin D_2
PGE_2	Prostaglandin E_2
PGES	PGE_2 synthase
PGF2α	Prostaglandin F2α
PGG_2	Prostaglandin G_2
PGH_2	Prostaglandin H_2
PGI_2	Prostaglandin I_2
PI	Propidium iodide
PLA_2	Phospholipases A_2
PLC	Phospholipase C
PPA	Polyphosphoric acid
P-TEFb	Positive transcription elongation factor
PTM	Post-transcriptional modification
PxxP	Proline-rich domain
Q-ToF	Quadrupole time of flight
Rac1	Ras-related C3 botulinum toxin substrate 1
RD	Regulatory domain
RLUC	Renilla Luciferase
RP - HPLC	Reversed-phase high performance liquid chromatography
RT-qPCR	Quantitative reverse transcription PCR
SDS	Sodium dodecyl sulfate
SIRT1	Silent mating type information regulation 2 homolog - 1
SP	Phosphorylation site
SPR	Surface Plasmon Reference
SRC	Proto-oncogene tyrosine-protein kinase Src
STAT3	Signal transducer and activator of transcription 3
SUMO	Small ubiquitin-like modifier protein
SWI/SNF	SWItch/Sucrose non-fermentable
TAD	Trans-activation domain
TFA	Trifluoroacetic acid
THF	Tetrahydrofuran
TLC	Thin layer chromatography

TMEDA	Tetramethylethylenediamine
TNFα	Tumor necrosis factor α
TP53	Tumor protein P53
TRiC/CCT	T-complex protein ring complex/Chaperonin containing TCP-1
TXA_2	Thromboxane A_2
UBL	Ubiquitin-like domain
WW	Tryptophan-tryptophan domain

Ringraziamenti…

Chi mi conosce sa bene che non esterno facilmente i miei sentimenti, ma vorrei esprimere la mia riconoscenza a tutti coloro che mi hanno affiancata e supportata nel lungo cammino del dottorato.

Ho pensato che il modo migliore per farlo fosse tramite alcune foto che ci ritraggono insieme!

La mia profonda gratitudine va alla Prof.ssa Ines Bruno che mi ha accolta nel suo laboratorio, creduto nelle mie capacità e guidata nel mondo della chimica organica.

Un sincero ringraziamento anche alla Prof.ssa Stefania Terracciano che è stata per me un punto di riferimento nel corso di questi anni.

Sicuramente il mio percorso non sarebbe stato lo stesso senza il Prof. Giuseppe Bifulco e tutti i componenti del gruppo computazionale, la Dott.ssa Maria Giovanna Chini, il Dott. Gianluigi Lauro e il Dott. Simone Di Micco. Grazie a tutti voi per avermi stimolata e incoraggiata.

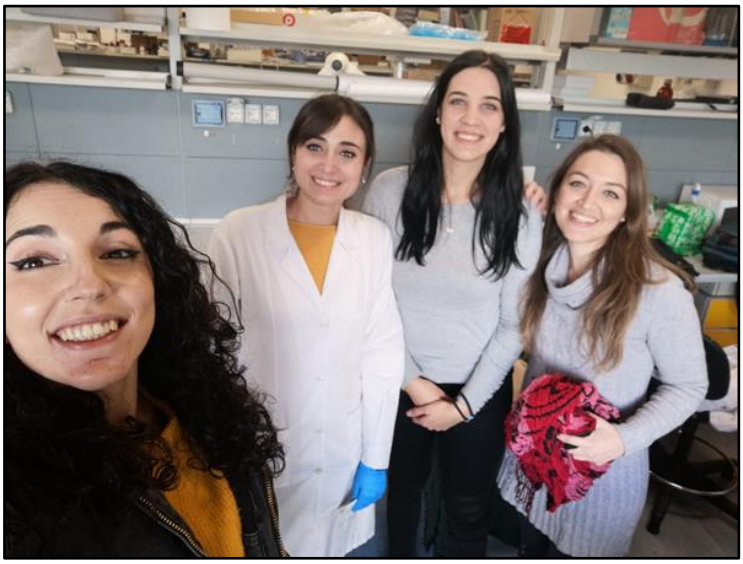

Grazie alle mie colleghe ed amiche Marianna Potenza, Ester Colarusso e Martina Pierri. Ho imparato tanto da ognuna di voi sia dal punto di vista professionale che dal punto di vista umano. Ricorderò sempre i giorni trascorsi insieme in laboratorio con molto affetto. Non avrei potuto desiderare delle compagne di viaggio migliori.

In questi 3 anni tanti tesisti si sono alternati nel laboratorio 10, ognuno con la propria storia, ognuno con le proprie qualità. Tutti voi avete contribuito a rendere

unico il mio dottorato per cui, a mia volta, spero di essere riuscita a trasmettervi l'amore per la ricerca e la passione per lo studio. Auguro a tutti voi un futuro ricco di soddisfazioni.

Uno speciale ringraziamento alla Dott.ssa Nuria Vilaboa e a tutto il suo gruppo di ricerca per avermi fatta sentire a "casa" durante il periodo che ho trascorso presso l'istituto IdiPAZ di Madrid.

Vorrei infine ringraziare la mia famiglia ed i miei amici per essere stati costantemente al mio fianco. Mi avete sostenuta in tutti i modi possibili ed aiutata ad andare avanti anche quando credevo di non farcela. Siete stati essenziali. Senza di voi difficilmente avrei raggiunto quest'obiettivo.

Per quanto mi riguarda, considero il dottorato un punto di partenza e non un punto di arrivo. Sono pronta ad affrontare le sfide che verranno.

Grazie a tutti!